UC Berkeley
UC Berkeley Electronic Theses and Dissertations

Title
Fetal immunity and the developing brain: implications for neurodevelopmental disorders.

Permalink
https://escholarship.org/uc/item/61n850tv

Author
Nichols, Eva K.

Publication Date
2020

Peer reviewed|Thesis/dissertation

eScholarship.org Powered by the California Digital Library
University of California

Fetal immunity and the developing brain: implications for neurodevelopmental disorders.

By

Eva K. Nichols

A dissertation submitted in partial satisfaction of the

requirements for the degree of

Doctor of Philosophy

in

Molecular and Cell Biology

in the

Graduate Division

of the

University of California, Berkeley

Committee in charge:

Professor Kaoru Saijo, Chair
Professor Ellen Robey
Professor David Raulet
Professor Daniela Kaufer

Spring 2020

Abstract

Fetal immunity and the developing brain:
implications for neurodevelopmental disorders.

By

Eva K. Nichols

Doctor of Philosophy in Molecular and Cell Biology

University of California, Berkeley

Professor Kaoru Saijo, Chair

The brain has innate immune myeloid cells (including microglia and border-associated macrophages) that have dynamic roles in homeostasis and the response to tissue injury and infection. Given the ability of brain myeloid cells to sense a variety of environmental cues, several studies have investigated their roles in neurodegenerative disease onset and progression. But, the impact of fetal myeloid cells on neurodevelopmental disorders is relatively unexplored in comparison. We used two mouse models of neurodevelopmental disorders to uncover the impact of fetal myeloid cell immunity to both normal and abnormal brain development. We found that an inflammatory lytic form of cell death, termed pyroptosis, in microglia may be required for establishing certain normal behavioral circuits. With genetic deficiency in the pyroptosis pathway, or upon pharmacological inhibition thereof, mice have attention-deficit/hyperactivity disorder (ADHD)-like behavior changes. Using the maternal immune activation (MIA) model of autism spectrum disorder (ASD), we identified a fetal myeloid responder population, likely to be border-associated macrophages, which directly sense MIA challenge. Thus, we learned that fetal immunity, mediated by myeloid cells, has important consequences for brain formation. Disruption or activation of these roles may constitute an upstream arm in neurodevelopmental disorder etiology.

Table of Contents

Abstract.....1

Table of Contents.....i

List of Figures.....iv

Tables.....vi

Dedication.....vii

Acknowledgements.....viii

Chapter 1: Introduction.....1

1.1: Microglia as the brain-resident immune cell: roles in health and disease.....2
1.2: Microglia and fetal brain development.....5
1.3: Attention-deficit/hyperactivity disorder (ADHD).....9
1.4: ADHD and the connection to immunity.....11
1.5: Autism-spectrum disorder (ASD).....12
1.6: ASD and the connection to immunity.....14

References.....16

Chapter 2: Microglial inflammasome activation may be required for normal brain development.

Abstract.....32

Introduction
2.1: Current animal models used to study ADHD.....32
2.2: Inflammasome activation and lytic cell death.....34
2.3: Known cases of inflammasome activation in the brain.....35

Results
2.4: Mice deficient in caspase-1 exhibit behaviors reminiscent of ADHD.....39
2.5: Mice deficient in *Nlrp3*, *Gsdmd*, and *Il1r1* exhibit behavioral tendencies reminiscent of ADHD.....40
2.6: Re-expression of CASP1 in a *Cx3cr1*-dependent manner restores behavior changes to WT levels.....40
2.7: In the fetal brain, microglial pyroptosis may occur in a spatiotemporal manner.....42
2.8: CASP1 deficiency causes discrete changes in cell patterning within the thalamus of adult *Casp1*$^{-/-}$ brains.....44

2.9: Pharmacological disruption of the pyroptosis pathway produces some ADHD-like behavior changes in mice.....45

Discussion
2.10: Lytic cell death and development: outstanding questions.....48
2.11: Study limitations and future directions.....49
2.12: *Casp1*$^{-/-}$ mice: A new model of ADHD? Additional considerations.....52

Figures.....54

Methods.....86

References.....92

Chapter 3: Fetal brain myeloid cells respond to maternal immune challenge.

Abstract.....103

Introduction
3.1: The maternal immune activation model (MIA) is a robust mouse model of ASD.....104
3.2: Known immune response mechanisms during the MIA mouse model of ASD.....105
3.3: Investigating fetal immunity during MIA: design and rationale for our study.....107

Results
3.4: Only Poly(I:C)-induced MIA causes ASD-like behavior changes.....109
3.5: Fetal immunity, mediated by TRIF signaling, is required for ASD-like defects in sociability.....110
3.6: Trans-placental viral infections cause ASD-like behavior changes.....111
3.7: We recovered robust microglial and border-associated macrophage (BAM) populations in the E13.5 brain by scRNA-seq.....112
3.8: We identified a putative WT fetal responder cell population to Poly(I:C)-induced MIA.....112
3.9: Putative fetal responder cells to Poly(I:C)-induced MIA resolve back towards a BAM-like state.....113

Discussion
3.10: Fetal brain myeloid cells are responsive to MIA.....115
3.11: Study limitations and future experimental modifications.....115

Figures.....118

Supplementary Table 1.....149

Methods.....158

References.....164

Chapter 4: Conclusions and future directions.....168

4.1: Fetal immunity and development: considerations for public health.....169
4.2: Outstanding questions and future directions of study.....170
4.3: Conclusion.....172

References.....173

Figures

Figure 2.1: *Casp1*$^{-/-}$ mice exhibit ADHD-like behavior change.....54

Figure 2.2: *Nlrp3*$^{-/-}$, *Il-1r*$^{-/-}$, and *Gsdmd*$^{-/-}$ mice phenocopy *Casp1*$^{-/-}$ ADHD-like behavior changes.....56

Figure 2.3: Re-expression of CASP1 in a *Cx3cr1*-dependent manner restores behavior changes to WT levels.....58

Figure 2.4: *Cx3cr1*-GFP^{+} cells are present in the fetal brain parenchyma and borders at E12.5.....60

Figure 2.5: RT-qPCR validation of *Cx3cr1*-GFP^{+} and *Cx3cr1*-GFP^{-} fetal brain cell fractions and *Casp1* expression in the *iCasp1* system.....62

Figure 2.6: Microglial lytic cell death occurs in a spatiotemporal manner in the fetal brain.....64

Figure 2.7: Visualizing active inflammasome assembly through ASC staining.....66

Figure 2.8: A fetal microglia lytic cell cluster was positive for ASC specks and exhibits morphological characteristics of active lysis.....68

Figure 2.9: Fetal microglial pyroptotic clusters are diminished on a *Casp1*$^{-/-}$ background.....70

Figure 2.10: Fetal microglial pyroptotic clusters localize near Pax6^{+} neural precursor cells.....72

Figure 2.11: *Casp1*$^{-/-}$ adult brains have no overt structural brain anomalies.....74

Figure 2.12: *Casp1*$^{-/-}$ adult brains have cellular patterning have increased cell density within the thalamic reticular nucleus.....76

Figure 2.13: Pharmacological inhibition of pyroptosis in development produces some ADHD-like behavior changes in mice.....78

Figure 2.14: Acetaminophen downregulates inflammasome pathway elements, but does not decrease the frequency of lytic microglial clusters.....80

Figure 2.15: Acetaminophen exposure to dams at E12.5-E14.5 produce offspring with hyperactivity.....82

Figure 2.16: Working model—microglial pyroptosis of key subsets promotes normal cell numbers within thalamic nuclei.....84

Figure 3.1: Only the TLR3 agonist, Poly(I:C), was sufficient to promote core ASD-like behavior changes in the MIA model.....118

Figure 3.2: Maternal TRIF sensing is necessary for producing restricted/repetitive behaviors in male offspring of Poly(I:C)-induced MIA mice.....120

Figure 3.3: Fetal TRIF sensing is necessary and sufficient for producing a core sociability deficit in male offspring of Poly(I:C)-induced MIA mice.....122

Figure 3.4: Infection of MHV-68, and not MCMV, at E12.5 promoted ASD-like behavior changes in male offspring.....124

Figure 3.5: MHV-68 can cross the placenta.....126

Figure 3.6: Using a single-cell RNA sequencing approach to identify potential fetal myeloid cells following MIA.....128

Figure 3.7: Quality control metrics of our scRNAseq dataset show high-quality cells.....130

Figure 3.8: We recovered 49,865 cells that are primarily E13.5 microglia and border-associated macrophage cells.....132

Figure 3.9: Heatmap of some of the top differentially expressed genes that distinguish the cell clusters.....134

Figure 3.10: We identify a putative WT fetal responder cell population to Poly(I:C)-induced MIA.....136

Figure 3.11: The putative WT fetal responder cells are inflammatory, and express both microglial and BAM-associated genes.....138

Figure 3.12: Batch composition and downsampling: testing for robustness.....140

Figure 3.13: RNA velocity analysis shows that the putative WT fetal responder cells resolve back toward a BAM cell state.....142

Figure 3.14: Cell cycle phasing of the dataset.....144

Figure 3.15: Working model—WT fetal myeloid cells, likely BAMs, respond to Poly(I:C)-induced MIA and promote the formation of ASD-like behavior changes.....146

Tables

Supplementary Table 1.....148

Dedication

I dedicate this dissertation to my mother, Christina, whose personal sacrifices made this possible. I love you so much.

Acknowledgements

"I have always depended on the kindness of strangers" is what Blanche DuBois, a fictional character in Tennessee William's *A Streetcar Named Desire*, famously says as she loses her grip on reality. It's a sentiment that remains with me, because, for very different (and un-tragic) reasons, I also depended on the kindness of strangers. Without them, my journey to a career in science would have been exceedingly more difficult (or may not have even happened at all). I'm lucky to have the names (and even friendship) of some of these strangers—they will be acknowledged here. However, there are many more strangers whose names and friendship I may never get to know, and I can only hope that my gratitude will reach them and that I someday can pay it forward. I leave myself forever accountable for that. Of course, I also relied on a lot of non-strangers—the family and friends that have emotionally supported me throughout my life. They have kindly lent me their ears and shoulders. I am forever indebted to them.

In this Acknowledgements section, readers will hopefully understand how I didn't accomplish this alone. I feel like my graduate school story began before I started college, which is why I include these three major groups of individuals to express gratitude toward: from my time in college (2010-2014), from graduate school itself (2014-2020), and from my personal life.

I'm a first-generation scholar, which means that I'm first-in-family to go to college and graduate school. Graduating debt-free from the University of Arizona and University of California, Berkeley, is bewildering. I owe much of that to Rosenna Trejo, my Flowing Wells High School counselor, who recognized that I was a bit lost after moving to a new school from out-of-state. Rosenna was instrumental in connecting me with scholarship opportunities and in helping me to navigate the college application process. She encouraged me to apply to the Dorrance Scholarship Program. Thank you, Rosenna, for pointing me in the right direction, and continuing on to be a dear friend in my life. The Dorrance Scholarship Program miraculously awarded me with financial and academic support for all four years of college at the University of Arizona. Jacquie and Bennett Dorrance founded the Dorrance Scholarship Program out of their unparalleled passion to improve the quality of life in their community. Through them, I was instilled with the values of environmental stewardship, volunteering, innovation, and cultural appreciation of the arts and humanities. Words cannot express my gratitude for their colossal gift. I thank Dr. Lindsey Buckman and Jim Hensley (psychologist and executive director of the Dorrance Scholarship Program, respectively) as pillars of consistent insight and guidance throughout college. I remember our meetings, cultural events, and travel experiences very fondly—a million thanks to the Dorrance Scholarship Program! I also thank the unknown donors and coordinators behind the Wildcat Excellence Tuition Award, the Valley Foundation Scholarship, and the American taxpayers behind the Pell Grant and Federal Work-Study Program. All of these individuals opened doors that were previously inaccessible to me—I deeply thank every last one of them.

In college, Dr. Liwen Lai opened the "science door" for me. I originally started out as a veterinary science major, and was looking for any job position through the Federal Work-Study program. I wasn't having much luck, so I started applying to jobs that I had no qualifications for—including, being a research assistant. Dr. Lai interviewed me for

the position on the first day of college (Monday October 23, 2010). Her first question was, “can you pipette?” I didn’t know what that was, so I said no. Her second question was, “are you a work-study student?” Thankfully, I was. Dr. Lai offered me a place in her lab, and I remained there under training by Dr. Kim Yong until graduating in May 2014. Kim remains the most patient person that I know, who gently encouraged and coached me in the lab despite my innumerable mistakes. Thanks to Kim and Dr. Lai, I became proficient in mouse handling and microscopy. At one point in college, my time with the Federal Work-Study program was drawing to a close. This threatened my ability to stay in the lab because I would need a paying job.

Dr. Lai supported my application to the Undergraduate Biology Research Program (UBRP), which provided structured scientific development in addition to wages. Dr. Carol Bender graciously accepted my application, was reviewed favorably enough to get a spot in UBRP. Thanks to Carol and UBRP, I was able to continue my lab work as a job while simultaneously getting training. It wasn’t until I arrived at UC Berkeley, where I realized how rare it is for undergraduates to get paid for research experience. My participation in UBRP absolutely paved my way to graduate school, and I am extremely grateful for that gift. Carol also went above and beyond in connecting me with opportunities for science outreach and mentorship, which taught me how I can share my science passion with the community around me. Carol became another mentor that I went to. She helped me understand what the world of science outside of the lab was like. I also want to thank the donors to UBRP, which include federal agencies, private non-profit organizations, internal university funds, and private industry: the National Science Foundation, the National Institutes of Health, the Western Alliance to Expand Student Opportunities, the Howard Hughes Medical Institute, the Arnold and Mabel Beckman Foundation, the American Society for Pharmacology and Experimental Therapeutics, Sanofi, and the Bioindustry Organization of Southern Arizona.

With guidance from Carol, Jennifer Cubeta, and advisors in the Molecular and Cellular Biology (MCB) department, I changed my major from veterinary science to MCB and pursued minors in biochemistry and microbiology. I worked with Dr. Jim Collins as an undergraduate teaching assistant for introductory microbiology, which began my interest in university teaching. He also was a window into the lifestyle of a university professor. I thank him for his encouragement and candid advice. From microbiology at the UA, I also thank Dr. V.K. Viswanathan who opened his doors to an independent study and many thought experiments. From both Dr. Collins and Dr. Viswanathan, I had a growing interest in innate immunity and microbial pathogenesis (though, unbeknownst to me then, innate immunity would “win”).

Dr. Lai, Dr. Bender, and Dr. Collins strongly supported my applications to graduate school (with help once again from the Dorrance Scholarship Program in paying application fees and travel expenses). I thank them all deeply for their support, especially because I applied to fifteen graduate programs (later, I found that most students apply to half as many!). To my astonishment, MCB at UC Berkeley was among the programs that offered me an interview. During the interview, it was clear that this was the best fit for me, and that still remains clear as I reflect on my experience here. I thank the unknown faculty and students that supported my entry into the program—especially as I was someone with no publication record and no hardcore classic molecular biology expertise.

My first science experience at UC Berkeley was rotating in Dr. Kaoru Saijo's lab. Kaoru's patience rivals that of Kim's; she taught me many classic molecular biology techniques by hand, even though she was insanely busy starting her new lab and writing grants. Her actions showed me that she would have a deep investment in my scientific training. Her out-of-the-box ideas at the frontier of immunology and neuroscience were an added bonus. I knew that I needed to join her lab. I joined officially on April 30th, 2015, and it was honestly one of the happiest days in my life for the beautiful feeling that so much was possible. Kaoru's steadfast confidence in me was a rock throughout my Ph.D., even when I felt it was unwarranted; she'd simply say, "Be confident!" And I would pretend to be (until I started to feel it for real). Kaoru's boundless positivity and cheerful disposition also became a rock in the moments nothing was working. She encouraged scientific creativity by enabling experiments that I wanted to do (even when she was fairly certain they wouldn't work). Like any mother figure, she also knew when to deal out hard truths, and when to curb my stubbornness. Upon interviewing for jobs, comments describing my scientific style included "dynamic", "enthusiastic", and "passionate". I thought it was funny because these are the exact words I would use to describe Kaoru—I'm happy that a little bit of her rubbed off on me. Kaoru, I will never be able to accurately express the depth of my gratitude for our journey together—I'm really sad it is about to end. You had an immeasurable impact on my scientific and personal development. I hope you can agree that we share a steel bond forged by fire! And, that we'll be life long friends. Thank you for your incredible gift of mentorship.

Along with Kaoru, I had another fantastic mentor to go to who was just across the hall: Dr. Ellen Robey. Thank you, Ellen, for providing valuable insight and perspective alongside Kaoru. From you, I appreciated most the lessons in rigorously producing and analyzing science, having laser eye attention to detail, and learning how to efficiently communicate my science. You went above and beyond in support of me, including chairing my qualifying exam, being a part of my thesis committee, attending my lab meetings, and editing numerous proposals. You helped my confidence grow for the simple reason of always taking my science seriously. Thank you for having been my sounding board throughout grad school, and in helping me grow as a better scientist.

I deeply thank the other members of my thesis committee: Dr. David Raulet, and Dr. Daniela Kaufer. I thank you, David, for your unrelenting curiosity. Kaoru and I didn't know whom to approach to include on my committee due to our strange mix of immunology and developmental neuroscience, but knew you might be curious enough to be involved. I appreciate your willingness and thoughtfulness in approaching my science, as well your confidence in me. Daniela, I thank you for your essential contributions throughout my Ph.D.: your neuroscience perspective was invaluable on my otherwise immunology committee! There have been quite a few times that your advice has saved us a lot of time at the bench. Thank you also for attending every last one of my thesis committee meetings. I've been so lucky to have a fantastic committee.

I also found other mentor figures in my own lab: Dr. Hsiu-Chun Chuang, and Dr. Greg Timblin. I have immense gratitude for Hsiu-Chun; my science presented here would not make sense without hers. In fact, a lot of her data is also presented here (indicated, and with her permission). Hsiu-Chun is the scientific "yin" to my scientific "yang": her mouse behavioral studies highlighted the major consequences of disrupting

fetal immunity to the brain, while I filled in some mechanistic details with non-behavior methods. Hsiu-Chun is amazing: she started a family and continued science seemingly without skipping a beat. I admire how she set up a large behavioral core in our lab, and juggled 4-5 projects. On top of all of that, her scientific intuition is marvelous. I will forever look up to Hsiu-Chun. Thank you, Hsiu-Chun, for being my role model in the lab, and for working with me so closely. I had tons of fun doing science with you.

I deeply thank Dr. Greg Timblin for his excellent (and sometimes unforgiving) scientific advice. I can always count on Greg to be honest, because he does not sugar coat anything (perhaps, in fear that it may increase diabetes risk). He continually challenged my thinking, which taught me when I needed to re-evaluate my strategy (or, when to defend it). I will always value Greg for his exquisite eye for experimental rigor, and his unparalleled pursuit for the scientific truth. Where others would have given up in their science, Greg would continue without breaking a sweat. Thank you, Greg, for always holding me to a higher standard—I look forward to your future works.

I thank others in the Saijo Lab for an enriching experience and shared laughter over lab snacks and drinks: Daniel Araujo, Sandra Muroy, Kurtresha Worden, Laura Craciun, Matt Davis, Madeline Arnold, Rhea Misra, Patirck Lin, Stella Zhu, Jerome Wang, Shannon Louie, Karensa Tjoa, Andrew Sun, Paulina Cedillo, and Fernanda Castro. I also thank the undergraduate students I have mentored in the lab, who gave me an opportunity to learn how to guide others in lab science: Arielle Illano, Timothy Corpuz, Georgia Shepperd, and Yousef Josef. I thank them for their contribution, and for teaching me important lessons. I especially thank Madeline Arnold and Matt Davis for helping me on long experiment days! Even though our days started as early as 6:30 AM, you managed to make them fun. I am sad that I won't get to personally witness your future science in the Saijo Lab.

I found additional fantastic mentors beyond my lab: Kathleen Pestal and Alex Tiriac. Kathleen and Alex are postdocs in the Barton and Feller labs (respectively). Kathleen was always so kind in sharing her exquisite knowledge and expertise in macrophage biology with me, whether it came in the form of casual conversation by the bench, or in careful editing and review of my funding proposals. Thank you so much, Kathleen! I hope we will continue to cross paths in the future, like at conferences. And Alex, it was a joy to learn from you, from technical guidance at the microtome to the softer skills in science: overcoming rejection and persisting through failure. It was also always fun to talk about shared video game and sci-fi book interests! I hope I can be a "Kathleen" and an "Alex" to future students around me.

I sincerely thank my collaborators at MIT for making what I thought was impossible, possible: Dr. Kwanghun Chun ("K.C."), Minyoung Kim, Katherine "Kitty" Xie, Nick Evans, Gabi Drummond, and YoungGyun Park. When I began looking at the fetal microglial landscape with light sheet microscopy, it was exciting for all of the data we could acquire. However, that data remained qualitative because, due to its size, was exceedingly difficult to computationally process and analyze. K.C., your inspiring vision of section-less tissue processing, imaging, and hardcore quantitative analysis is one that resonates with me strongly. Thank you for sharing your lab's expertise and resources in helping us to define the fetal brain landscape. Minyoung, working with you has been one of the best experiences in grad school. Seeing you develop your software was simply the most amazing accomplishment I have witnessed! Your example has

inspired my growing interest in computational biology. Kitty, thank you for your impressive work in optimizing the upstream tissue processing for our difficult samples! And Nick, I hope to hone my imaging skills in hopes of becoming a microscopy professional like you. Thanks once again Chung Lab for this wonderful collaboration, even though the work is not presented here in this dissertation.

I also want to thank Tara Essock-Burns, a stellar postdoc that I met at an imaging conference coordinated by UC Berkeley Cancer Research Lab Molecular Imaging Center (Advanced Imaging Methods 2018). We initiated a collaboration to image bobtail squid light organ development by fluorescence light sheet microscopy. It was immensely fun to visualize these elegant creatures in a way that hasn't been done before (at least, to our knowledge). One of our beautiful images won a calendar prize. While our collaboration ended due to unforeseen circumstances, I hope we can resume our work together in the future.

I also thank members of the Barton Lab (Greg Barton and Bethany Russell) and Vance Lab (Russell Vance and Isabella Rauch) for kindly donating mouse strains in our studies. They really enabled some cool science. I also thank the Coscoy Lab (Laurent Coscoy and Kristi Geiger) for their expertise in virology, and aiding in critical experiments for one of our manuscripts. These individuals exemplify the amazing collaborative research environment on the 4th floor of LSA—many thanks to all of them.

I want to deeply thank the UC Berkeley Single-Cell User Group. Our monthly group meetings were essential in guiding my progress. In particular, I want to especially thank Nick Everetts. Nick graciously spent a lot of time helping me to troubleshoot my code, share his own code, and in the process taught me a few tricks with my data. Having someone like Nick who understands biology and computational science was super fantastic! I also thank John Blair, who patiently helped me follow in his footsteps to get my dry lab analysis going. Thank you, John! I thank the founders of the group, Diya Das and Caroline Cypranowska, for offering fantastic insight as I began this project. I also thank Rick Z. Li from the Glass Lab at UCSD. Rick spent a lot of time advising and evaluating my work, which was essential because this was the first time the Saijo Lab began doing advanced transcriptional work. Rick also sat in on my last lab meeting, and performed the RNA velocity analysis included in this dissertation. Thank you, Rick! I have so much gratitude toward all of these single cell experts.

I also want to thank my fellow 2014 cohort of students who made my transition to graduate school easier through camaraderie. In the beginning of grad school, my laptop was stolen while studying outside in the grass. When my classmates found out, so many people pitched in money to help recover the cost. This remains one of the greatest acts of kindness I've had. A thousand thanks! I didn't know that this was only the beginning of a close bond among classmates that have always come together in times of crisis. Additionally, we knew how to have fun. I will treasure memories from our various class activities (such as backpacking, camping, and skiing/snowboarding, Amy Wednesdays, Friendsgivings, and Movie Night). No matter where we all go in the world, I hope we can continue to count on each other. Please think of me as someone you can go to. Special thanks to my roommates from "Roosevelt Manor": Robyn Jong and Emma Carroll (and to honorary guest Eric Greene). Thank you all for your gentle positivity, and sharing delicious food! It was a joy to live with you both. I also thank Dominic Castanzo, whose humor and heart-to-heart conversations were a godsend in

grad school. Thanks Dom also for being an awesome roommate in “Chateaux Dwight”! I especially cherished my time with Rose Hill and Rory McCallion during many game nights—it was the best to look forward to seeing you at the end of the week. I also thank the frequent flyers of our Movie Night group: Tim Turkalo, Lydia Lutes, Dan Kramer, George Otto, Franziska Lorbeer, John Blair, Shally Margolis, Kelsey Hennick, and Ellen Cushing. I also thank Djem Kissiov and Natalie Wolf for our wonderful times getting coffee and smoothies during breaks at work.

In grad school, I did a lot of science outreach with Dom Castanzo and Dan Kramer, primarily at elementary schools. Thank you both so much for embarking on our outreach initiative together! I learned so much by working together. Dan, when you commit to something, it is awe-inspiring because 100% of you is all-in. I love that you put your best effort in every task, especially the ones that have no bearing on your future success—a true testament to your character. Thanks for inspiring me to do the same! Dom, your creativity in lesson design was superb, and chemistry knowledge sublime. I wish we had more shared lessons together. Thanks to Alyssa Bormann for her outstanding dedication to science outreach and education in general—it was a blast working with you. I thank the other student volunteers we worked with: Franziska Lorbeer, Graham Woolley, Rebecca Bartke, and Daniel Saxton. Many thanks to Crystal Nie, who helped us get started at Madera Elementary School. Crystal, thank you also for your enthusiasm and passion to get more science everywhere! Many more thanks to the teachers and staff at Madera, Sheldon, and Sankofa Elementary schools for opening their doors to our science.

Another extracurricular activity I participated in graduate school was the new inclusive MCB+, or iMCB+, initiative aimed at advocating for and supporting underrepresented first-year graduate students entering the Berkeley MCB graduate program. iMCB was started by Dr. Lisa Eshun-Wilson when she was a graduate student and co-founded by Dr. Susan Marqusee. iMCB is now co-directed by Michelle Soto Reid and Dr. David Weisblat. I deeply thank these individuals for not only recognizing that underrepresented MCB students were facing additional challenges in graduate school, but also deciding to do something about it. iMCB sought to explore actionable ways to improve support for underrepresented first-year graduate students by starting a research group. I joined the iMCB research group in hopes of learning how to increase diversity, equity, and inclusion in the current and future departments that I will be a part of. The iMCB research group became an awesome think tank where we built on each other’s personal and literature research insights to make improvements to the iMCB framework that will hopefully achieve our goal in increasing support for underrepresented students. I am so thankful to be a part of this group with Sophia Friesen, Sonali Mali, Danielle Spitzer, Maia Reyes, Amanda González-Segarra, and Anthony Rodriguez-Vargas, Michelle Soto Reid, and Lisa Eshun-Wilson—thanks to all of you for your boundless creativity, fierce passion, and visions for a better future.

I want to thank a variety of support staff that I relied heavily on during my work. My data literally would not be here if it weren’t for these amazing individuals! I thank the MCB Graduate Affairs Office for their hard work in recruiting students, managing student milestones, and orchestrating payroll. In particular I thank Sara Bottger, Sarah Hamilton, Hannah Bloom, Carlos Garcia, Berta Parra, Mark Jenkinson, and Eric Buhlis. GAO staff has always patiently answered my questions throughout grad school. I

sincerely thank Hector Nolla and Alma Valeros for helping with my flow cytometry and sorting experiments. I especially thank Hector for his continuous flexibility and grace, especially at the height of sorter traffic; if it weren't for Hector, it would not have been possible to schedule my experiments. I thank Hector and Alma for providing assistance even when self-sorting! I sincerely thank the UC Berkeley Cancer Research Lab Molecular Imaging Center: Holly Aaron, Feather Ives, and Jen-Yi Lee. Holly and Jen helped train me on the light sheet microscope after it had arrived, as well as several other instruments on campus. Holly went above and beyond to include me in professional development activities (such as conferences, courses, and an analysis software bootcamp). Thank you, Holly! Feather, thank you for continually helping me at the scope with patience and humor (remember the time I couldn't find the power button?), as well as insight to my histology experiments. I'm so glad you joined the MIC! Holly, Feather, and Jen—you three will forever remain my microscopy muses; I am going to miss you all very much. I also thank Justin Choi and Ariane Baudhuin of the Ngai Lab and the Functional Genomics Laboratory. Justin's work was essential in preparation of single-cell libraries and was my go-to source for sequencing information. Thank you Justin for the fantastic work, and being patient on days where I didn't get any cells back. Thanks also to the QB3-Berkeley Genomics core and Dr. Eric Chow at the UCSF Center for Advanced Technology for sequencing my libraries. I especially thank Dr. Derek Pappas that went above and beyond in helping me get to the bottom of various sequencing related issues. Many thanks to Ariane, who gave me access and training to the cryostat. I sincerely thank the OLAC veterinarians, technicians, and other staff members overseeing the ethical care and use of mice—their work is extremely demanding, and they are the superstars of biomedical research. I thank also individuals from Research IT at UC Berkeley that helped me many times work with the cluster computing resources. I extend special thanks to Erik Newman and Rickey Victoriano, who frequently went above and beyond to provide excellent care for our mice. I also want to express gratitude to the various custodial staff, security, and building management in LSA and LKS to ensure we have safe and clean workspaces. In particular, I thank Mike and Alfredo for conversations that brightened my day.

I also thank my therapist, Jeff. Graduate school is a super tough journey. I've always been prone to anxiety, but grad school seemed to magnify that a lot. I benefited tremendously from the Counseling and Psychological Services at the Tang health center. I deeply thank Jeff of for teaching me how to manage my anxiety. Jeff, my life felt so much better after therapy with you. Thank you for teaching me these essential tools!

I want to deeply thank the individuals who contributed to the funding that supported my work. I was supported with an NIH T32 training grant, which is funded by taxpayer money. I was also supported with the UC Berkeley Chancellor's fellowship, Elizabeth Roboz-Einstein fellowship, and UC Dissertation-Year fellowship. I sincerely thank the taxpayers and donors behind my funding.

Many friends have rallied to support me every step of the way. I owe them so much! I want to first thank the friends outside of the science bubble that were still kind and patient enough to maintain their friendship with me, despite my dis-engagement with social media, slow response times to messages, and my unpredictable schedule: Alexis Recto, Patsy Nelson, Paola Pereyra, Laline Wang, Minh Tran, Michael Flagg,

Blake Hamby, and Yujie He. Even though we are far apart, it felt like no time had passed when we would visit each other. When I would see them again, I felt like how I imagine sailors feel after seeing land after being on sea for a long time. I will address them directly below.

Alexis, thanks for being there for me, ever since we met in the 5th grade! I'm just amazed, feeling so lucky that we've been friends for over seventeen years. You're just an incredible light and joy in this world. Every time I even think of you, I smile! Especially while remembering when you surprised me for my 27th birthday. That is one of my favorite highlights from my time in grad school. I'm glad we shared a period of time together when we were both in a grad program. Even though are subjects are really different, it was comforting to have a lifelong friend who understood what being a grad student was like. I'm so happy that you visited me multiple times while I was in school. Thanks so much for being a shoulder to lean on. I'm so proud of your accomplishments!

Patsy and Paola, I've known you both almost as long as I have known Alexis. I'm so glad I got to know you during the most awkward years of my life: middle school. I remember weekend and summer days reading at Border's bookstore super fondly; I catch myself wishing that I could re-live another one of those days. Patsy, I'm so happy and proud that you found your calling in the care of special needs' children. Paola, I'm also happy and proud of you—I have another lab sister! Thank you both for being my friends for so long. I also want to thank both of your families. Kim and Nick Nelson, thank you for always hosting me in your home, and for all of the laughter we had together! I miss you so much, Nick. I also thank Paola's family for their hospitality and encouragement: her brother Chris, and parents Jenny and Iver. Though we've all been a part so long, it's amazing that we come together as if no time passed at all. I look forward to future visits together.

I thank you, Laline, for your dear letters that you wrote to me while I was in school; I saved every single one. I apologize for not returning them promptly! I also thank you and your mom Ruby for visiting me during my first year. Laline, I admire your boundless creativity in all of your projects. Your imagination has always inspired me to try to think differently, and find ways to explore and channel my own creativity. I'm excited about your new life beginning with James! I hope that we can connect together really soon.

Thank you, Minh, for being one of the first friends I made after moving to Tucson! Not only that, thanks for continuing to be my friend despite my slow responsiveness to your messages. I appreciate you so much for taking time to hang out with me when I'm in town, and connecting with me over our shared interest in video games and yoga. When you came to the bay area with the rest of our high school crew, it was so much fun; I won't forget the time we collaborated to avoid the zombie in our escape room. Thanks for that great visit.

Michael, I'm so glad I met you at the piano in the summer of 2010. I didn't know then how impactful on my life you'd be! We shared so many adventures and life experiences. Whenever I have a funny story to tell, nine times out of ten you were involved. I'm over the moon that you met Blake, because our paths were otherwise unlikely to cross….Michael and Blake, you're that "spice of life" where everything becomes so much more fun and enjoyable simply because you're there. Thank you for

being my oasis. Spending time with you both while in graduate school was truly restorative, and now that I'm done, I look forward to taking the many fun trips together that we have imagined for a long while now.

Yujie, thank you for being one of my dearest friends, and for sharing your soulful wisdom—it has centered me time and time again. I count my lucky stars that we happened to live across from each other in the dorms during our freshman year. When you, Steve, Michael, and Blake visited me in the bay area, it was one of the best times that I fondly look back on. I'll never forget when you told me that you and Steve were pregnant with Irma. Getting to know her after she was born has been one of the greatest personal joys of the past year and a half. I thank you so much for naming me Irma's *kai-ma*, and for generally including me in your new family. I also thank you and Steve for not only hosting me when I'm in town, but also for taking a genuine interest in my lab work. Yujie, thank you for so much happiness.

Lydia, I'm most grateful to not only have had you as a close friend in college, but for all of grad school as well. My greatest sadness is that we won't be across the hall from each other. We won't be able to have another "workover" at each other's benches, or another happy hour at the Pacific Standard Taproom before we graduate. But, I know that our bond is ionic! It will survive any distance. Lydia, thank you so much for being a constant reservoir of strength and encouragement for me. When I started grad school, I didn't know that our friendship would be my greatest advantage in navigating science and normal life difficulties. We're like Sam and Frodo (and, I'm determined for us to become Grace and Frankie!). A favorite uncle of ours once said, "While it is always best to believe in oneself, a little help from others can be a great blessing." Thank you for being that blessing for me. Even more importantly, thanks for letting me use your Netflix account. Shout out to Lydia's family—it was wonderful to get to know you when you all have visited. Not only did they raise a person that I wish the world had more of, they helped me out a lot. I have special thanks for Todd, Susan, Oakley, and Karen who have graciously helped me move alongside Lydia to Berkeley from Tucson. Thank you all so much—it would have been a lot harder for me to make it on my own. Todd also paid for Lydia's Netflix account (thank you Todd!). I also have special gratitude for Elaine Drees, who made very nice matching masks for Lydia and I during the SARS-CoV-2 pandemic—thank you Elaine!

I've been so lucky to have a wonderful and supportive family. I thank my dad, Paul Nichols, for always working so hard throughout my life to provide for our family. I've never seen him take a vacation until after we were grown (and, one of those breaks was due to a global pandemic!). I will always cherish our time together in Seattle after my post-doc interview, and when we flew to Wales to see Bri. Now that I will be moving to Seattle, I hope that we will get to spend more time together there in the future. Josh, you're my favorite brother (even though you're my only brother). I'm thrilled that our next chapters are bringing us up north—more adventures await us! Thank you so for bringing me so much smiles and laughter (both in person, and virtually over social media). I also thank my lovely sisters, Bri and Amberlin, for coming together in stressful times. Bri completed her Ph.D. program from Bangor University in Wales, and I could not be more proud. Our grad school journeys had several parallels, and it was always wonderful to talk to her about it. Bri, thanks so much for being there—you even managed to be the only family member to visit me, despite being the one furthest away! Thank you so very

much. I'm comforted that, despite the distance between us, we've managed to see each other in person quite a few times in recent years. I plan to be the one going to see *you* more often in the future. I had the best time in Wales to celebrate your graduation, and I intend to go back soon. Amberlin, thank you for hosting me and Tim often when we were in town—we had so much fun at Aunt Cheryl's wedding, and it's been an absolute joy spending more time with you, Laila, Hailey, and Matt. I love you all so much. I also thank my aunt Cheryl, Uncle Mark, and cousin Johnnie for all of the fun along the way. Visiting for Thanksgiving and summer barbeques were wonderful respites toward the end and after a stressful semester. I love you all.

Our family suffered tremendous losses. My young cousin Mark passed away in March 2020; he was taken far too soon and we miss him dearly. My dear Grandma Doris Nichols passed in November 2019, and my beloved Grandma Robin Huckins in November 2019. I thank my Grandma Dee for encouraging a positive attitude to school, and for supporting me financially at times (such as when I needed a mattress and a co-signer for a line of credit). I thank my Grandma Robin for teaching me the important lesson to love and appreciate life. I will always remember her contagious laughter! I desperately love and miss these individuals so much; I'm grateful to them for the light and love they had given me in my life.

I want to especially thank my Uncle Mike. Most of us in science recall interests in science beginning in childhood—Uncle Mike was that gateway for me. I credit him for my interest in science and the natural world. Growing up (it being the 90's), he'd share his Ranger Rick magazines and collectible wildlife cards with me. I was fascinated with learning about nature, and Uncle Mike taught me a lot about animals and the outdoors. Importantly, he always went out of his way to spend quality time with me. He's also one of the few people who have taken genuine interest in what I've been up to in school, and even remembering names of cells and proteins I've been interested in. Thank you, Uncle Mike—I don't know if you're aware, but you've had a huge impact on me. I love you so much.

I want to give a special thanks to my stepfather, Rick Cordova. In late 2017, the GOP proposed a tax plan that would make graduate student tuition wavers count as taxable income. These tuition waivers effectively functioned as coupons since we taught for the university, and these were dollars that never reached our pockets. This tax reform would have devastated everyone's finances, at particular detriment to non-traditional students. Needing to pay four times as much in taxes would have threatened my and others' ability to stay in the program. Without any hesitation, Rick started to think of solutions to financially help me out so that I would be able to finish my program. Luckily, this aspect of the tax plan did not come to fruition. Rick, I will never forget that kindness. To me, it was more than just the offer to help—it was the demonstration that you counted me as your kid. I'm lucky to have you as a parent. Thank you so much for your love and support!

As this chapter in my life closes, I am most happy and grateful that I get to open another with Tim Turkalo (and our cat Charlie!). Tim, when I met you for the second time outside of the BART station, something inside of me knew that you were going to be really special. Each day after that only confirmed the feeling. Thank you so much for being by my side—you were always a source of consistent love, comfort, and support; I really hope that I've been the same for you. You're my safe harbor. I've relied so much

on your steadfastness to feel grounded (I've also relied a lot on your excellent cooking to survive). No matter where we go, I know that I'll feel at home with you. I love you so much, and I eagerly look forward to our future together (especially, our future with Charlie). Adopting Charlie has been our best moment together, and it's super hard to imagine our life without him. I thank Charlie for not only bringing Tim and I closer together, but for adding so much excitement and love to our life. I also have a lot of gratitude toward Tim's family for including me so openly, and for thinking of me as family (as I do for them). It almost feels like I've known you all for much longer than I actually do! Thank you so much Taylor, Aaron, Katie, Drew, Joanie, and Mike (and Janie and Mack!). I really appreciated all of your support for both of us, especially during the home stretch. I love you all.

My mother Christina Cordova, to whom this dissertation is dedicated, has remained my strongest supporter of all. Her colossal personal sacrifices made everything possible for me. She has worked so hard to provide for our family, even to her own detriment, to make sure my brother and I were well taken care of. I struggle to adequately convey her impact and meaning to me, but I think her greatest lesson was to "make sure I get my own" first—meaning, don't sacrifice your own goals for others. Fiercely pursue them, and don't be afraid while doing so. Her greatest gift was that she always believed that I could successfully accomplish my goals. I didn't know how beautiful that was to have someone believe in you so completely that you didn't have to always rely on yourself. I know that I wouldn't have been brave enough to start college and graduate school if it wasn't for my mom. Her confidence in me was a bit like wearing invisible armor: I was immune to doubt from others and myself. Admittedly, grad school shook me several times. When that happened, a phone call with my mom helped to center me again. I found peace and love in her wisdom. She was always found a way to distill down my problems and share a time when she felt the same way or experienced a similar situation. Often, we were able to laugh about it. In the end, she was right—I was able to accomplish my goal of finishing my Ph.D. program. The more people I get to know, the more I see how rare it is for someone to have a person like my mom in their lives. I love you so much mom. Thank you for everything.

Chapter 1

Introduction

1.1 Microglia as the brain-resident immune cell: roles in health and disease.

For decades, the brain was believed to be "immune privileged"—one of few organs invisible to the vast network of cells armed to respond to injury and infection[1]. This notion has prevailed for many years, despite the discovery of an immune cell within the brain over a century ago termed "microglia." Microglia are the resident immune cells of the central nervous system, also known as the CNS's tissue-resident macrophage cell due to the similar origins and functions to peripheral macrophages[2-5]. Indeed, microglia express the same equipment as peripheral macrophages. These include the classic Toll-like receptors (TLRs) and other pattern recognition receptors (PRRs) like inflammasome proteins[3,6]. Thus, microglia have the capacity to mount and sustain an immune response upon recognition of damage-associated molecular patterns (DAMPs) and pathogen-associated molecular patterns (PAMPs). Despite this, T cell infiltration is notably restricted during homeostasis, and dendritic cells around the CNS suppress T cell activation[7,8]. These data suggest quiescence mechanisms within the CNS. Therefore, the degree of the immune privileged state of the CNS is being questioned and reconsidered[1,8,9].

But, microglial roles extend beyond immunity[10,11]. Microglia are present from the earliest stages of brain formation and are required for normal brain development (discussed in detail within section 1.2 of this chapter). In adulthood, microglia persist throughout the brain where they occupy 5-20% of brain cells dependent on the region[2,12,13]. Microglia adopt tiled non-overlapping arrays of cell bodies and highly motile cell processes[14,15] that screen synapses within their territory. Via these processes, microglia are thought to monitor neural function and support homeostasis through the action of neuromodulatory and neurohormone receptors[11,16]. Altogether, microglia are dynamic cellular sensors that integrate changes in the environment to produce a response. These dynamic functions can be summarized as "butler" and "security guard" roles that maintain tissue homeostasis and surveillance.

Increasing attention has been drawn to microglia and brain disease because decades of research into the neural origins of brain pathologies have yielded unsatisfactory progress in finding novel intervention strategies. Excellent strides in cancer immunotherapy, which have provided cures for subsets of cancer patients—have bolstered the efforts in exploring the immune origins of brain disease[17-20]. As with brain disease, cancer was once thought to not involve immune responses. Therefore, studying microglial immunity in the context of brain disease has been a hot area of research for the last decade, in which most of these studies have focused on models of neurodegenerative disease. I will discuss key studies that highlight the microglial roles in brain homeostasis and in brain disease (i.e., Alzheimer's disease). This introduction to microglia biology in health and disease is not exhaustive of the literature. I direct the reader to a number of excellent reviews that have guided much of this writing[2,10,11,14,15,21].

First, I will discuss the known microglial roles in brain homeostasis in adulthood. Microglial processes are highly motile and make numerous physical contacts with neural soma, axons, and dendritic synapses of which some are transient and some of which are terminal[14,15]. *Wake et al.* in 2009 found microglial contact with pre-synaptic boutons and post-synaptic spines[14,15]. Contact persisted longer following ischemia;

about a quarter of contacted boutons were lost[14]. Microglial arms seem to prefer contacting smaller spines, and these are three times more likely to be eliminated within two days than non-contacted ones[15]. In a sensory deprivation model, microglia preferred to contact larger spines that ultimately reduced in size[22-24]. *Tremblay et al.* found that microglial contact of spines differed in an experience-dependent manner that contributed to synapse elimination[15,25]. These data collectively suggest that microglia impact neural synapse stability.

Microglial purinergic signaling through the purinergic receptor P2Y12 (P2Y12R), and neural N-methyl-D-aspartate receptor (NMDAR) signaling, is thought to mediate much of microglial process motility and physical contact with neurons[15,26]. Neural NMDR activation initiated microglial process outgrowth radially and increased contact[15,27,28]. Focal outgrowth occurred after global glutamatergic activation[15,29]. Knocking out P2Y12R abolished these phenomena and exacerbated seizure intensity in a kainic acid induced seizure model[15,27,28]. P2Y12R signaling in microglia is also important for sensing tissue injury and may be the primary regulatory mechanism[26,30]. After laser injury, microglial processes rapidly converged to the focal lesion[31,32], and *ex vivo* studies have shown that ATP-mediated purinergic receptor activation is sufficient to induce chemotaxis[26,33,34]. Microglial motility may also be impacted during long term potentiation[35] (LTP; thought to be the cellular basis for neural plasticity regarding learning and memory[36]) and long term depression[37] (LTD; cellular basis for weakening synapse strength[38]). These data suggest possible roles of microglia participating in the regulation of synaptic plasticity. Between P8 and P10 days after birth, microglial deletion was correlated with a decrease in spine densities and reduced functional synapses within the cortex[39] suggesting that microglia promote proper synaptogenesis. Indeed, microglia were found to promote learning-dependent synaptogenesis in a brain derived neurotrophic factor (BDNF)-dependent manner[15,40].

Synapse elimination and refinement are a critical part of normal brain development, because many more synapses are made than ultimately used. Weak or inactive synapses are thought to be removed using cell-intrinsic and cell-extrinsic methods. Since microglia are acknowledged as highly phagocytic cells, exploration of the putative microglial roles in synapse refinement began in earnest after 2005. Synaptic material was found in the microglia within the developing hippocampus, and mice lacking CX3CR1 had increased numbers of immature synapses[41]. Intriguingly, the innate immune complement compounds have roles in synapse engulfment by microglia. Hints about the involvement of complement came from the fact that C1q is upregulated in postnatal neurons[42], and C1q-deficient mice lack efficient synaptic refinement[42]. In contrast, microglia express the complement C3 receptors (C3R)[43]. Genetic ablation of C3 or C3R reduced microglial pre-synaptic phagocytosis and increased synapse density[42-44].

In support of the previously discussed studies that suggest microglial involvement in synaptogenesis, remodeling, plasticity, and elimination, a number of behavioral alterations were noted in mice where microglial functions were disrupted and/or following transient depletions. *Cx3cr1*-deficient mice exhibit impaired behaviors[11]. These include sociability, grooming, LTP, and learning-dependent memory defects[11,45,46]. Transient deletion of microglia also impacted behavior. Transient depletion of microglia with a conditional tamoxifen-inducible diphtheria toxin caused

behavioral deficits in learning and memory[11,40]. Depleting locally hippocampal microglia with clodronate impaired learning and social interaction tasks, while using a CSF1R inhibitor transiently impaired spatial learning[11,47]. These defects were resolved after microglial re-population[11,47]. Taken altogether, microglia in normal brain homeostasis impact normal behaviors presumably through active synapse maintenance.

Microglial functions are often involved in brain disease[11]. Whether or not disrupted microglial functions are causative, or secondary to changes in other brain cells, is unknown and a frequent subject in a flourishing area of investigation. Here, I will discuss a few case examples in the context of neurodegeneration, primarily Alzheimer's disease (AD). I direct the reader to a number of excellent reviews that consider microglial immunity in other brain disease contexts, like multiple sclerosis[48], Parkinson's disease[49], retinal degeneration[50], and amyotrophic lateral sclerosis[51].

AD is likely the most thoroughly studied brain disease in relation to the microglia-mediated immune response[52-55]. AD is a primarily neurological disease, with onset generally later in life characterized by symptoms of memory loss and impaired cognition[54]. The mainstream hypothesis for AD etiology is the amyloid beta (Aβ) hypothesis that has dominated for over twenty-five years[56]. In this model, Aβ in healthy individuals is made from amyloid precursor protein (APP)[56]. APP is cleaved precursor protein by β- and γ-secretase, and Aβ is released outside of the cell to be rapidly degraded[57]. However, this process becomes pathological when the metabolic activity to control extracellular Aβ is diminished and Aβ begins to accumulate and deposit[56]. Amyloid fibrils begin to form, which progress into plaques[56]. This, in turn, causes neurotoxicity from the formation of intracellular tau neurofibrillary tangles[56]. Ultimately, loss of synapses and neuronal death occurs and this constitutes the neurodegenerative aspects of AD[56]. While there are several problems with the Aβ hypothesis[58,59] (which will not be discussed here), microglia are seen as essential components to the Aβ model[60] due to several compelling pieces of data. A review by *Wang and Colonna* has guided much of this present discussion, which is not exhaustive of the literature[54].

A lot of genetic evidence implicated in non-familial sporadic AD has suggested that microglia dysfunction may contribute to the onset and progression of neurodegeneration. For example, the immune and microglia module was identified as having the greatest number of neuropathology traits compared to others, and several immune-related genes were identified as novel risk factors in other studies[61,62]. Upon investigation, Aβ plaques rapidly recruit microglia, and microglia were found to remove Aβ peptides[54,63]. When microglia are pharmacologically depleted using a diphtheria toxin model, Aβ plaques did not decrease, but their size increased until microglia returned, suggesting that microglia restrict the expansion of Aβ plaques[54,64]. Microglia also release enzymes to aid in Aβ clearance; these include insulin degrading enzyme, matrix metalloproteinases, and plasminogen[54,65]. A key microglial receptor, TREM2, is thought to mediate Aβ uptake because TREM2-deficient mice had excessive Aβ deposition and dystrophic neurites around the plaques[54,66]. Also, TREM2 haploinsufficiency and total deficiency on the APP/PS1-21 and 5XFAD AD mouse model backgrounds prevented microglial proliferation and clustering around Aβ plaques[54,67-69]. Thus, in the early stages, microglial reduction of Aβ via TREM2 is beneficial. However, at some point, Aβ accumulation becomes a DAMP signal and initiates a pro-inflammatory and neurotoxic programming in microglia by activation of the

NLRP3 inflammasome[54] (as discussed in greater length in Chapter 2 sections 2.2 and 2.3). As an outcome of inflammasome sensing, a lytic cell death termed pyroptosis occurs, with release of neurotoxic pro-inflammatory cytokines and ASC specks[6,70]; ASC specks in turn nucleate additional Aβ deposition[54,71]. Additionally, *Joshi et al.* delineated another mechanism: reactive microglia can secrete extracellular vesicles that promote the conversion of insoluble Aβ fibrils into a soluble Aβ species considered to be more neurotoxic[54,72]. Thus, a vicious cycle is propagated in this fashion. Multiple therapeutic trials are underway to see how the beneficial aspects of microglial functions can be harnessed in the prevention and/or treatment of AD.

In conclusion, microglia cells in the brain perform vital functions in the maintenance of brain homeostasis and contribute meaningfully to brain pathology, as exemplified by the multitude of AD studies. Modulating microglial functions may therefore offer novel intervention strategies for brain disease. In contrast, microglial roles in fetal brain development have less mechanistic clarity. Next, I discuss what is known about the microglial contribution to brain formation.

1.2 Microglia and fetal brain development.

The role of microglia during brain formation (and in context of neurodevelopmental disorders) is relatively unexplored in comparison to the plethora of adult brain studies. Understanding microglia-mediated immunity in brain formation may offer insight to how neurodevelopmental disorders develop. In the process, we may learn how fetal brain immunity shapes neural circuits. The rationale to study this topic comes from the compelling observations that mice and humans lacking microglia in development have striking anatomical brain defects that may contribute to an early death[73-76]. The mouse model is the colony-stimulating factor 1 receptor (CSF1R) knockout mouse[76]. CSF1R is required for sensing colony-stimulating factor 1 (CSF) and interleukin 34 (IL-34), which promote the survival, recruitment, proliferation, and migration of mononuclear phagocytes in development (which include microglia and monocytes) [77-79]. Mice without CSF1R (on a C57BL/6 background) have general drastic structural tissue anomalies and rarely survive past weaning[76,80]. Within the brains of *Csf1r*$^{-/-}$ mice, there are enlarged ventricles and compressed parenchyma[74]. Strikingly, a human case was discovered in which two mutations in the *Csf1r* gene caused two dysfunctional copies of the CSF1R[75]. Unfortunately, this human patient had overt brain abnormalities (such as agenesis of the corpus callosum and tiny cerebellum), and died at a young age[75].

Therefore, microglia are essential in orchestrating normal brain development. It is hypothesized that embryonic microglia do so by secretion of trophic brain factors that support the proliferation of neural precursor cells (NPCs), clearance of dead or dying NPCs, and/or promote normal levels of neural apoptosis in a cell-extrinsic manner[81]. Thus, changes in specific microglial functions during brain development may translate to specific neural changes, of which may not gross structural abnormalities, but could cause symptomatic behavioral abnormalities. I will discuss what is known about prenatal microglial development framed by classic concepts in neuronal development.

Microglia descend from the first wave of C-KIT^{+}/CD41^{+} erythomyeloid progenitor cells (EMPs) from the yolk sac island in early embryogenesis[11,82]. These EMPs migrate

seed the embryonic brain at day 9.5 (E9.5) to become microglia. Microglia do not require the transcription factor *Myb* as hematopoietic stem cells (HSCs) do, but microglia depend on the transcription factor *Pu.1* instead[83]. Thus, they are distinct from HSCs[83]. There are two major cellular phenotypes from E10.5 onward in the brain, with differing ratios over time: amoeboid shaped cells and ramified cells[84]. Amoeboid cells in development are thought to be actively migrating cells[84] (however, in the adult brain, amoeboid microglia are thought to be in a responsive "activated" cell state[10,85]). Meanwhile, ramified microglial cells are characterized by a smaller central cell body and multiple extended cell arms or processes that sample the local environment[3,10,32]. Thus, ramified cells are considered to be resting cells with minimal movement aside from the radial projections of the central cell body. At E12.5, the vast majority of microglial cells are amoeboid shaped until E15.5 and later[84].

It is proposed that EMPs utilize the developing vasculature, such as the vitelline vein, to traffic to their destination organs[86]. The main evidence supporting this comes from Na^+/Ca^{2+} exchanger-1 deficient mice (*Ncx-1*$^{-/-}$) that lack a heartbeat and blood circulation[87]. *Ncx-1*$^{-/-}$ mice did not have microglial cells in the brain rudiment at E10.5[82]. However, there are inconsistencies in this model. The CNS derives from the ectoderm germ cell layer, which does not contain vascular progenitor cells[88]. Thus, mesoderm-derived angioblasts, the vascular progenitor cells, need to invade the brain[88]. They first seed the outer neural tube and form a mesh-like network termed the perineural vascular plexus (PNVP) by day E8.5 above the cortical plate[88,89]. Vascular sprouts descend from the PNVP and infiltrate the developing brain parenchyma toward the ventricular zone (VZ) at E9.5[88,89]. Thus, if microglial cell progenitors were indeed traveling by developing vasculature, they should populate the cortical plate before reaching the VZ. By extension, microglial cells would have decreased accessibility to developing neural cells at the VZ and therefore have limited impact on NPC development. Yet, several accounts describe the opposite: microglial cells populate the ventricles and VZ as early as E10.5[84] and closely associate with neural progenitors and apoptotic cells[84,90-92] where microglia begin to orchestrate neural outgrowth[91]. Putative microglial precursors, marked by *Cx3cr1*-GFP signal, appear as free-floating cells in the ventricles or attached to the ventricle walls, seemingly poised to enter the brain parenchyma[84,93-95]. Moreover, microglial invasion to the cortical plate doesn't begin until E16.5, and this is thought to proceed in an "inside-out" manner using radial glial cells as guideposts[84,96]. Indeed, in support of this idea, microglia were found to be necessary for proper dopaminergic axons in the forebrain and neocortical interneuron lamination[96]. Other reports in human fetal brain found evidence for three routes of entry: meninges, choroid plexus, and ventricles[94,95,97]. A couple reviews largely accept that microglial progenitors deriving from the yolk sac invade the brain using vasculature[98,99], while others cite alternative routes of entry[97,100], perhaps dependent on region and timing[100,101]. Ultimately, it is highly likely that microglial precursor cells utilize multiple routes of invasion into the brain, which may or may not reflect two microglial ontogenies. Indeed, only a third of adult microglia were marked in fate-mapping studies at E7-E7.5[82], suggesting contributions from a non-yolk sac source. In support of this idea, homeobox B8 (*Hoxb8*) positive and negative microglia were discovered in the murine brain[102,103]. *Hoxb8*$^-$ microglial cells were the majority of adult microglia, likely coming from the yolk sac, while *Hoxb*$^+$ microglia may come from the fetal liver[102,103]. Future studies using lineage-

tracing tools are required to clarify the possible differing ontogenies and migratory routes utilized by microglial precursor cells to infiltrate the brain over time.

Microglial development follows a stepwise program[104]. Data from population-level from embryonic and adult brains via chromatin immunoprecipitation sequencing (ChIP-seq), assay for transposase-accessible chromatin using sequencing (ATAC-seq), and RNA-seq highlighted three distinct stages: early, pre-, and adult-microglial stages[104]. Early microglia is characterized as E10.5-13.5, pre-microglia from E14.5 to a few weeks after birth, and adult microglia as a few weeks after birth onward[104]. Intriguingly, the yolk sac and early microglia transcriptional profiles shared a high concordance over time despite disparate regions, suggesting either microglial precursors don't immediately adapt after entry to the brain, or that aspects of microglial development are pre-determined before brain entry[104]. Early microglia had high expression of genes involved with cell differentiation and cell cycling[104]—consistent with the idea of prenatal expansion. Early microglia also expressed genes associated with neural migration, neurogenesis, and cytokine secretion[104]; this supports the idea that microglia shape brain formation by orchestrating aspects of NPC development[11,101]. Genes associated with neural development peaked a few days before birth[104], consistent with the flourishing of neurogenesis and migration. After the brain matures, the gene expression profiles of adult microglia adopt more of a surveillance and homeostasis state, and express classic known microglial genes such as *Fcrls* and *Sall1*[104]. The timing is consistent with the idea that microglial development is completed about two weeks after birth, in which 95% of microglia have settled in their final adult brain niche[5,82].

Matcovitch-Natan and colleagues found four major chromatin states: enhancers that are only open in the yolk sac, enhancers open in the early- and pre-microglia (but not adult), adult microglial enhancers that are open (i.e., *Sal1* and *MafB*) and adult microglial enhancers that are closed (i.e., *Irf8*)[104]. Intriguingly, the pre-microglia stage does not seem to undergo unique chromatin remodeling because there was nothing unique about remodeling in this stage; this suggests different usage of the epigenetic landscape in early microglial development[104]. Certain open enhancers defined some stages over others. For the yolk sac stage, *Ctsb* and *Ifit3* have high ATAC signal intensity[104]. For the adult microglia stage, *Fcrls* and *MafB* have high ATAC signal intensity[104]. Collectively, the data identify two key transitions in development: from early microglia to pre-microglia around E13.5-E14.5, and pre-microglia to adult microglia a few weeks after birth, around weaning. These data may be consistent with observations in fetal brain development of microglial morphologies. There is a drastic switch in ratios from mostly amoeboid microglia to mostly ramified microglia at E15.5[84]. Thus, it stands to reason that any alterations to microglial functions before E15.5 and after E15.5 may likely produce different effects on the brain.

A prominent single-cell RNA sequencing (scRNA-seq) study by *Hammond et al.* characterized the transcriptional heterogeneity of microglia throughout the mouse lifespan[105]. They found that microglia are most transcriptionally diverse in the developing, aged, and injured brain[105]. Embryonic microglia also separate out from other lifespan stages[105-107]. Thus, we can infer that, during homeostasis in non-development contexts, microglia are fairly homogenous with similar homeostasis and surveillance programs. It isn't until aging or pathogenic contexts that this programming is disrupted[105]. In support of this, a scRNA-seq study from *Qingyun et al.* found only

limited transcriptional heterogeneity of microglia in adulthood irrespective of brain region[107]. Observations from *Hammond et al.* suggest that microglial cells in development are most diverse when they are differentiating, which matches well with the early- and pre-microglial stages identified by *Matcovitch-Natan et al.*[104]. However, additional scRNA-seq studies and a fate map study identify a surprisingly large contribution of border-associated macrophages (BAMs) to the myeloid cell fraction[108,109] in development that was previously identified as microglial[105]. Thus, the perceived developmental heterogeneity of microglia may actually be less due to the contributions of BAM populations.

To summarize, microglia come from yolk sac island progenitor cells and depend on CSF1R signaling to traffic to the developing brain[78,79]. Microglial precursors arrive to the brain rudiment at E9.5[82]. Microglia alter chromatin, epigenetic, and transcriptional profiles throughout their developmental programming, defining three key stages: E10.5-E13.5 early microglia, E14.5-P9 pre-microglia, and mature microglia after weaning[104]. Microglial cells collectively appear more transcriptionally diverse in development, but otherwise this diversity resolves over the lifespan to become general homeostasis and surveillance programs (except during aging and pathological conditions)[105]. Microglial morphology in the developing brain switches from mostly amoeboid to mostly ramified by E15.5[84]. The contribution of BAMs should not be ignored in the fetal brain, as they are a sizeable portion of the brain $Cd45^{+}Cd11b^{+}$ myeloid cell fraction[109].

Milestones in microglial development overlap with neural cell development milestones. Neurogenesis from radial glial cells begins at E12.5, when microglia are present in a mostly amoeboid cell state[84]. By E14.5, approximately all of the brain's requisite neural subtypes have been generated, and neural cells begin to migrate[110]—a time when microglia are about to enter a key transition point in their programming[104]. At the same time, asymmetric division of immature neurons begins to generate oligodendrocytes and astrocytes[100,101,111]; these also integrate into developing circuits. By E16.5 through E18.5, the cellular basis of circuits is largely settled; early synaptogenesis events begin[111]. Microglia have since passed a key developmental switch after E14.5-E15.5[104], and are mostly in a ramified state[84]. This suggests that microglia are at the right place and time to begin surveying synapses. From birth until three weeks of age, neural circuits undergo a critical period of synaptogenesis followed by pruning[100,111]; after, microglia are in a mature state[104]. Unnecessary synaptic connections are removed (by cell-intrinsic mechanisms[112]) and also in a microglia- and complement-dependent manner[44]) while other synapses are strengthened[112]. By postnatal day 20 (P20), brain development is considered largely complete in mouse[100]. Microglia are self-renewing cells with very limited contribution from the periphery at steady-state[113-117]. Neurons are largely post-mitotic, save for the adult neurogenesis in the sub-ventricular zone (SVZ)[118].

Because milestones in microglial and neural cell development overlap, lack of fetal microglia causes drastic brain abnormalities in mouse and humans, fetal microglia localize near NPCs, and microglial immunity is involved in normal brain homeostasis in adulthood, my guiding hypothesis is that disrupting microglial immunity during brain formation negatively affects neural development and is an upstream mechanism in the formation of aberrant circuitry underlying neurodevelopmental disorders. Indeed, there are a few case examples already of alterations to microglial functions in development

that affect the neural compartment, causing behavioral changes and/or disease in adulthood. For example, a single somatic mutation in the BRAF gene (V600E) induced in mouse EMPs causes a severe neurodegenerative disorder[119]. This disorder was characterized by deposition of APP, astrogliosis, synaptic loss, and death on top of neurobehavioral signs of paralysis[119]. This was shown to be driven by ERK-activated microglia, and prevented with BRAF inhibition[119]. In another afore-cited study, perturbing activity of microglia (through cell-depletion and *Cx3cr1*, *Cr3*, and *Dap12* deficient mice) affected dopaminergic axonal outgrowth and interneuron lamination[96]. Compellingly, mice deficient in *Cx3cr1* had transient reductions in microglia with defects in synaptic pruning; these mice had deficits in social interaction and increases in restricted and repetitive behaviors[46]. In another study, which highlighted a secondary hematopoietic derived population of microglia marked by *Hoxb8*, showed that *Hoxb8* mutant mice had compulsive grooming and hair removal tendencies[103]. Lastly, microglia have been implicated in a mouse model of Rett syndrome[120,121]. Expressing the wildtype methyl CpG binding protein 2 gene (*Mecp2*) in microglia (mutations in *Mecp2* is responsible for most Rett syndrome cases) on an otherwise *Mecp2*-null mouse, arrested disease pathology which is due in part to microglial phagocytic activity[120,121].

Taken altogether, it is not unreasonable to propose that disruptions in immune functions of microglia in development mediate an upstream arm of neurodevelopmental disease etiology. In this dissertation, I introduce two mouse models of neurodevelopmental disorders that I used to further investigate microglial immune roles in brain formation: attention/deficit-hyperactivity disorder (ADHD) produced by disruption of a specialized form of cell death in microglia, and autism spectrum disorder (ASD) induced by exposure to maternal inflammation.

1.3: Attention-deficit/hyperactivity disorder (ADHD).

ADHD is diagnosed in about 7% of children worldwide[122,123], making ADHD the most common neurodevelopmental disorder. ADHD is characterized by the core symptoms of hyperactivity, impulsivity, and inattention [124,125] (https://www.cdc.gov/ncbddd/adhd/diagnosis.html). In about half of children, symptoms persist into adulthood[126]. Curiously, despite ADHD being among the most common neurodevelopmental disorders in children, the etiology and mechanism is still not clear though genetic and environmental factors are thought to play a role. Twin and adoption studies put estimates of ADHD heritability as high as 76%[127], suggesting a strong genetic component. Intriguingly, ADHD has a different presentation in males than in females, suggesting a sex bias; inattentive ADHD is more common among girls while hyperactive-impulsive is more common among boys[128-131]. In this section, I will briefly discuss the current ideas surrounding ADHD neurobiology and neurochemistry.

A variety of brain regions and networks are proposed to mediate ADHD behavioral symptoms. The regions include the prefrontal cortex (PFC), cerebellum, striatum, inferior parietal cortex, and the dorsal anterior cingulate cortex because of abnormalities found during brain scans[122]. The PFC in particular may be a strong nexus point for ADHD symptoms, as it has several connections with the cerebellum and caudate nuclei[122,132,133]. Studies have found reduced volume and function in white and gray matter in the PFC, as well as reduced maturation, in ADHD patients. Additional

evidence supporting the PFC roles in ADHD behaviors come from lesions of the PFC that yield a similar presentation to ADHD in people[122,134-136], which are particularly pronounced on the right hemisphere versus the left hemisphere[122,137,138]. The cerebellum, which is classically thought to mediate balance, was structurally different in ADHD patients[122,139-144]. The cerebellum receives inputs from the PFC[122]. The striatum is a prominent brain region of interest, because it is the largest reservoir of the dopamine neurotransmitter and the "dopamine hypothesis" is the prevailing theory of ADHD neurochemistry (discussed below). The striatum includes the caudate, nucleus accumbens, putamen, and globus pallidus; neural circuits here connect with those in the PFC[122]. Neuroimaging studies found reduced size of the globus pallidus in young ADHD patients[122,139,144-147] and also larger size of the nucleus accumbens in adults with ADHD[122,148]. Additional studies found size differences also in the inferior parietal cortex, of differing directions in children and adults[122,149,150], which also implicates this region. Lastly, abnormalities in the dorsal anterior cingulate cortex were found in ADHD patients during a continuous performance and response inhibition tasks[122,151-156]. This region is thought to be involved with many brain tasks: cognition, motor control, reward-based decision-making, and error detection among many others[122,151]. The thalamus may also be an important relay station among these interconnected regions: it receives inputs from the cerebellum and has inputs to the accumbens nucleus and PFC[122].

Some of the regions described above are implicated in mice that have hyperactive and/or inattentive behavioral phenotypes. For example, *Wells et al.* found that thalamic reticular impairment (through deletion of patched domain containing 1; *Ptchd1*) causes attention-deficit and hyperactivity[157]. Indeed, this region is thought to be a broad circuit endophenotype for other neurodevelopmental disorders[158]. And, lesions of the cerebellum produced hyperactivity[159,160]. These observations suggest conserved neural mechanisms from rodents to humans related to activity and attention.

Because many regions appear involved in ADHD behaviors and ADHD-like behaviors in mice, perhaps more unifying explanations can be found in neurochemistry. The prevailing hypothesis related to ADHD neurochemistry is the dopamine hypothesis—the idea that alterations to the dopaminergic system explain ADHD hyperactivity, inattention, and impulsivity symptoms[161]. This hypothesis arose from genetic studies of ADHD patients that showed associations with dopamine signaling pathway elements[162-165]. For example, polymorphisms in the dopamine receptors (DRD4, DRD5) and transporter (DAT1)[166,167] were found that impair the dopamine system such that there was a deficit in extracellular dopamine within cells[122,168]. In support of this idea, ADHD medication includes the stimulants methylphenidate (MPH) and amphetamine[169,170] (AMPH). MPH and AMPH work by antagonizing the action of dopamine, and increases the amount of extracellular dopamine and norepinephrine[122]. Since increasing available dopamine helps to attenuate the symptoms of ADHD in patients, this is another reason why dopamine deficiency is thought to be at the core of ADHD physiology. Furthermore, functional brain imaging studies demonstrated a wide array of hypofunctional anomalies in the cortical-striatal-thalamic brain circuits of ADHD patients[122,168]; these regions involve dopaminergic signaling. And, a binding study with [^{11}C]raclopride showed depressed dopamine activity in the caudate nucleus of ADHD adults[171].

While the above data appear compelling at first glance, a number of other observations weaken this hypothesis. There is lack of association of DAT1 or DRD4 mutations in samples of the French, Chinese Han, and Irish populations in ADHD patients[172-174] suggesting that associations from the foundational studies[162-165] may not extend to all populations. Furthermore, many other susceptible loci identified by genome-wide linkage or association studies do not contain dopamine-related genes[175-181]. For example, another genetic risk factor includes polymorphisms in the human norepinephrine (NET) gene, *SCLC6A2*, which suggests disruptions in norepinephrine signaling[182]. When considering pharmacology, psychostimulants used in the treatment of ADHD have a nonresponse rate as high as 30-40%[183]. It is also known that these psychostimulants are also effective for neurotypical subjects and produce the same behavioral effects[184-186]; indeed, these stimulants are prone to substance abuse[187,188], weakening the idea that ADHD patients have a dopamine defect corrected by psychostimulants. Furthermore, MPH and AMPH also modulate norepinephrine signaling; specific inhibitors of norepinephrine transporter can be as effective as psychostimulants when treating ADHD symptoms[184,189]. These data suggest contributing mechanisms from norepinephrine signaling. Lastly, a meta-analysis taking into account functional brain imaging data from several studies does not support the idea that ADHD is a result of hypofunction in discrete isolated brain regions[184,190]. In the binding study involving [^{11}C]raclopride could not rule out that ADHD patients had a higher basal tone of dopamine[171,184].

Thus, while dopamine signaling is involved with ADHD symptoms, it does not explain all aspects of ADHD physiology. Because multiple brain regions and neurochemistry are implicated, the neurobiology underlying ADHD etiology is complex with likely many contributing mechanisms of genetic and environmental origin. Since ADHD is a neurodevelopmental disorder, investigating the origins of ADHD using mouse models that are not solely due to disruptions in dopaminergic signaling may shed light on ADHD physiology. Investigations with such models may encourage research toward non-stimulant treatments for ADHD symptoms.

1.4: ADHD and the connection to immunity.

Intriguingly, most of the major neuropsychiatric conditions have been linked to disrupted immunity. These disorders include bipolar disorder, depression, and schizophrenia. For these disorders, interleukin-6 (IL-6), tumor necrosis factor-α (TNF-α), soluble cytokine receptor (sIL-2R), and cytokine receptor antagonist (IL-1RA) were all significantly increased in chronically ill patients compared to controls[191]. For autism spectrum disorder (ASD), a multitude of studies support immunity being involved in ASD development (see Chapter 3 for details). These data suggest underlying pathways of immune dysfunction that contribute to neuropsychiatric and neurodevelopmental disorders.

Despite ADHD being the most common neuropsychiatric condition[122,123], the connection of ADHD to immunity has been less explored compared to others[192]. However, the precedence to do so is there—ADHD has a high comorbidity with T_H1- and T_H2-mediated disorders and/or allergic diseases such as Celiac disease, otitis media, allergic hypersensitivity disorder, asthma, rhinitis, and atopic dermatitis[193-200].

Maternal and paternal autoimmunity was found to be associated with an increased risk of ADHD in children[201,202]. In particular, maternal multiple sclerosis, rheumatoid arthritis, type 1 diabetes, asthma, and hypothyroidism were associated with ADHD in offspring[202]. Within ADHD patients themselves, associations with autoimmune conditions were found in a sex-dependent manner[203]. The strongest association identified by Hegvik and colleagues was found between ADHD and psoriasis in females, with additional associations between ADHD, Crohn's disease, and ulcerative colitis [203]. In contrast, males with ADHD had lower chances of having Crohn's disease and ulcerative colitis[203]. Within ADHD patients, significant increases in serum IgE, IgG, and IL-6 were found relative to control patients[204,205]. Furthermore, associations between patients treated for infection and ADHD risk in children and adolescents were also found[206].

While these studies discussed herein should be regarded cautiously, the data collectively supports the idea that there is a connection between immunity and ADHD. Yet, to my best knowledge, no known mechanisms have been yet delineated. A mouse model may clarify ADHD etiology and identify the putative circuitries mediating the core hyperactivity and inattention symptoms. Understanding the neural basis of ADHD, and possible contributions from the immune system, can help direct additional research in identifying and testing neuromodulatory or immunomodulatory compounds that relieve ADHD symptoms in patients.

1.5: Autism spectrum disorder (ASD).

ASD is a neurodevelopmental disorder characterized by impairments in social interaction and restricted repetitive behaviors[124] (https://www.cdc.gov/ncbddd/autism/facts.html). ASD is approximately 4.5 times more common in males than females, revealing a sex bias[207-209]. Currently, about 1 in 54 children have ASD (https://www.cdc.gov/ncbddd/autism/data.html). The neurobiology of ASD is complex, with a multitude of brain regions thought to be involved. Thus, an in-depth review including primary works is beyond the scope of this introductory chapter. A few reviews have guided the brief amount of information included here; I direct the reader to look to these reviews for the original references[210-214]. Regions mediating social impairment are thought to include the orbitofrontal cortex (OFC), anterior cingulate cortex (ACC), fusiform gyrus, superior temporal sulcus (STS), amygdala mirror neuron regions, inferior frontal gyrus (IFG), and posterior parietal cortex [210]. The OFC, ACC, basal ganglia (BG), and thalamus (Th) are thought to mediate the restricted and repetitive stereotyped behaviors in ASD patients[210]. For communication in particular, the IFG, STS, supplementary motor area, BG, substantia nigra, Th, and pontine nuclei cerebellum are thought to be involved[210]. Only some of these areas are consistently supported by imaging and functional imaging studies. The neocortex is one of these regions; a common finding seems to be that ASD patients have altered columnar structures in the neocortex and paucity of Purkinje neurons of the cerebellum[210,211,215]. The cerebellum and caudate nucleus is enlarged in ASD patients compared to controls, and total brain volume in general in 25-30% of ASD patients' brains is increased significantly in size between the first and second year of life, which may be due to increases in white matter rather than gray matter[210,211,214].

Because of the variety of brain regions are involved, the field is seeking a more unifying theory of ASD physiology. As a result, some propose that ASD is a condition of aberrant connectivity[211,213]. In support of this, adults with ASD tend to have long-distance "under connectivity" and local short-range "over connectivity" in which there is ineffective integration among various brain regions (particularly of intrahemispheric and intracortical origin)[211,213]. Disrupted neurochemistry is also proposed to be a facet of ASD physiology, which may provide explanatory power for the plethora of brain regions involved. Indeed, disrupted excitation/inhibition (E/I) ratio is a core theory of ASD physiology[215,216]. It posits that unbalanced synaptic inputs to a circuit (i.e., too much or too little excitation/inhibition) lead to disrupted function. The E/I ratio hypothesis is attractive, because it may also explain the connectivity and integration issues proposed to underlie ASD. Within the E/I ratio hypothesis, there are two opposing models: that ASD has reduced excitability via hypoglutamatergic signaling, or that ASD has decreased inhibition[215]. Suppressed GABAergic signaling is also proposed, in addition to de-regulated serotonergic signaling, dopaminergic signaling, and disrupted norepinephrine signaling[215]. Because ASD patients exhibit a large range of phenotypes, this almost assuredly obfuscates efforts to clarify "typical" ASD physiology—if that exists.

The pursuit of defining core ASD neurobiology is further confounded with its highly heterogeneous genetic component. ASD is thought to be among the most heritable of neurodevelopmental disorders because of the high concordance rate among monozygotic twins (up to 96 percent)[217-222]. Various genome-wide association studies (GWAS) and whole exome analyses have been underway in the past decade in effort to dissect ASD's complex genetic milieu[223-228]. There appears to be a large burden of extremely rare *de novo* copy number variant (CNV) mutations among hundreds of genes, as well as single nucleotide variants (SNVs) that often appear in the six loci identified to be implicated with ASD[229]. In general, these mutations alter the dosage of genes but do not completely abrogate their presence. They are absent from the general population and are likely to be highly penetrant. A recessive model does not fit the behavior of these mutations, as they mostly occur as duplications or hemizygous deletions. In about a fraction of ASD cases, a single genetic alteration (such as a CNV) could be penetrant enough to cause the main symptoms[230]. All in all, it is estimated that there are between 350 to 400 ASD susceptibility genes, of which a single gene is not attributed more than 1% of the cause for ASD[226,228]. Given all the mutant variations among hundreds of genes, it seemingly becomes a game of educated guesswork to assimilate these into a cohesive picture of ASD etiology. Despite the immense difficulties in interpreting conclusions from sequencing studies on a gene-by-gene basis, consistent patterns emerge at a functional level. Common modules associated with mutant gene variations include networks involved synaptic function and chromatin remodeling[231-233].

Environmental factors could represent a "second-hit" that modulates existing genetic factors predisposing an individual to ASD (or possibly induce mutations). For example, maternal exposure to toxins, teratogens, certain drugs, infection & autoimmunity, and nutrient deficiency are identified environmental risk factors for developing ASD[234-237]. In support of epigenetic factors, advanced parental age and alterations in genetic imprinting may increase the risk of ASD[238,239]. Curiously,

transcriptome studies of ASD subjects identified another environmental risk module: the immune system[240,241], which supports the identification of maternal infection and autoimmunity as a risk factor[234-236,239]. Mounting evidence suggests that an early immune activation could be a core feature of ASD pathophysiology. In fact*, Ziats and Rennert* in 2001 found that 219 of the previously identified putative ASD risk genes may converge unto cytokine signaling pathways[242], and *Krishnan et al.* demonstrated that many ASD genes converge on key pathways that includes immunity[231]. The connection of ASD and immunity is discussed in the next section.

1.6: ASD and the connection to immunity.

Infection during pregnancy is an environmental risk factor for developing ASD. In a landmark epidemiological study, *Atladottir et al.* investigated Danish medical records and performed a retrospective study including all children born in Denmark from 1980 through 2005—over 10,000 cases[243]. *Atladottir et al*. found that hospital entry due to maternal viral infection in the first trimester, and bacterial infection in the second trimester, were associated with ASD diagnosis in the offspring[243]. Other studies also identified and reviewed maternal infection as a risk factor[234-236,239]. Maternal autoimmunity was also associated with increasing ASD risk[235,244-246]. Thus, collectively, the connection between the ASD etiology and immunity was solidified.

This connection is reinforced with data supporting that individuals with ASD often display features of permanent immune deregulation[247]. Postmortem brain tissue from patients with ASD (and non-neurological case controls) demonstrated that there was an increase in microglial and astroglial "activation" in the postmortem brains of autistic patients—increased GFAP reactivity in astroglia and MHC-II expression in microglia[248]. Furthermore, *Vargas et al.* also observed increased levels of proinflammatory cytokines (such as IL-6) in freshly obtained tissue[248]. In living patients, cerebrospinal fluid (CSF) shows a pro-inflammatory profile with significant increases in cytokines including macrophage chemoattractant protein-1 (MCP-1), interferon gamma (IFN-γ), and transforming growth factor beta (TGF-β)[248]. *Vargas et al.* did not note significant contribution of adaptive immune features, such as $CD3^+$ T cell or $CD20^+$ B cell infiltration into post-mortem brain tissue, and absence of immunoglobulin deposition[248]. In a study by Voineagu and colleagues, post-mortem brain tissue samples from 19 ASD cases and 17 control cases were analyzed by microarray[249]. *Voineague et al.* found a set of genes downregulated in the cortex of ASD patients related to synaptic function, while upregulated genes are implicated in the immune response[249].

In further support of the connection between ASD and immunity are elevated levels of cytokines and chemokines in the blood of children with ASD relative to non-ASD controls. For example, increases in interleukin-1β (IL-1β), IL-6, and IL-8 have been noted, and the magnitude of these changes was correlated with the severity of the behavioral abnormalities[241]. These data suggest that permanent immune deregulation also extends peripherally beyond the CNS. In support of this, there is a higher prevalence of inflammatory bowel disease (IBD) and other gastrointestinal (GI) disorders among ASD patients[250]. Lastly, treatment of ASD patients with anti-inflammatory drugs moderately alleviated a subset of ASD symptoms[251]. Mothers of ASD children often report that fever reduces symptom severity, a finding corroborated in

2007[252]. Thus, it appears that the role of the immune system in ASD etiology is gaining appreciation.

While these studies discussed herein should be regarded cautiously, the data collectively supports the idea that there is a connection between immunity and ASD that persists into the lifespan. Since ASD is a neurodevelopmental disorder, studying the immune component during the development of ASD *in utero* is worthy of investigation. Luckily, a robust mouse model of ASD exists—the maternal immune activation model (MIA)—which is discussed in Chapter 3.

References

1. Carson, M. J., Doose, J. M., Melchior, B., Schmid, C. D. & Ploix, C. C. CNS immune privilege: hiding in plain sight. *Immunol. Rev.* **213,** 48–65 (2006).
2. Saijo, K. & Glass, C. K. Microglial cell origin and phenotypes in health and disease. *Nat. Rev. Immunol.* **11,** 775–787 (2011).
3. Kettenmann, H., Hanisch, U.-K., Noda, M. & Verkhratsky, A. Physiology of microglia. *Physiological Reviews* **91,** 461–553 (2011).
4. Kierdorf, K. *et al.* Microglia emerge from erythromyeloid precursors via Pu.1- and Irf8-dependent pathways. *Nature Publishing Group* **16,** 273–280 (2013).
5. Ginhoux, F., Lim, S., Hoeffel, G., Low, D. & Huber, T. Origin and differentiation of microglia. *Front. Cell. Neurosci.* **7,** 45 (2013).
6. Walsh, J. G., Muruve, D. A. & Power, C. Inflammasomes in the CNS. *Nat Rev Neurosci* **15,** 84–97 (2014).
7. Suter, T. *et al.* The brain as an immune privileged site: dendritic cells of the central nervous system inhibit T cell activation. *Eur. J. Immunol.* **33,** 2998–3006 (2003).
8. Harris, M. G. *et al.* Immune privilege of the CNS is not the consequence of limited antigen sampling. *Sci. Rep.* **4,** 4422 (2014).
9. Engelhardt, B., Vajkoczy, P. & Weller, R. O. The movers and shapers in immune privilege of the CNS. *Nat Immunol* **18,** 123–131 (2017).
10. Wolf, S. A., Boddeke, H. W. G. M. & Kettenmann, H. Microglia in Physiology and Disease. *Annu. Rev. Physiol.* **79,** 619–643 (2017).
11. Wright-Jin, E. C. & Gutmann, D. H. Microglia as Dynamic Cellular Mediators of Brain Function. *Trends in Molecular Medicine* **25,** 967–979 (2019).
12. Lawson, L. J., Perry, V. H., Dri, P. & Gordon, S. Heterogeneity in the distribution and morphology of microglia in the normal adult mouse brain. *NEUROSCIENCE* **39,** 151–170 (1990).
13. Perry, V. H., Hume, D. A. & Gordon, S. Immunohistochemical localization of macrophages and microglia in the adult and developing mouse brain. *NEUROSCIENCE* **15,** 313–326 (1985).
14. Wake, H., Moorhouse, A. J., Miyamoto, A. & Nabekura, J. Microglia: actively surveying and shaping neuronal circuit structure and function. *Trends in Neurosciences* **36,** 209–217 (2013).
15. Uweru, J. O. & Eyo, U. B. A decade of diverse microglial-neuronal physical interactions in the brain (2008-2018). *Neuroscience Letters* **698,** 33–38 (2019).
16. Kettenmann, H., Kirchhoff, F. & Verkhratsky, A. Microglia: new roles for the synaptic stripper. *Neuron* **77,** 10–18 (2013).
17. Pardoll, D. M. Immunology beats cancer: a blueprint for successful translation. *Nat Immunol* **13,** 1129–1132 (2012).
18. Littman, D. R. *Releasing the Brakes on Cancer Immunotherapy. Cell* **162,** 1186–1190 (2015).
19. Lynch, M. A. & Mills, K. H. G. Immunology meets neuroscience--opportunities for immune intervention in neurodegenerative diseases. *Brain Behavior and Immunity* **26,** 1–10 (2012).

20. Deczkowska, A. *et al.* PD-1 immune checkpoint blockade reduces pathology and improves memory in mouse models of Alzheimer's disease. *Nature Medicine* 1–5 (2016). doi:10.1038/nm.4022
21. Eyo, U. B. & Wu, L.-J. Microglia: Lifelong patrolling immune cells of the brain. *Progress in Neurobiology* **179,** 101614 (2019).
22. la Peña, de, J. B. *et al.* Exploring the Validity of Proposed Transgenic Animal Models of Attention-Deficit Hyperactivity Disorder (ADHD). *Mol Neurobiol* **55,** 3739–3754 (2018).
23. Gainetdinov, R. R. *et al.* Role of serotonin in the paradoxical calming effect of psychostimulants on hyperactivity. *Science* **283,** 397–401 (1999).
24. Leo, D. & Gainetdinov, R. R. Transgenic mouse models for ADHD. *Cell Tissue Res* **354,** 259–271 (2013).
25. Tremblay, M.-È., Lowery, R. L. & Majewska, A. K. Microglial interactions with synapses are modulated by visual experience. *PLoS Biol.* **8,** e1000527 (2010).
26. Calovi, S., Mut-Arbona, P. & Sperlágh, B. Microglia and the Purinergic Signaling System. *NEUROSCIENCE* **405,** 137–147 (2019).
27. Dissing-Olesen, L. *et al.* Activation of neuronal NMDA receptors triggers transient ATP-mediated microglial process outgrowth. *J. Neurosci.* **34,** 10511–10527 (2014).
28. Eyo, U. B. *et al.* Neuronal hyperactivity recruits microglial processes via neuronal NMDA receptors and microglial P2Y12 receptors after status epilepticus. *J. Neurosci.* **34,** 10528–10540 (2014).
29. Eyo, U. B. *et al.* Regulation of Physical Microglia-Neuron Interactions by Fractalkine Signaling after Status Epilepticus. *eNeuro* **3,** (2016).
30. Haynes, S. E. *et al.* The P2Y12 receptor regulates microglial activation by extracellular nucleotides. *Nat Neurosci* **9,** 1512–1519 (2006).
31. Davalos, D. *et al.* ATP mediates rapid microglial response to local brain injury in vivo. *Nat Neurosci* **8,** 752–758 (2005).
32. Nimmerjahn, A., Kirchhoff, F. & Helmchen, F. Resting microglial cells are highly dynamic surveillants of brain parenchyma in vivo. *Science* **308,** 1314–1318 (2005).
33. Wu, L.-J., Vadakkan, K. I. & Zhuo, M. ATP-induced chemotaxis of microglial processes requires P2Y receptor-activated initiation of outward potassium currents. *Glia* **55,** 810–821 (2007).
34. Irino, Y., Nakamura, Y., Inoue, K., Kohsaka, S. & Ohsawa, K. Akt activation is involved in P2Y12 receptor-mediated chemotaxis of microglia. *J. Neurosci. Res.* **86,** 1511–1519 (2008).
35. Pfeiffer, T., Avignone, E. & Nägerl, U. V. Induction of hippocampal long-term potentiation increases the morphological dynamics of microglial processes and prolongs their contacts with dendritic spines. *Sci. Rep.* **6,** 32422–9 (2016).
36. Lynch, M. A. Long-term potentiation and memory. *Physiological Reviews* **84,** 87–136 (2004).
37. Zhang, J. *et al.* Microglial CR3 Activation Triggers Long-Term Synaptic Depression in the Hippocampus via NADPH Oxidase. *Neuron* **82,** 195–207

(2014).
38. Ito, M. Long-term depression. *Annu. Rev. Neurosci.* **12,** 85–102 (1989).
39. Eyo, U. B. *et al.* The GluN2A Subunit Regulates Neuronal NMDA receptor-Induced Microglia-Neuron Physical Interactions. *Sci. Rep.* **8,** 828–10 (2018).
40. Parkhurst, C. N. *et al.* Microglia Promote Learning-Dependent Synapse Formation through Brain-Derived Neurotrophic Factor. *Cell* **155,** 1596–1609 (2013).
41. Paolicelli, R. C. *et al.* Synaptic pruning by microglia is necessary for normal brain development. *Science* **333,** 1456–1458 (2011).
42. Stevens, B. *et al.* The classical complement cascade mediates CNS synapse elimination. *Cell* **131,** 1164–1178 (2007).
43. Stephan, A. H., Barres, B. A. & Stevens, B. The Complement System: An Unexpected Role in Synaptic Pruning During Development and Disease. *Annu. Rev. Neurosci.* **35,** 369–389 (2012).
44. Schafer, D. P. *et al.* Microglia Sculpt Postnatal Neural Circuits in an Activity and Complement-Dependent Manner. *Neuron* **74,** 691–705 (2012).
45. Rogers, J. T. *et al.* CX3CR1 deficiency leads to impairment of hippocampal cognitive function and synaptic plasticity. *J. Neurosci.* **31,** 16241–16250 (2011).
46. Zhan, Y. *et al.* Deficient neuron-microglia signaling results in impaired functional brain connectivity and social behavior. *Nature Publishing Group* 1–10 (2014). doi:10.1038/nn.3641
47. Torres, L. *et al.* Dynamic microglial modulation of spatial learning and social behavior. *Brain Behavior and Immunity* **55,** 6–16 (2016).
48. Wang, J. *et al.* Targeting Microglia and Macrophages: A Potential Treatment Strategy for Multiple Sclerosis. *Front Pharmacol* **10,** 286 (2019).
49. Gao, H.-M. *et al.* Microglial activation-mediated delayed and progressive degeneration of rat nigral dopaminergic neurons: relevance to Parkinson's disease. *J. Neurochem.* **81,** 1285–1297 (2002).
50. Langmann, T. Microglia activation in retinal degeneration. *J. Leukoc. Biol.* **81,** 1345–1351 (2007).
51. Rizzo, F. *et al.* Cellular therapy to target neuroinflammation in amyotrophic lateral sclerosis. *Cell. Mol. Life Sci.* **71,** 999–1015 (2014).
52. Moore, Z., Taylor, J. M. & Crack, P. J. The involvement of microglia in Alzheimer's disease: a new dog in the fight. *Br J Pharmacol* **176,** 3533–3543 (2019).
53. Streit, W. J. Microglia and Alzheimer's disease pathogenesis. *J. Neurosci. Res.* **77,** 1–8 (2004).
54. Wang, S. & Colonna, M. Microglia in Alzheimer's disease: A target for immunotherapy. *J. Leukoc. Biol.* **106,** 219–227 (2019).
55. Cameron, B. & Landreth, G. E. Inflammation, microglia, and alzheimer's disease. *Neurobiology of Disease* **37,** 503–509 (2010).
56. Selkoe, D. J. & Hardy, J. The amyloid hypothesis of Alzheimer's disease at 25 years. *EMBO Molecular Medicine* **8,** 595–608 (2016).
57. Baranello, R. J. *et al.* Amyloid-beta protein clearance and degradation (ABCD) pathways and their role in Alzheimer's disease. *Curr Alzheimer Res*

12, 32–46 (2015).
58. Herrup, K. The case for rejecting the amyloid cascade hypothesis. *Nat Neurosci* **18,** 794–799 (2015).
59. Kametani, F. & Hasegawa, M. Reconsideration of Amyloid Hypothesis and Tau Hypothesis in Alzheimer's Disease. *Front. Neurosci.* **12,** 25 (2018).
60. Gandy, S. & Heppner, F. L. Microglia as Dynamic and Essential Components of the Amyloid Hypothesis. *Neuron* **78,** 575–577 (2013).
61. Bin Zhang *et al.* Integrated Systems Approach Identifies Genetic Nodes and Networks in Late-Onset Alzheimer's Disease. *Cell* **153,** 707–720 (2013).
62. Lambert, J.-C. *et al.* Implication of the immune system in Alzheimer's disease: evidence from genome-wide pathway analysis. *J. Alzheimers Dis.* **20,** 1107–1118 (2010).
63. Bolmont, T. *et al.* Dynamics of the microglial/amyloid interaction indicate a role in plaque maintenance. *J. Neurosci.* **28,** 4283–4292 (2008).
64. Zhao, R., Hu, W., Tsai, J., Li, W. & Gan, W.-B. Microglia limit the expansion of β-amyloid plaques in a mouse model of Alzheimer's disease. *Mol Neurodegener* **12,** 47–11 (2017).
65. Hickman, S. E., Allison, E. K. & Khoury, El, J. Microglial dysfunction and defective beta-amyloid clearance pathways in aging Alzheimer's disease mice. *J. Neurosci.* **28,** 8354–8360 (2008).
66. Wang, Y. *et al.* TREM2-mediated early microglial response limits diffusion and toxicity of amyloid plaques. *J. Exp. Med.* **213,** 667–675 (2016).
67. Wang, Y. *et al.* TREM2 lipid sensing sustains the microglial response in an Alzheimer's disease model. *Cell* **160,** 1061–1071 (2015).
68. Ulrich, J. D. *et al.* Altered microglial response to Aβ plaques in APPPS1-21 mice heterozygous for TREM2. *Mol Neurodegener* **9,** 20 (2014).
69. Jay, T. R. *et al.* Disease Progression-Dependent Effects of TREM2 Deficiency in a Mouse Model of Alzheimer's Disease. *J. Neurosci.* **37,** 637–647 (2017).
70. Bergsbaken, T., Fink, S. L. & Cookson, B. T. Pyroptosis: host cell death and inflammation. *Nat. Rev. Microbiol.* **7,** 99–109 (2009).
71. Venegas, C. *et al.* Microglia-derived ASC specks cross-seed amyloid-β in Alzheimer's disease. *Nature* **552,** 355–361 (2017).
72. Joshi, P. *et al.* Microglia convert aggregated amyloid-β into neurotoxic forms through the shedding of microvesicles. *Cell Death and Differentiation 2015 22:10* **21,** 582–593 (2014).
73. Dai, X.-M. *et al.* Targeted disruption of the mouse colony-stimulating factor 1 receptor gene results in osteopetrosis, mononuclear phagocyte deficiency, increased primitive progenitor cell frequencies, and reproductive defects. *Blood* **99,** 111–120 (2002).
74. Erblich, B., Zhu, L., Etgen, A. M., Dobrenis, K. & Pollard, J. W. Absence of colony stimulation factor-1 receptor results in loss of microglia, disrupted brain development and olfactory deficits. *PLoS ONE* **6,** e26317 (2011).
75. Oosterhof, N. *et al.* Homozygous Mutations in CSF1R Cause a Pediatric-Onset Leukoencephalopathy and Can Result in Congenital Absence of Microglia. *Am. J. Hum. Genet.* **104,** 936–947 (2019).

76. Li, J., Chen, K., Zhu, L. & Pollard, J. W. Conditional deletion of the colony stimulating factor-1 receptor (c-fms proto-oncogene) in mice. *Genesis* **44,** 328–335 (2006).
77. Cecchini, M. G. *et al.* Role of colony stimulating factor-1 in the establishment and regulation of tissue macrophages during postnatal development of the mouse. *Development* **120,** 1357–1372 (1994).
78. Chitu, V. & Stanley, E. R. Regulation of Embryonic and Postnatal Development by the CSF-1 Receptor. *Curr. Top. Dev. Biol.* **123,** 229–275 (2017).
79. Chitu, V., Gokhan, S., Nandi, S., Mehler, M. F. & Stanley, E. R. Emerging Roles for CSF-1 Receptor and its Ligands in the Nervous System. *Trends in Neurosciences* **39,** 378–393 (2016).
80. Hume, D. A. *et al.* Phenotypic impacts of CSF1R deficiencies in humans and model organisms. *J. Leukoc. Biol.* (2019). doi:10.1002/JLB.MR0519-143R
81. Anderson, S. R. & Vetter, M. L. Developmental roles of microglia: A window into mechanisms of disease. *Dev. Dyn.* **248,** 98–117 (2019).
82. Ginhoux, F. *et al.* Fate mapping analysis reveals that adult microglia derive from primitive macrophages. *Science* **330,** 841–845 (2010).
83. Shulz, C., Perdiguero, E. G., Science, L. C.2012. *A lineage of myeloid cells independent of Myb and hematopoetic stem cells*. doi:10.1126/science.1213307
84. Swinnen, N. *et al.* Complex invasion pattern of the cerebral cortex bymicroglial cells during development of the mouse embryo. *Glia* **61,** 150–163 (2013).
85. Ransohoff, R. M. & Perry, V. H. Microglial physiology: unique stimuli, specialized responses. *Annu. Rev. Immunol.* **27,** 119–145 (2009).
86. Stremmel, C. *et al.* Yolk sac macrophage progenitors traffic to the embryo during defined stages of development. *Nature Communications* **9,** 75–14 (2018).
87. Koushik, S. V. *et al.* Targeted inactivation of the sodium-calcium exchanger (Ncx1) results in the lack of a heartbeat and abnormal myofibrillar organization. *FASEB J.* **15,** 1209–1211 (2001).
88. Engelhardt, B. & Liebner, S. Novel insights into the development and maintenance of the blood-brain barrier. *Cell Tissue Res* **355,** 687–699 (2014).
89. Arnold, T. & Betsholtz, C. The importance of microglia in the development of the vasculature in the central nervous system. *Vasc Cell* **5,** 4 (2013).
90. Ashwell, K. The distribution of microglia and cell death in the fetal rat forebrain. *Brain Res. Dev. Brain Res.* **58,** 1–12 (1991).
91. Cunningham, C. L. & Martinez-Cerdeno, V. Microglia regulate the number of neural precursor cells in the developing cerebral cortex. *Journal of …* (2013). doi:10.1523/JNEUROSCI.3441-12.2013
92. Sierra, A. *et al.* Microglia shape adult hippocampal neurogenesis through apoptosis-coupled phagocytosis. *Cell Stem Cell* **7,** 483–495 (2010).
93. Arnò, B. *et al.* Neural progenitor cells orchestrate microglia migration and positioning into the developing cortex. *Nature Communications* **5,** 5611

(2014).
94. Cuadros, M. A. & Navascués, J. The origin and differentiation of microglial cells during development. *Progress in Neurobiology* **56,** 173–189 (1998).
95. Monier, A. *et al.* Entry and distribution of microglial cells in human embryonic and fetal cerebral cortex. *J. Neuropathol. Exp. Neurol.* **66,** 372–382 (2007).
96. Squarzoni, P. *et al.* Microglia modulate wiring of the embryonic forebrain. *Cell Rep* **8,** 1271–1279 (2014).
97. Verney, C., Monier, A., Fallet-Bianco, C. & Gressens, P. Early microglial colonization of the human forebrain and possible involvement in periventricular white-matter injury of preterm infants. *Journal of Anatomy* **217,** 436–448 (2010).
98. Silva, C. G., Peyre, E. & Nguyen, L. Cell migration promotes dynamic cellular interactions to control cerebral cortex morphogenesis. *Nat Rev Neurosci* **20,** 318–329 (2019).
99. Bjornsson, C. S., Apostolopoulou, M., Tian, Y. & Temple, S. It takes a village: constructing the neurogenic niche. *Dev. Cell* **32,** 435–446 (2015).
100. Thion, M. S. & Garel, S. On place and time: microglia in embryonic and perinatal brain development. *Current Opinion in Neurobiology* **47,** 121–130 (2017).
101. Reemst, K., Noctor, S. C., Lucassen, P. J. & Hol, E. M. The Indispensable Roles of Microglia and Astrocytes during Brain Development. *Front Hum Neurosci* **10,** 566 (2016).
102. De, S. *et al.* Two distinct ontogenies confer heterogeneity to mouse brain microglia. *Development* **145,** (2018).
103. Chen, S.-K. *et al.* Hematopoietic origin of pathological grooming in Hoxb8 mutant mice. *Cell* **141,** 775–785 (2010).
104. Matcovitch-Natan, O. *et al.* Microglia development follows a stepwise program to regulate brain homeostasis. *Science* **353,** aad8670 (2016).
105. Hammond, T. R. *et al.* Single-Cell RNA Sequencing of Microglia throughout the Mouse Lifespan and in the Injured Brain Reveals Complex Cell-State Changes. *Immunity* **50,** 253–271.e6 (2019).
106. Masuda, T. *et al.* Spatial and temporal heterogeneity of mouse and human microglia at single-cell resolution. *Nature* **566,** 388–392 (2019).
107. Li, Q. *et al.* Developmental Heterogeneity of Microglia and Brain Myeloid Cells Revealed by Deep Single-Cell RNA Sequencing. *Neuron* **101,** 207–223.e10 (2019).
108. Van Hove, H. *et al.* A single-cell atlas of mouse brain macrophages reveals unique transcriptional identities shaped by ontogeny and tissue environment. *Nat Neurosci* **22,** 1021–1035 (2019).
109. Utz, S. G. *et al.* Early Fate Defines Microglia and Non-parenchymal Brain Macrophage Development. *Cell* (2020). doi:10.1016/j.cell.2020.03.021
110. Martínez, S., Puelles, E., system, L. P. T. M. N.2012. Molecular regionalization of the developing neural tube. *Elsevier* doi:10.1016/B978-0-12-369497-3.10001-9
111. Semple, B. D., Blomgren, K., Gimlin, K., Ferriero, D. M. & Noble-Haeusslein, L. J. Brain development in rodents and humans: Identifying benchmarks of

maturation and vulnerability to injury across species. *Progress in Neurobiology* **106-107,** 1–16 (2013).
112. Feldman, D. E. Synaptic mechanisms for plasticity in neocortex. *Annu. Rev. Neurosci.* **32,** 33–55 (2009).
113. Waisman, A., Ginhoux, F., Greter, M. & Bruttger, J. Homeostasis of Microglia in the Adult Brain: Review of Novel Microglia Depletion Systems. *Trends in Immunology* **36,** 625–636 (2015).
114. Hashimoto, D. *et al.* Tissue-Resident Macrophages Self-Maintain Locally throughout Adult Life with Minimal Contribution from Circulating Monocytes. *Immunity* **38,** 792–804 (2013).
115. Bruttger, J. *et al.* Genetic Cell Ablation Reveals Clusters of Local Self-Renewing Microglia in the Mammalian Central Nervous System. *Immunity* 1–16 (2015). doi:10.1016/j.immuni.2015.06.012
116. Tay, T. L. *et al.* A new fate mapping system reveals context-dependent random or clonal expansion of microglia. *Nature Publishing Group* **20,** 793–803 (2017).
117. Ajami, B., Bennett, J. L., Krieger, C., Tetzlaff, W. & Rossi, F. M. V. Local self-renewal can sustain CNS microglia maintenance and function throughout adult life. *Nat Neurosci* **10,** 1538–1543 (2007).
118. Zhao, C., Deng, W. & Gage, F. H. Mechanisms and functional implications of adult neurogenesis. *Cell* **132,** 645–660 (2008).
119. Mass, E. *et al.* A somatic mutation in erythro-myeloid progenitors causes neurodegenerative disease. *Nature* **549,** 389–393 (2017).
120. Derecki, N. C. *et al.* Wild-type microglia arrest pathology in a mouse model of Rett syndrome. *Nature* **484,** 105–109 (2012).
121. Derecki, N. C., Cronk, J. C. & Kipnis, J. The role of microglia in brain maintenance: implications for Rett syndrome. *Trends in Immunology* **34,** 144–150 (2013).
122. Mehta, T. R., Monegro, A., Nene, Y., Fayyaz, M. & Bollu, P. C. Neurobiology of ADHD: A Review. *Curr Dev Disord Rep* **6,** 235–240 (2019).
123. Thomas, R., Sanders, S., Doust, J., Beller, E. & Glasziou, P. Prevalence of attention-deficit/hyperactivity disorder: a systematic review and meta-analysis. *PEDIATRICS* **135,** e994–1001 (2015).
124. American Psychiatric Association. *Diagnostic and statistical manual of mental disorders* (5th ed.). Arlington, VA: Author. (2013).
125. Epstein, J. N. & Loren, R. E. A. Changes in the Definition of ADHD in DSM-5: Subtle but Important. *Neuropsychiatry (London)* **3,** 455–458 (2013).
126. Lara, C. *et al.* Childhood predictors of adult attention-deficit/hyperactivity disorder: results from the World Health Organization World Mental Health Survey Initiative. *Biological Psychiatry* **65,** 46–54 (2009).
127. Faraone, S. V. *et al.* Molecular genetics of attention-deficit/hyperactivity disorder. *BPS* **57,** 1313–1323 (2005).
128. Trent, S. & Davies, W. The influence of sex-linked genetic mechanisms on attention and impulsivity. *Biol Psychol* **89,** 1–13 (2012).
129. Arnold, L. E. Sex differences in ADHD: conference summary. *J Abnorm Child Psychol* **24,** 555–569 (1996).

130. May, T., Adesina, I., McGillivray, J. & Rinehart, N. J. Sex differences in neurodevelopmental disorders. *Current Opinion in Neurology* **32,** 622–626 (2019).
131. Davies, W. Sex differences in Attention Deficit Hyperactivity Disorder: Candidate genetic and endocrine mechanisms. *FRONTIERS IN NEUROENDOCRINOLOGY* 1–16 (2014). doi:10.1016/j.yfrne.2014.03.003
132. Arnsten, A. F. T. & Pliszka, S. R. Catecholamine influences on prefrontal cortical function: relevance to treatment of attention deficit/hyperactivity disorder and related disorders. *Pharmacology Biochemistry and Behavior* **99,** 211–216 (2011).
133. Kesner, R. P. & Churchwell, J. C. An analysis of rat prefrontal cortex in mediating executive function. *Neurobiol Learn Mem* **96,** 417–431 (2011).
134. McLEAN, A. *et al.* Characteristic neurocognitive profile associated with adult attention-deficit/hyperactivity disorder. *Psychol Med* **34,** 681–692 (2004).
135. Bedard, A.-C. *et al.* Selective inhibition in children with attention-deficit hyperactivity disorder off and on stimulant medication. *J Abnorm Child Psychol* **31,** 315–327 (2003).
136. Itami, S. & Uno, H. Orbitofrontal cortex dysfunction in attention-deficit hyperactivity disorder revealed by reversal and extinction tasks. *Neuroreport* **13,** 2453–2457 (2002).
137. Aron, A. R., Robbins, T. W. & Poldrack, R. A. Inhibition and the right inferior frontal cortex. *Trends Cogn. Sci. (Regul. Ed.)* **8,** 170–177 (2004).
138. Godefroy, O. & Rousseaux, M. Divided and focused attention in patients with lesion of the prefrontal cortex. *Brain Cogn* **30,** 155–174 (1996).
139. Castellanos, F. X. *et al.* Quantitative brain magnetic resonance imaging in attention-deficit hyperactivity disorder. *Arch. Gen. Psychiatry* **53,** 607–616 (1996).
140. Berquin, P. C. *et al.* Cerebellum in attention-deficit hyperactivity disorder: a morphometric MRI study. *Neurology* **50,** 1087–1093 (1998).
141. Hill, D. E. *et al.* Magnetic resonance imaging correlates of attention-deficit/hyperactivity disorder in children. *Neuropsychology* **17,** 496–506 (2003).
142. Mostofsky, S. H., Reiss, A. L., Lockhart, P. & Denckla, M. B. Evaluation of cerebellar size in attention-deficit hyperactivity disorder. *J. Child Neurol.* **13,** 434–439 (1998).
143. Bussing, R., Grudnik, J., Mason, D., Wasiak, M. & Leonard, C. ADHD and conduct disorder: an MRI study in a community sample. *World J. Biol. Psychiatry* **3,** 216–220 (2002).
144. Castellanos, F. X. *et al.* Developmental trajectories of brain volume abnormalities in children and adolescents with attention-deficit/hyperactivity disorder. *JAMA* **288,** 1740–1748 (2002).
145. Castellanos, F. X. *et al.* Quantitative brain magnetic resonance imaging in girls with attention-deficit/hyperactivity disorder. *Arch. Gen. Psychiatry* **58,** 289–295 (2001).
146. Overmeyer, S. *et al.* Distributed grey and white matter deficits in hyperkinetic disorder: MRI evidence for anatomical abnormality in an attentional network.

Psychol Med **31,** 1425–1435 (2001).
147. Aylward, E. H. *et al.* Basal ganglia volumes in children with attention-deficit hyperactivity disorder. *J. Child Neurol.* **11,** 112–115 (1996).
148. Seidman, L. J. *et al.* Dorsolateral prefrontal and anterior cingulate cortex volumetric abnormalities in adults with attention-deficit/hyperactivity disorder identified by magnetic resonance imaging. *BPS* **60,** 1071–1080 (2006).
149. Sowell, E. R. *et al.* Cortical abnormalities in children and adolescents with attention-deficit hyperactivity disorder. *Lancet* **362,** 1699–1707 (2003).
150. Makris, N. *et al.* Cortical thinning of the attention and executive function networks in adults with attention-deficit/hyperactivity disorder. *Cereb. Cortex* **17,** 1364–1375 (2007).
151. Bush, G., Luu, P. & Posner, M. Cognitive and emotional influences in anterior cingulate cortex. *Trends Cogn. Sci. (Regul. Ed.)* **4,** 215–222 (2000).
152. Zametkin, A. J. *et al.* Cerebral glucose metabolism in adults with hyperactivity of childhood onset. *N Engl J Med* **323,** 1361–1366 (1990).
153. Rubia, K. *et al.* Hypofrontality in attention deficit hyperactivity disorder during higher-order motor control: a study with functional MRI. *AJP* **156,** 891–896 (1999).
154. Tamm, L., MENON, V., RINGEL, J. & REISS, A. L. Event-related FMRI evidence of frontotemporal involvement in aberrant response inhibition and task switching in attention-deficit/hyperactivity disorder. *J Am Acad Child Adolesc Psychiatry* **43,** 1430–1440 (2004).
155. Duncan, J. & Owen, A. M. Common regions of the human frontal lobe recruited by diverse cognitive demands. *Trends in Neurosciences* **23,** 475–483 (2000).
156. Goldman-Rakic, P. S. Topography of cognition: parallel distributed networks in primate association cortex. *Annu. Rev. Neurosci.* **11,** 137–156 (1988).
157. Wells, M. F., Wimmer, R. D., Schmitt, L. I., Halassa, M. M. & Feng, G. Thalamic reticular impairment underlies attention deficit in Ptchd1Y/− mice. *Nature* 1–20 (2016). doi:10.1038/nature17427
158. Krol, A., Wimmer, R. D., Halassa, M. M. & Feng, G. Thalamic Reticular Dysfunction as a Circuit Endophenotype in Neurodevelopmental Disorders. *Neuron* **98,** 282–295 (2018).
159. Sontag, T. A., Tucha, O., Walitza, S. & Lange, K. W. Animal models of attention deficit/hyperactivity disorder (ADHD): a critical review. *Atten Defic Hyperact Disord* **2,** 1–20 (2010).
160. Ferguson, S. A. & Holson, R. R. Neonatal dexamethasone on day 7 causes mild hyperactivity and cerebellar stunting. *Neurotoxicol Teratol* **21,** 71–76 (1999).
161. Levy, F. The dopamine theory of attention deficit hyperactivity disorder (ADHD). *Aust N Z J Psychiatry* **25,** 277–283 (1991).
162. Cook, E. H. *et al.* Association of attention-deficit disorder and the dopamine transporter gene. *The American Journal of Human Genetics* **56,** 993–998 (1995).
163. Gill, M., Daly, G., Heron, S., Hawi, Z. & Fitzgerald, M. Confirmation of association between attention deficit hyperactivity disorder and a dopamine

transporter polymorphism. *Molecular Psychiatry* **2,** 311–313 (1997).
164. Swanson, J. M. *et al.* Association of the dopamine receptor D4 (DRD4) gene with a refined phenotype of attention deficit hyperactivity disorder (ADHD): a family-based approach. *Molecular Psychiatry* **3,** 38–41 (1998).
165. LaHoste, G. J. *et al.* Dopamine D4 receptor gene polymorphism is associated with attention deficit hyperactivity disorder. *Molecular Psychiatry* **1,** 121–124 (1996).
166. Gizer, I. R., Ficks, C. & Waldman, I. D. Candidate gene studies of ADHD: a meta-analytic review. *Hum. Genet.* **126,** 51–90 (2009).
167. Li, D., Sham, P. C., Owen, M. J. & He, L. Meta-analysis shows significant association between dopamine system genes and attention deficit hyperactivity disorder (ADHD). *Hum. Mol. Genet.* **15,** 2276–2284 (2006).
168. Swanson, J. M. *et al.* Etiologic subtypes of attention-deficit/hyperactivity disorder: brain imaging, molecular genetic and environmental factors and the dopamine hypothesis. *Neuropsychol Rev* **17,** 39–59 (2007).
169. Childress, A. C. & Berry, S. A. Pharmacotherapy of attention-deficit hyperactivity disorder in adolescents. *Drugs* **72,** 309–325 (2012).
170. Wigal, S. B. Efficacy and safety limitations of attention-deficit hyperactivity disorder pharmacotherapy in children and adults. *CNS Drugs* **23 Suppl 1,** 21–31 (2009).
171. Volkow, N. D. *et al.* Depressed dopamine activity in caudate and preliminary evidence of limbic involvement in adults with attention-deficit/hyperactivity disorder. *Arch. Gen. Psychiatry* **64,** 932–940 (2007).
172. Wohl, M. *et al.* Lack of association of the dopamine transporter gene in a French ADHD sample. *Am. J. Med. Genet. B Neuropsychiatr. Genet.* **147B,** 1509–1510 (2008).
173. Wang, Y. *et al.* Lack of association between the dopamine transporter gene 3' VNTR polymorphism and attention deficit hyperactivity disorder in Chinese Han children: case-control and family-based studies. *Kobe J Med Sci* **53,** 327–333 (2008).
174. Hawi, Z. *et al.* No association of the dopamine DRD4 receptor (DRD4) gene polymorphism with attention deficit hyperactivity disorder (ADHD) in the Irish population. *Am. J. Med. Genet.* **96,** 268–272 (2000).
175. Fisher, S. E. *et al.* A genomewide scan for loci involved in attention-deficit/hyperactivity disorder. *The American Journal of Human Genetics* **70,** 1183–1196 (2002).
176. Ogdie, M. N. *et al.* A genomewide scan for attention-deficit/hyperactivity disorder in an extended sample: suggestive linkage on 17p11. *The American Journal of Human Genetics* **72,** 1268–1279 (2003).
177. Ogdie, M. N. *et al.* Attention deficit hyperactivity disorder: fine mapping supports linkage to 5p13, 6q12, 16p13, and 17p11. *The American Journal of Human Genetics* **75,** 661–668 (2004).
178. Zhou, K. *et al.* Meta-analysis of genome-wide linkage scans of attention deficit hyperactivity disorder. *Am. J. Med. Genet. B Neuropsychiatr. Genet.* **147B,** 1392–1398 (2008).
179. Arcos-Burgos, M. *et al.* Attention-deficit/hyperactivity disorder in a population

isolate: linkage to loci at 4q13.2, 5q33.3, 11q22, and 17p11. *The American Journal of Human Genetics* **75,** 998–1014 (2004).
180. Franke, B., Faraone, S. V., Asherson, P. & Buitelaar, J. The genetics of attention deficit/hyperactivity disorder in adults, a review. (2012). doi:10.1038/mp.2011.138
181. Bakker, S. C. *et al.* A whole-genome scan in 164 Dutch sib pairs with attention-deficit/hyperactivity disorder: suggestive evidence for linkage on chromosomes 7p and 15q. *The American Journal of Human Genetics* **72,** 1251–1260 (2003).
182. Hohmann, S. *et al.* Association of norepinephrine transporter (NET, SLC6A2) genotype with ADHD-related phenotypes: findings of a longitudinal study from birth to adolescence. *Psychiatry Research* **226,** 425–433 (2015).
183. Findling, R. L. Evolution of the treatment of attention-deficit/hyperactivity disorder in children: a review. *Clinical Therapeutics* **30,** 942–957 (2008).
184. Gonon, F. The dopaminergic hypothesis of attention-deficit/hyperactivity disorder needs re-examining. *Trends in Neurosciences* **32,** 2–8 (2009).
185. Rapoport, J. L. *et al.* Dextroamphetamine: cognitive and behavioral effects in normal prepubertal boys. *Science* **199,** 560–563 (1978).
186. Rapoport, J. L. & Inoff-Germain, G. Responses to methylphenidate in Attention-Deficit/Hyperactivity Disorder and normal children: update 2002. *J Atten Disord* **6 Suppl 1,** S57–60 (2002).
187. Gerlach, K. K., Dasgupta, N., Schnoll, S. H. & Henningfield, J. E. Epidemiology of stimulant misuse and abuse: implications for future epidemiologic and neuropharmacologic research. *Neuropharmacology* **87,** 91–96 (2014).
188. Harstad, E., Levy, S.COMMITTEE ON SUBSTANCE ABUSE. Attention-deficit/hyperactivity disorder and substance abuse. *PEDIATRICS* **134,** e293–301 (2014).
189. Pliszka, S. R. The neuropsychopharmacology of attention-deficit/hyperactivity disorder. *BPS* **57,** 1385–1390 (2005).
190. Dickstein, S. G., Bannon, K., Castellanos, F. X. & Milham, M. P. The neural correlates of attention deficit hyperactivity disorder: an ALE meta-analysis. *J Child Psychol Psychiatry* **47,** 1051–1062 (2006).
191. Goldsmith, D. R., Rapaport, M. H. & Miller, B. J. A meta-analysis of blood cytokine network alterations in psychiatric patients: comparisons between schizophrenia, bipolar disorder and depression. *Molecular Psychiatry* **21,** 1696–1709 (2016).
192. Hoekstra, P. J. Attention-deficit/hyperactivity disorder: is there a connection with the immune system? *Eur Child Adolesc Psychiatry* **28,** 601–602 (2019).
193. Güngör, S., Celiloğlu, Ö. S., Özcan, Ö. Ö., Raif, S. G. & Selimoğlu, M. A. Frequency of celiac disease in attention-deficit/hyperactivity disorder. *J. Pediatr. Gastroenterol. Nutr.* **56,** 211–214 (2013).
194. Minter, K. R., Roberts, J. E., Hooper, S. R., Burchinal, M. R. & Zeisel, S. A. Early childhood otitis media in relation to children's attention-related behavior in the first six years of life. *PEDIATRICS* **107,** 1037–1042 (2001).
195. Pelsser, L. M. J., Buitelaar, J. K. & Savelkoul, H. F. J. ADHD as a (non)

allergic hypersensitivity disorder: a hypothesis. *Pediatr Allergy Immunol* **20,** 107–112 (2009).
196. Schmitt, J., Buske-Kirschbaum, A. & Roessner, V. Is atopic disease a risk factor for attention-deficit/hyperactivity disorder? A systematic review. *Allergy* **65,** 1506–1524 (2010).
197. Tsai, S.-J. Signal transducer and activator of transcription 6 (STAT6) and attention-deficit hyperactivity disorder: a speculative hypothesis. *MEDICAL HYPOTHESES* **67,** 1342–1344 (2006).
198. Ceylan, M. F., Sener, S., Bayraktar, A. C. & Kavutcu, M. Changes in oxidative stress and cellular immunity serum markers in attention-deficit/hyperactivity disorder. *Psychiatry Clin. Neurosci.* **66,** 220–226 (2012).
199. Suwan, P., Akaramethathip, D. & Noipayak, P. Association between allergic sensitization and attention deficit hyperactivity disorder (ADHD). *Asian Pac. J. Allergy Immunol.* **29,** 57–65 (2011).
200. Schans, J. V. D., Çiçek, R., de Vries, T. W., Hak, E. & Hoekstra, P. J. Association of atopic diseases and attention-deficit/hyperactivity disorder: A systematic review and meta-analyses. *Neuroscience and Biobehavioral Reviews* **74,** 139–148 (2017).
201. Nielsen, P. R., Benros, M. E. & Dalsgaard, S. Associations Between Autoimmune Diseases and Attention-Deficit/Hyperactivity Disorder: A Nationwide Study. *J Am Acad Child Adolesc Psychiatry* **56,** 234–240.e1 (2017).
202. Instanes, J. T. *et al.* Attention-Deficit/Hyperactivity Disorder in Offspring of Mothers With Inflammatory and Immune System Diseases. *Biological Psychiatry* **81,** 452–459 (2017).
203. Hegvik, T.-A., Instanes, J. T., Haavik, J., Klungsøyr, K. & Engeland, A. Associations between attention-deficit/hyperactivity disorder and autoimmune diseases are modified by sex: a population-based cross-sectional study. *Eur Child Adolesc Psychiatry* **27,** 663–675 (2018).
204. Darwish, A. H., Elgohary, T. M. & Nosair, N. A. Serum Interleukin-6 Level in Children With Attention-Deficit Hyperactivity Disorder (ADHD). *J. Child Neurol.* **34,** 61–67 (2019).
205. Verlaet, A. A. J. *et al.* Oxidative stress and immune aberrancies in attention-deficit/hyperactivity disorder (ADHD): a case-control comparison. *Eur Child Adolesc Psychiatry* **28,** 719–729 (2019).
206. Köhler-Forsberg, O. *et al.* A Nationwide Study in Denmark of the Association Between Treated Infections and the Subsequent Risk of Treated Mental Disorders in Children and Adolescents. *JAMA Psychiatry* **76,** 271–279 (2019).
207. Ferri, S. L., Abel, T. & Brodkin, E. S. Sex Differences in Autism Spectrum Disorder: a Review. *Curr Psychiatry Rep* **20,** 9 (2018).
208. Lai, M.-C., Lombardo, M. V., Auyeung, B., Chakrabarti, B. & Baron-Cohen, S. Sex/gender differences and autism: setting the scene for future research. *J Am Acad Child Adolesc Psychiatry* **54,** 11–24 (2015).
209. Loomes, R., Hull, L. & Mandy, W. P. L. What Is the Male-to-Female Ratio in Autism Spectrum Disorder? A Systematic Review and Meta-Analysis. *J Am*

Acad Child Adolesc Psychiatry **56,** 466–474 (2017).
210. Amaral, D. G., Schumann, C. M. & Nordahl, C. W. Neuroanatomy of autism. *Trends in Neurosciences* **31,** 137–145 (2008).
211. Parellada, M. *et al.* The neurobiology of autism spectrum disorders. *Eur. Psychiatry* **29,** 11–19 (2014).
212. DiCicco-Bloom, E. *et al.* The developmental neurobiology of autism spectrum disorder. *J. Neurosci.* **26,** 6897–6906 (2006).
213. Minshew, N. J. & Williams, D. L. The New Neurobiology of Autism: Cortex, Connectivity, and Neuronal Organization. *Arch Neurol* **64,** 945–950 (2007).
214. Anagnostou, E. & Taylor, M. J. Review of neuroimaging in autism spectrum disorders: what have we learned and where we go from here. *Mol Autism* **2,** 4–9 (2011).
215. Polleux, F. & Lauder, J. M. Toward a developmental neurobiology of autism. *Ment Retard Dev Disabil Res Rev* **10,** 303–317 (2004).
216. Rubenstein, J. L. R. & Merzenich, M. M. Model of autism: increased ratio of excitation/inhibition in key neural systems. *Genes Brain Behav.* **2,** 255–267 (2003).
217. Muhle, R., Trentacoste, S. V. & Rapin, I. The genetics of autism. *PEDIATRICS* **113,** e472–86 (2004).
218. Rosenberg, R. E. *et al.* Characteristics and concordance of autism spectrum disorders among 277 twin pairs. *Arch Pediatr Adolesc Med* **163,** 907–914 (2009).
219. Ritvo, E. R., Freeman, B. J., Mason-Brothers, A., Mo, A. & Ritvo, A. M. Concordance for the syndrome of autism in 40 pairs of afflicted twins. *AJP* **142,** 74–77 (1985).
220. Hallmayer, J. *et al.* Genetic heritability and shared environmental factors among twin pairs with autism. *Arch. Gen. Psychiatry* **68,** 1095–1102 (2011).
221. Steffenburg, S. *et al.* A twin study of autism in Denmark, Finland, Iceland, Norway and Sweden. *J Child Psychol Psychiatry* **30,** 405–416 (1989).
222. Smalley, S. L., Asarnow, R. F. & Spence, M. A. Autism and genetics. A decade of research. *Arch. Gen. Psychiatry* **45,** 953–961 (1988).
223. O'Roak, B. J. *et al.* Multiplex Targeted Sequencing Identifies Recurrently Mutated Genes in Autism Spectrum Disorders. *Science* **338,** 1619–1622 (2012).
224. O'Roak, B. J. *et al.* Sporadic autism exomes reveal a highly interconnected protein network of de novo mutations. *Nature* **485,** 246–250 (2012).
225. Iossifov, I. *et al.* The contribution of de novo coding mutations to autism spectrum disorder. *Nature* **515,** 216–221 (2014).
226. Iossifov, I. *et al.* De Novo Gene Disruptions in Children on the Autistic Spectrum. *Neuron* **74,** 285–299 (2012).
227. Sanders, S. J. *et al.* Multiple recurrent de novo CNVs, including duplications of the 7q11.23 Williams syndrome region, are strongly associated with autism. *Neuron* **70,** 863–885 (2011).
228. Krumm, N., O'Roak, B. J., Shendure, J. & Eichler, E. E. A de novo convergence of autism genetics and molecular neuroscience. *Trends in Neurosciences* **37,** 95–105 (2014).

229. Sanders, S. J. *et al.* Insights into Autism Spectrum Disorder Genomic Architecture and Biology from 71 Risk Loci. *Neuron* **87,** 1215–1233 (2015).
230. Bourgeron, T. From the genetic architecture to synaptic plasticity in autism spectrum disorder. *Nat Rev Neurosci* **16,** 551–563 (2015).
231. Krishnan, A., Zhang, R., Yao, V. & Theesfeld, C. L. Genome-wide prediction and functional characterization of the genetic basis of autism spectrum disorder. *Nature* (2016). doi:10.1038/nn.4353
232. Bourgeron, T. A synaptic trek to autism. *Current Opinion in Neurobiology* **19,** 231–234 (2009).
233. Mbadiwe, T. & Millis, R. M. Epigenetics and autism. *Autism Research and Treatment* **2013,** 826156 (2013).
234. Dietert, R. R., Dietert, J. M. & Dewitt, J. C. Environmental risk factors for autism. *Emerg Health Threats J* **4,** 7111 (2011).
235. Matelski, L. & van de Water, J. Risk factors in autism: Thinking outside the brain. *Journal of Autoimmunity* **67,** 1–7 (2016).
236. Lyall, K., Schmidt, R. J. & Hertz-Picciotto, I. Maternal lifestyle and environmental risk factors for autism spectrum disorders. *Int J Epidemiol* **43,** 443–464 (2014).
237. Kinney, D. K., Barch, D. H., Chayka, B., Napoleon, S. & Munir, K. M. Environmental risk factors for autism: do they help cause de novo genetic mutations that contribute to the disorder? *MEDICAL HYPOTHESES* **74,** 102–106 (2010).
238. Gardener, H., Spiegelman, D. & Buka, S. L. Perinatal and neonatal risk factors for autism: a comprehensive meta-analysis. *PEDIATRICS* **128,** 344–355 (2011).
239. Chaste, P. & Leboyer, M. Autism risk factors: genes, environment, and gene-environment interactions. *Dialogues Clin Neurosci* **14,** 281–292 (2012).
240. Chow, M. L. *et al.* Age-Dependent Brain Gene Expression and Copy Number Anomalies in Autism Suggest Distinct Pathological Processes at Young Versus Mature Ages. *PLoS Genet* **8,** e1002592–14 (2012).
241. Ginsberg, M. R., Rubin, R. A., Falcone, T., Ting, A. H. & Natowicz, M. R. Brain transcriptional and epigenetic associations with autism. *PLoS ONE* **7,** e44736 (2012).
242. Ziats, M. N. & Rennert, O. M. Expression profiling of autism candidate genes during human brain development implicates central immune signaling pathways. *PLoS ONE* **6,** e24691 (2011).
243. Atladóttir, H. Ó. *et al.* Maternal Infection Requiring Hospitalization During Pregnancy and Autism Spectrum Disorders. *J Autism Dev Disord* **40,** 1423–1430 (2010).
244. Edmiston, E., Ashwood, P. & van de Water, J. Autoimmunity, Autoantibodies, and Autism Spectrum Disorder. *Biological Psychiatry* **81,** 383–390 (2017).
245. Chen, S.-W. *et al.* Maternal autoimmune diseases and the risk of autism spectrum disorders in offspring: A systematic review and meta-analysis. *Behavioural Brain Research* **296,** 61–69 (2016).

246. Atladóttir, H. Ó. *et al.* Association of family history of autoimmune diseases and autism spectrum disorders. *PEDIATRICS* **124,** 687–694 (2009).
247. Patterson, P. H. Maternal infection and immune involvement in autism. *Trends in Molecular Medicine* **17,** 389–394 (2011).
248. Vargas, D. L., Nascimbene, C., Krishnan, C., Zimmerman, A. W. & Pardo, C. A. Neuroglial activation and neuroinflammation in the brain of patients with autism. *Ann Neurol.* **57,** 67–81 (2005).
249. Voineagu, I. *et al.* Transcriptomic analysis of autistic brain reveals convergent molecular pathology. *Nature* **474,** 380–384 (2011).
250. Kohane, I. S. *et al.* The co-morbidity burden of children and young adults with autism spectrum disorders. *PLoS ONE* **7,** e33224 (2012).
251. Rossignol, D. A. Novel and emerging treatments for autism spectrum disorders: a systematic review. *Ann Clin Psychiatry* **21,** 213–236 (2009).
252. Curran, L. K. *et al.* Behaviors associated with fever in children with autism spectrum disorders. *PEDIATRICS* **120,** e1386–92 (2007).

Chapter 2

Microglial inflammasome activation may be required for normal brain development.

Material presented in this chapter has been adapted with permission from:
Chuang, H. C.*, Nichols, E. K.*, Rauch, I., Chang, W. C., bioRxiv, R. M., 2019. (n.d.). Defective cell death of distinct microglial subsets contributes to ADHD-like behavior in mice. *Biorxiv.org*. http://doi.org/10.1101/749390.
* = co-first authors.

Abstract

Microglia are resident immune cells in the central nervous system that play essential roles to maintain homeostasis and neuronal function[1-5]. Microglia are transcriptionally heterogeneous cells[6,7], but the mechanisms by which they contribute to normal brain development remain unclear. Here, we show that microglia in the developing striatum and thalamus undergo pyroptosis, a type of lytic cell death that occurs as a result of Caspase-1 (CASP1) activation downstream of inflammasomes[8]. We observe that pyroptosis occurs in a spatiotemporally regulated and Casp1-dependent manner during fetal brain development. Mice lacking Casp1 or the inflammasome regulating molecules, NLRP3, IL-1R, and Gasdermin D exhibit behavior changes characterized by hyperactivity, inattention, and impulsivity that are similar to attention-deficit/hyperactivity disorder (ADHD). Furthermore, re-expression of Casp1 in Cx3cr1+ cells, including microglia, restores normal behavior and cell death. We demonstrate that injection of an NLRP3 inhibitor into pregnant wild-type mice is sufficient to induce ADHD-like behaviors in offspring. These data suggest that microglial inflammasome activation and pyroptosis are essential for normal brain development, and that genetic and pharmacological disruptions in this pathway may represent new ADHD risk factors.

Introduction

2.1 Current animal models used to study ADHD.

ADHD is a neurodevelopmental disorder of unknown origins[9], so it is unsurprising that a multitude of rodent models of varying genetic and pharmacological manipulations have been proposed to study ADHD etiology. Often, these rodent mouse models have unclear genetics, such as the inbred spontaneously hypersensitive rat (SHR)[10,11] and the Naples high-excitability rat (NHR)[10,12]. A model using an environmental insult is also popular: the neonatal 6-hydroxydopamine (6-OHDA) lesioned mouse model[10]. The three SHR, NHR, and 6-OHDA models are considered to be among the most popular animal models used to study ADHD etiology due to their high face-validity to human ADHD symptoms: they all display core inattention, hyperactivity, and impulsivity behavioral defects[10,13]. Because these models have unclear genetics or require unnatural chemical lesions[13], I refer the reader to consider a number of reviews wherein these and other models of similar modalities are discussed in greater detail[10,14-20]. I focus the remaining discussion on available genetically modified mouse models that are highly validated[10].

The most validated genetically modified mouse model to study ADHD is the dopamine transporter knockout (DAT-KO) mouse[10,21]. The DAT-KO mouse lacks the dopamine transporter (encoded by the *Slc6a3* gene), and exhibit all three core symptoms of ADHD: hyperactivity, impulsivity, and inattention[21-26]. Furthermore, DAT-KO hyperactivity was ameliorated by the drugs methylphenidate (MPH) and amphetamine (AMPH)—drugs used to treat ADHD in people[21,22,27]—suggesting that the DAT-KO mouse model has predictive value for exploring ADHD correlates to the human condition. The DAT-KO mouse is particularly popular because it has a disrupted dopamine system. The “dopamine hypothesis” has gained traction as one of the better-supported hypotheses of ADHD neurobiology[28], and is discussed more in the main Introduction (section 1.3). Thus, the DAT-KO mouse has “construct validity” in that it matches the theorized neurobiological basis of ADHD in people[29,30].

Briefly, other highly validated genetically modified ADHD mouse models include the Coloboma or *Snap25*-mutant mouse[21,31-33], the neurokinin-1 receptor knockout (NK1R-KO) mouse[21,34,35], and the mutant human thyroid hormone receptor beta gene knock-in[36-38]. All three of these mice exhibit the three core symptoms of ADHD: hyperactivity, impulsivity, and inattention, and MPH and/or AMPH attenuated the hyperactivity in these models[32,36-39]. At least seventeen additional mouse models have been proposed to study ADHD; they are reviewed by *de la Peña et al.*[21].

Genetic models have their limitations. Learning from the case of autism spectrum disorder (ASD), any one identified genetic mutation accounts for an extreme minority of all ASD cases, since a great multitude of risk genes have been identified (see Introductory Chapter 1.5 for details). Because of this, we may speculate that models relying on a single risk gene for either ADHD or ASD may not recapture the full aspects of neurodevelopmental disorder etiology. Another explanation is that multiple risk genes suggest multiple underlying mechanisms, all of which produce a similar neurobiological endophenotypes categorized as ADHD. These are reasons that studies using ADHD animal models should be cautiously interpreted despite the best efforts to match face,

predictive, and construct validity to ADHD in people. Using models that seem to prove the current concept(s) of ADHD etiology is also dangerous, because this may hinder and constrain identification of novel mechanisms that could lead to improved treatment options.

The considerations described above for ADHD genetic mouse models suggest yet another aspect of ADHD etiology: there are environmental components to ADHD that may facilitate or even drive ADHD behaviors that account for the remaining cases in the population that are not caused by a single and highly-penetrant mutation. The maternal-fetal environment during brain development is an example. Maternal immunity is one such risk factor already discussed in section 2.1 of this chapter.

2.2 Inflammasome activation and lytic cell death.

The study described in this chapter comes from a serendipitous discovery that involves inflammasome biology. In this section, I will discuss current concepts related to inflammasome activation and lytic cell death.

Inflammasomes are multimeric protein complexes that sense intracellular damage-associated molecular pattern (DAMP) and pathogen-associated molecular pattern (PAMP) signals. Inflammasome activation happens as a result of tissue damage and infection[8,40,41]. Inflammasomes activate pro-CASP1 and cleave multiple substrates that include the pro-inflammatory cytokines interleukin 1 beta (IL-1β) and interleukin 10 (IL-18) [8,40,41]. This action results in the cleavage of gasdermin D (GSDMD), the terminal executioner protein of the inflammasome cascade that oligomerizes into a pore at the surface of the cell[42-44]. Formation of the pore allows contents to exit and enter the cell, causing a characteristic swelling before lysis[42-44]. This lytic cell death is termed *pyroptosis*, and pyroptosis is thought to launch adaptive immunity by exposing intracellular DAMPs and PAMPs to the extracellular space where antigen-presenting cells can engulf them[45]. Thus, inflammasome biology constitutes an arm of innate immunity. This type of innate immunity has been defined relatively recently—in the 2000s[40]—compared to the classically defined methods of pathogen sensing (such as through Toll-like receptors; TLRs)[46].

Upstream of CASP1 are the sensor and adaptor proteins that recognize specific DAMP and PAMP stimuli; these are named after their structural domains[8,41]. The more famous and well characterized of these include the NLRs (nucleotide-binding domain and leucine-rich repeat containing) and CARD (Caspase activation and recruitment domain) containing adaptor molecule ASC (apoptosis-associated speck-like protein containing a CARD). I will discuss a few of the better-described upstream inflammasome proteins: NLRP1, NLRP3, NAIP-NLRC4, and AIM2. NLRP1 was the first NLR to be shown to form an inflammasome complex, and is responsive to *Bacillus antracis* lethal toxin[40,41,47,48]. NLRP3 responds to a wide array of diverse stimuli: extracellular ATP, pore-forming toxins, particulate matter, and many pathogens[49]. The NAIP-NLRC4 inflammasome responds to bacterial flagellin and the rod and needle subunits of bacterial type 3 secretion systems[41,45]. The AIM2 inflammasome responds to foreign cytosolic DNA, such as that coming from DNA viruses and intracellular bacterial infections[8,41].

While multiple sensors may form the inflammasome complex, the majority of them converge at pro-CASP1 cleavage; these are representing the so-called canonical inflammasome signaling pathway. Non-canonical inflammasome signaling pathway exists and converges on pro-caspase-11 cleavage; caspase-11 then cleaves GSDMD prior to pore formation and pyroptosis[50,51]. Thus, pyroptosis is distinguished from apoptosis by cleavage of pro-CASP1 or pro-caspase-11 instead of pro-caspase-3[52]. Other distinguishing features of pyroptosis from apoptosis are how the cells die. Apoptosis is considered to be more "immunologically silent"—meaning, there is limited release of intracellular contents due to a coordinated shrinkage and a "blebbing" that occurs, while pyroptosis involves cell swelling and expulsion of intracellular contents[45,53,54]. Another distinguishing feature is ASC speck formation for most, but not all, inflammasome activation pathways[8,41,45,55]. ASC specks are visualized by microscopy, and are indicative of active caspase-1 cleavage[8,41,45,55]. Thus, there are four major hallmarks of inflammasome activation (in order of the inflammasome cascade events): ASC speck formation, CASP1 cleavage, enlarged cell volume, and IL-1β/IL-18 release[8,41,45,53-55]. However, it should be noted that these hallmarks are often, but not always, guaranteed indicators of activation for each of the described upstream inflammasome sensors; I refer the reader to a few excellent reviews for more details[8,41,45].

While pyroptosis is clearly important for attenuation and resolution of infection[45], it is unknown whether or not pyroptosis plays a developmental role during organogenesis. Since pyroptosis occurs in tissue damage and infectious contexts, and results in pro-inflammatory cytokine production[45], it is not expected to occur in development because tissue damage or infection in the fetus is not expected to occur. Furthermore, pro-inflammatory compounds are generally regarded as harmful; they are another reason why we would not expect pyroptosis to be active during organogenesis. Meanwhile, it is very well appreciated that apoptosis is critical for normal development[56].

Contrary to our expectations, we discovered that Caspase-1 knockout mice (*Casp1*$^{-/-}$) had striking behavior changes that reminded us of core ADHD-like behavioral traits—suggesting a developmental role of inflammasomes in shaping normal brain development. These data are shared and discussed in the subsequent sections of this chapter. First, I discuss known cases of inflammasome activation (and the action of IL-1β, IL-18) within the brain.

2.3 Known cases of inflammasome activation in the brain.

Inflammasome biology research has centered on cells of the myeloid lineage, because myeloid cells are the main sentinels to injury and infection in tissues and as a result are well equipped with a wide array of damage and pattern recognition receptors[57-59]. As a result, the literature concerning inflammasome biology and the brain has typically been examined in microglial cells, which are the principle innate immune cell of the central nervous system (as discussed in the main Introduction of this dissertation in section 1.1)[1,3,60,61]. The most common investigated inflammasome in the brain is the NLRP3 inflammasome[62], and the NLRP3 inflammasome has been implicated in the context of several brain pathologies: Alzheimer disease (AD)[62-64], Parkinson disease (PD)[62,65-67], amyotrophic lateral sclerosis (ALS)[62,68-70], viral infections

in the brain[62,71-73], and traumatic brain injury (TBI)[62,74,75]. NLRP3 expression appears be mostly restricted to microglia in homeostasis[62,76], but is detected in mice or rats in certain disease contexts[62,68,77,78]. Other inflammasomes have been studied, though to a lesser degree: the NLRP1b, NLRP2, NLRC4, and AIM2[62,79]. Because NLRP3 is the best-characterized inflammasome in the brain, and is most relevant to our study presented herein, I will focus most of the remaining discussion about known cases of the NLRP3 inflammasome activation in the brain. The excellent reviews of Heneka and colleagues[62] (and others[79]**)** have guided the discussion herein, as case examples are not exhaustive of all of the available literature. I direct the reader to these reviews for more detailed information about non-NLRP3 inflammasome activation in the brain.

The microglia-mediated immune response is increasingly being appreciated for having a clear association to AD pathology[80-83]. In this context, the NLRP3 inflammasome has been most frequently investigated. The famous hallmarks of AD pathogenesis are the accumulation and deposition of fibrillar Aβ and intraneuronal formation of neurofibrillary tangles (NFTs) composed of tau proteins[84]. Both Aβ and NFT, upon accumulation into plaques, become DAMPs known to activate microglial NLRP3 inflammasomes[62,79,85]. This was first shown *in vitro* in which fibrillar Aβ induced IL-1β release in an NLRP3- and ASC-dependent manner[62,85]. Incubation with z-YVAD, a CASP1 inhibitor, inhibited IL-1β release[62,85]. In mice, Aβ injection into the striatum caused an increase in cell surface expression of the glycoprotein F4/80 in microglia and macrophages, suggesting an activation phenotype; this phenomenon was abolished in ASC, CASP1, IL-1R, and MYD88 knockout mice[62,85]. These data suggest that Aβ initiates a cascade involving MYD88 activation, and the NLRP3 inflammasome ultimately cleaves CASP1[62,85]. A series of experiments were done with transgenic mice that express known genes and mutations with familial early-onset AD. These are amyloid precursor protein (APP) and presenilin 1 (PS1) containing an exon 9 deletion (APP/PS1) mice; these were crossed with NLRP3-knockout mice[62,86]. Strikingly, these mice showed signs of two-fold enhanced Aβ phagocytosis and increased expression of insulin-degrading enzyme (IDE) [62,86], which has been shown previously to degrade extracellular Aβ[87]. NLRP3 was restricted to microglia, so it was concluded that the NLRP3 inflammasome in microglia were responsible for enhanced Aβ clearance[62,86]. There was also attenuation of neuronal spine loss in the neocortex, and hippocampal long-term potentiation (LTP; measure for memory consolidation) was protected[62,86]. APP/PS1-NLRP3$^{-/-}$ mice performed better in several behavior tests assaying many learning and memory paradigms compared to APP/PS1 mice alone[62,86]. NLRP3$^{-/-}$ mice alone did not show any behavioral deficits in LTP or spatial memory performance[62,86],. And strikingly, ASC specks were detected in activated microglia cells, solidifying that inflammasome activation and pyroptosis were underway[62,86]. Furthermore, ASC specks were shown to seed Aβ deposition[62,88]. Taken altogether, the data suggest a model that innate immune cell pyroptosis in the brain by microglia is involved in the early stages of Aβ deposition and AD progression[62].

PD is another context in which NLRP3 inflammasome activation has been discovered. PD pathology involves alpha-synuclein protein (α-Syn), a pre-synaptic protein, which becomes fibrillar and disrupts cell homeostasis and precipitates neural cell death[89]. Fibrillar α-Syn was shown to increase microglial IL-1β release in a CASP1 dependent manner[62,65-67]. α-Syn may utilize a TLR-MYD88-mediated signaling pathway

for microglial inflammasome activation, as α-Syn activation was blocked by an anti-TLR2 antibody in human monocytes[62,65,90] consistent with the idea that the NLRP3 inflammasome needs initial priming by TLR signaling[49]. α-SynA53T mutant mice model PD by overexpressing α-Syn, crossed into a CASP1 knockout mouse resulted in a strong reduction of microglial immunoreactivity[62,66]. α-Syn and inflammasomes may engage in a vicious cycle of activation: α-Syn can be truncated by CASP1 cleavage itself, increasing the chances of oligomerization and additional inflammasome activation and cytokine release; this outcome further exacerbates neural death[62,91]. Inhibition of inflammasome activation is therefore neuroprotective in the PD context[62].

Signs of inflammasome activation were found in ALS mouse models and human patients. In humans, mutations in the superoxide dismutase 1 (SOD1) gene, like SOD1G93A, cause familial forms of dominantly inherited ALS[62,68,69]. A mouse model carries this mutation. In SOD1G93A mice, CASP1 is cleaved in an NLRP3- and ASC-dependent manner[62,68,69]; these data suggest that mutant SOD1 expression itself (and related consequences thereof) are sufficient to drive NRLP3 inflammasome activation and IL-1β release. Genetic ablation of CASP1 and IL-1β crossed into the SOD1G93A line had the following effects: prolonged survival of these mice, reduced choline acetyltransferase (ChAT) motor neuron death in the spinal cord, and reduced astrocytic and microglial activation[62,68,69]. In the cerebrospinal fluid of sporadic ALS cases, significantly higher amounts of the cytokine IL-18 was found, suggesting the outcome of inflammasome activation[62,70]. In support of this, increased detection of NLRP3, ASC, cleaved CASP1, and mature IL-18 were found in the spinal cords of similar ALS patients[62,68].

In the previous case examples, DAMP signals were found to activate inflammasomes in the brain. Unsurprisingly, PAMPs from viral infections in the brain were also found to activate inflammasomes. One example comes from HIV infection. HIV infections produce a neurocognitive disorder (called HANDs) in up to half of infected patients[92]. Signs and symptoms of HANDs include learning, memory, and executive dysfunctions[92]. mRNA levels of IL-1β/IL-18 were increased in HIV-infected brains[62,71]. In an *in vitro* model of human microglial infection by HIV, ASC speck formation was dependent on the NLRP3 inflammasome with subsequent IL-1β release[62,71]. The HIV-1 transactivator of transcription (Tat) protein was found to be instrumental for NLRP3 and ASC upregulation and increase in CASP1 cleavage and IL-1β release[62,72]. A similar trend was seen with the HIV-1 viral protein R (Vpr)[62,73]. In Vpr transgenic mice, the CASP1 inhibitor VX-765 improved behavioral deficits[62,73] suggesting a CASP1 dependent mechanism downstream of inflammasome activation.

The above discussion was mostly centered on microglial inflammasome sensing in the brain, with some evidence for contributions from astrocytes[62]. Are neurons themselves capable of inflammasome sensing? Case examples from traumatic brain injury and colitis suggest that neurons are indeed capable of inflammasome activation and pyroptosis. In a spinal cord injury model (SCI) in rats, increased CASP1 and caspase-11 cleavage (and resulting IL-1β/IL-18 secretion) was detected post-SCI in motor neurons[62,74]. This was found to be NLRP1b- and ASC-dependent[62,74]. The AIM2 inflammasome was also involved in neurons. Using an AIM2 activator caused ASC specks to form, as well as CASP1 cleavage and IL-1β release in embryonic cortical neurons—indicating pyroptosis[62,75]. Neuronal pyroptosis was prevented by addition of a

cell-permeable irreversible inhibitor of CASP1, Ac-YVAD-CMK[62,75]. In humans, CSF derived from TBI patients induced AIM2 activation, CASP1 cleavage, and neuronal pyroptosis *in vitro*[62,75]. This process was abolished with the addition of an ATP release channel inhibitor, suggesting this is a death signal for neuronal pyroptosis[62,75]. In a rat model of cerebral cortex TBI, NLRP3 activation (and downstream effectors) were detectable six hours after TBI[62,78]. NLRP3 itself was found in neurons, microglia, and astrocytes [62,78]. However, in mice, a similar model did not find a neuroprotective effect from either an NLRP1 or ASC knockout despite increased IL-1β levels[62,93]. There is an intriguing case example of neuronal pyroptosis in enteric gut neurons that innervate the colon. Using experimental mouse models of colitis, *Gulbransen et. al* found that inflammation activates a neuronal signaling complex comprised of P2X7 receptors, pannexin-1 channels, ASC, and caspases that lead to neuron death[94]. However, it is unclear if this is neuronal pyroptosis, because IL-1β was not a feature of neuron death, and the authors used a pan-caspase inhibitor (zVAD(OMe)-fmk) so the requirement for CASP1 in this phenomena is unknown[94]. In another case example from the gut, exclusive production of IL-18 from neurons was necessary for barrier protection from the microbe *Salmonella typhimurium*[95]. This is intriguing because IL-18 production is generally thought to be restricted to immune cells. Altogether, these data force us to realize that we shouldn't expect inflammasome activation to be entirely restricted to immune cells. I believe that further investigation is required to fully understand which inflammasome proteins are present in all brain cells during homeostasis, and which are upregulated during tissue distress.

IL-1β and IL-18 cytokines are produced as the final outcome of inflammasome activation. What are the known effects on bystander cells, particularly for neurons? Since attenuating inflammasome activation (and/or the products thereof) by antibodies, chemical inhibition, or genetic deficiency ameliorated the neurological symptoms in the variety of models discussed above, we may infer that IL-1β is generally neurotoxic. Further studies are needed to characterize the distribution of inflammasome protein and cytokine release in the brain during homeostasis and disease.

To conclude, the discussed studies above solidify competent microglia-mediated (and neural-mediated) inflammasome sensing, pyroptosis, and IL-1β/IL-18 release in the brain, with relevance to neurodegenerative and infectious conditions. Our own data surprisingly suggest that microglia-mediated inflammasome activation and pyroptosis may occur in development. The subsequent sections in this chapter will present and discuss the results.

Results

2.4 Mice deficient in caspase-1 exhibit behaviors reminiscent of ADHD.

In the beginning of this study, we originally wanted to test the hypothesis that CASP1 deficient mice (*Casp1*$^{-/-}$) are protected against maternal immune activation (MIA), a mouse model of autism spectrum disorder (ASD) (as discussed in Chapter 3). Our rationale was that, since an inflammasome protein was identified as an ASD risk gene, perhaps the absence of CASP1 would be neuroprotective[96]. To infer baseline *Casp1*$^{-/-}$ behaviors, we performed a number of behavior assays targeting key traits: sociability, anxiety, learning & memory, depression, hyperactivity, and restricted-repetitive behaviors. For sociability, three assays were utilized: the reciprocal social interaction, three-chamber, and food preference social transmission assays. For anxiety-like behaviors, we used the elevated plus maze and the open field assay (center vs. peripheral ratio). For learning and memory, the T-maze and fear conditioning (contextual and cued) assays were used. For depression, the force-tail suspension test was utilized. For hyperactivity-like behaviors, we relied on the open field assay for general movement. For repetitive-restricted-like behaviors, the marble burying and open field (for grooming) assays were used. For most behaviors presented here, we first used *Casp1*$^{-/-}$*Casp11*$^{-/-}$ mice that were available to us (a kind gift from Russell Vance); unless otherwise noted, these mice will be referred to as *Casp1*$^{-/-}$ mice.

To our surprise, male *Casp1*$^{-/-}$ mice exhibited an intriguing pattern of behavior changes at baseline. Not all behaviors were affected—only a discrete set of behavior changes were observed. Male *Casp1*$^{-/-}$ mice had traveled a significantly greater amount of distance during the open field assay, suggesting a more hyperactive phenotype relative to WT controls (**Figure 2.1A**). Male *Casp1*$^{-/-}$ mice also spent more time exploring the open arms of the elevated-plus maze assay, suggesting a hypo-anxious phenotype compared to WT (**Figure 2.1B**). Though, it is possible that an innately higher level of activity drove this behavior. Strangely, male *Casp1*$^{-/-}$ mice also had a statistically significant tendency relative to WT mice in climbing the behavior apparatus during the three-chamber assay (**Figure 2.1C**). Combined with the result from the elevated-plus maze assay, we interpreted this result as a possible indicator of impulsivity. The other behaviors we tested in male *Casp1*$^{-/-}$ mice (sociability, learning & memory, and repetitive-restricted behaviors were comparable to WT (data not shown). Intriguingly, female *Casp1*$^{-/-}$ mice had no behavior changes compared to WT (data not shown). Therefore, we captured a male bias in our dataset.

We collectively interpret these alterations in male *Casp1*$^{-/-}$ mice as “ADHD-like” behavior changes, as they are similar to what has been observed from other established mouse models of ADHD[10]—including the male bias. Since inattention is a core diagnostic symptom of ADHD (along with hyperactivity and impulsivity), we also wanted to use an assay to measure attention. We chose the five-choice serial reaction time task (5-CSRTT) in which mice are trained to pay attention to a stimulus light; this appears to be a standard assay in evaluating rodent models of ADHD[10,15,97]. Upon seeing the light, the mouse learns to poke its nose into an aperture to retrieve a food pellet reward dispensed by a magazine. Upon subsequent trials, the duration of the light stimulus decreases; the mouse must pay attention to the light stimulus in order to know when to retrieve the food pellet reward. In contrast to the previous assays, this

experiment was run on a pure *Casp1*$^{-/-}$ background. Relative to WT controls, male *Casp1*$^{-/-}$ mice had a significantly decreased percent accuracy of nose pokes (**Figure 2.1D**); in an attempt to retrieve a food pellet, they erroneously poked their noses in multiple apertures regardless of light stimulus. These data suggest that male *Casp1*$^{-/-}$ mice are less attentive than their WT counterparts. We interpret this result as male *Casp1*$^{-/-}$ mice having an inattentive phenotype.

Taken altogether, we suggest that male *Casp1*$^{-/-}$ mouse behavior changes are reminiscent of ADHD-like behavior changes. Because *Casp1*$^{-/-}$ mice had behavior changes that deviated significantly from WT, we inferred that inflammasome activation itself is important to establish normal behaviors. We further reasoned that, if this is indeed the case, mice deficient in the upstream and downstream inflammasome pathway elements would phenocopy male *Casp1*$^{-/-}$ mouse behavior patterns.

2.5 Mice deficient in Nlrp3*,* Gsdmd*, and* Il1r1 *exhibit behavioral tendencies reminiscent of ADHD.*

Since CASP1 is downstream of a wide array of inflammasome proteins, and upstream of effectors gasdermin D and IL-1β (**Figure 2.3A** and as discussed in section 2.2 of this chapter), we sought to test mice deficient in upstream and downstream inflammasome pathway elements. We reasoned that, since there is no expected damage or infection to the fetus *in utero*, the inflammasome protein most likely to be activated is the NLRP3 inflammasome, which is activated by a multitude of stimuli. During brain development, it is known that there is a high degree of apoptosis[56]; perhaps, any limited release of intracellular contents from dying cells could activate the NLRP3 inflammasome. We also chose to test gasdermin D (*Gsdmd*$^{-/-}$) deficient mice, because GSDMD is the terminal executioner protein of inflammasome activation and pyroptosis. We also tested mice deficient in IL-1β sensing; as such, we used the IL-1R knockout mouse line (*Il-1r*$^{-/-}$ mice). Therefore, both upstream and downstream elements of inflammasome activation and sensing are represented in our behavior analyses.

Strikingly, the *Nlrp3*$^{-/-}$, *Gsdmd*$^{-/-}$, and *Il-1r*$^{-/-}$ male mice phenocopied many of the male *Casp1*$^{-/-}$ behavior changes. Male *Nlrp3*$^{-/-}$, *Gsdmd*$^{-/-}$, and *Il-1r*$^{-/-}$ mice traveled a significantly greater distance in the open field assay (**Figure 2.3B,E**) and spent more time in the open arms of the elevated-plus maze assay (**Figure 2.3C,F**). Male *Gsdmd*$^{-/-}$, but not *Il-1r*$^{-/-}$, mice exhibited a statistically significant tendency to climb the behavioral apparatuses within the three-chamber assay (**Figure 2.3D,G**). We did not run *Nlrp3*$^{-/-}$, *Gsdmd*$^{-/-}$, and *Il-1r*$^{-/-}$ mice in the 5-CSRTT assay. However, we interpret that male *Nlrp3*$^{-/-}$, *Gsdmd*$^{-/-}$, and *Il-1r*$^{-/-}$ mice phenocopy *Casp1*$^{-/-}$ mouse hyperactivity. *Nlrp3*$^{-/-}$ and *Gsdmd*$^{-/-}$ also phenocopied *Casp1*$^{-/-}$ mouse impulsivity. We also recaptured the male bias—female *Nlrp3*$^{-/-}$, *Gsdmd*$^{-/-}$, and *Il-1r*$^{-/-}$ mouse behavior was normal compared to WT (data not shown). Compellingly, a previous publication also found that *Il-1r*$^{-/-}$ mice exhibited hyperactivity and low anxiety[98].

2.6 Re-expression of CASP1 in a Cx3cr1*-dependent manner restores behavior changes to WT levels.*

Collectively, we identified a core set of behavior changes in mice deficient in the inflammasome pathway. Because not all behavioral traits were impacted, these data suggest that a subset of cells in the developing brain have the NLRP3 inflammasome activated. Since the current dogma is that inflammasome is restricted to the myeloid lineage, we wanted to test if CASP1 expression in the myeloid compartment would rescue WT behaviors on an otherwise CASP1 deficient mouse background. Because the *Casp1* deficient mice we used previously are also deficient in *Casp11*, we wanted to test the requirement of *Casp1* to the behavioral abnormalities.

To do so, we took advantage of the inducible *Casp1* expression line (*iCasp1* mice[99]) in which we can re-express CASP1 in a *Cx3cr1*-dependent manner (termed *iCasp1* mice) on an otherwise *Casp1*$^{-/-}$ background. CX3XR1^{+} cells are myeloid—they include microglia, monocytes, and border-associated macrophages[100]. It is not expected that neural cells have CX3CR1 expression. Therefore, in these *iCasp1* mice, Cre will recombine the stop-flox-cassette in CX3CR1^{+} cells, allowing for *Casp1* transcription. We bred male *Casp1*$^{-/-}$*;iCasp1;Cx3cr1-Cre* mice with *Casp1*$^{-/-}$*; iCasp1* female mice such that each litter had "control" mice (*Casp1*$^{-/-}$*;iCasp1*—effectively *Casp1*$^{-/-}$ mice with an intact stop-flox-cassette) and "experimental" mice (*Casp1*$^{-/-}$*;iCasp1;Cx3cr1-Cre*—CASP1 expression in CX3CR1^{+} cells) (**Figure 2.3A**). Since obtaining WT mice was not possible in this cross, we used age-matched WT mice for comparisons. Notably, in our system, *Casp1*$^{-/-}$*;iCasp1;Cx3cr1-Cre* had almost three-fold higher expression of *Casp1* compared to WT mice (**Figure 2.5E**).

Strikingly, experimental male *Casp1*$^{-/-}$*;iCasp1;Cx3cr1-Cre* mice traveled a comparable amount of distance to WT mice in the open field assay, while the control male *Casp1*$^{-/-}$*;iCasp1* mice traveled a significantly greater amount of distance (**Figure 2.3B**). These data suggest that the re-expression of CASP1 in CX3CR1^{+} cells restored hyperactivity seen in male *Casp1*$^{-/-}$ mice to baseline levels. Male *Casp1*$^{-/-}$*;iCasp1;Cx3cr1-Cre* mice did not spend a significantly greater amount of time in the open arms comparable to WT mice in the elevated plus maze assay, while the control *Casp1*$^{-/-}$*;iCasp1* mice spent a greater amount of time in the open arms (**Figure 2.3C**). The experimental male *Casp1*$^{-/-}$*;iCasp1;Cx3cr1-Cre* mice also did not climb the behavior apparatus of the three-chamber assay as often as the control *Casp1*$^{-/-}$*;iCasp1* mice (**Figure 2.3D**). These data suggest that the re-expression of CASP1 in CX3CR1^{+} cells restored impulsive characteristics seen in male *Casp1*$^{-/-}$ mice to baseline levels.

Collectively, these data suggest that CASP1 re-expression in the CX3XR1^{+} cell compartment restores the ADHD-like behavioral traits of hyperactivity and impulsivity to baseline WT levels, and that CASP1, and not CASP11, is important for the behavioral phenotype. We initially interpreted these data as CASP1 expression in the myeloid cell compartment as being important for helping to establish normal behaviors in mice. However, a paper from *Haimon et. al* proposed that CX3CR1 expression has leakiness in the neural compartment[101], which may complicate our interpretation of this data. Essentially, *Haimon et. al's* RiboTag analysis revealed that developmental *Cx3cr1*-Cre (but not inducible *Cx3cri*^{CreER}) had rearrangements in neurons[101]. In order to double check that *Casp1* and *Nlrp3* mRNA was enriched in the myeloid cell fraction, and not neural cell fraction, we obtained CD45^{+}Cd11b^{+} myeloid and CD45^{-}Cd11b^{-} neural cell mRNA from E14.5 embryonic brains and performed RT-qPCR. Indeed, *Casp1* and *NLRP3* mRNA was significantly enriched in the CD45^{+}Cd11b^{+} myeloid cell fraction

relative to the $CD45^{-}Cd11b^{-}$ neural cell fraction (**Figure 2.5A,B**). In contrast, *Cd200* and *Celf4* mRNA shown to be "contaminating" neural transcripts in the *Cx3cr1*-GFP^{+} fraction in Haimon and colleagues' RiboTag data, were highly enriched in the *Cx3cr1*-GFP^{-} cell fraction of fetal E14.5 brains compared to the *Cx3cr1*-GFP^{+} cell fraction **Figure 2.5C,D**). We inferred that neural expression of *Cx3cr1* may occur later in brain development.

We reasoned that microglia might be the most populous of the $CD45^{+}Cd11b^{+}$ myeloid cell fraction in the developing brain, as they seed the brain approximately day E10.5 in development (as discussed in the main Introduction, section 1.2). Because microglia are defined as $CX3CR1^{+}$ cells in the brain parenchyma, we next used an imaging approach to see if we can detect active microglial inflammasome activation and pyroptosis in the developing fetal brain.

2.7 In the fetal brain, microglial pyroptosis may occur in a spatiotemporal manner.

Since there were no significant behavior changes across all traits assayed in male *Casp1*$^{-/-}$ mice—only a select few—we reasoned that if indeed microglial inflammasome activation and pyroptosis were taking place, it would occur in discrete brain regions. Furthermore, we reasoned that if the NLRP3 inflammasome were active, it would likely be active during the onset of neurogenesis (~E12.5 as discussed in the main Introduction) and resolve after the majority of neural populations have been generated and the cellular basis of circuits established (~E16.5 as discussed in the main Introduction) because that is when the greatest amount of neural apoptosis and possible DAMP release is happening[54,102,103].

In order to test our hypothesis that microglial inflammasome activation and pyroptosis is occurring during fetal brain development, I developed an imaging screening method for two main reasons: we anticipated a discrete nature of the phenomena with limited knowledge as to which brain regions are involved, and traditional methods of serial sectioning and staining are difficult and laborious for embryonic tissues. To improve our chances of visualizing possible microglial inflammasome activation and pyroptosis, I combined a tissue clearing method, CUBIC[104,105], and lightsheet fluorescence microscopy (LSFM), on E12.5, E14.5, and E16.5 embryos (**Figure 2.4A**). Combining a tissue clearing methods and LSFM allowed for an unbiased acquisition of the entirety of the developing brain. Instead of physically sectioning tissue, LSFM allowed for serial optical sections thinner than that which is easily acquired with a frozen cryostat[106-109]. After imaging, sections were reconstructed in three dimensions. It is possible to reconstruct entire embryonic bodies and individual brain sections at once (**Figure 2.4B**). As we anticipated, we visualized *Cx3cr1*-GFP^{+} cells in the parenchyma and brain borders, including the neurogenic zone (**Figure 2.4C**).

Visualizing pyroptosis is technically challenging, and the most common method is to use the propidium iodide (PI) dye for staining[43,110-113]. The PI dye has to intercalate with DNA in order to fluoresce. Since pyroptosis is a lytic form of cell death, we reasoned that GSDMD pores will allow PI dye inside cells where it can intercalate with exposed DNA[110]. In contrast, blebbing and contraction of a cell during apoptosis occurs with no pore formation; it is not expected that PI will highlight apoptotic cells. We also reasoned that, after lysis, PI can intercalate with DNA in the extracellular environment. It

should be noted that using PI is not an exclusive dye for pyroptosis, because other forms of cell death can also be lytic, such as necroptosis[114]. However, since we are utilizing this method as a screening tool and intended to validate inflammasome activation with a secondary method and mutant mice, we reasoned using PI was a good first start. We intravenously injected E12.5-E16.5 WT dams (crossed to male *Cx3cr1-GFP*$^{+/+}$ mice; embryos are *Cx3cr1-GFP*$^{+/-}$) with PI for at least ten minutes before collecting embryos for tissue processing (**Figure 2.6A**). Heterozygous *Cx3cr1-GFP*$^{+/-}$ litters allowed for visualization of brain myeloid cells (including microglia, monocytes, and border-associated macrophages[100]). If microglial pyroptosis is occurring, we would expect to see GFP signal in the brain parenchyma co-localize with the PI signal, resulting in high-intensity pixels.

Intriguingly, we observed co-localization of *Cx3cr1*-GFP^{+} and PI signal primarily occurred in two regions of the fetal brain of male mice: the lateral ganglionic eminence (LGE) and primitive thalamus (iTh) of the brain parenchyma (**Figure 2.6B-D**). These clusters started at day E12.5 (**Figure 2.6B,D**), reached a flourish and E14.5 (**Figure 2.6C**), and largely diminished at E16.5 (data not shown). These data suggest that two major loci in the fetal brain are undergoing lysis, and that these cells are likely microglial due to their presence in the brain parenchyma.

Since PI is not exclusive to pyroptosis, we sought additional validation. Since the NLRP3 inflammasome involves ASC[49], we wanted to see if we would find ASC speck formation. Finding ASC specks would suggest active inflammasome and CASP1 cleavage. We chose ASC staining over cleaved CASP1 staining, because colleagues regarded the available antibodies for cleaved CASP1 as untrustworthy. ASC specks are approximately 1-2 μm large, and could be easily be mistaken as non-specific “junk” signal. In order to ensure that we can detect ASC signal with an effective antibody, we used gut tissue as orthogonal controls. In the gut environment, there is close proximity of host cells to microbial communities, in which invasive bacterial species may be expected to invade intestinal cells and induce pyroptosis[99]. To increase the probability of seeing ASC speck formation, we utilized *Casp8*$^{+/-}$*Casp1*$^{-/-}$ mice[99] in which 4.0 cm of jejunum was collected and sectioned from two independent mice. In these mice, cells do not pyroptose, but ASC speck formation is expected to occur in a greater frequency. 8 cm of jejunum was screened, and ASC speck formation observed (**Figure 2.7A,B**). In parallel, we have similarly screened about 8 cm of jejunum tissue from two independent *ASC*$^{-/-}$ mice and did not observe ASC specks (**Figure 2.7C,D**). Despite screening the entirety of five WT embryonic brains from three independent litters, we found only one instance of ASC formation in a lytic cell cluster of the LGE within a male E12.5 brain (**Figure 2.8B**). While this suggests inflammasome activation within the fetal brain, I am not confident in this result since one case was found. However, strikingly, the cells within these characteristic clusters (as previously visualized by LSFM) appear swollen and bulbous in contrast to the surrounding tissue when imaged by simple brightfield differential interference contrast (DIC) microscopy (**Figure 2.8A,C**). Consistent with the expectation that *Cx3cr1*-GFP^{+} PI^{+} cells are undergoing cell swelling and lysis, *Cx3cr1*-GFP^{+} PI^{+} cells had a significantly larger diameter compared to *Cx3cr1*-GFP^{+} cells around the cluster without PI (**Figure 2.8D**). We also found restoration of these lytic cell death clusters in *iCasp1* mice (data not shown).

The data thus far collectively suggest that microglial lytic cell death occurs in primarily two zones in the fetal brain—the LGE and iTh—which may involve active inflammasome assembly. We also observed that this lytic death process primarily occurred between E12.5-E14.5. This process may proceed differently in female mice, as the temporal dynamics did not match as well with male mice; more investigation is required on this end (data not shown). We used mouse genetics next to infer if lytic cells could be microglial, and if CASP1 is required. We crossed *Cx3cr1-GFP* mice unto a pure *Casp1*$^{-/-}$ background, producing male *Cx3cr1-GFP*$^{+/+}$*Casp1*$^{-/-}$ mice, which were then crossed to female *Casp1*$^{-/-}$ mice. The genotype of these litters was *Cx3cr1-GFP*$^{+/-}$ *Casp1*$^{-/-}$. We repeated the previous experiments and found that the frequency of lytic *Cx3cr1*-GFP$^{+/+}$PI^{+} was significantly reduced (**Figure 2.9A,B**). Thus, using CASP1 as the main definitive criteria for pyroptosis, these genetic data suggest that microglial pyroptosis is occurring in fetal brain development.

2.8 CASP1 deficiency causes discrete changes in cell patterning within the thalamus of adult Casp1$^{-/-}$ *brains.*

From the anatomical location of the microglial pyroptotic cell clusters, we infer that they are in the LGE and iTh of the fetal brain. Since their location is close to the known zones of neurogenesis, near the ventricles, we hypothesized that they are near neural precursor cells (NPCs) that are dividing from radial glia[115-117]. In order to test this hypothesis, we sectioned more *Cx3cr1-GFP*$^{+/-}$ fetal brain tissue and stained for Pax6. Pax6 is a transcription factor that exercises great control over early brain development for many, but not all, neural subsets[118,119]. Using the LGE as an example, we found that *Cx3cr1*-GFP$^{+/-}$PI^{+} lytic cells are in close proximity to Pax6^{+} NPCs (**Figure 2.10A**) confirming that *Cx3cr1*-GFP$^{+/-}$PI^{+} lytic clusters are in the neighborhood of active neurogenesis. Intriguingly, cells that are both PI^{+} and GFP^{+} appear to have reduced GFP expression compared to GFP^{+} cells alone, consistent with previous observations from Russell Vance's group.

Since pyroptosis involves release of pro-inflammatory cytokines, it could be those bystanders NPCs sense this inflammation. Since we observed behavior changes in *Casp1*$^{-/-}$ mice that differ from WT mice, it could be that this inflammation is required for shaping proper neural numbers or neural cell fate within these discrete brain areas. To understand how lack of microglial pyroptosis affects the developing brain, we serial sectioned age-matched adult WT and *Casp1*$^{-/-}$ mice to perform classic stereology and histology experiments in order to find features in the brain that may help explain the ADHD-like behavior changes of *Casp1*$^{-/-}$ mice. Given that fetal brain imaging implicated the LGE and iTh, we anticipated finding cellular changes rather than global anatomical changes in regions descending from the LGE and iTh. In the adult brain, the largest regions that descend from the LGE and iTh include the striatum and thalamus[115,119,120].

To first test if there were any gross structural anomalies in the *Casp1*$^{-/-}$ brains compared to WT, we used the Cavalieri stereological method[121] to measure the gross brain volume in three independent age-matched mice from each genotype. *Casp1*$^{-/-}$ cerebrum volume did not differ significantly from WT brains (**Figure 2.11A**), suggesting that there are no major anomalies in structure that would result in a smaller or larger brain volume. Since the fetal LGE and iTh brain regions contained the microglial lytic

cell clusters, we also measured the brain volumes of the striatum and thalamus—the largest structures descending from these fetal brain regions[115,120,122-124]. The *Casp1*$^{-/-}$ striatum and thalamus volume did not differ from WT (**Figure 2.11B,C**), suggesting that even in these regions there were no overt structural anomalies that would help explain *Casp1*$^{-/-}$ behavior changes. Since *Casp1*$^{-/-}$ behavior changes were not widespread, perhaps it makes sense that we did not find global structural irregularities in *Casp1*$^{-/-}$ brains.

Since we found the lytic cell clusters mainly occur on days E12.5 and E14.5, we reasoned that we might find cellular changes, such as differing cell numbers, in neural compartments rather than synapse-level changes. This is because the cellular basis of circuits are not there until E18.5, and synaptogenesis begins shortly thereafter[102]. In a preliminary experiment comparing *iCasp1* and *Casp1*$^{-/-}$ brains, we did not find any changes within the striatum. Interestingly, we did find cell patterning changes in the rostral thalamus of the *Casp1*$^{-/-}$ mouse brain. We found that the thalamic reticular nucleus (TRN), was enriched with neural, and not microglial, cells (**Figure 2.12**). We also found other compartments that appeared to have decreases in cell number, but these regions were not quantified (data not shown). The TRN was already previously found to have a central role in attention[125], and alterations within this compartment are proposed to mediate a central circuit endophenotype for many neurodevelopmental disorders[126]. The TRN is one of few thalamic nuclei composed entirely of GABAergic neurons[115,127,128]. We used parvalbumin staining to demarcate the TRN within the thalamus and counted neuron cell bodies (NeuN^{+}) in WT and *Casp1*$^{-/-}$ brains. We found that *Casp1*$^{-/-}$ brains have a significantly higher amount of neurons in the TRN compared to WT (**Figure 2.12A,B**). Since GABAergic neurons are inhibitory, it could be that a greater amount of GABAergic neurons in the TRN of *Casp1*$^{-/-}$ mice drive more inhibition in the brain regions that they project to. This disruption to the excitatory/inhibitory balance may mediate the ADHD-like behavior changes seen in *Casp1*$^{-/-}$ mice. However, future studies using electrophysiology and optogenetics will be needed to test this hypothesis. Intriguingly, the amount of microglia in the same region did not differ between WT and *Casp1*$^{-/-}$ (**Figure 2.12C,D**). The expectation is that there would be more microglial cells filling the niche in *Casp1*$^{-/-}$ mice in the absence of lytic cell death. Perhaps, this is reflective of how immune cells generally regulate their population size in tissue niches.

To conclude, we found a neural consequence as an outcome of CASP1 deficiency (in addition to the behavioral studies). These data may support a working model in which a pro-inflammatory cytokine or cytokines (released from microglial pyroptosis) promote the neural death of NPCs that populate the TRN. However, future studies are required, both in the fetus and the adult brain, to explore the neural basis of the *Casp1*$^{-/-}$ behavioral phenotype.

2.9 Pharmacological disruption of the pyroptosis pathway produces some ADHD-like behavior changes in mice.

While it is possible that the NLRP3/CASP1/GSDMD/IL1-R inflammasome pathway may represent novel genetic risk factors for ADHD, we found no evidence from current studies in the literature that supports this idea. Furthermore, since genetics

alone cannot account for the large amount of ADHD cases in the population, we began to consider the possibility that maternally derived environmental factors may impact the NLRP3/CASP1/GSDMD/IL1-R inflammasome pathway during brain development. Therefore, we began to think about possible medications that, when taken during pregnancy, could promote the formation of ADHD behaviors in offspring.

We wanted see if the *Casp1*$^{-/-}$ behavioral phenotype can be recaptured with a known CASP1 (ICE) inhibitor, VX-765[129], along with an NLRP3 drug inhibitor, MCC950[130]. ICE inhibitors have been used in the treatment of autoimmune conditions[131,132], and maternal autoimmunity is already a known risk factor for ADHD[133,134]. We injected pregnant mice through the height of neurogenesis and differentiation (E12.5-E14.5) to see if we can produce the ADHD-like behavior changes seen in *Casp1*$^{-/-}$ mice (**Figure 2.13A**). Strikingly, offspring of dams injected with MCC950 traveled a significantly greater amount of distance within the open field assay compared to vehicle controls (**Figure 2.13B**), suggesting hyperactivity. Offspring of dams injected with MCC950 also spent more time in the open arms of the elevated-plus maze assay compared to vehicle controls (**Figure 2.13C**). Offspring of dams injected with VX-765 did not travel a significantly greater amount of distance or spend a significantly greater amount of time in the open arms of the elevated-plus maze assay compared to vehicle controls (**Figure 2.13B,C**). Neither offspring from VX-765- or MCC950-injected dams exhibited a significant amount of climbing relative to vehicle controls (**Figure 2.13D**). Collectively, these data demonstrate that pharmacological disruption of the pyroptosis pathway during development (at least for the NLRP3 inhibitor MCC950) could recapture the hyperactive and partial impulsive tendencies of the *Casp1*$^{-/-}$ mice.

Intriguingly, over-the-counter use of acetaminophen (ACP) by pregnant mothers was associated with an increase in hyperactivity of offspring[135-142]. ACP is considered to be a safe source of pain and fever relief for pregnant women[143]. Perhaps, its widespread use contributes to the high percentage of individuals with ADHD in the population. In a series of *in vitro* experiments using a microglial cell line (SIMA9 cells), we found that ACP downregulated both *Nlrp3* and *Casp1* mRNA in a dose-dependent manner (**Figure 2.14A,B**). Another study showed suppression of the NLRP3 inflammasome in LPS-challenged piglet mononuclear phagocytes after acetaminophen treatment[144]. As a result, we hypothesized that maternal use of ACP may suppress the active inflammasome pathway during brain development of the offspring *in utero*. In order to test this hypothesis, we injected ACP (using a dose comparable to the human daily equivalent intake) throughout the onset and flourishing of active neurogenesis (E12.5-E14.5) and ran the offspring through behavior assays. In contrast to the *in vitro* data, we did not observe downregulation of *Casp1* mRNA in E14.5 *ex-vivo* isolated $Cd45^{+}Cd11b^{+}$ myeloid cell fraction at E14.5 (**Figure 2.14C**). However, we only observed a modest downregulation of *Nlrp3* mRNA in E14.5 *ex-vivo* isolated $Cd45^{+}Cd11b^{+}$ myeloid cell fraction (**Figure 2.14D**). In order to see if the depression of *Nlrp3* was enough to decrease the lytic zones previously identified in the LGE and iTh, we treated WT dams (crossed to *Cx3cr1-GFP*$^{+/+}$ males) with ACP from E12.5-E14.5 of pregnancy. On the day of the experiment, we intravenously tail-injected dams with PI, collected the embryos, and processed for imaging by LSFM as previously described in section 2.9 and **Figure 2.6A** of this chapter. We cleared and imaged the embryos to count the

frequency of observed *Cx3cr1*-GFP$^{+/-}$PI^{+} lytic cell clusters. The modest reduction of *Nlrp3* mRNA (**Figure 2.14D**) was not enough to significantly reduce the frequency of lytic cell death clusters at E14.5 (**Figure 2.14E**).

While we did not observe reduction of lytic cell death in the fetal brain following exposure to ACP, offspring from ACP-injected mothers did have behavior changes reminiscent of hyperactivity and impulsivity. ACP-exposed offspring traveled a significantly greater amount of distance during the open field assay (**Figure 2.15A**), but did not spend a significantly greater amount of time in the open arms of the elevated-plus maze assay (**Figure 2.15B**), and climbed the equipment of the three-chamber sociability assay more frequently than vehicle controls (**Figure 2.16C**). Taken altogether, exposure to maternal ACP reproduced some of the ADHD-like behavior changes similar to what was seen with *Casp1*$^{-/-}$ mice.

Taken altogether, pharmacological disruption of the inflammasome pathway, likely in the myeloid compartment, was sufficient to recapture some or all aspects of the ADHD-like behavior changes seen from the *Casp1*$^{-/-}$ offspring. However, these changes were to a lesser degree compared to genetic ablation of the pyroptosis pathway, and we did not recapture an effect on lytic clusters when using our previous LSFM screening assay.

Discussion

2.10 Lytic cell death and development: outstanding questions.

Altogether, the data may support a working model in which fetal brain DAMPs activate the microglial NLRP3 inflammasome and induce pyroptosis (**Figure 2.16A,B**). As a consequence of microglial pyroptosis, released factor(s) (perhaps including IL-1β) modulate the bystander NPC pool (**Figure 2.16A,B**). When considering the iTh, these released factors may promote death of GABAergic interneuron precursor cells that eventually fill the TRN (**Figure 2.16A,B**). An increase in inhibition driven by more GABAergic interneurons of the TRN may help to drive the ADHD-like behavior changes seen in *Casp1*$^{-/-}$ mice. However, much work is needed to test this model (as discussed in section 2.13). And, this model weakens when we consider the major outstanding questions.

First, why would an inflammatory and lytic form cell death in the fetal brain be required in shaping normal brain circuitry? And, if the working model in **Figure 2.16** is correct, why wouldn't the entire neurogenic zone along the ventricle have lytic zones? These are difficult questions to answer without additional exploration. However, I am free to speculate below.

For the first question, I hypothesize that embryonic macrophages in general support organogenesis through the secretion of trophic factors and possibly immunomodulatory compounds. However, the ways in which embryonic macrophages do this are largely unknown. The reason I think embryonic macrophages are important for normal organogenesis is from the colony-stimulating factor 1 receptor (CSF1R) knockout mouse[145,146] (also discussed in the Introduction Chapter section 1.2). CSF1R is required for sensing colony-stimulating factor 1 (CSF) and interleukin 34 (IL-34), which promote the survival, recruitment, proliferation, and migration of mononuclear phagocytes in development (which include microglia and monocytes)[147-149]. Mice without CSF1R (on a C57BL/6 background) have drastic structural tissue anomalies and rarely survive past weaning[145,146,150,151]. Indeed, without microglia, the mouse brain has missing and malformed structures[150]. A human case was recently discovered in which two mutations in the *Csf1r* gene that caused two dysfunctional copies of the CSF1R[151]. Unfortunately, the young patient had similar brain abnormalities as the mouse model and died at a young age[151]. These studies suggest that embryonic macrophages may support organogenesis, because in their absence, massive structural anomalies were found—particularly for bone and brain[145,146,150-152]. And, the ways in which macrophages support organogenesis is largely unknown and appear to be organ-dependent. In adult tissues, it is known that macrophages shape proper tissue function[57,58]. Thus, it is not out of the realm of possibility that in development, macrophages respond to "damage" from ongoing apoptosis and generally respond in similar ways as seen in adulthood. It would be interesting to see if there are subtle physiological abnormalities in other organs not immediately detectable by eye.

Yet, why wouldn't lytic zones be broadly seen throughout the neurogenic zones of the fetal brain? I speculate it may have to do with the timing and direction of migration of microglial precursors to the brain parenchyma. While microglial cells have been found to be in the developing brain as early as E10.5, this was discovered by flow cytometry

and therefore lacked spatial information[153]. With the advent of single-cell RNA sequencing, many of these "microglial" cells are actually border-associated macrophages[154,155]. Of these, there are actually quite few putative microglial cells in the developing brain parenchyma at E12.5[156] (**Figure 2.4C**). Some appear to be within vasculature, and others in the lumen of the ventricles (**Figure 2.4C**). From my LSFM studies, the distinction between parenchymal microglia and vascular microglia is often unclear. Perhaps, microglial cells don't encounter DAMPs until they exit the vessels and enter the neurogenic brain parenchymal space and the LGE and iTh are the first places to do so. A second reason for why there are not more lytic zones is the possibility that the brain myeloid cell program is heterogeneous, and that this heterogeneity encode differing susceptibility to possible DAMPs signals. But, future studies are needed to address these questions like these (also discussed in Chapter 4 section 4.2).

To conclude, we are not sure why microglial pyroptosis may be required for properly shaping a few, but not all, brain circuits. However, I can propose future directions that may shed light on this phenomenon (below in Section 2.13 and in Chapter 4 section 4.2).

2.11 Study limitations and future directions.

The data presented here are largely correlative, and can benefit from further investigation with more refined tools. I will discuss some of the limitations of this study and future experiments that can be done.

At this time, using the *Cx3cr1-GFP* reporter and *Cx3cr1-Cre* mice remains the best-defined genetic tool to study microglia from early development. CX3CR1 is broadly expressed microglia, other macrophages, monocytes, dendritic cells, and even in certain lymphoid cell populations[100]. Thus, in our interpretation of the re-expression behavior data presented in **Figure 2.3** and Section 2.6, we can't be certain that re-expression of CASP1 in the microglia cells themselves is responsible for the rescue. It could be that contributions from other brain myeloid cells (such as monocytes and border-associated macrophages)[154,155] are present, and/or from peripheral $CX3CR1^{+}$ cells. The recently defined genetic mouse tools identified during my Ph.D., which include using the *Tmem119* and *Sall1* loci, is more restricted to microglia[157-160]. However, their expression does not begin until later in brain development; TMEM119 is robustly and consistently expressed after P14[157,161], and prenatal expression of SALL1 was not explored[160]. With the advent of single-cell RNA sequencing technology, it is our hope that more microglia-specific genetic tools, from the earliest stages of brain entry, will be available to validate our results.

Furthermore, the *Haimon et al.* study brought forth the observation that there were recombination events in neurons of developmental RiboTag *Cx3cr1-Cre* animals, suggesting the existence of CX3CR1-expressing neurons[101]. While we did our best to demonstrate by RT-qPCR that *Nlrp3* and *Casp1* mRNA expression levels were significantly enriched in the *ex-vivo* E14.5 myeloid cell fraction ($CD45^{+}Cd11b^{+}$ cells; including microglia) compared to the *ex-vivo* E14.5 non-myeloid cell fraction ($CD45^{-}$ $Cd11b^{-}$ cells; including neurons), we can't exclude the possibility that there is limited expression of the *Cx3cr1* gene in a subset of neurons that would affect our interpretation of the *iCasp1* re-expression experiment in **Figure 2.3**.

Evaluating the upstream activators of NLRP3 can test our working model further. Experimentally testing the requirement for NLRP3 activators is exceedingly challenging for *in vivo* studies, partly due to the diverse array of possible stimuli[49] and also because many activators cannot be simply deleted or inhibited *in vivo*. For example, removing exogenous ATP, a theorized DAMP-NLRP3 activator in our system, may cause a multitude of effects that would render the data uninterpretable. However, we could consider conditionally deleting the purinergic receptor using mice that has the floxed purinergic receptor P2Y12 (*P2y12r*$^{fl/fl}$)[162] deleted from CX3CR1-Cre expressing cells[100]. Microglial P2Y12R recognizes extracellular ATP[163,164]. Assuming P2Y12R is the main ATP sensor for microglia, deletion of P2Y12 in CX3CR1^{+} cells would test our hypothesis that ATP is the NLRP3 activator in our system. If our hypothesis is correct, ADHD-like behavior changes will be restored to WT levels with the absence of microglial P2Y12R. There would also be an absence of the lytic cell clusters in the LGE and iTh fetal brain regions.

Testing the downstream effects of NLRP3 activation can also test our working model further. IL-1β and IL-18 are the classic cytokines defined as a result of pyroptosis[8,40,41,45]. In our study, we used IL-1R deficient mice and found that *Il-1r*$^{-/-}$ mice partially phenocopied the *Casp1*$^{-/-}$ ADHD-like behavior changes. Our study did not test the requirements of IL-18 sensing, which may contribute to the phenotype. Repeating our experiments with *Il18r*$^{-/-}$ mice, and seeing if the *Casp1*$^{-/-}$ ADHD-like behaviors are partially recaptured may explain why *Il-1r*$^{-/-}$ mice partially phenocopied the *Casp1*$^{-/-}$ ADHD-like behavior changes. If crossing *Il-1r*$^{-/-}$ and *Il18r*$^{-/-}$ together completely recaptures all *Casp1*$^{-/-}$ ADHD-like behavior changes, then we would confirm that both IL-18 and IL-1β shape formation of the circuits underlying these behavior changes.

Though we used *Il-1r*$^{-/-}$ mice, we did not confirm which cell population has IL-1R expression and is sensing IL-1β. In order to test that bystander NPCs are sensing IL-1β, we can cross *Il-1r*$^{fl/fl}$[165] and/or *Il18r*$^{fl/fl}$ mice[166] to different neuron-specific Cre mice[167]. In crossed mice, the IL-1R or IL-18R will be deleted from neurons. Indeed, some neurons have been shown to express the IL-1R[168,169]. If the ADHD-like behavior changes are reproduced in these mice, then that would support our current working model that neuronal sensing of IL-1β and/or IL-18, factors released from pyroptosis, shape proper circuit formation.

Without using mouse genetics, testing the requirement of IL-1β and/or IL-18 in our system can be done with intra-ventricular injection of antibodies targeting IL-1β and/or IL-18 during at E12.5-E16.5. This could be particularly important to do, as I failed to detect IL-1β by ELISA when taking fluid out of the ventricles of embryos (data not shown). It could be that levels were beyond the limit of detection of the assay, as an estimated 400-500 microglial cells may undergo pyroptosis; these are relatively few cells in the total fetal brain cell population. Injection of antibodies targeting IL-1β and/or IL-18 during at E12.5-E16.5 would hypothetically prevent interaction of these cytokines with their cognate IL-1Rs and/or IL-18Rs. If the *Casp1*$^{-/-}$ ADHD-like behavior changes are reproduced with the intra-ventricular α-IL-1β and/or α-IL-18, then that behavior data would also suggest that IL-1β and/or IL-18 neural sensing is important for shaping a proper circuit.

In our study, we used live staining with PI to visualize lytic cell death clusters. This limits our interpretation, since PI is not exclusive to pyroptotic cells. So, we

screened multiple WT fetal brains for ASC speck formation for additional validation. We found only one example of ASC specks (**Figure 2.8B**). While visualizing ASC formation is already an uncommon occurrence, it is unsafe to rely on one replicate to solidify our conclusion. In future studies, repeating our assay with a transgenic ASC assembly reporter mouse (ASC-citrine mice)[170] could improve detection of ASC specks in our system. For now, our main conclusion of identifying microglial pyroptosis comes from the following observations: *Cx3cr1*-GFP^{+}PI^{+} cells are in the brain parenchyma, suggesting they are microglial; *Cx3cr1*-GFP^{+}PI^{+} cells are very bulbous and large, suggesting they are undergoing cell swelling and lysis; and, our behavior result is from CASP1 deficient mice. Since CASP1 activation may be the most agreed-upon definitive characteristic of pyroptosis[8,41,45], and re-expression in a *Cx3cr1*-dependent manner restored behaviors to WT, we think we are visualizing microglial pyroptosis. Using improved tools to visualize cleaved CASP1 would benefit this study.

Our study also has limitations when it came to our LSFM assay. We used one 488 laser with two bandpass filters (505-545 nm and 575-615 nm) to capture GFP and PI signals, respectively. One downside is that there is some spillover of PI fluorescence into the GFP channel. To compound this, there was significant autofluorescence in the PI channel from the developing vasculature. Therefore, I limited my analysis to counting the frequency of lytic cell clusters (using the criteria I defined in the Methods section) rather than the fluorescence intensity. Furthermore, maintaining the exact degree of clarity in processed samples is extremely difficult; though they were processed for the same minimum length of time, sample-to-sample variability of the tissue and reagents could account for differences in clearing. Definitely, the inner regions of the fetal brain far from the surface (which includes the iTh) had decreased signal compared to cells closer to the surface; this is because tissue clearing is more efficient closer to the surfaces of tissue. To help overcome this effect, dual-laser illumination was used whenever possible. We also did not confirm PI labeling efficiency; we only processed samples that had successful tail IV injections. Because of the limitations of our LSFM assay, I recommend its utility for mainly screening purposes.

Lytic cell clusters were not completely absent in *Cx3cr1-GFP*$^{+/-}$*Casp1*$^{-/-}$ mice (**Figure 2.9B**). One explanation could be the large degree of redundancy among cell death pathways. Perhaps, crossing *Cx3cr1-GFP*$^{+/-}$*Casp1*$^{-/-}$ mice with additional knockouts of alternative cell death pathways elements could completely abolish *Cx3cr1*-GFP^{+}PI^{+} lytic cell clusters and cells. It is also curious that these lytic cell clusters were primarily unilateral—only seen on one hemisphere, and not the other. With discussion among colleagues, it was appreciated that other features of the mouse brain exhibit unilateral properties. It is unknown why this is the case. Perhaps, neural cells descending from regions in our study (such as the LGE or iTh) have axonal projections that cross the midline and these are sufficient for a normal behavioral circuit. Further considering the LSFM assay, I did not see any significant decreases of in lytic cluster frequency of ACP-treated dams despite the ADHD-like behavior changes (**Figure 2.15E**). Since I begin the assay many hours after ACP injections on the last E14.5 day, perhaps timing is an issue and/or sensitivity of our assay. Lastly, though we found restoration of the lytic cell death clusters in *iCasp1* mice (in which CASP1 was re-expressed in a *Cx3cr1*-dependent manner) (data not shown), we still found few bright-

intensity GFP^+PI^+ cells in *iCasp1* mice (without re-expressed CASP1). We are not sure of the origin of this fluorescence.

Modern neuroscience tools can help us explore the neural circuitry of *Casp1*$^{-/-}$ behavior changes. Our data implicates thalamic GABAergic neurons (within the TRN) as a possible driver of the behavior changes we found. It is unknown which regions TRN GABAergic interneurons project to in our system. We can stereotaxically inject anterograde fluorescent tracers within the TRN of the mouse brain, which would propagate fluorescence to the terminal axonal processes[171]. In the *Casp1*$^{-/-}$ brain, we might expect to see more fluorescence at the end of the axons relative to WT. This effectively indicates potential region(s) that are receiving an imbalance of inhibitory signal resulting from the overabundance of GABAergic interneurons in *Casp1*$^{-/-}$ brains. Injection of retrograde tracers within the region (or regions) identified by anterograde tracing from the TRN (or, perhaps trans-synaptic labeling[171]) may further identify additional brain regions affected by lack of excitatory signal. Thus, these experiments would be the beginning of a connectome study. Identifying fluorescence can be streamlined by tissue clearing of whole adult mouse brains and LSFM imaging. This described connectome experiment can inform future electrophysiology and optogenetics studies. Slice electrophysiology can be used to test the hypothesis that there is excitatory/inhibitory imbalance within the TRN-mediated circuit. Perhaps, driving more excitation into the TRN-mediated circuit via optogenetics would restore the ADHD-like behavior of *Casp1*$^{-/-}$ mice to WT levels. We will not completely understand the basis of the behavioral phenotype of *Casp1*$^{-/-}$ mice until these experiments are done.

Altogether, I encourage the reader to cautiously interpret our results in light of our limitations and imperfect assays. We hope for the development of more refined tools, (and the motivation of future students/postdocs), to carry out the future directions and alternative experiments described in this section.

2.12 Casp1$^{-/-}$ *mice: A new model of ADHD? Additional considerations.*

As always, studies using animals to model human neuropsychiatric disorders should be interpreted cautiously as no animal model can truly recapitulate the human condition. It is largely agreed that an animal model for ADHD should exhibit three key criteria: have face (similarity in symptoms), predictive (similarity in response to medical interventions), and construct (similarity in etiology) validity[10,21,172]. Because ADHD etiology is unknown in humans, demonstrating construct validity in ADHD models is limited. In this section, I discuss the ways in which *Caspase-1*$^{-/-}$ mice may or may not be taken seriously as a new model to study ADHD.

Casp1$^{-/-}$ may have face validity for modeling ADHD in that these mice recaptured the three core traits: hyperactivity, inattention, and impulsivity. To assay the hyperactivity trait, we primarily used the open-field assay and measured the distance that mice traveled. To assay attention, we used the 5-CSRTT assay and measured percent accuracy of nose pokes[97]. To assay impulsivity, we measured the time spent in the open arms of the elevated-plus maze assay and quantified the amount of climbing during the three-chamber sociability assay. According to the standards of the field[10,172], the assays that we had used to test hyperactivity and attention appear to be fairly standard; however, our assessment of impulsivity via the elevated-plus maze assay and

three-chamber assay is unconventional. Our interpretation of impulsivity was motivated by the features seen in children with ADHD (https://www.cdc.gov/ncbddd/adhd/diagnosis.html). Furthermore, we did not distinguish the temporal and novel aspects of the *Casp1*$^{-/-}$ behaviors in our study. For example, thinking of the human condition, hyperactivity should not be present in novel environments, impulsiveness should develop gradually over time, and sustained attention-deficit should be present only when stimuli are widely spaced apart[172]. Therefore, we should wait to propose *Casp1*$^{-/-}$ mice as a novel model for ADHD until we can behaviorally phenotype them further to thoroughly test the face validity of the traits we observed.

It is not known if *Casp1*$^{-/-}$ mice have any predictive validity to model ADHD—we did not test if the common drug treatments (like amphetamine and methylphenidate[10,173]) improve the hyperactivity, inattention, and impulsivity that we observed in *Casp1*$^{-/-}$ mice. In order to demonstrate the possible utility of *Casp1*$^{-/-}$ mice as a new ADHD model, we should treat them with amphetamine and methylphenidate drugs to see if their behaviors return to WT levels[10,173]. If pharmacological intervention does not improve the hyperactive, inattentive, and impulsive characteristics in *Casp1*$^{-/-}$ mice, it's unlikely that *Casp1*$^{-/-}$ mice would be accepted as a novel model of ADHD.

And, the etiology of ADHD is unknown. As discussed previously in the Introduction of this chapter, the dopamine hypothesis is the most popular theory. In *Casp1*$^{-/-}$ mice, we implicated a subset of GABAergic interneurons of the thalamus as a possible zone that mediates the ADHD-like behavior changes that we saw. We did not observe cellular changes in the striatum, which is a site containing many dopaminergic neurons. If GABAergic interneurons are indeed involved in the behavioral patterns we saw in *Casp1*$^{-/-}$ mice, it is possible that pharmacological treatment with the common stimulants that modulate dopamine and norepinephrine will not correct *Casp1*$^{-/-}$ mouse behavior. Thus, it is unlikely that *Casp1*$^{-/-}$ would be considered to have construct validity as a model for ADHD so long as the dopamine hypothesis prevails.

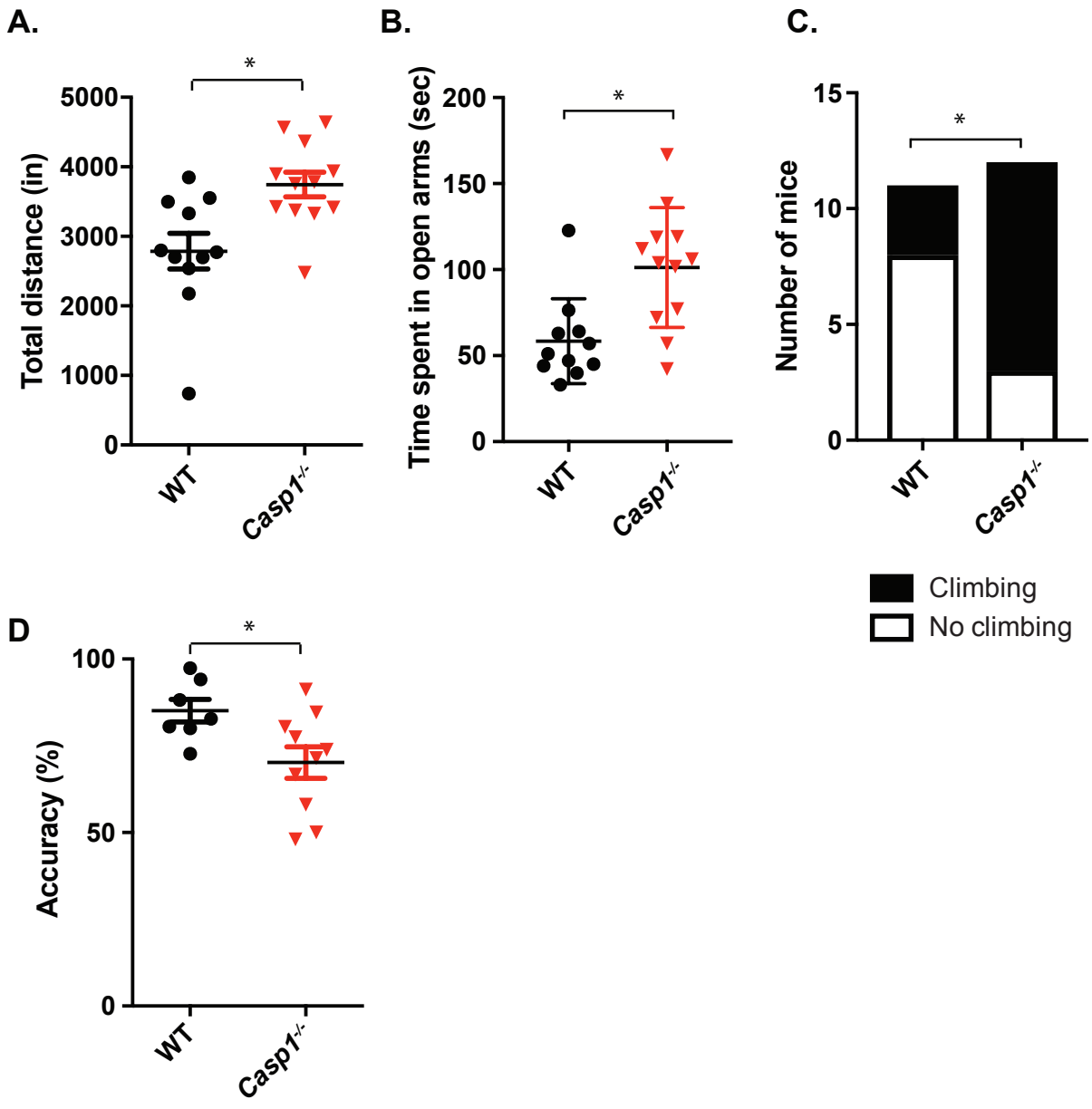

A.
B.
C.
D
Total distance (in)
5000
4000
3000
2000
1000
0
WT
Casp1-/-
*
Time spent in open arms (sec)
200
150
100
50
0
Number of mice
15
10
5
Climbing
No climbing
Accuracy (%)
100
50

Figure 2.1: Casp1$^{-/-}$ *mice exhibit ADHD-like behavior changes.*
A. General activity of male WT (black circles, N=11) and *Casp1*$^{-/-}$ (red triangles, N=12) mice was determined by the open field assay and is shown as total distance traveled (inches).
B. Level of anxiety of male WT (black circles, N=11) and *Casp1*$^{-/-}$ (red triangles, N=12) mice and is shown as time spent in the open arms (seconds).
C. Climbing behavior of male WT (N=11) and *Casp1*$^{-/-}$ (N=12) mice determined from the three-chamber social interaction assay.
D. Attention behavior of male WT (N=7) and *Casp1*$^{-/-}$ (N=10) was determined by the five-choice serial reaction time task and is shown as accuracy of their response (%).
(*) shows $p < 0.05$.

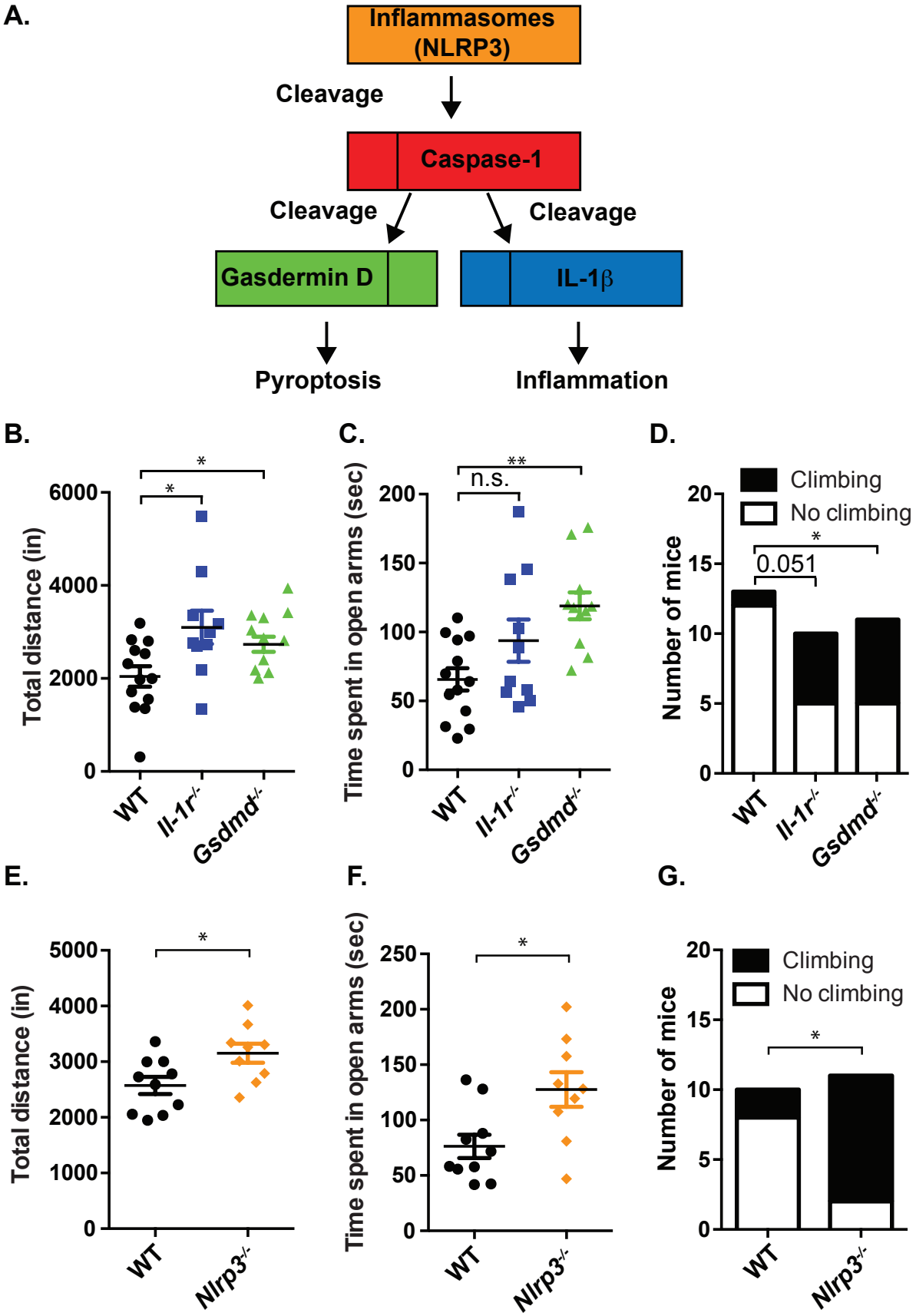

A.
Inflammasomes (NLRP3)
Cleavage
Caspase-1
Cleavage
Cleavage
Gasdermin D
IL-1β
Pyroptosis
Inflammation
B.
Total distance (in)
6000
4000
2000
0
*
*
WT
Il-1r-/-
Gsdmd-/-
C.
Time spent in open arms (sec)
200
150
100
50
0
**
n.s.
WT
Il-1r-/-
Gsdmd-/-
D.
Number of mice
20
15
10
5
0
Climbing
No climbing
*
0.051
WT
Il-1r-/-
Gsdmd-/-
E.
Total distance (in)
5000
4000
3000
2000
1000
0
*
WT
Nlrp3-/-
F.
Time spent in open arms (sec)
250
200
150
100
50
0
*
WT
Nlrp3-/-
G.
Number of mice
20
15
10
5
0
Climbing
No climbing
*
WT
Nlrp3-/-

Figure 2.2: Nlrp3$^{-/-}$, Il-1r$^{-/-}$, *and* Gsdmd$^{-/-}$ *mice phenocopy* Casp1$^{-/-}$ *ADHD-like behavior changes.*
A. Simplified canonical NLRP3 inflammasome pathway.
B. General activity of male WT (black circles, N=13), *Il-1r*$^{-/-}$ (blue squares, N=10), and *Gsdmd*$^{-/-}$ (green triangles, N=11) mice was determined by the open field assay and is shown as total distance traveled (inches).
C. Level of anxiety of male WT (black circles, N=13), *Il-1r*$^{-/-}$ (blue squares, N=10), and *Gsdmd*$^{-/-}$ (green triangles, N=11) mice was determined by the elevated plus maze assay and is shown as time spent in the open arms (seconds).
D. Climbing behavior of male WT (N=11), *Il-1r*$^{-/-}$ (N = 10), and *Gsdmd*$^{-/-}$ (N=11) mice was determined from the three-chamber social interaction assay.
E. General activity of male WT (black circles, N=10) and *Nlrp3*$^{-/-}$ (orange diamonds, N=9) mice was determined by the open field assay and is shown as total distance traveled (inches).
F. Level of anxiety of male WT (black circles, N=10) and *Nlrp3*$^{-/-}$ (orange diamonds, N=9) mice was determined by the elevated plus maze assay and is shown as time spent in the open arms (seconds).
G. Climbing behavior of male WT (black circles, N=10) and *Nlrp3*$^{-/-}$ (orange diamonds, N=12) was determined from the three-chamber social interaction assay.
* shows $p < 0.05$, ** shows $p < 0.01$; n.s. = not significant.

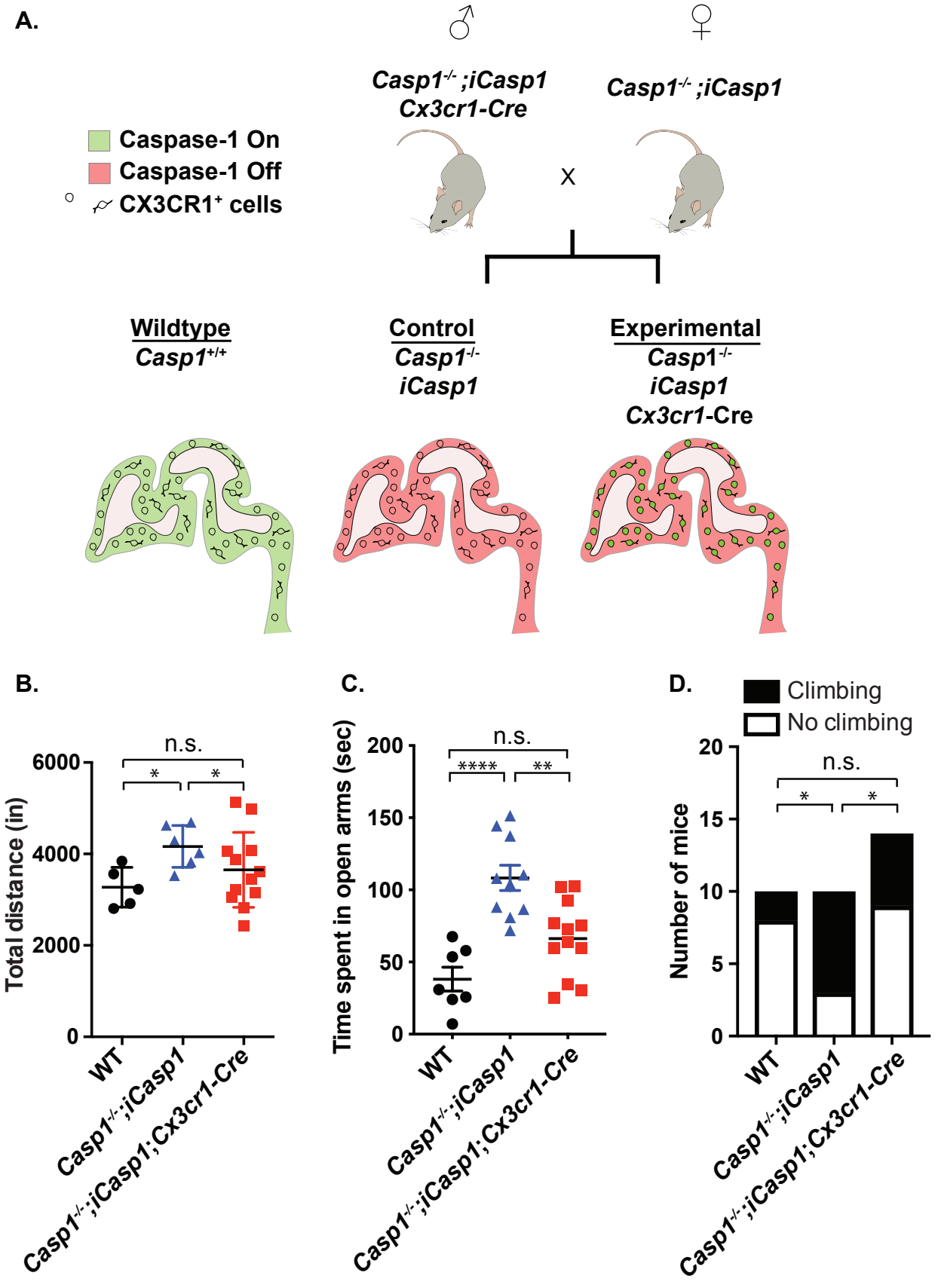

A.
♂
♀
Casp1-/- ;iCasp1 Cx3cr1-Cre
Casp1-/- ;iCasp1
X
Caspase-1 On
Caspase-1 Off
CX3CR1+ cells
Wildtype
Casp1+/+
Control
Casp1-/-
iCasp1
Experimental
Casp1-/-
iCasp1
Cx3cr1-Cre
B.
Total distance (in)
6000
4000
2000
0
n.s.
*
*
WT
Casp1-/-;iCasp1
Casp1-/-;iCasp1;Cx3cr1-Cre
C.
Time spent in open arms (sec)
200
150
100
50
0
n.s.
****
**
WT
Casp1-/-;iCasp1
Casp1-/-;iCasp1;Cx3cr1-Cre
D.
Climbing
No climbing
Number of mice
20
15
10
5
0
n.s.
*
*
WT
Casp1-/-;iCasp1
Casp1-/-;iCasp1;Cx3cr1-Cre

Figure 2.3: *Re-expression of CASP1 in a* Cx3cr1-*dependent manner restores behavior changes to WT levels.*
A. Breeding strategy is shown. We crossed three mouse lines (*Casp1*$^{-/-}$, *iCasp1*, and *Cx3cr1*-Cre) to generate *Casp1*$^{-/-}$;*iCasp1*;*Cx3cr1*-Cre positive (Experimental) mice and *Casp1*$^{-/-}$;*iCasp1*;Cre negative (Control) littermates. Expected *Casp1* expression pattern depicted in sagittal embryonic brain illustrations.
B. General movement of male WT (black circles, N=5), littermate Control (blue triangles, N=6), and Experimental (red squares, N=12) mice was determined by the open field assay and is shown as total distance (inches).
C. Anxiety levels of male WT (black circles, N=7), littermate Control (blue triangles, N=10), and Experimental (red squares, N=12) mice was determined by the elevated plus maze assay and is shown as time spent in the open arms.
D. Climbing behavior of male WT, littermate Control, and Experimental mice determined from the three-chamber social interaction assay.
(*) shows $p < 0.05$, (**) shows $p < 0.01$, (****) shows $p < 0.0001$; n.s. = not significant.

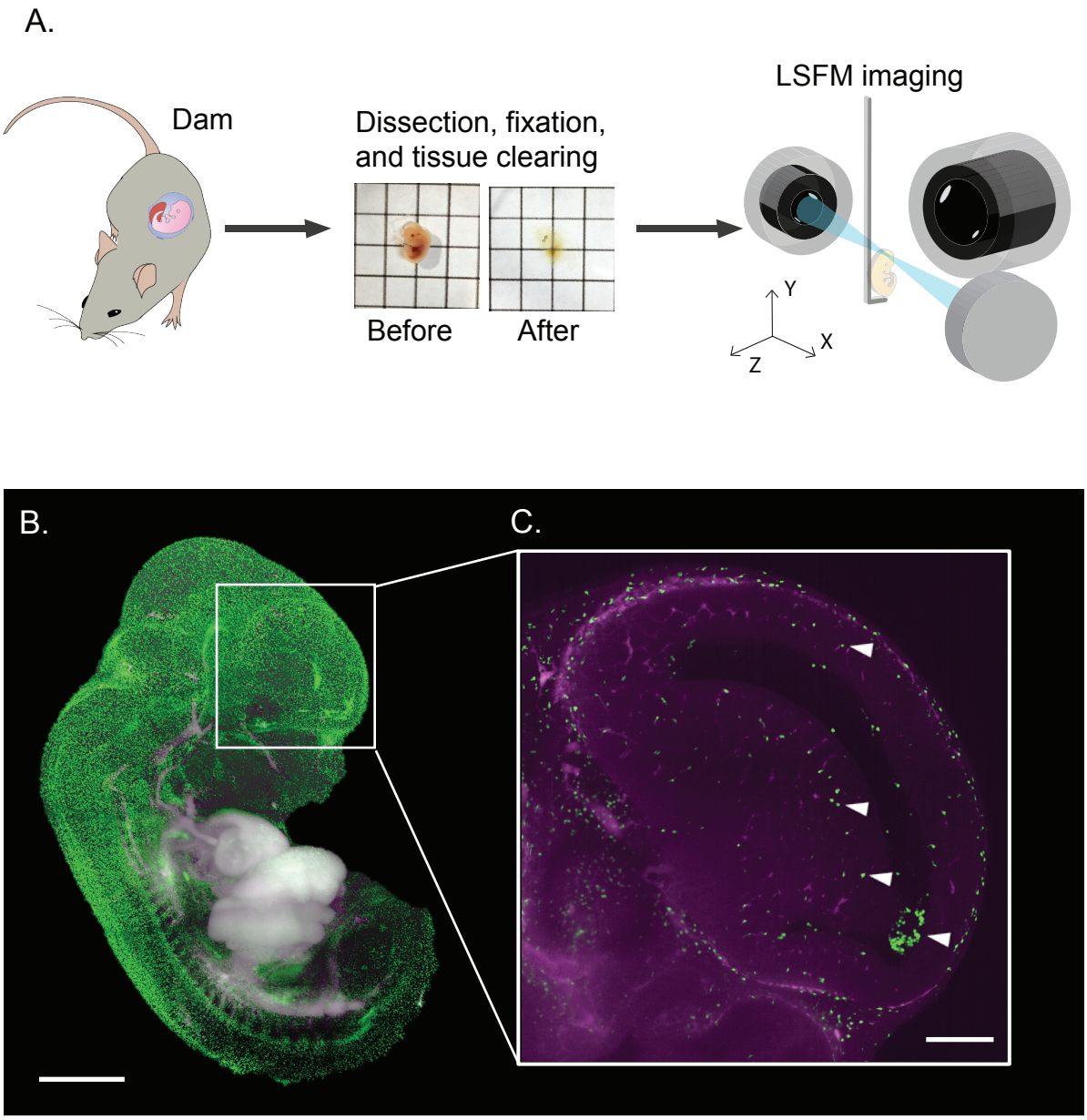

A.
Dam
Dissection, fixation,
and tissue clearing
Before
After
LSFM imaging
Y
X
Z
B.
C.

Figure 2.4: Cx3cr1-GFP^{+} *cells are present in the fetal brain parenchyma and borders at E12.5.*
A. Light sheet fluorescence microscopy (LSFM) assay experimental scheme.
B. A representative *Cx3cr1*-GFP$^{+/-}$ male E12.5 embryo imaged by LSFM and reconstructed as a 3D maximum-intensity projection. Green is *Cx3cr1*-GFP signal, and magenta is autofluorescence. Scale bar is approximately 2 mm.
C. Example *z*-slice from the embryonic forebrain. Green is *Cx3cr1*-GFP signal, and magenta is autofluorescence. Scale bar is approximately 500 μm.

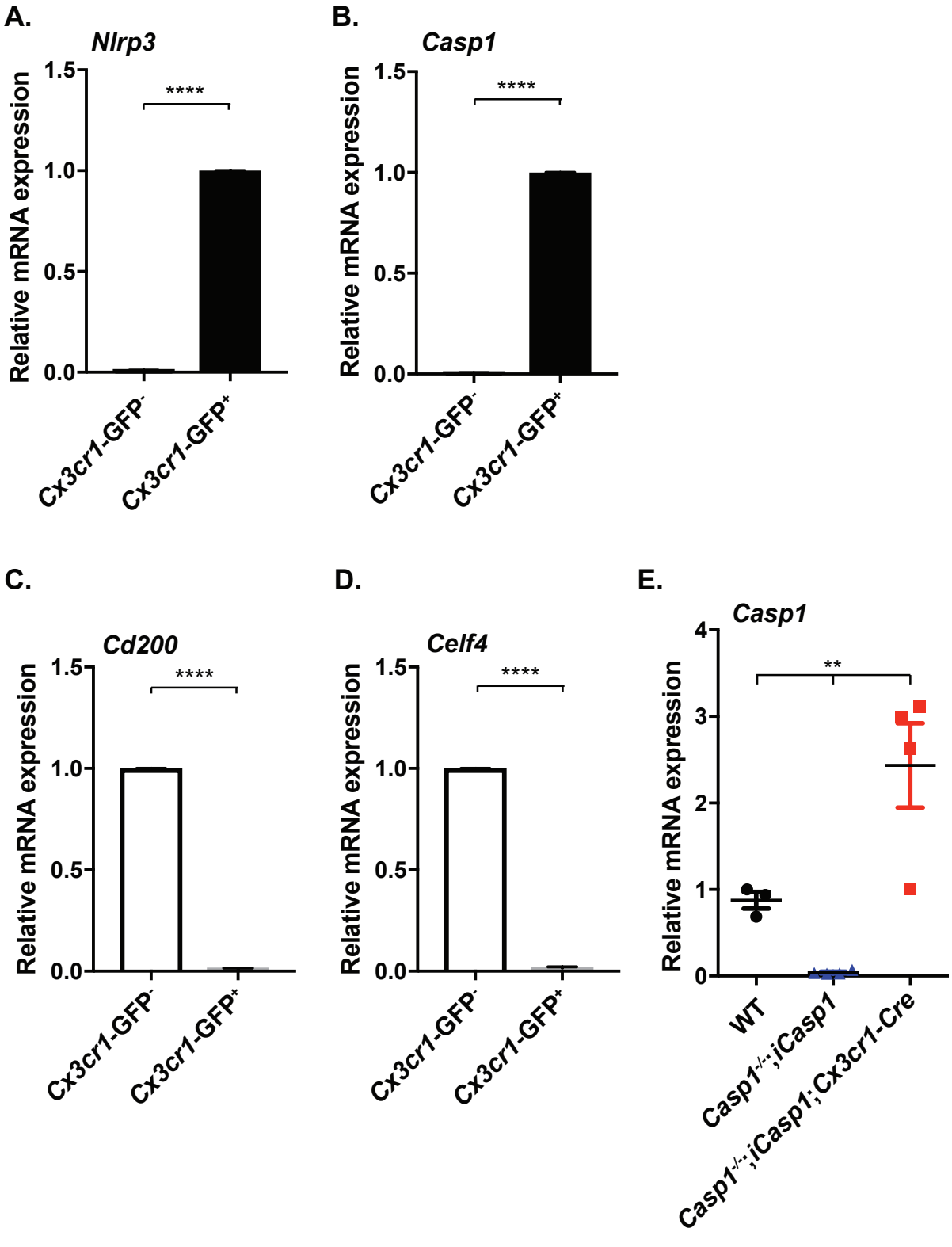
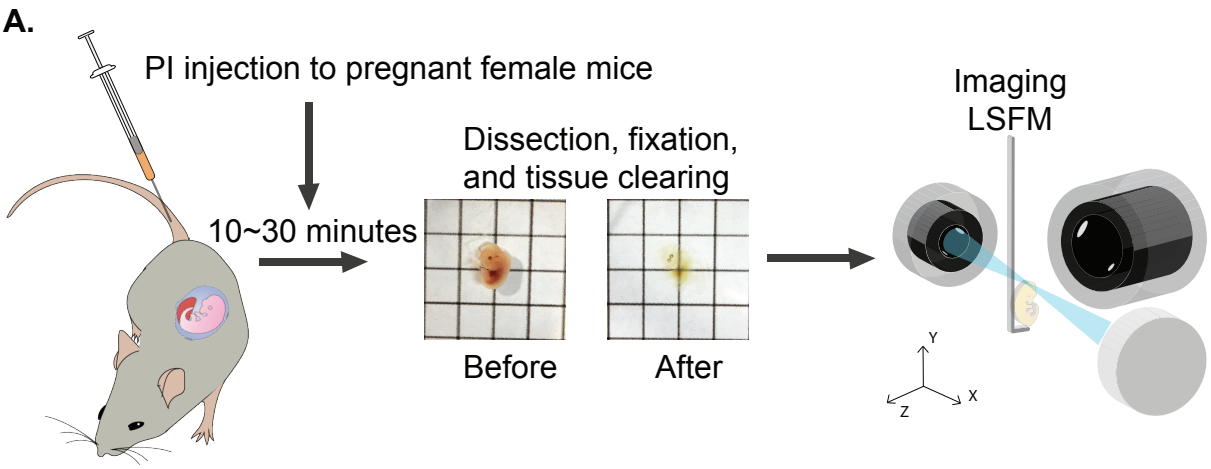
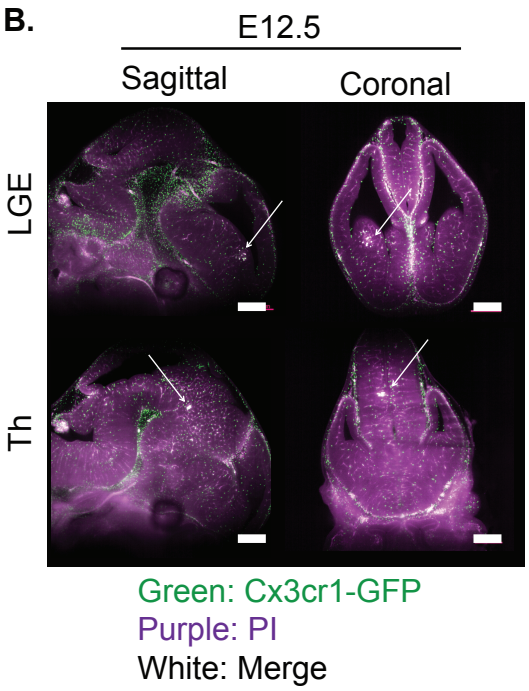
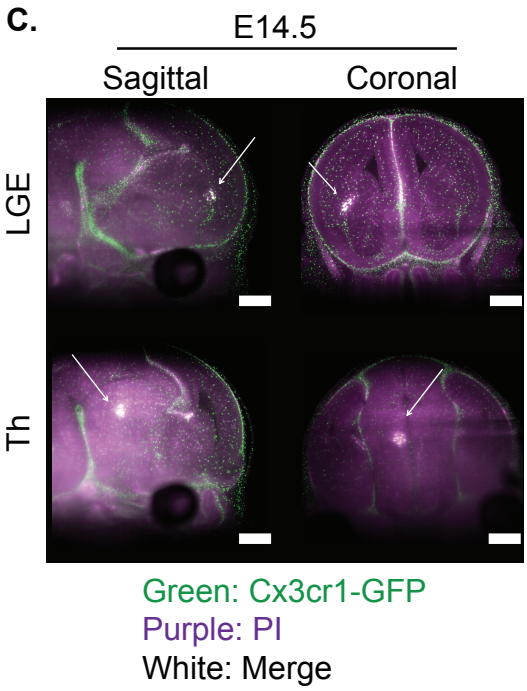

A.
Nlrp3
Relative mRNA expression
1.5
1.0
0.5
0.0
****
Cx3cr1-GFP-
Cx3cr1-GFP+
B.
Casp1
Relative mRNA expression
1.5
1.0
0.5
0.0
****
Cx3cr1-GFP-
Cx3cr1-GFP+
C.
Cd200
Relative mRNA expression
1.5
1.0
0.5
0.0
****
Cx3cr1-GFP-
Cx3cr1-GFP+
D.
Celf4
Relative mRNA expression
1.5
1.0
0.5
0.0
****
Cx3cr1-GFP-
Cx3cr1-GFP+
E.
Casp1
Relative mRNA expression
4
3
2
1
0
**
WT
Casp1-/-;iCasp1
Casp1-/-;iCasp1;Cx3cr1-Cre

Figure 2.5: *RT-qPCR validation of* Cx3cr1-GFP^{+} *and* Cx3cr1-GFP^{-} *fetal brain cell fractions and Casp1 expression in the iCasp1 system.*
A. Relative *Nlrp3* mRNA expression in the *Cx3cr1*-GFP^{+} and *Cx3cr1*-GFP^{-} *ex-vivo* sorted cells from a male E14.5 fetal brain.
B. Relative *Casp1* mRNA expression in the *Cx3cr1*-GFP^{+} and *Cx3cr1*-GFP^{-} *ex-vivo* sorted cells from a male E14.5 fetal brain.
C. Relative *Cd200* mRNA expression in the *Cx3cr1*-GFP^{+} and *Cx3cr1*-GFP^{-} *ex-vivo* sorted cells from a male E14.5 fetal brain.
D. Relative *Celf4* mRNA expression in the *Cx3cr1*-GFP^{+} and *Cx3cr1*-GFP^{-} *ex-vivo* sorted cells from a male E14.5 fetal brain.
E. Relative *Casp1* mRNA expression in the Cd45^{+}Cd11b^{+} *ex-vivo* myeloid cell fraction from male adult WT, *Casp1*$^{-/-}$;*iCasp1*;*Cx3cr1*-Cre positive and *Casp1*$^{-/-}$;*iCasp1*;Cre negative mice.
(***) shows $p < 0.001$, (****) shows $p < 0.0001$.


A.
PI injection to pregnant female mice
10~30 minutes
Dissection, fixation,
and tissue clearing
Before
After
Imaging
LSFM
Y
X
Z


B.
E12.5
Sagittal
Coronal
LGE
Th
Green: Cx3cr1-GFP
Purple: PI
White: Merge


C.
E14.5
Sagittal
Coronal
LGE
Th
Green: Cx3cr1-GFP
Purple: PI
White: Merge

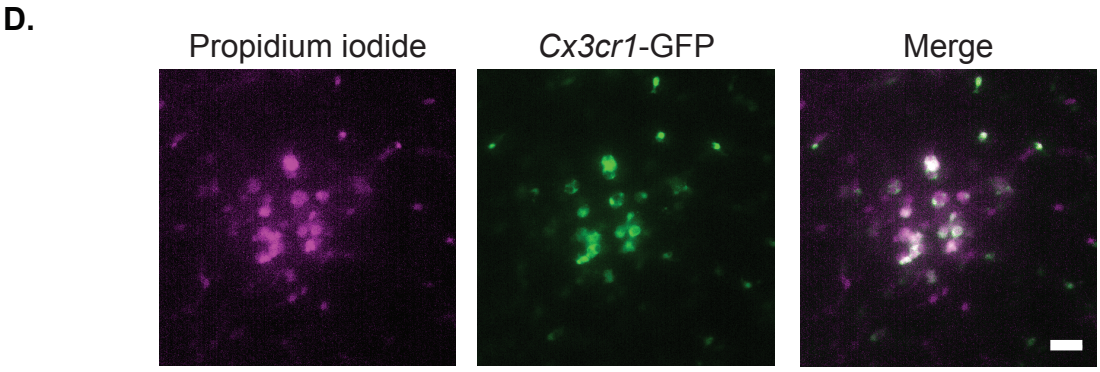

D.
Propidium iodide
Cx3cr1-GFP
Merge

Figure 2.6: Microglial lytic cell death occurs in a spatiotemporal manner in the fetal brain.
A. Propidium-iodide (PI) light sheet fluorescence microscopy (LSFM) assay experimental scheme. PI was injected into pregnant female mice at specific gestational stages. Ten to thirty minutes after PI injection, total embryos were recovered, cleared, and imaged by LSFM.
B. Representative sagittal and coronal LSFM images of the LGE and primitive thalamus (iTh) of a male E12.5 fetal brain are shown (N=6). Arrows indicate the location of a PI+ cell cluster. Green signal is GFP, purple signal is PI, White signal is colocalized signal. Scale bars indicate 500 μm.
C. Representative sagittal and coronal LSFM images of the LGE and iTh of a male E14.5 fetal brain are shown (N=5). Arrows indicate the location of a *Cx3cr1*-GFP^+PI^+ cell cluster. Green signal is GFP, purple signal is PI, White signal is colocalized signal. Scale bars indicate 500 μm.
D. Representative zoomed in *Cx3cr1*-GFP^+PI^+ cluster of the LGE at E12.5. Scale bar indicates 50 μm.

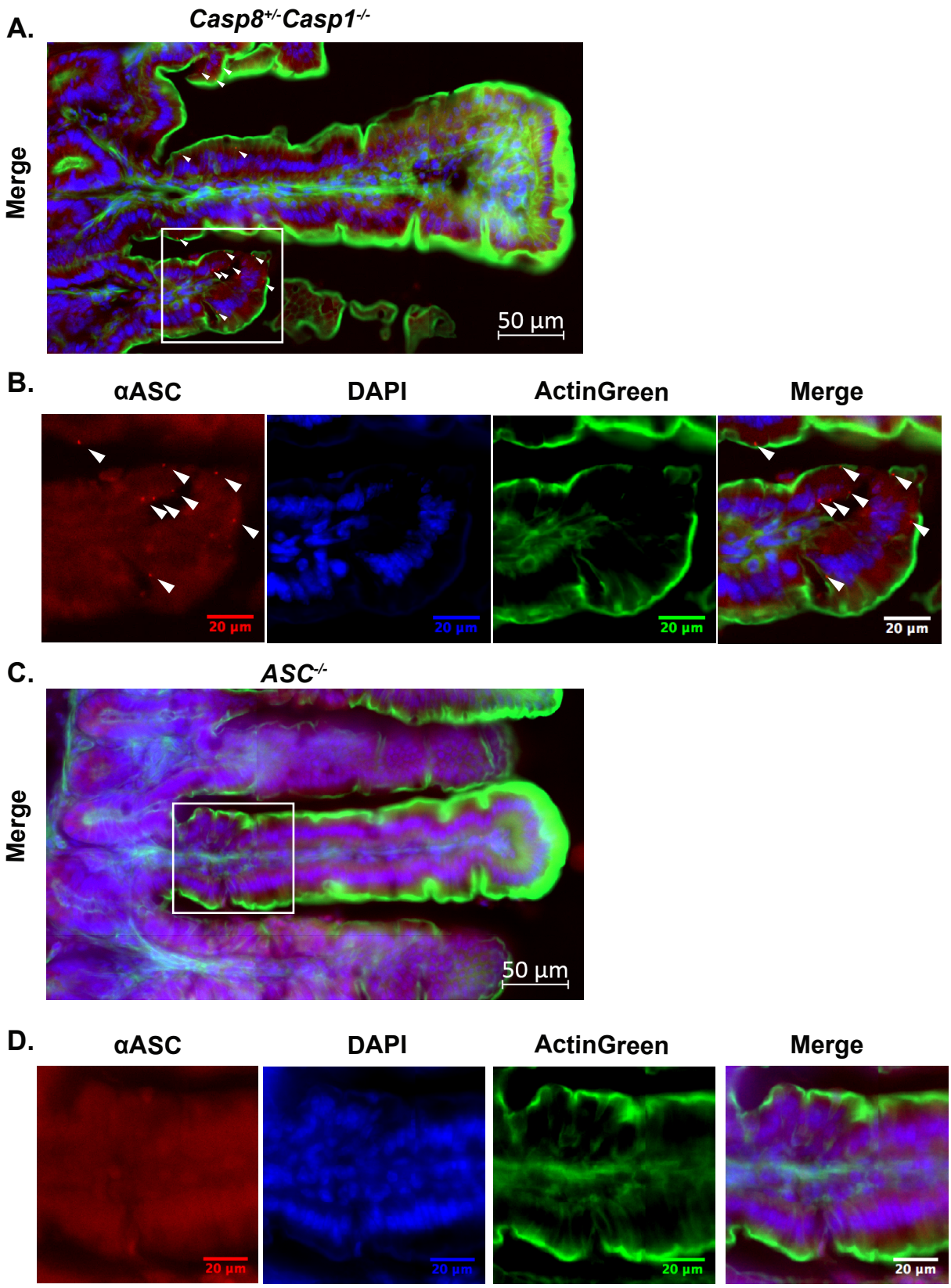
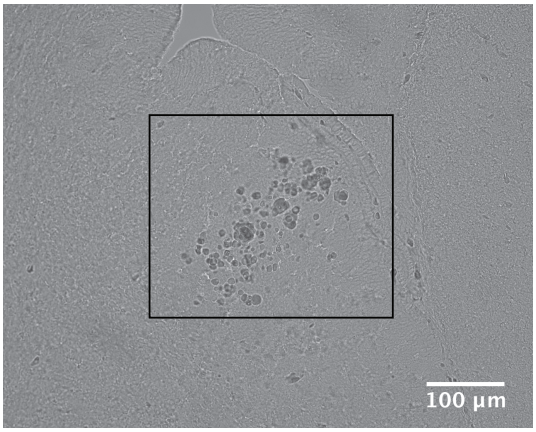
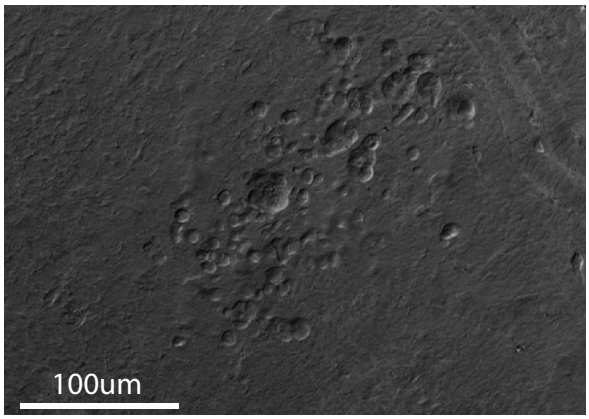

A.
Casp8+/-Casp1-/-
Merge
50 µm
B.
αASC
DAPI
ActinGreen
Merge
20 µm
C.
ASC-/-
Merge
50 µm
D.
αASC
DAPI
ActinGreen
Merge
20 µm

Figure 2.7: *Visualizing active inflammasome assembly through ASC staining.*
A. Representative intestinal jejenum section from a *Casp8*$^{+/-}$*Casp1*$^{-/-}$ mouse stained with Rb α hASC primary antibody (1:200, red), DAPI (1:2000, blue), and ActinGreen (Molecular Probes, 2 drops/mL, green) serving as a positive control. In this genetic scheme, ASC speck formation is expected, but cells are unable to undergo pyroptosis—thus, yielding more ASC specks. Scale bar indicates 50 μm. White arrowheads point to ASC specks.
B. Inset with channels split. From left to right: ASC, DAPI, ActinGreen, and merged signals. Scale bar indicates 20 μm. White arrowheads point to ASC specks.
C. Intestinal section from an *ASC*$^{-/-}$ mouse stained with Rb α hASC primary antibody (1:200), DAPI (1:2000), and ActinGreen (Molecular Probes, 2 drops/mL, green) serving as a positive control. Scale bar indicates 50 μm.
D. Inset with channels split. From left to right: ASC, DAPI, ActinGreen, and merged signals. Scale bar indicates 20 μm.
Per genotype, at least 4.0 cm of the jejunum from N=2 mice were examined. *ASC*$^{-/-}$ sections were stained and imaged with the same conditions as *Casp8*$^{+/-}$*Casp1*$^{-/-}$ sections. Histogram was adjusted to enhance brightness and contrast for all images. Images collected on Zeiss AxioScan slide scanner.

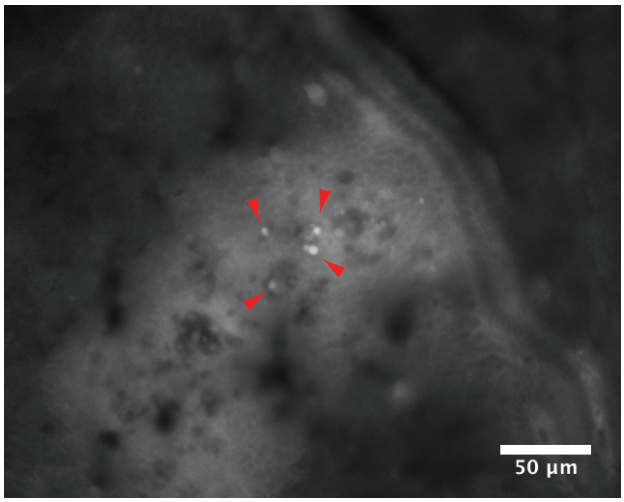
A.


Brightfield
100 µm

B.


DIC
100um

C.


αASC
50 µm

D.

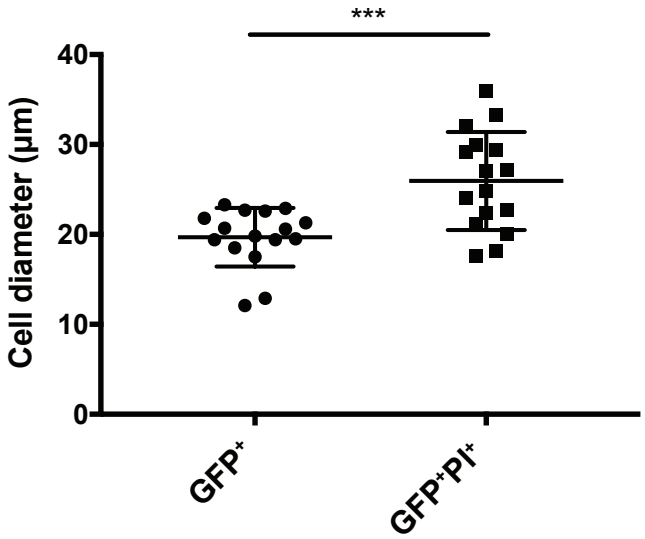

***
Cell diameter (µm)
40
30
20
10
0
GFP+
GFP+PI+

Figure 2.8: *A fetal microglia lytic cell cluster was positive for ASC specks and exhibits morphological characteristics of active lysis.*
A. A representative E12.5 lytic cell death cluster in the male LGE visualized by brightfield microscopy. Scale bar is 100 μm.
B. The representative E12.5 lytic cell death cluster in the LGE from the inset in panel (**A.**) visualized by differential interference contrast (DIC) microscopy. Scale bar is 100 μm.
C. αASC signal in the lytic cell death LGE cluster in the inset from panel (**A.**). Scale bar is 50 μm. Red arrows point to punctate ASC specks. N=1.
D. Cell diameters of cells from a representative *Cx3cr1*-GFP^+PI^+ cluster acquired by LSFM and quantified using the Imaris (Bitplane) program. Diameters of *Cx3cr1*-GFP^+ cells within the cluster, but without, PI were quantified (GFP^+) in addition to PI-containing *Cx3cr1*-GFP^+ cells (GFP^+PI^+).
(***) indicates $p < 0.001$.

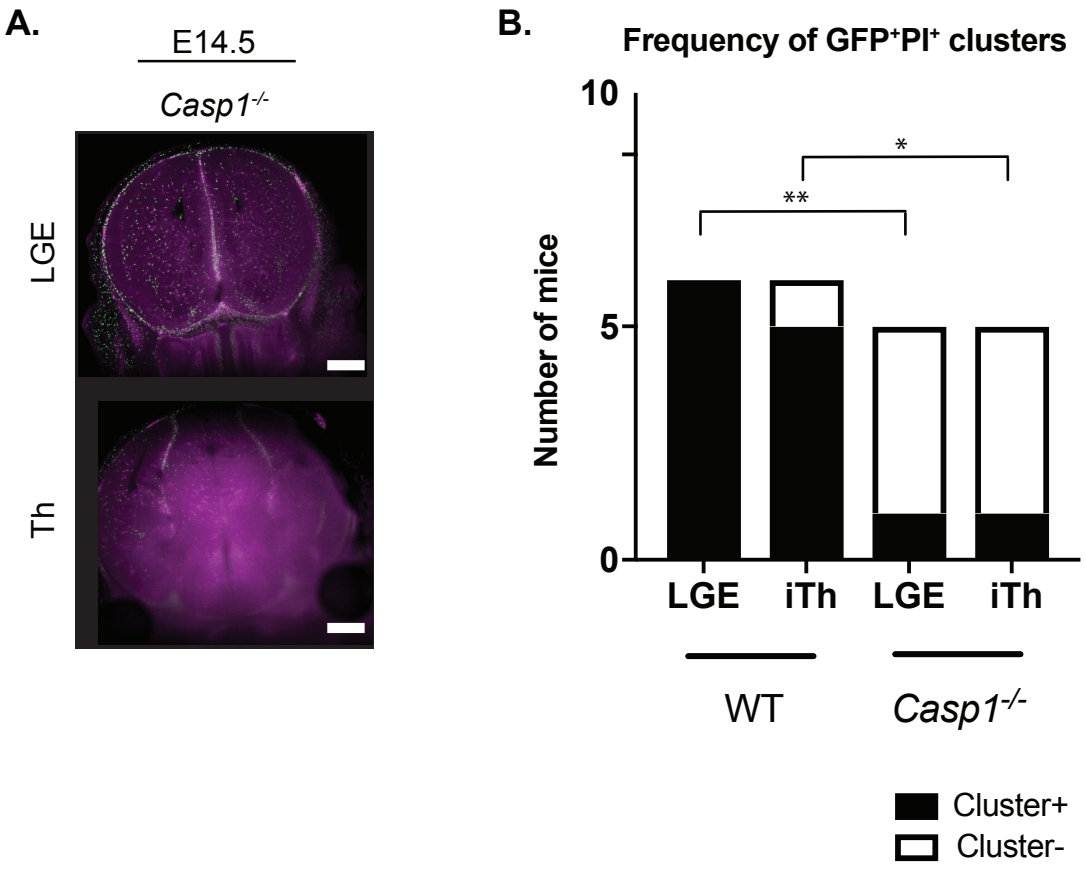

A.
E14.5
Casp1-/-
LGE
Th
B.
Frequency of GFP+PI+ clusters
10
5
0
Number of mice
*
**
LGE
iTh
LGE
iTh
WT
Casp1-/-
Cluster+
Cluster-

Figure 2.9: *Fetal microglial pyroptotic clusters are diminished on a* Casp1$^{-/-}$ *background.*
A. Representative coronal LSFM images of a male *Casp1*$^{-/-}$ E14.5 fetal brain shown (N=5). Scale bars indicate 500 µm.
B. Numbers of male mice that exhibited at least one GFP^{+}PI^{+} cluster in the E14.5 LGE and iTh are shown. exhibited clusters in the LGE and iTh are shown.
(*) shows $p < 0.05$ and (**) shows $p < 0.01$; n.s. = not significant.

A.

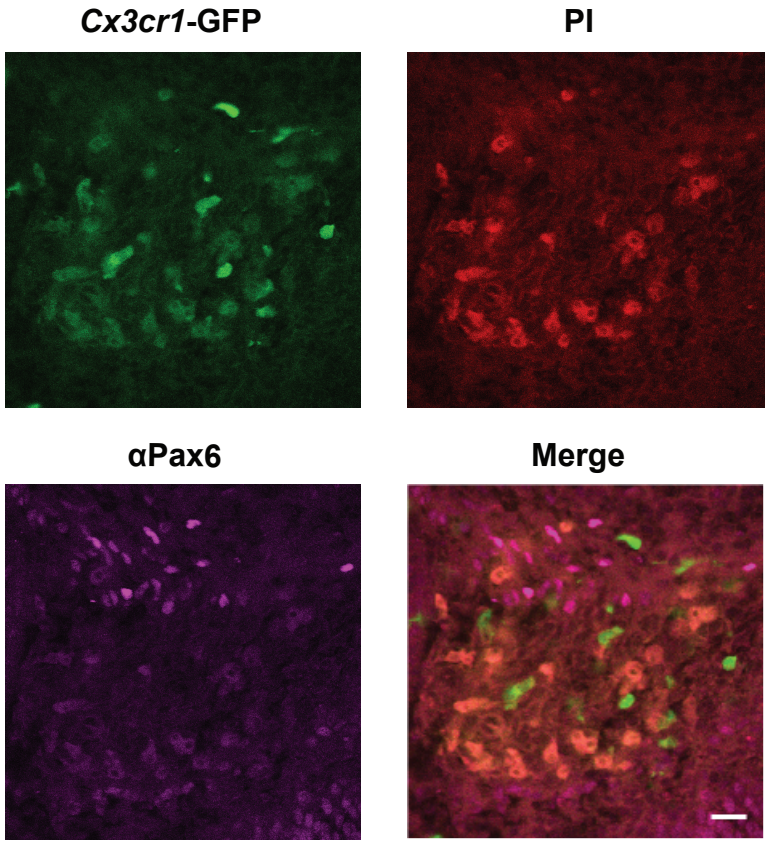
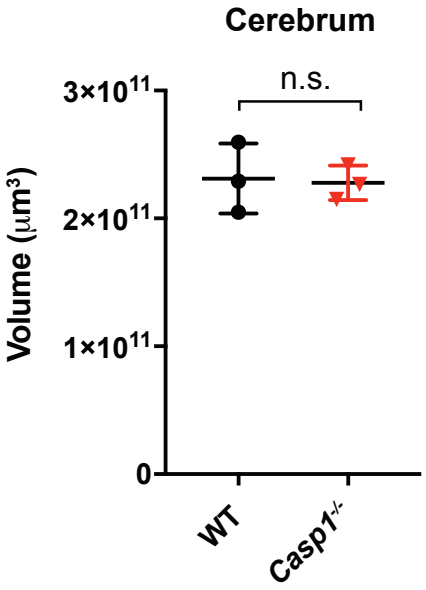
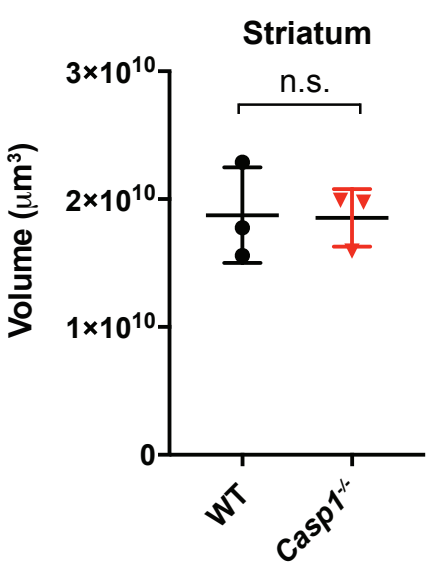


Figure 2.10: *Fetal microglial pyroptotic clusters localize near Pax6^{+} neural precursor cells.*
A. Enlarged image of an E12.5 *Cx3cr1*-GFP^{+}PI^{+} cluster is shown. Dams were injected with PI, embryos collected, and fetal brain sections stained with an anti-Pax6 antibody. Images of Cx3cr1-GFP (top left), PI (top right), anti-Pax6 (bottom left), and merged signals are shown. Scale bar indicates 50 μm. Imaged by Zeiss LSM 880 with Airyscan.

A.


Cerebrum
n.s.
3×10^11
2×10^11
1×10^11
0
Volume (μm^3)
WT
Casp1-/-

B.


Striatum
n.s.
3×10^10
2×10^10
1×10^10
0
Volume (μm^3)
WT
Casp1-/-

C.

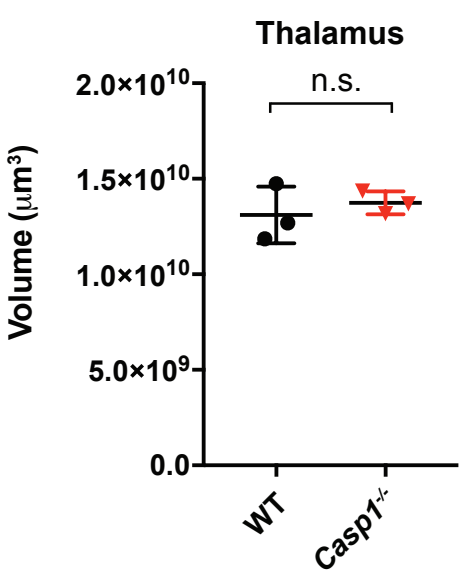

Thalamus
n.s.
2.0×10^10
1.5×10^10
1.0×10^10
5.0×10^9
0.0
Volume (μm^3)
WT
Casp1-/-

Figure 2.11: Casp1$^{-/-}$ *adult brains have no overt structural brain anomalies*.
A. Volume of the cerebrum from age-matched adult male WT (black circle, N=3) and *Casp1*$^{-/-}$ (red triangle, N=3) brains determined by Nissl staining and stereology using the Cavalieri Method.
B. Volume of the striatum from age-matched adult male WT (black circle, N=3) and *Casp1*$^{-/-}$ (red triangle, N=3) brains determined by Nissl staining and stereology using the Cavalieri Method.
C. Volume of the thalamus from age-matched adult male WT (black circle, N=3) and *Casp1*$^{-/-}$ (red triangle, N=3) brains determined by Nissl staining and stereology using the Cavalieri Method.
Data is shown as volumes (mm^3) of individual mice and their averages. Error bars indicate S.E.M.
n.s. = not significant.

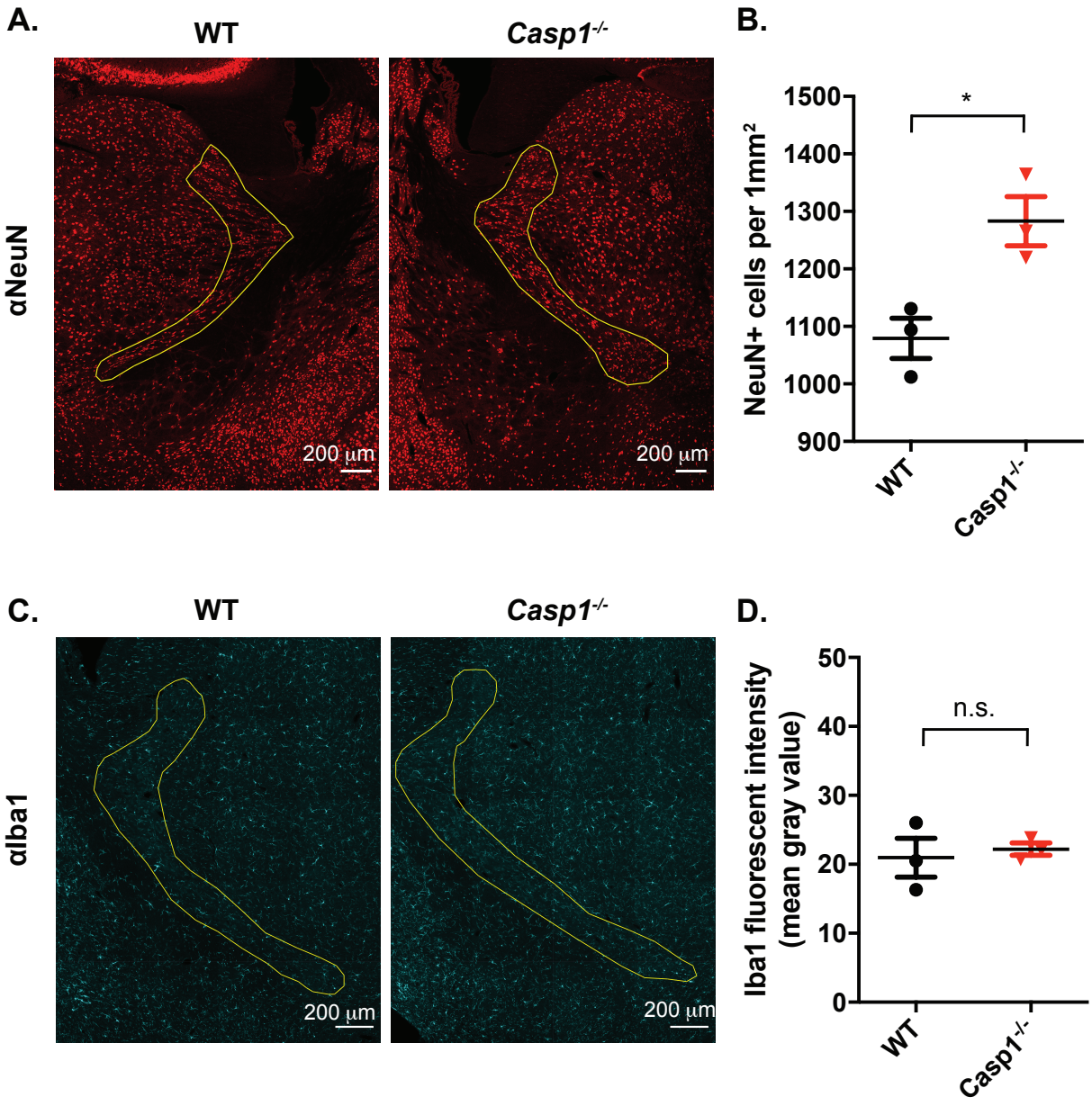

A.
WT
Casp1-/-
αNeuN
200 μm
200 μm
B.
NeuN+ cells per 1mm2
1500
1400
1300
1200
1100
1000
900
*
WT
Casp1-/-
C.
WT
Casp1-/-
αIba1
200 μm
200 μm
D.
Iba1 fluorescent intensity
(mean gray value)
50
40
30
20
10
0
n.s.
WT
Casp1-/-

Figure 2.12: Casp1$^{-/-}$ *adult brains increased cell density within the thalamic reticular nucleus.*
A. Representative images of anti-NeuN staining signals from age-matched male *Casp1*$^{-/-}$ (N=3, right) and WT (N=3, left) adult brains are shown. Yellow lines indicate the TRN regions defined by anti-parvalbumin staining.
B. Average anti-NeuN signals from age-matched male *Casp1*$^{-/-}$ (red triangle) and WT (black circle) mice brain sections are shown as cell number/mm^2. Dots indicate individual animals and are the average cell numbers from a total of 6 serial sections shown.
C. Representative images of anti-Iba1 staining signals from age-matched male *Casp1*$^{-/-}$ (N=3, right) and WT (N=3, left) adult brains are shown. Yellow lines indicate the TRN regions defined by anti-parvalbumin staining.
D. Average anti-Iba1 staining fluorescence intensities of age-matched male *Casp1*$^{-/-}$ (red triangle) and WT (black circle) mouse brain sections are shown as mean gray value/mm^2. Dots indicate individual animals and are the average of fluorescence intensities from a total of 6 serial sections shown.
(*) shows $p < 0.05$; n.s. = not significant.

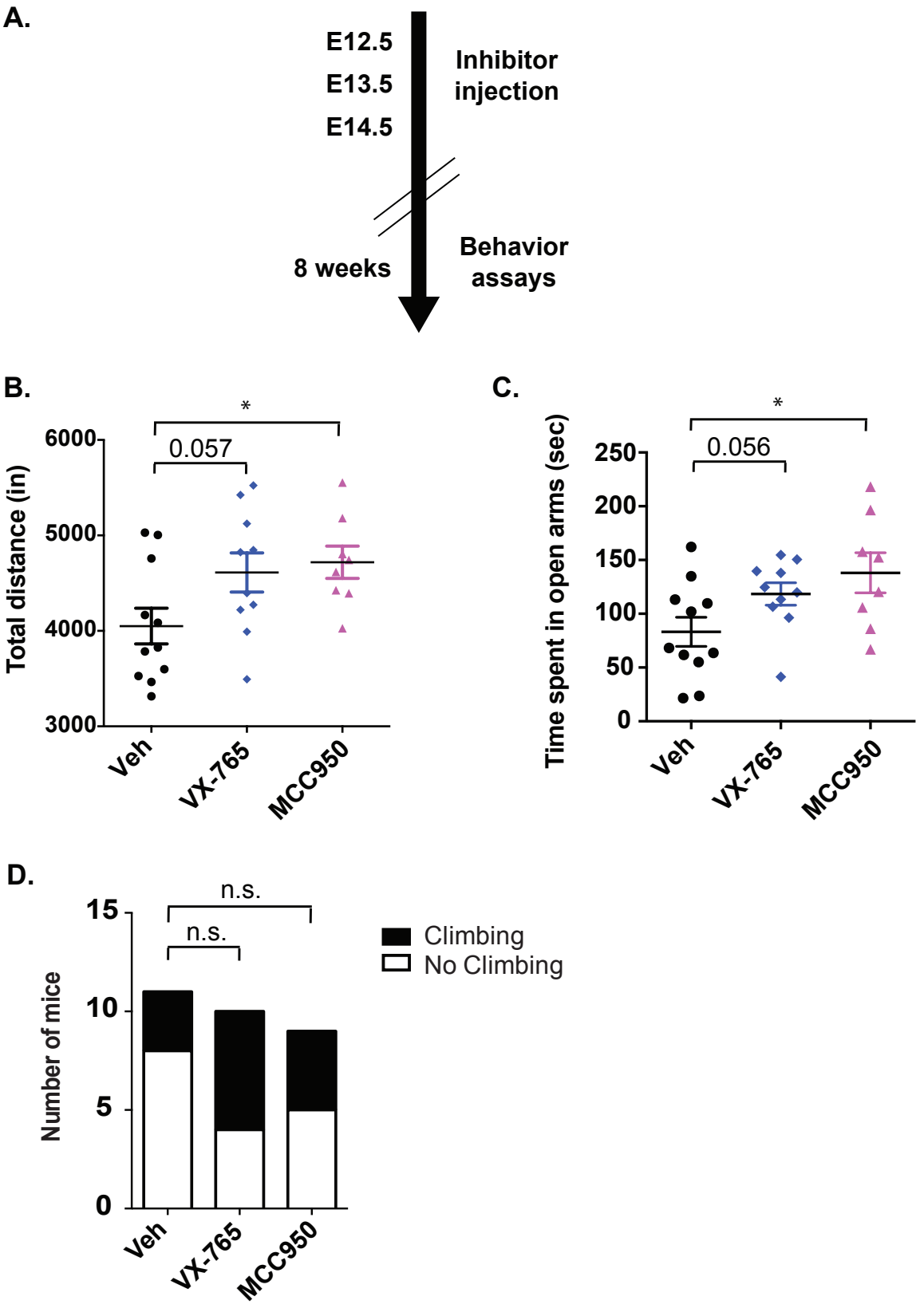

A.
E12.5
E13.5
E14.5
Inhibitor injection
8 weeks
Behavior assays
B.
Total distance (in)
6000
5000
4000
3000
*
0.057
Veh
VX-765
MCC950
C.
Time spent in open arms (sec)
250
200
150
100
50
0
*
0.056
Veh
VX-765
MCC950
D.
Number of mice
15
10
5
0
n.s.
n.s.
Climbing
No Climbing
Veh
VX-765
MCC950

Figure 2.13: *Pharmacological inhibition of pyroptosis in development produces some ADHD-like behavior changes in mice.*
A. Experimental scheme. Inhibitors were injected intraperitoneally to dams days E12.5-E14.5 in gestation. After birth and 8 weeks of age, behavior assays were run.
B. General movement of offspring of male WT mice treated with PBS (black circles), VX-765 (blue diamonds), and MCC950 (pink triangles) was determined by open field assay and is shown as total distance (inches).
C. Level of anxiety was determined by elevated plus maze assay and is shown as time spent in open arms (seconds).
D. Climbing behavior was determined using the three-chamber social interaction assay. (*) shows $p < 0.05$; n.s. = not significant.

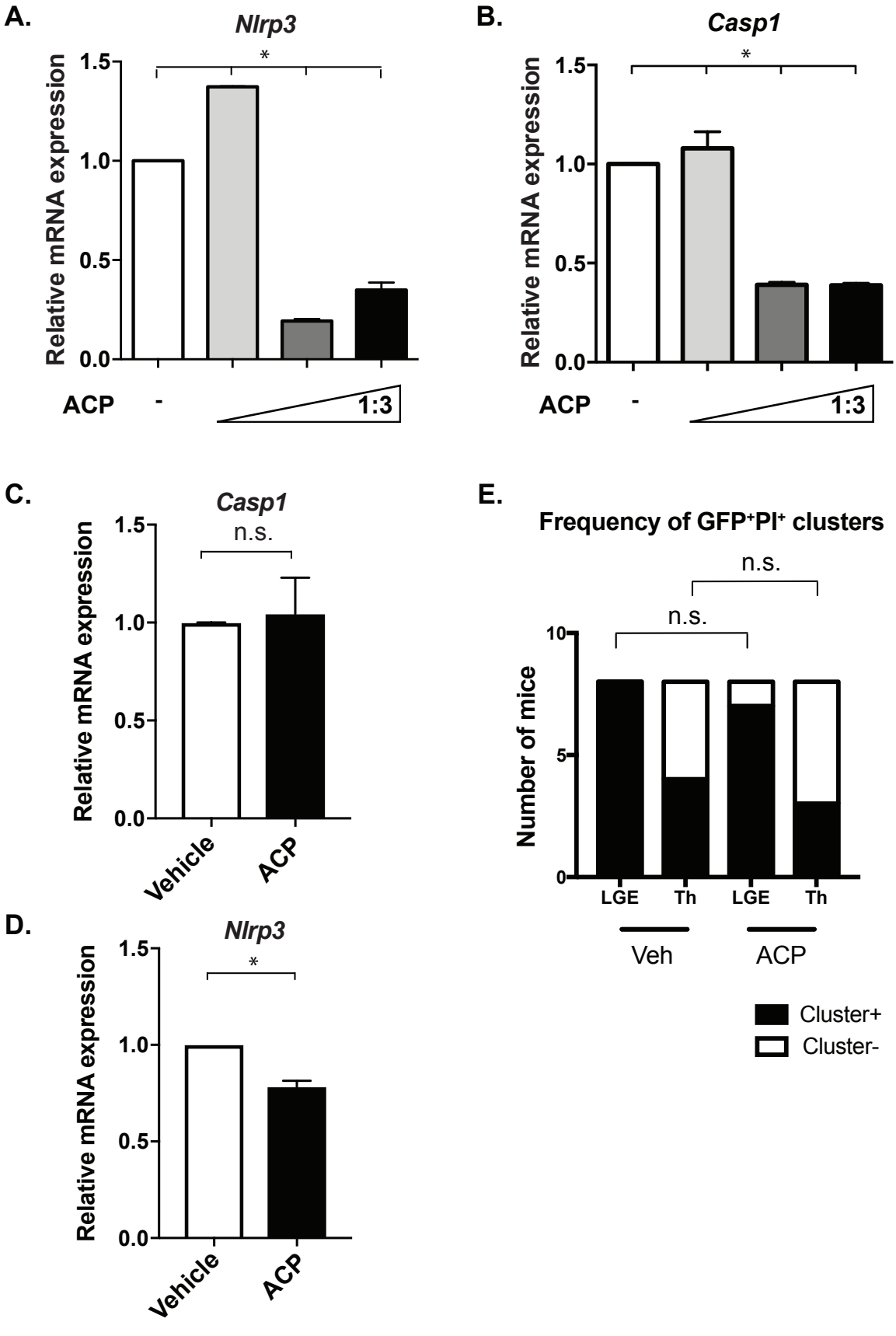
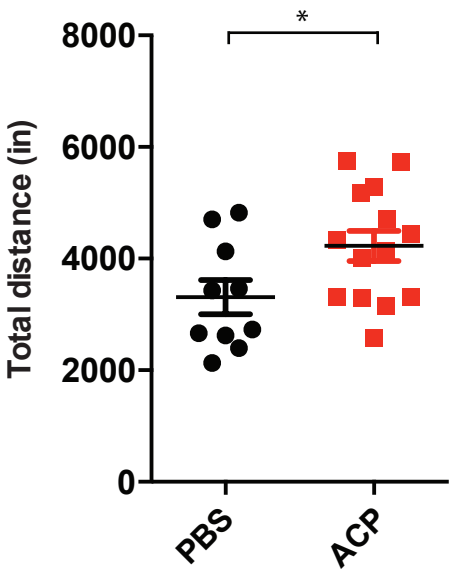
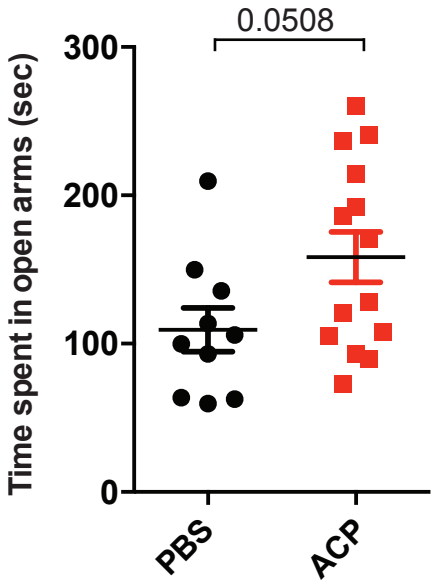

A.
Nlrp3
Relative mRNA expression
1.5
1.0
0.5
0.0
*
ACP
-
1:3
B.
Casp1
Relative mRNA expression
1.5
1.0
0.5
0.0
*
ACP
-
1:3
C.
Casp1
n.s.
Relative mRNA expression
1.5
1.0
0.5
0.0
Vehicle
ACP
D.
Nlrp3
Relative mRNA expression
1.5
1.0
0.5
0.0
*
Vehicle
ACP
E.
Frequency of GFP+PI+ clusters
n.s.
n.s.
Number of mice
10
5
0
LGE
Th
LGE
Th
Veh
ACP
Cluster+
Cluster-

Figure 2.14: *Acetaminophen downregulates inflammasome pathway elements, but does not decrease the frequency of lytic microglial clusters.*
A. A mouse microglial cell line (SIMA9) was treated with 3-fold serial dilutions of 1.5 mg/ml acetaminophen (the highest concentration) for 12 hours and the relative mRNA expression of *Nlrp3* was determined by RT-qPCR.
B. A mouse microglial cell line (SIMA9) was treated with 3-fold serial dilutions of 1.5 mg/ml acetaminophen (the highest concentration) for 12 hours and the relative mRNA expression of *Casp1* was determined by RT-qPCR.
C. *Casp1* relative mRNA expression from *ex-vivo* isolated E14.5 $Cd45^{+}Cd11b^{+}$ male cells from fetal brains exposed to daily maternal intraperitoneal ACP injections at E12.5 and E14.5, determined by RT-qPCR.
D. *Nlrp3* relative mRNA expression from *ex-vivo* isolated E14.5 $Cd45^{+}Cd11b^{+}$ cells from fetal brains exposed to daily maternal intraperitoneal ACP injections at E12.5 and E14.5, determined by RT-qPCR.
E. Numbers of male mice that exhibited at least one $GFP^{+}PI^{+}$ cluster in the E14.5 LGE and iTh are shown from vehicle- and ACP-exposed offspring.
(*) shows $p < 0.05$.

A.


*
8000
6000
4000
2000
0
Total distance (in)
PBS
ACP

B.


0.0508
300
200
100
0
Time spent in open arms (sec)
PBS
ACP

C.

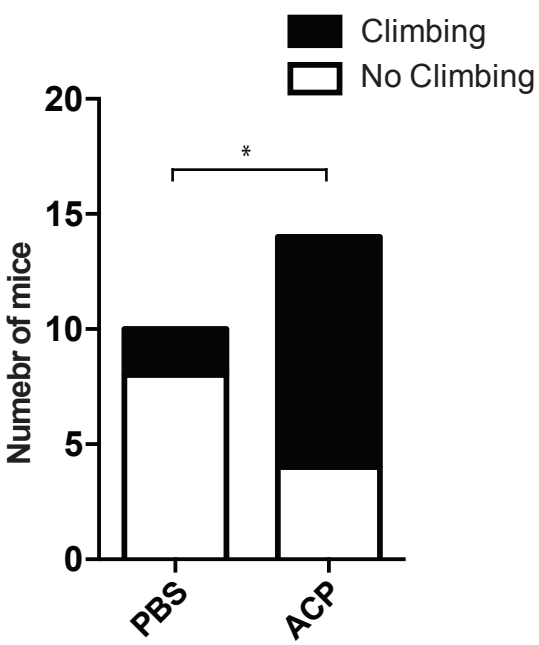
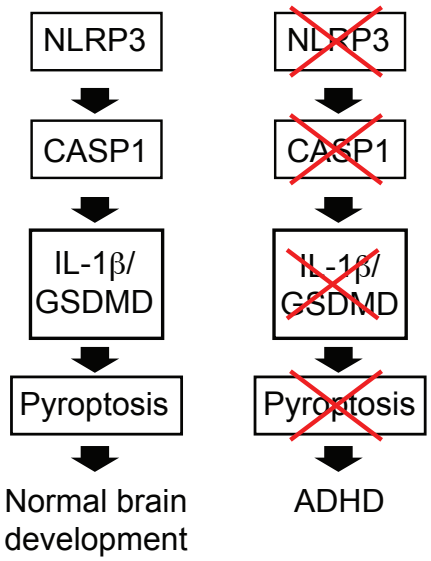

Climbing
No Climbing
*
20
15
10
5
0
Numebr of mice
PBS
ACP

Figure 2.15: *Acetaminophen exposure to dams at E12.5-E14.5 produce offspring with hyperactivity.*
A. General movement of offspring of male WT (black circles) and acetaminophen (ACP)-injected (red squares) mice was determined by open field assay and is shown as total distance (inches).
B. Level of anxiety was determined by elevated plus maze assay and is shown as time spent in open arms (seconds).
C. Climbing behavior was determined by three-chamber social interaction assay.
(*) shows $p < 0.05$.

A.


NLRP3
CASP1
IL-1β/
GSDMD
Pyroptosis
Normal brain
development
NLRP3
CASP1
IL-1β/
GSDMD
Pyroptosis
ADHD

B.

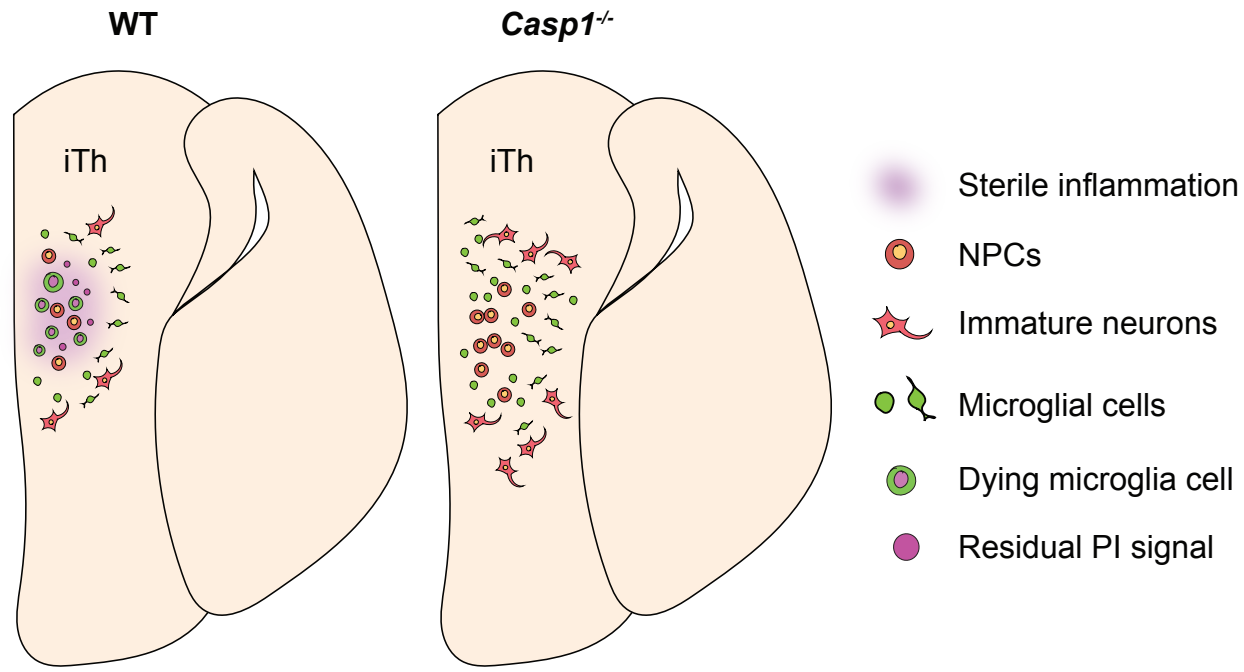

WT
Casp1-/-
iTh
iTh
Sterile inflammation
NPCs
Immature neurons
Microglial cells
Dying microglia cell
Residual PI signal

Figure 2.16: *Working model—microglial pyroptosis of key subsets promotes normal cell numbers within thalamic nuclei.*
A. Working model is shown. Specific microglial subsets in the male LGE and iTh undergo pyroptosis during fetal brain development. Activation of the NLRP3-CASP1-IL-1β/GSDMD pathway is required for normal brain development. Genetic and pharmacological disruptions of this pathway may increase the risk of the offspring developing ADHD.
B. Illustration of the fetal brain iTh at E14.5. Damage-associated molecular patterns (DAMPs), such as ATP, released from dead or dying neural cells activates microglial NLRP3 initiating the NLRP3-CASP1-IL-1β/GSDMD pathway depicted in panel (**A.**). As a result, sterile inflammation (perhaps mediated in part by IL-1β) influences the development of bystander neural precursor cells (NPCs). We propose that pro-inflammatory cytokines are required to promote the death of TRN precursor cells in the iTh.

Methods

Animals

All animals were maintained in specific pathogen-free conditions under a 12-hr light-dark cycle (7 am to 7 pm) and were given a standard chow diet and water *ad libitum*. Wild-type C57BL/6 mice were obtained from Charles River Laboratories and The Jackson Laboratory. *Casp1*$^{-/-}$*Casp11*$^{-/-}$ mice were kindly provided by A. Van der Velden and M. Starnbach. The generation of *iCasp1* and *Gsdmd*$^{-/-}$ mice was completed as described previously[99]. *IL-1R*$^{-/-}$*, Cx3cr1-Cre,* and *Cx3cr1-GFP* mice were purchased from The Jackson Laboratory. All animals were cohoused in mixed-genotype groups of 3-5 mice per cage upon weaning. If cohousing was not done, their bedding was mixed regularly to normalize the microenvironment. All experiments were approved by the Animal Care and Use Committee and were performed under the institutional guidelines of the University of California, Berkeley.

Behavioral assays
Male and female animals that were 2-4 months old were used for behavior assays.

Open field test

Mice were individually placed in the center of a plastic box (22 x 42.5 x 21 cm) for 1 hour and allowed to freely explore the arena. Animal movement was monitored by computerized photobeam using the MotorMonitor SmartFrame System (Kinder Scientific).

Elevated plus maze

Mice were individually placed onto the center of a platform (5 x 5 cm) of the maze that consisted of two open and two closed arms (30 x 5 cm) that were elevated 30 cm from the floor. Mice were allowed to freely explore the maze for 10 min and the Smart Video Tracking System (Panlab) was used to determine the time spent in the open and closed arms, as well as the center, during the test.

Three-chamber social behavior test

A three-chambered rectangular box with two dividing walls that marked the left, center, and right chambers (20 x 40 x 22 cm, each) was used. Two walls had openings that allowed a test mouse to freely move into each chamber. After a 10-minute habituation phase, a cylindrical grid cage (7 cm diameter and 15 cm height) housing a stranger mouse (age- and sex-matched) (S1) and another empty cylindrical grid cage (E) were placed on opposite sides of the apparatus. The test mouse was allowed to freely explore the chambers with the S1 and E cages for 10 min. The movement of the test mouse was recorded, and the time spent interacting or sniffing each cylindrical cage was measured using the Smart Video Tracking System (Panlab). The time spent on the

top of the cylindrical cage was designated as the climbing behavior and was also measured using the Smart Video Tracking System (Panlab).

The 5 choice serial reaction time task (5-CSRTT)

The procedures used in this task were as previously described with modifications[97]. A Plexiglas operator chamber (19 x 22 x 24 cm) with five response apertures and a food magazine was automatically controlled by the software (Packwin, Panlab). The procedure consisted of the pre-training, magazine training and 5-CSRTT training phase. Before the test and then throughout the entire experiment, the mice were food-restricted (1.8-2 g per day). On the first day of food restriction, mice were introduced some reward pellets (TestDiet 14 mg sugar pellets) to familiarize the mice to their taste. During the pre-training phase involved habituation to the chamber, five reward pellets in the food magazine and one reward pellet in each of the five apertures were placed for each operant chamber, and magazine light and all five stimulus lights were remained illuminated for the duration of the session. The mice were individually placed in the chamber and allowed to freely explore for 10 minutes. The habituation session was repeated until all the pellets were consumed. On the day of magazine training, the mice were placed in chamber for a 4-min period of free exploration, followed by all five stimulus lights switched on throughout the remaining session. After a random nose-poke response was made in one of the five apertures, the mouse was given 1 pellet in the food magazine. Once mice earned 20 pellets, they commenced to the 5-CSRTT training, which graduates through increasingly challenging stages (stage 1-6) on a schedule of progressively decreasing stimulus duration (SD) and increasing inter-trial intervals (ITI). The percentage of accuracy was calculated as [(number of correct trials/(number of correct and incorrect trials)) x 100]. The number of days taken to achieve the criteria for stage 6 (accuracy > 75 %, correct trials> 20) was recorded to indicate the attention performance. After meeting the criteria of stage 6 for at least two consecutive days, mice were moved forward in the testing schedule in which the variable ITI (5, 8.75, and 12.5 seconds) was randomly presented with an SD of 1.25 s. The percent accuracy was also calculated in this testing.

PI injection and tissue clearing

A total volume of 100 µl of propidium iodide (PI, 1.0 mg/ml) solution was intravenously injected into pregnant female mice at specific gestational dates. After 10-30 min of incubation, the mice were sacrificed. After recovering intact fetal bodies, we fixed fetal bodies and used the CUBIC tissue clearing method[104]. Briefly, embryos were incubated in R1 for approximately 2 days, replacing with fresh R1 after 24 hours, until the tissue was clarified (by eye). Embryos were rinsed in PBS before immersion in R2. They remained in R2, replacing with fresh R2 after 24 hours, until the tissue became fully clarified by eye. This step normally took 3-4 days before imaging.

Light sheet fluorescence microscopy and analysis

LSFM was performed using the Zeiss Lightsheet Z.1 system and 5X objective set (EC Plan-Neofluar 5x/0.16 detection and LSFM 5x/0.1 illumination lens) at 0.36x zoom. Samples were mounted on the stage using superglue and FEP tubing. CUBIC R2 solution was used as the refractive index-matched solution. Coronal acquisitions captured the entirety of the embryonic forebrain (about 620 Z slices). GFP and PI signals were simultaneously acquired using one image track and 488 laser at 12% power, with two bandpass filters, 505-545 nm and 575-615 nm, to capture GFP and PI signals, respectively. Light sheet thickness set at 13.13 µm and exposure to 39.9 ms. Shannon-Nyquist sampling was observed, with voxel sizes approx. X =2.13 µm, Y=2.13 µm, and Z=6.16 µm. Imaging data was processed and analyzed by Imaris 9.1.0 software (Bitplane). The Lightsheet Z.1 microscope was available from the UC Berkeley Cancer Research Lab Molecular Imaging Center.

Ex-vivo fetal brain cell isolation

Unless otherwise noted, all isolation steps took place using ice-cold solutions on ice to prevent microglial activation; spins occurred at 1200*xg* at 4^{o}C for 10 minutes. E14.5 fetal brains were individually dissected and minced in PBS, then placed in 5 mL of F-12 media containing 8 U/mL DNAse-I (Roche, Ref. #04716728001). Each sample was triturated with a flame-polished glass pipet to obtain tissue pieces <1 mm. Samples were spun down and re-suspended in 10 mL of digestion buffer (HBSS buffer containing Ca_2^+ Mg_2^+ and 0.13 U/mL Liberase-TM, Sigma Aldrich cat. no. 5401119001). Samples were transferred to a 37^{o}C chamber to rotate, undergoing trituration every 5 minutes three times. While dissections, trituration, and digestion were ongoing, gDNA was isolated from fetal tails and used in a fast SRY PCR (fwd primer 5'-TTGTCTAGAGAGCATGGAGGGC-3', rev primer 5'-CCACTCCTCTGTGACACTTTAGC-3'; KAPA2G Fast HotStart PCR kit, Kapa Biosystems cat. no. KK5503) to determine sex. Samples were pooled by sex, filtered through a 100 µm cell strainer, and rinsed with 4 mL of Wash Buffer 1 (HBSS buffer without Ca_2^+ Mg_2^+, 10% FBS, and 10 U/mL DNAse-I). Filtrate was then filtered once more with a 70 µm cell strainer, rinsed by 4 mL of Wash Buffer 1, and then washed with 22 mL of Wash Buffer 2 (HBSS buffer without Ca_2^+ Mg_2^+ and 10% FBS). If fetal brains were Cx3cr1-GFP$^{+/-}$, samples were concentrated to about 3x10^6 cells/mL in Wash Buffer 2 and a viability dye (DAPI or TOPRO3; 1:10^4) was added immediately prior to sorting. At least 1x10^4 live GFP$^+$ and GFP$^-$ cells from either gender were simultaneously sorted into two tubes of Trizol-LS and frozen at -80^{o}C until RNA isolation. If fetal brains were WT, at least 1x10^6 cells were stained with Cd45.2-PE (1:100; Invitrogen ref. no. 12-0454-83) and Cd11b-PE-Cy7 (1:100; eBioscience cat. no. 25-0112-81) in 800 µL of Wash Buffer 2 for at least 15 minutes. After, 500 µL of Wash Buffer 2 was added and sample was spun down at 800*xg* (4^{o}C for 5 minutes), and re-suspended to about 3x10^6 cells/mL. A viability dye (DAPI, 1:10^4) was added immediately prior to sorting. At least 1x10^4 live Cd45$^+$Cd11b$^+$ and Cd45$^-$Cd11b$^-$ cells from either gender were simultaneously sorted into two tubes of Trizol-LS and frozen at -80^{o}C until RNA isolation. GFP$^+$ and Cd45$^+$Cd11b$^+$ cells both constituted about 1-2% of the total brain cell population.

Fetal brain immunofluorescence staining and imaging

Fetal bodies were recovered and drop-fixed in 4% PFA in PBS solution overnight on rotation at 4^{o}C, and rinsed the next day three times in PBS for two hours at RT. Fetal bodies then underwent a sucrose gradient up to 30% wt/vol PBS prior to embedding in a 1:1 mix of 30% sucrose in PBS and OCT compound (Sakura VWR) and sectioning on cryostat at 40µm thickness. Sections were dried and permeabilized with 0.1% Triton X-100 in PBS and blocked with 3-5% BlockAid solution (ThermoFisher, B10710). For ASC staining, sections were then stained with KO-verifed rabbit α hASC primary antibody (1:200; Adipogen, AL177, cat. no. AG-25B-0006-C100) overnight at 4^{o}C and donkey α rabbit AF350 secondary antibody (1:1000; ThermoFisher, cat. no. A10039) for at least 2 hours at RT. Sections were imaged using an upright Zeiss Axioskop 2 plus wide-field epifluorescence microscope. A 100 HAL lamp was used for illumination and images were captured with Plan Apochromat 20x/0.75 objective with standard DAPI and FITC cubes. An exposure time of 80.525 ms was used. Image brightness and contrast was changed throughout the image to enhance visibility of ASC specks. At least five embryos were serial sectioned from three different litters to detect ASC signal in the forebrain. Rabbit α hASC antibody was KO-verified using *ASC*$^{-/-}$ gut tissue, and positive signal was confirmed in parallel using gut tissue from *Casp8*$^{+/-}$*Casp1*$^{-/-}$ mice; these were imaged using a Zeiss Axio Scan.Z1 slide scanner microscope. Differential interference contrast (DIC) imaging was done on a Nikon Widefield Epifluorescent microscope. For Pax6 staining, a *Cx3cr1-GFP*$^{+/-}$ E12.5 embryonic sections (harvested after maternal exposure to PI) were stained with a primary antibody against mouse Pax6 and imaged by the Zeiss LSM 880 with Airyscan. Microscopes were available from the UC Berkeley Cancer Research Lab Molecular Imaging Center.

Nissl staining

Three adult age-matched WT and Casp1$^{-/-}$ mice underwent transcardial perfusion with PBS and 4% PFA in PBS prior to dissection of whole brain and post-fixation overnight in 4% PFA in PBS. Next day, brains were rinsed three times for at least two hours in PBS at RT. Brains were embedded in OCT compound (Sakura VWR) before serial sectioning at 40 µm in a cryostat. Sections were stored at -80^{o}C until Nissl staining. For Nissl staining, OCT was washed from sections and then air dried at room temperature for 1 hour. Sections were then rinsed in ddH_2O and stained in Cresyl Violet solution (0.3% wt/vol Cresyl Violet Acetate in water plus 0.3% glacial acetic acid v/v; Sigma C-1791 and 537020) for 45 minutes. Sections were quickly rinsed in ddH_2O before undergoing an ethanol dehydration series (1 minute steps; 70%, 95%, 100% EtOH) before clearing in Xylenes for 3 minutes (Sigma 214736). Sections were mounted in Permount and dried for overnight before imaging.

Stereology

The Cavalieri volume estimation method (MicroBrightField) was used to estimate the volume of whole cerebrum, striatum, and thalamus of three adult age-matched WT and Casp1$^{-/-}$ mouse brains (from approximately Bregma +1.5 mm to Bregma -4.6 mm). 40 µm Nissl-stained sections were visualized using the bright field setting on a Imager.M1

microscope (Zeiss) connected to a camera (MicroFire A/R, Optronics) and computer running Stereo Investigator 11.03 software (MicroBrightField). Afterwards, markers were placed (using a grid spacing of 200μm and a section evaluation interval of 6) over these regions. Contours were drawn according to regions defined by the Allen Brain Atlas. Total volumes were then determined using the built-in software estimator. All volume estimations except for two possessed a Gundersen coefficient of error <0.10.

TRN staining, imaging, and quantification

WT and *Casp1*$^{-/-}$ adult brains were sectioned into 40 μm-thick coronal sections and blocked in PBST (0.1% Triton X-100 in PBS) containing 5% normal donkey serum and then incubated with primary anti-NeuN antibody, anti-Iba1 antibody, and anti-parvalbumin antibody overnight at 4°C. After washing, the brain sections were incubated with the corresponding secondary antibodies conjugated with Alexa Fluor® 488, Alexa Fluor® 555, and Alexa Fluor® 647 at RT for 2 h, followed by staining with iamidino-2-phenylindole (DAPI, 1:10000). The primary antibodies used in this study are as follows: rabbit anti-NeuN (1:300; ABN78, MilliporeSigma), mouse anti-parvalbumin (1:1000; P3088, MilloporeSigma), goat anti-Iba1 (1:250; PA5-18039, Thermo Fisher Scientific). The images were acquired using a confocal microscope (LSM 710 AxioObserver; Carl Zeiss) and then quantitatively analyzed with ImageJ (Fiji). The numbers of NeuN-positive cells in the regions of the thalamic reticular nucleus (TRN), which were defined with the parvalbumin staining, were measured with the Cell Counter plugin on ImageJ. To examine the expression levels of microglia, the mean gray value of Iba1 signaling in TRN regions was measured by ImageJ to indicate the mean fluorescent intensity of Iba1. For each mouse, 6 images were collected in each treatment. Three independent experiments were carried out. The LSM 710 AxioObserver microscope was available from the UC Berkeley Cancer Research Lab Molecular Imaging Center.

Acetaminophen *in vitro* assays

About $0.2x10^6$ SIM-A9 cells (a murine microglial cell line, were kindly provided by Dr. K. Nagamoto-Coms at the University of North Dakota) were plated onto a 6-well plate. Next day, cells were treated with acetaminophen (ACP) at three concentrations: 0.166 mg/mL, 0.5 mg/mL, and 1.5 mg/mL. Every well in the plate (including vehicle control wells) received the same amount of 100% ethanol (EtOH) to control for EtOH toxicity effects—concentrations beyond 1.5 mg/mL induced widespread cell death. ACP was prepared at a stock concentration of 25 mg/mL in 100% ethanol and stored at -20^{o}C. 12 hours after treatment, RNA was extracted in Trizol solution for RT-qPCR.

RT-qPCR

SIM-A9 cells, a murine microglial cell line, were kindly provided by Dr. K. Nagamoto-Coms (University of North Dakota). Total RNA from either SIM-A9 cells or *ex-vivo* microglia was isolated using the DirectZol kit (Zymo research). RT reactions were performed using the random hexamers protocol from the SuperScript III First-Strand

Synthesis System kit (Invitrogen, cat. no. 18080051) and RT-qPCRs were performed using the KAPA SYBR qPCR 2X master mix (Kapa Biosystems, KK5503), all following the manufacturer protocols. $2^{-\Delta\Delta Ct}$ method was used for analysis using *Hprt* expression for normalization. Primers used in this study include:
Hprt (fwd 5'- TCAGTCAACGGGGGACATAAA-3', rev 5'-GGGGCTGTACTGCTTAACCAG-3'), *Casp1* (fwd 5'-TGGGACCCTCAAGTTTTGCCC-3', rev 5'-GGCAAGACGTGTACGAGTGGTT-3'), *Nlrp3* (fwd 5'-CTTTGCTGCGATCAACAGGCG-3', rev 5'-TCAAGGCTGTCCTCCTGGCATA-3'), *Celf4* (fwd 5'-CAAGGAGCGCACAATGCGAC-3', rev 5'-ATGAGGGCTGCTTGCTGCTG-3'), *Cd200* (fwd 5'-TCACTTGCTCTGCGACTGCC-3', rev 5'-GGGGTCTTTGACCCGGAGGA-3').

Statistical analyses

Statistical analysis was performed using the Prism 6 (GraphPad) software. We used the Student's t-test to compare two groups and one-way ANOVA to compare more than three groups with the Tukey post-test, except when showing the differences between the littermate controls and experimental groups. Fisher's exact test was used to correlate climbing behavior changes with genotype, as well as the appearance of clusters and their correlations with time point and genotype. P-values <0.05 were considered to be statistically significant.

References

1. Saijo, K. & Glass, C. K. Microglial cell origin and phenotypes in health and disease. *Nat. Rev. Immunol.* **11,** 775–787 (2011).
2. Wright-Jin, E. C. & Gutmann, D. H. Microglia as Dynamic Cellular Mediators of Brain Function. *Trends in Molecular Medicine* **25,** 967–979 (2019).
3. Kettenmann, H., Hanisch, U.-K., Noda, M. & Verkhratsky, A. Physiology of microglia. *Physiological Reviews* **91,** 461–553 (2011).
4. Eyo, U. B. & Wu, L.-J. Microglia: Lifelong patrolling immune cells of the brain. *Progress in Neurobiology* **179,** 101614 (2019).
5. Uweru, J. O. & Eyo, U. B. A decade of diverse microglial-neuronal physical interactions in the brain (2008-2018). *Neuroscience Letters* **698,** 33–38 (2019).
6. Hammond, T. R. *et al.* Single-Cell RNA Sequencing of Microglia throughout the Mouse Lifespan and in the Injured Brain Reveals Complex Cell-State Changes. *Immunity* **50,** 253–271.e6 (2019).
7. Li, Q. *et al.* Developmental Heterogeneity of Microglia and Brain Myeloid Cells Revealed by Deep Single-Cell RNA Sequencing. *Neuron* **101,** 207–223.e10 (2019).
8. Broz, P. & Dixit, V. M. Inflammasomes: mechanism of assembly, regulation and signalling. *Nat. Rev. Immunol.* **16,** 407–420 (2016).
9. Mehta, T. R., Monegro, A., Nene, Y., Fayyaz, M. & Bollu, P. C. Neurobiology of ADHD: A Review. *Curr Dev Disord Rep* **6,** 235–240 (2019).
10. Sontag, T. A., Tucha, O., Walitza, S. & Lange, K. W. Animal models of attention deficit/hyperactivity disorder (ADHD): a critical review. *Atten Defic Hyperact Disord* **2,** 1–20 (2010).
11. OKAMOTO, K. & AOKI, K. Development of a strain of spontaneously hypertensive rats. *Jpn. Circ. J.* **27,** 282–293 (1963).
12. Sadile, A. G., Lamberti, C., Siegfried, B. & Welzl, H. Circadian activity, nociceptive thresholds, nigrostriatal and mesolimbic dopaminergic activity in the Naples High- and Low-Excitability rat lines. *Behavioural Brain Research* **55,** 17–27 (1993).
13. Leo, D. & Gainetdinov, R. R. Transgenic mouse models for ADHD. *Cell Tissue Res* **354,** 259–271 (2013).
14. Russell, V. A. Overview of animal models of attention deficit hyperactivity disorder (ADHD). *Curr Protoc Neurosci* **Chapter 9,** Unit9.35 (2011).
15. Sagvolden, T., DasBanerjee, T., Zhang-James, Y., Middleton, F. & Faraone, S. Behavioral and genetic evidence for a novel animal model of Attention-Deficit/Hyperactivity Disorder Predominantly Inattentive Subtype. *Behav Brain Funct* **4,** 56 (2008).
16. Fernando, A. B. P. & Robbins, T. W. Animal models of neuropsychiatric disorders. *Annu Rev Clin Psychol* **7,** 39–61 (2011).
17. Meneses, A. *et al.* Spontaneously hypertensive rat (SHR) as an animal model for ADHD: a short overview. *Rev Neurosci* **22,** 365–371 (2011).
18. Kostrzewa, R. M., Kostrzewa, J. P., Kostrzewa, R. A., Nowak, P. & Brus, R.

Pharmacological models of ADHD. *J Neural Transm (Vienna)* **115,** 287–298 (2008).
19. Davids, E., Zhang, K., Tarazi, F. I. & Baldessarini, R. J. Animal models of attention-deficit hyperactivity disorder. *Brain Res. Brain Res. Rev.* **42,** 1–21 (2003).
20. Paule, M. G. *et al.* Attention deficit/hyperactivity disorder: characteristics, interventions and models. *Neurotoxicol Teratol* **22,** 631–651 (2000).
21. la Peña, de, J. B. *et al.* Exploring the Validity of Proposed Transgenic Animal Models of Attention-Deficit Hyperactivity Disorder (ADHD). *Mol Neurobiol* **55,** 3739–3754 (2018).
22. Gainetdinov, R. R. *et al.* Role of serotonin in the paradoxical calming effect of psychostimulants on hyperactivity. *Science* **283,** 397–401 (1999).
23. Leo, D. & Gainetdinov, R. R. Transgenic mouse models for ADHD. *Cell Tissue Res* **354,** 259–271 (2013).
24. Li, B., Arime, Y., Hall, F. S., Uhl, G. R. & Sora, I. Impaired spatial working memory and decreased frontal cortex BDNF protein level in dopamine transporter knockout mice. *European Journal of Pharmacology* **628,** 104–107 (2010).
25. Ralph, R. J., Paulus, M. P., Fumagalli, F., Caron, M. G. & Geyer, M. A. Prepulse inhibition deficits and perseverative motor patterns in dopamine transporter knock-out mice: differential effects of D1 and D2 receptor antagonists. *J. Neurosci.* **21,** 305–313 (2001).
26. Yamashita, M. *et al.* Norepinephrine transporter blockade can normalize the prepulse inhibition deficits found in dopamine transporter knockout mice. *Neuropsychopharmacology* **31,** 2132–2139 (2006).
27. Leo, D. & Gainetdinov, R. R. Transgenic mouse models for ADHD. *Cell Tissue Res* **354,** 259–271 (2013).
28. Swanson, J. M. *et al.* Dopamine genes and ADHD. *Neuroscience and Biobehavioral Reviews* **24,** 21–25 (2000).
29. la Peña, de, J. B. *et al.* Exploring the Validity of Proposed Transgenic Animal Models of Attention-Deficit Hyperactivity Disorder (ADHD). *Mol Neurobiol* **55,** 3739–3754 (2018).
30. Gainetdinov, R. R. Strengths and limitations of genetic models of ADHD. *Atten Defic Hyperact Disord* **2,** 21–30 (2010).
31. Bruno, K. J. *et al.* Abnormal latent inhibition and impulsivity in coloboma mice, a model of ADHD. *Neurobiology of Disease* **25,** 206–216 (2007).
32. Hess, E. J., Collins, K. A. & Wilson, M. C. Mouse model of hyperkinesis implicates SNAP-25 in behavioral regulation. *Journal of Neuroscience* **16,** 3104–3111 (1996).
33. Wilson, M. C. Coloboma mouse mutant as an animal model of hyperkinesis and attention deficit hyperactivity disorder. *Neuroscience and Biobehavioral Reviews* **24,** 51–57 (2000).
34. Sharp, S. I. *et al.* Genetic association of the tachykinin receptor 1 TACR1 gene in bipolar disorder, attention deficit hyperactivity disorder, and the alcohol dependence syndrome. *Am. J. Med. Genet. B Neuropsychiatr. Genet.* **165B,** 373–380 (2014).

35. Yan, T. C., Hunt, S. P. & Stanford, S. C. Behavioural and neurochemical abnormalities in mice lacking functional tachykinin-1 (NK1) receptors: a model of attention deficit hyperactivity disorder. *Neuropharmacology* **57,** 627–635 (2009).
36. Siesser, W. B., Cheng, S.-Y. & McDonald, M. P. Hyperactivity, impaired learning on a vigilance task, and a differential response to methylphenidate in the TRbetaPV knock-in mouse. *Psychopharmacology (Berl.)* **181,** 653–663 (2005).
37. Siesser, W. B., Zhao, J., Miller, L. R., Cheng, S. Y. & McDonald, M. P. Transgenic mice expressing a human mutant beta1 thyroid receptor are hyperactive, impulsive, and inattentive. *Genes Brain Behav.* **5,** 282–297 (2006).
38. Wong, R. *et al.* Transgenic mice bearing a human mutant thyroid hormone beta 1 receptor manifest thyroid function anomalies, weight reduction, and hyperactivity. *Mol. Med.* **3,** 303–314 (1997).
39. Hess, E. J., Jinnah, H. A., Kozak, C. A. & Wilson, M. C. Spontaneous locomotor hyperactivity in a mouse mutant with a deletion including the Snap gene on chromosome 2. *Journal of Neuroscience* **12,** 2865–2874 (1992).
40. Martinon, F., Burns, K. & Tschopp, J. The inflammasome: a molecular platform triggering activation of inflammatory caspases and processing of proIL-beta. *Molecular Cell* **10,** 417–426 (2002).
41. Place, D. E. & Kanneganti, T.-D. Recent advances in inflammasome biology. *Current Opinion in Immunology* **50,** 32–38 (2018).
42. He, W.-T. *et al.* Gasdermin D is an executor of pyroptosis and required for interleukin-1β secretion. *Cell Res.* **25,** 1285–1298 (2015).
43. Liu, X. *et al.* Inflammasome-activated gasdermin D causes pyroptosis by forming membrane pores. *Nature* **535,** 153–158 (2016).
44. Evavold, C. L. *et al.* The Pore-Forming Protein Gasdermin D Regulates Interleukin-1 Secretion from Living Macrophages. *Immunity* (2017). doi:10.1016/j.immuni.2017.11.013
45. Bergsbaken, T., Fink, S. L. & Cookson, B. T. Pyroptosis: host cell death and inflammation. *Nat. Rev. Microbiol.* **7,** 99–109 (2009).
46. Takeda, K. & Akira, S. TLR signaling pathways. *Seminars in Immunology* **16,** 3–9 (2004).
47. Boyden, E. D. & Dietrich, W. F. Nalp1b controls mouse macrophage susceptibility to anthrax lethal toxin. *Nature Genetics* **38,** 240–244 (2006).
48. Chavarría-Smith, J. & Vance, R. E. Direct Proteolytic Cleavage of NLRP1B Is Necessary and Sufficient for Inflammasome Activation by Anthrax Lethal Factor. *PLoS Pathog* **9,** e1003452–10 (2013).
49. He, Y., Hara, H. & Núñez, G. Mechanism and Regulation of NLRP3 Inflammasome Activation. *Trends Biochem. Sci.* **41,** 1012–1021 (2016).
50. Kayagaki, N. *et al.* Caspase-11 cleaves gasdermin D for non-canonical inflammasome signalling. *Nature* **526,** 666–671 (2015).
51. Shi, J. *et al.* Cleavage of GSDMD by inflammatory caspases determines pyroptotic cell death. *Nature* **526,** 660–665 (2015).
52. Kuranaga, E. Beyond apoptosis: caspase regulatory mechanisms and

functions in vivo. *Genes Cells* **17,** 83–97 (2012).
53. Fink, S. L. & Cookson, B. T. Caspase-1-dependent pore formation during pyroptosis leads to osmotic lysis of infected host macrophages. *Cell. Microbiol.* **8,** 1812–1825 (2006).
54. Albert, M. L. Death-defying immunity: do apoptotic cells influence antigen processing and presentation? *Nat. Rev. Immunol.* **4,** 223–231 (2004).
55. Fernandes-Alnemri, T. *et al.* The pyroptosome: a supramolecular assembly of ASC dimers mediating inflammatory cell death via caspase-1 activation. *Cell Death and Differentiation 2015 22:10* **14,** 1590–1604 (2007).
56. Fuchs, Y. & Steller, H. Programmed cell death in animal development and disease. *Cell* **147,** 742–758 (2011).
57. Stefater, J. A., Ren, S., Lang, R. A. & Duffield, J. S. Metchnikoff's policemen: macrophages in development, homeostasis and regeneration. *Trends in Molecular Medicine* **17,** 743–752 (2011).
58. Wynn, T. A., Chawla, A. & Pollard, J. W. Macrophage biology in development, homeostasis and disease. *Nature* **496,** 445–455 (2013).
59. Lavin, Y. & Merad, M. Macrophages: gatekeepers of tissue integrity. *Cancer Immunol Res* **1,** 201–209 (2013).
60. Kierdorf, K. *et al.* Microglia emerge from erythromyeloid precursors via Pu.1- and Irf8-dependent pathways. *Nature Publishing Group* **16,** 273–280 (2013).
61. Ginhoux, F., Lim, S., Hoeffel, G., Low, D. & Huber, T. Origin and differentiation of microglia. *Front. Cell. Neurosci.* **7,** 45 (2013).
62. Heneka, M. T., McManus, R. M. & Latz, E. Inflammasome signalling in brain function and neurodegenerative disease. *Nat Rev Neurosci* **19,** 610–621 (2018).
63. Sims, R. *et al.* Rare coding variants in PLCG2, ABI3, and TREM2 implicate microglial-mediated innate immunity in Alzheimer's disease. *Nature Genetics* **49,** 1373–1384 (2017).
64. Griciuc, A. *et al.* Alzheimer's Disease Risk Gene CD33 Inhibits Microglial Uptake of Amyloid Beta. *Neuron* **78,** 631–643 (2013).
65. Codolo, G. *et al.* Triggering of inflammasome by aggregated α-synuclein, an inflammatory response in synucleinopathies. *PLoS ONE* **8,** e55375 (2013).
66. Zhou, Y. *et al.* MicroRNA-7 targets Nod-like receptor protein 3 inflammasome to modulate neuroinflammation in the pathogenesis of Parkinson's disease. *Mol Neurodegener* **11,** 28 (2016).
67. Gustot, A. *et al.* Amyloid fibrils are the molecular trigger of inflammation in Parkinson's disease. *Biochem. J.* **471,** 323–333 (2015).
68. Johann, S. *et al.* NLRP3 inflammasome is expressed by astrocytes in the SOD1 mouse model of ALS and in human sporadic ALS patients. *Glia* **63,** 2260–2273 (2015).
69. Meissner, F., Molawi, K. & Zychlinsky, A. Mutant superoxide dismutase 1-induced IL-1beta accelerates ALS pathogenesis. *Proc. Natl. Acad. Sci. U.S.A.* **107,** 13046–13050 (2010).
70. Italiani, P. *et al.* Evaluating the levels of interleukin-1 family cytokines in sporadic amyotrophic lateral sclerosis. *J Neuroinflammation* **11,** 94 (2014).
71. Walsh, J. G. *et al.* Rapid inflammasome activation in microglia contributes to

brain disease in HIV/AIDS. *Retrovirology* **11,** 35 (2014).
72. Chivero, E. T. *et al.* HIV-1 Tat Primes and Activates Microglial NLRP3 Inflammasome-Mediated Neuroinflammation. *J. Neurosci.* **37,** 3599–3609 (2017).
73. Mamik, M. K. *et al.* HIV-1 Viral Protein R Activates NLRP3 Inflammasome in Microglia: implications for HIV-1 Associated Neuroinflammation. *J Neuroimmune Pharmacol* **12,** 233–248 (2017).
74. de Rivero Vaccari, J. P. *et al.* Therapeutic neutralization of the NLRP1 inflammasome reduces the innate immune response and improves histopathology after traumatic brain injury. *J. Cereb. Blood Flow Metab.* **29,** 1251–1261 (2009).
75. Adamczak, S. E. *et al.* Pyroptotic neuronal cell death mediated by the AIM2 inflammasome. *J. Cereb. Blood Flow Metab.* **34,** 621–629 (2014).
76. Gustin, A. *et al.* NLRP3 Inflammasome Is Expressed and Functional in Mouse Brain Microglia but Not in Astrocytes. *PLoS ONE* **10,** e0130624 (2015).
77. Maturana, C. J., Aguirre, A. & Sáez, J. C. High glucocorticoid levels during gestation activate the inflammasome in hippocampal oligodendrocytes of the offspring. *Devel Neurobio* **77,** 625–642 (2017).
78. Liu, H.-D. *et al.* Expression of the NLRP3 inflammasome in cerebral cortex after traumatic brain injury in a rat model. *Neurochem. Res.* **38,** 2072–2083 (2013).
79. Walsh, J. G., Muruve, D. A. & Power, C. Inflammasomes in the CNS. *Nat Rev Neurosci* **15,** 84–97 (2014).
80. Moore, Z., Taylor, J. M. & Crack, P. J. The involvement of microglia in Alzheimer's disease: a new dog in the fight. *Br J Pharmacol* **176,** 3533–3543 (2019).
81. Streit, W. J. Microglia and Alzheimer's disease pathogenesis. *J. Neurosci. Res.* **77,** 1–8 (2004).
82. Wang, S. & Colonna, M. Microglia in Alzheimer's disease: A target for immunotherapy. *J. Leukoc. Biol.* **106,** 219–227 (2019).
83. Cameron, B. & Landreth, G. E. Inflammation, microglia, and alzheimer's disease. *Neurobiology of Disease* **37,** 503–509 (2010).
84. Selkoe, D. J. & Hardy, J. The amyloid hypothesis of Alzheimer's disease at 25 years. *EMBO Molecular Medicine* **8,** 595–608 (2016).
85. Halle, A. *et al.* The NALP3 inflammasome is involved in the innate immune response to amyloid-beta. *Nat Immuno* **9,** 857–865 (2008).
86. Heneka, M. T. *et al.* NLRP3 is activated in Alzheimer's disease and contributes to pathology in APP/PS1 mice. *Nature* **493,** 674–678 (2013).
87. Baranello, R. J. *et al.* Amyloid-beta protein clearance and degradation (ABCD) pathways and their role in Alzheimer's disease. *Curr Alzheimer Res* **12,** 32–46 (2015).
88. Venegas, C. *et al.* Microglia-derived ASC specks cross-seed amyloid-β in Alzheimer's disease. *Nature* **552,** 355–361 (2017).
89. Lücking, C. B. & Brice, A. Alpha-synuclein and Parkinson's disease. *Cell. Mol. Life Sci.* **57,** 1894–1908 (2000).

90. Daniele, S. G. *et al.* Activation of MyD88-dependent TLR1/2 signaling by misfolded α-synuclein, a protein linked to neurodegenerative disorders. *Sci Signal* **8,** ra45–ra45 (2015).
91. Wang, W. *et al.* Caspase-1 causes truncation and aggregation of the Parkinson's disease-associated protein α-synuclein. *Proc. Natl. Acad. Sci. U.S.A.* **113,** 9587–9592 (2016).
92. Woods, S. P., Moore, D. J., Weber, E. & Grant, I. Cognitive neuropsychology of HIV-associated neurocognitive disorders. *Neuropsychol Rev* **19,** 152–168 (2009).
93. Brickler, T. *et al.* Nonessential Role for the NLRP1 Inflammasome Complex in a Murine Model of Traumatic Brain Injury. *Mediators Inflamm.* **2016,** 6373506 (2016).
94. Gulbransen, B. D. *et al.* Activation of neuronal P2X7 receptor-pannexin-1 mediates death of enteric neurons during colitis. *Nature Medicine* **18,** 600–604 (2012).
95. Jarret, A. *et al.* Enteric Nervous System-Derived IL-18 Orchestrates Mucosal Barrier Immunity. *Cell* **180,** 50–63.e12 (2020).
96. Talkowski, M. E. *et al.* Sequencing Chromosomal Abnormalities Reveals Neurodevelopmental Loci that Confer Risk across Diagnostic Boundaries. *Cell* **149,** 525–537 (2012).
97. Asinof, S. K. & Paine, T. A. The 5-choice serial reaction time task: a task of attention and impulse control for rodents. *JoVE* e51574 (2014). doi:10.3791/51574
98. Murray, C. L., Obiang, P., Bannerman, D. & Cunningham, C. Endogenous IL-1 in cognitive function and anxiety: a study in IL-1RI-/- mice. *PLoS ONE* **8,** e78385 (2013).
99. Rauch, I. *et al.* NAIP-NLRC4 Inflammasomes Coordinate Intestinal Epithelial Cell Expulsion with Eicosanoid and IL-18 Release via Activation of Caspase-1 and -8. *Immunity* **46,** 649–659 (2017).
100. Yona, S. *et al.* Fate mapping reveals origins and dynamics of monocytes and tissue macrophages under homeostasis. *Immunity* **38,** 79–91 (2013).
101. Haimon, Z. *et al.* Re-evaluating microglia expression profiles using RiboTag and cell isolation strategies. *Nat Immunol* **19,** 636–644 (2018).
102. Semple, B. D., Blomgren, K., Gimlin, K., Ferriero, D. M. & Noble-Haeusslein, L. J. Brain development in rodents and humans: Identifying benchmarks of maturation and vulnerability to injury across species. *Progress in Neurobiology* **106-107,** 1–16 (2013).
103. Martínez, S., Puelles, E., system, L. P. T. M. N.2012. Molecular regionalization of the developing neural tube. *Elsevier* doi:10.1016/B978-0-12-369497-3.10001-9
104. Susaki, E. A. *et al.* Whole-brain imaging with single-cell resolution using chemical cocktails and computational analysis. *Cell* **157,** 726–739 (2014).
105. Susaki, E. A. *et al.* Advanced CUBIC protocols for whole-brain and whole-body clearing and imaging. *Nature Protocols* **10,** 1709–1727 (2015).
106. Santi, P. A. Light sheet fluorescence microscopy: a review. *J. Histochem. Cytochem.* **59,** 129–138 (2011).

107. Keller, P. J. & Dodt, H.-U. Light sheet microscopy of living or cleared specimens. *Current Opinion in Neurobiology* **22,** 138–143 (2012).
108. Power, R. M. & Huisken, J. A guide to light-sheet fluorescence microscopy for multiscale imaging. *Nat Meth* **14,** 360–373 (2017).
109. Ueda, H. R. *et al.* Tissue clearing and its applications in neuroscience. *Nat Rev Neurosci* **21,** 61–79 (2020).
110. Vande Walle, L. & Lamkanfi, M. Pyroptosis. *Curr. Biol.* **26,** R568–R572 (2016).
111. Rauch, I. *et al.* NAIP-NLRC4 Inflammasomes Coordinate Intestinal Epithelial Cell Expulsion with Eicosanoid and IL-18 Release via Activation of Caspase-1 and -8. *Immunity* **46,** 649–659 (2017).
112. Miao, E. A. *et al.* Caspase-1-induced pyroptosis is an innate immune effector mechanism against intracellular bacteria. *Nat Immunol* **11,** 1136–1142 (2010).
113. Chen, X. *et al.* Pyroptosis is driven by non-selective gasdermin-D pore and its morphology is different from MLKL channel-mediated necroptosis. *Cell Res.* **26,** 1007–1020 (2016).
114. Linkermann, A. & Green, D. R. Necroptosis. *N Engl J Med* **370,** 455–465 (2014).
115. Martinez, S., Puelles, E., Puelles, L. & Echevarria, D. in *The Mouse Nervous System* 2–18 (Elsevier, 2012). doi:10.1016/B978-0-12-369497-3.10001-9
116. Thion, M. S. & Garel, S. On place and time: microglia in embryonic and perinatal brain development. *Current Opinion in Neurobiology* **47,** 121–130 (2017).
117. Bjornsson, C. S., Apostolopoulou, M., Tian, Y. & Temple, S. It takes a village: constructing the neurogenic niche. *Dev. Cell* **32,** 435–446 (2015).
118. Englund, C. *et al.* Pax6, Tbr2, and Tbr1 are expressed sequentially by radial glia, intermediate progenitor cells, and postmitotic neurons in developing neocortex. *J. Neurosci.* **25,** 247–251 (2005).
119. Puelles, L. *et al.* Pallial and subpallial derivatives in the embryonic chick and mouse telencephalon, traced by the expression of the genes Dlx-2, Emx-1, Nkx-2.1, Pax-6, and Tbr-1. *J. Comp. Neurol.* **424,** 409–438 (2000).
120. Puelles, L., Martinez-de-la-Torre, M., nervous, J. F. T. M.2012. Diencephalon. *Elsevier* doi:10.1016/B978-0-12-369497-3.10009-3
121. Schmitz, C. & Hof, P. R. Design-based stereology in neuroscience. *NEUROSCIENCE* **130,** 813–831 (2005).
122. Martinez-Ferre, A. & Martinez, S. Molecular regionalization of the diencephalon. *Front. Neurosci.* **6,** 73 (2012).
123. Scholpp, S. & Lumsden, A. Building a bridal chamber: development of the thalamus. *Trends in Neurosciences* **33,** 373–380 (2010).
124. Chatterjee, M. & Li, J. Y. H. Patterning and compartment formation in the diencephalon. *Front. Neurosci.* **6,** 66 (2012).
125. Wells, M. F., Wimmer, R. D., Schmitt, L. I., Halassa, M. M. & Feng, G. Thalamic reticular impairment underlies attention deficit in Ptchd1Y/− mice. *Nature* 1–20 (2016). doi:10.1038/nature17427
126. Krol, A., Wimmer, R. D., Halassa, M. M. & Feng, G. Thalamic Reticular

Dysfunction as a Circuit Endophenotype in Neurodevelopmental Disorders. *Neuron* **98,** 282–295 (2018).
127. Pinault, D. The thalamic reticular nucleus: structure, function and concept. *Brain Res. Brain Res. Rev.* **46,** 1–31 (2004).
128. Joyner, A. L. & Sudarov, A. *Chapter 3 - Genetic Neuroanatomy*. *The Mouse Nervous System* 36–50 (Elsevier Inc., 2011). doi:10.1016/B978-0-12-369497-3.10003-2
129. Wannamaker, W. *et al.* (S)-1-((S)-2-{[1-(4-amino-3-chloro-phenyl)-methanoyl]-amino}-3,3-dimethyl-butanoyl)-pyrrolidine-2-carboxylic acid ((2R,3S)-2-ethoxy-5-oxo-tetrahydro-furan-3-yl)-amide (VX-765), an orally available selective interleukin (IL)-converting enzyme/caspase-1 inhibitor, exhibits potent anti-inflammatory activities by inhibiting the release of IL-1beta and IL-18. *J Pharmacol Exp Ther* **321,** 509–516 (2007).
130. Coll, R. C. *et al.* A small-molecule inhibitor of the NLRP3 inflammasome for the treatment of inflammatory diseases. *Nature Medicine* **21,** 248–255 (2015).
131. Randle, J., Harding, M. W., on, G. K. E. O.2001. ICE/Caspase-1 inhibitors as novel anti-inflammatory drugs. *Taylor & Francis* doi:10.1517/13543784.10.7.1207
132. Wang, C.-C. *et al.* Caspase-1 inhibitor ameliorates experimental autoimmune myasthenia gravis by innate dendric cell IL-1-IL-17 pathway. *J Neuroinflammation* **12,** 118 (2015).
133. Hegvik, T.-A., Instanes, J. T., Haavik, J., Klungsøyr, K. & Engeland, A. Associations between attention-deficit/hyperactivity disorder and autoimmune diseases are modified by sex: a population-based cross-sectional study. *Eur Child Adolesc Psychiatry* **27,** 663–675 (2018).
134. Nielsen, P. R., Benros, M. E. & Dalsgaard, S. Associations Between Autoimmune Diseases and Attention-Deficit/Hyperactivity Disorder: A Nationwide Study. *J Am Acad Child Adolesc Psychiatry* **56,** 234–240.e1 (2017).
135. Liew, Z., Ritz, B., Rebordosa, C., Lee, P.-C. & Olsen, J. Acetaminophen use during pregnancy, behavioral problems, and hyperkinetic disorders. *JAMA Pediatr* **168,** 313–320 (2014).
136. Blaser, J. A. & Allan, G. M. Acetaminophen in pregnancy and future risk of ADHD in offspring. *Can Fam Physician* **60,** 642 (2014).
137. Thompson, J. M. D. *et al.* Associations between acetaminophen use during pregnancy and ADHD symptoms measured at ages 7 and 11 years. *PLoS ONE* **9,** e108210 (2014).
138. Stergiakouli, E., Thapar, A. & Davey Smith, G. Association of Acetaminophen Use During Pregnancy With Behavioral Problems in Childhood: Evidence Against Confounding. *JAMA Pediatr* **170,** 964–970 (2016).
139. Avella-Garcia, C. B., Julvez, J., journal, J. F. I.2016. Acetaminophen use in pregnancy and neurodevelopment: attention function and autism spectrum symptoms. *academic.oup.com* doi:10.1093/ije/dyw115
140. Andrade, C. Use of acetaminophen (paracetamol) during pregnancy and the

risk of attention-deficit/hyperactivity disorder in the offspring. *J Clin Psychiatry* **77,** e312–4 (2016).
141. Liew, Z., Ritz, B., Virk, J. & Olsen, J. Maternal use of acetaminophen during pregnancy and risk of autism spectrum disorders in childhood: A Danish national birth cohort study. *Autism Res* **9,** 951–958 (2016).
142. Bauer, A. Z., Kriebel, D., Herbert, M. R., Bornehag, C.-G. & Swan, S. H. Prenatal paracetamol exposure and child neurodevelopment: A review. *Horm Behav* **101,** 125–147 (2018).
143. Werler, M. M., Mitchell, A. A., Hernandez-Diaz, S. & Honein, M. A. Use of over-the-counter medications during pregnancy. *Am. J. Obstet. Gynecol.* **193,** 771–777 (2005).
144. Liu, Y. *et al.* The anti-inflammatory effects of acetaminophen and N-acetylcysteine through suppression of the NLRP3 inflammasome pathway in LPS-challenged piglet mononuclear phagocytes. *Innate Immun* **21,** 587–597 (2015).
145. Dai, X.-M. *et al.* Targeted disruption of the mouse colony-stimulating factor 1 receptor gene results in osteopetrosis, mononuclear phagocyte deficiency, increased primitive progenitor cell frequencies, and reproductive defects. *Blood* **99,** 111–120 (2002).
146. Li, J., Chen, K., Zhu, L. & Pollard, J. W. Conditional deletion of the colony stimulating factor-1 receptor (c-fms proto-oncogene) in mice. *Genesis* **44,** 328–335 (2006).
147. Cecchini, M. G. *et al.* Role of colony stimulating factor-1 in the establishment and regulation of tissue macrophages during postnatal development of the mouse. *Development* **120,** 1357–1372 (1994).
148. Chitu, V. & Stanley, E. R. Regulation of Embryonic and Postnatal Development by the CSF-1 Receptor. *Curr. Top. Dev. Biol.* **123,** 229–275 (2017).
149. Chitu, V., Gokhan, S., Nandi, S., Mehler, M. F. & Stanley, E. R. Emerging Roles for CSF-1 Receptor and its Ligands in the Nervous System. *Trends in Neurosciences* **39,** 378–393 (2016).
150. Erblich, B., Zhu, L., Etgen, A. M., Dobrenis, K. & Pollard, J. W. Absence of colony stimulation factor-1 receptor results in loss of microglia, disrupted brain development and olfactory deficits. *PLoS ONE* **6,** e26317 (2011).
151. Oosterhof, N. *et al.* Homozygous Mutations in CSF1R Cause a Pediatric-Onset Leukoencephalopathy and Can Result in Congenital Absence of Microglia. *Am. J. Hum. Genet.* **104,** 936–947 (2019).
152. Hume, D. A. *et al.* Phenotypic impacts of CSF1R deficiencies in humans and model organisms. *J. Leukoc. Biol.* (2019). doi:10.1002/JLB.MR0519-143R
153. Ginhoux, F. *et al.* Fate mapping analysis reveals that adult microglia derive from primitive macrophages. *Science* **330,** 841–845 (2010).
154. Van Hove, H. *et al.* A single-cell atlas of mouse brain macrophages reveals unique transcriptional identities shaped by ontogeny and tissue environment. *Nat Neurosci* **22,** 1021–1035 (2019).
155. Utz, S. G. *et al.* Early Fate Defines Microglia and Non-parenchymal Brain Macrophage Development. *Cell* (2020). doi:10.1016/j.cell.2020.03.021

156. Swinnen, N. *et al.* Complex invasion pattern of the cerebral cortex bymicroglial cells during development of the mouse embryo. *Glia* **61,** 150–163 (2013).
157. Bennett, M. L. *et al.* New tools for studying microglia in the mouse and human CNS. *Proc. Natl. Acad. Sci. U.S.A.* **113,** E1738–46 (2016).
158. Kaiser, T. & Feng, G. Tmem119-EGFP and Tmem119-CreERT2 Transgenic Mice for Labeling and Manipulating Microglia. *eNeuro* **6,** (2019).
159. Ruan, C. *et al.* A novel Tmem119-tdTomato reporter mouse model for studying microglia in the central nervous system. *Brain Behavior and Immunity* **83,** 180–191 (2020).
160. Buttgereit, A. *et al.* Sall1 is a transcriptional regulator defining microglia identity and function. *Nat Immunol* **17,** 1397–1406 (2016).
161. Kaiser, T. & Feng, G. Modeling psychiatric disorders for developing effective treatments. *Nature Medicine* **21,** 979–988 (2015).
162. Mo, M. *et al.* Microglial P2Y12 Receptor Regulates Seizure-Induced Neurogenesis and Immature Neuronal Projections. *J. Neurosci.* **39,** 9453–9464 (2019).
163. Wu, L.-J., Vadakkan, K. I. & Zhuo, M. ATP-induced chemotaxis of microglial processes requires P2Y receptor-activated initiation of outward potassium currents. *Glia* **55,** 810–821 (2007).
164. Calovi, S., Mut-Arbona, P. & Sperlágh, B. Microglia and the Purinergic Signaling System. *NEUROSCIENCE* **405,** 137–147 (2019).
165. Robson, M. J. *et al.* Generation and Characterization of Mice Expressing a Conditional Allele of the Interleukin-1 Receptor Type 1. *PLoS ONE* **11,** e0150068 (2016).
166. Nowarski, R. *et al.* Epithelial IL-18 Equilibrium Controls Barrier Function in Colitis. *Cell* **163,** 1444–1456 (2015).
167. Harris, J. A. *et al.* Anatomical characterization of Cre driver mice for neural circuit mapping and manipulation. *Front Neural Circuits* **8,** 76 (2014).
168. Liu, X. & Quan, N. Microglia and CNS Interleukin-1: Beyond Immunological Concepts. *Front. Neurol.* **9,** 8 (2018).
169. Liu, X. *et al.* Cell-Type-Specific Interleukin 1 Receptor 1 Signaling in the Brain Regulates Distinct Neuroimmune Activities. *Immunity* **50,** 317–333.e6 (2019).
170. Tzeng, T.-C. *et al.* A Fluorescent Reporter Mouse for Inflammasome Assembly Demonstrates an Important Role for Cell-Bound and Free ASC Specks during In Vivo Infection. *Cell Rep* **16,** 571–582 (2016).
171. Saleeba, C., Dempsey, B., Le, S., Goodchild, A. & McMullan, S. A Student's Guide to Neural Circuit Tracing. *Front. Neurosci.* **13,** 897 (2019).
172. Sagvolden, T., Russell, V. A., Aase, H., Johansen, E. B. & Farshbaf, M. Rodent models of attention-deficit/hyperactivity disorder. *BPS* **57,** 1239–1247 (2005).
173. Childress, A. C. & Berry, S. A. Pharmacotherapy of attention-deficit hyperactivity disorder in adolescents. *Drugs* **72,** 309–325 (2012).

Chapter 3

Fetal brain myeloid cells respond to maternal immune challenge.

Abstract

Maternal infection is an environmental risk factor for autism spectrum disorder (ASD) in offspring. This risk factor is modeled by using the maternal immune activation model (MIA) paradigm[1,2] in which a prenatally injected viral or bacterial mimetic promotes ASD-like behavior changes in the offspring. Here, we show that only the viral mimetic Poly(I:C) injected at embryonic day 12.5 (E12.5) promoted ASD-like behavior changes in male offspring (and not the TLR agonists CpG-ODN and LPS). Furthermore, we found that fetal TRIF, and not maternal TRIF, signaling was necessary and sufficient to promote the core sociability defects in offspring following Poly(I:C)-induced MIA. These data suggest direct fetal innate immune sensing of a viral threat that is independent of maternal viral sensing. In support of this, only transplacental infection of a virus induced ASD-like behavior changes in the offspring, while another viral infection that did not cross the placenta could not promote ASD-like behavior changes. In order to identify the putative fetal innate immune cell sensing viral MIA challenge, we used a single-cell RNA sequencing (scRNAseq) approach on WT and *Trif*$^{-/-}$ fetal brain myeloid cells 24 hours after Poly(I:C)-induced MIA. We discovered an inflammatory population of responsive brain myeloid cells, likely to be border-associated macrophages, responding to Poly(I:C) in the fetal brain. Responder cells were absent in *Trif*$^{-/-}$ and WT control fetal brains. Altogether, our work identifies a fetal innate immune component for the MIA-induced sociability deficits.

Introduction

3.1 The maternal immune activation model (MIA) is a robust mouse model of ASD.

A benefit of studying ASD is the possibility of better understanding the circuits that mediate social behaviors. Because a large variety of genes are implicated as risk factors to ASD (as discussed in the main Introduction section 1.5), it is difficult to model all genetic risk factors in mice. Current ASD mouse models that rely on gene mutations include *neuroligin*, *neurexin*, *Shank*, *Fmr1*, *Mecp2*, *Ube3a*, *Nf1*, *Pten*, and *Tsc1/Tsc2* mutant mice; I refer the reader to these excellent reviews for further details about these mice and the behavioral phenotypes they possess[3-5]. Because an estimated 75% of ASD cases have unknown cause (not rooted in mutations), perhaps environmental factors drive the majority of ASD cases in the population[4].

The Atladottir study[6] inspired the maternal immune activation (MIA) model of ASD[1,2], which is becoming regarded as among the most robust models of ASD not reliant on genetic perturbation(s). Maternal infection as an environmental ASD risk factor is recaptured by injecting pregnant mice with a viral or bacterial mimetic, such as polyriboinosinic polyribocytidylic acid (Poly(I:C)) and lipopolysaccharide (LPS), respectively, during embryonic days E10.5, E12.5, or E14.5. Male offspring born to treated dams exhibit the hallmarks of ASD-like behavior changes, such as decreased sociability and an increase in restricted/repetitive behavior[1,2]. Poly(I:C) is structurally similar to viral dsRNA, which is primarily sensed by Toll-like receptor 3 (TLR3) and induces type I interferon (IFN) among other pro-inflammatory cytokines and chemokines via a TRIF-dependent signaling cascade[7,8]. LPS is found in the outer membrane of Gram-negative bacteria, and is sensed by Toll-like receptor 4 (TLR4)[9,10]. LPS sensing through TLR4 induces robust inflammatory response via MyD88- and TRIF-dependent signaling cascades, and promotes IL-6, TNF-α, and IL-12 pro-inflammatory cytokines production[9,10].

The immunostimulatory properties of Poly(I:C) and LPS pose an advantage over using live viral or bacterial infections for a few reasons. Firstly, the precise pathogens mediating the maternal infection ASD risk factor is not known. Secondly, using live infections in the lab poses a greater health risk to personnel, and requires specialized resources that are very expensive (such as separate housing and equipment for infected mice). Thirdly, routinely using live infections is experimentally difficult, and has the potential to introduce a wide array of variables that are difficult to control and monitor. These factors include identifying a safe range of viral or bacterial titers sufficient to induce an immune response, ensuring the same consistent degree of infection for all animals, establishing humane endpoints, and daily monitoring of mouse health. Furthermore, using live infections can complicate biological interpretation, particularly for the viral ones. Whether or not a behavioral outcome is due to a single, transient immune response from the initial infection, or due to re-activation of the virus in adulthood, is difficult to determine. For the above reasons, injecting with immune-stimulatory viral- or bacterial-mimics is the preference among investigators using the MIA model of ASD.

Currently, using Poly(I:C) or LPS in the MIA model is thought to be interchangeable[2,11], though efforts are underway to unify the MIA model[12]. While both

Poly(I:C) and LPS are highly immune-stimulatory and produce pro-inflammatory cytokines and chemokines, the precise character if the pro-inflammatory milieu is different largely because TLR3 utilizes TRIF as its sole adapter molecule, and TLR uses MYD88 in addition to Trif[8-10]. If the pro-inflammatory milieu is indeed involved in ASD development *in utero*, it could be that different behaviors and/or behavior severity depends on which TLR agonist is used in the MIA model. It is also thought that the gestational time point of injection, E12.5 and E14.5, produce the same behavioral alterations. Yet, in mouse, a two days' difference *in utero* is staggering. During E12.5, neurogenesis is just beginning as immature neurons descend from radial glial precursors[13]. At E14.5, neurogenesis is flourishing and most of the major neural subtypes have been generated[13]. Inducing a maternal immune response at E12.5 or E14.5 could have drastically different outcomes on the fetal brain. Indeed, comparing to human development, two days' time in mouse approximates a twelve day difference in humans[14]. In support of this concept, it is acknowledged that injection MIA agonists to dams later in gestation produces schizophrenia-like behavior changes in offspring[11,15]. Later in development (after E16.5), neurogenesis is largely complete, and the cellular basis of neural circuits has been settled[13,14]; therefore, neural alterations resulting from MIA may exert impacts at the synapse-level in addition to the neural cell body itself. Taken altogether, the type of immune-stimulant and timing of injection in development should be carefully considered when investigating how immune activation translates to the aberrant circuitry underlying the MIA-induced ASD-like behavior changes in mice.

3.2 Known immune response mechanisms during the MIA mouse model of ASD.

The immune responses related to the MIA model of ASD have primarily been centered on maternal immunity. A foundational paper from *Smith et al.* was the first to implicate a maternal cytokine, IL-6, as a requirement for driving ASD-like behavior changes in offspring[16]. *Smith et al.* gave a single maternal injection of Poly(I:C) co-administered with an anti-IL-6 antibody at E12.5[16]. They found that it prevented an ASD-like sociability defect (as measured by the social interaction/social preference test)[16]. In IL-6$^{-/-}$ mice, Poly(I:C) had no effect on the behaviors of adult offspring[16], though they exhibited abnormal conditioning behaviors within the latent inhibition paradigm (suggesting IL-6 has steady-state functions in normal brain development[16]). Blocking IL-6 also prevented over 90% of the gene expression changes seen in the offspring of Poly(I:C)-injected dams as assayed by microarray[16]. IL-6 is a cytokine that exerts pleiotropic effects[17,18]. Because of this, secondary immune responses downstream of IL-6 may also mediate ASD-like behavior changes.

One such cytokine downstream of IL-6 is IL-17a[19,20]. In a landmark paper by *Choi et al.*, maternal IL-17 produced by T_H17 cells, downstream of IL-6, was shown to be necessary and sufficient for promoting ASD-like behavior changes following Poly(I:C)-induced MIA[21]. *Choi et al.* injected Poly(I:C) to E12.5 dams and showed that serum cytokines IL-6, TNF-α, IFN-β, and IL-1β are significantly produced 3 hours after injection, followed by IL-17a at E14.5[21]. Using an IL-6$^{-/-}$ failed to increase serum levels of IL-17a, confirming that IL-17a is downstream of IL-6[21]. Similarly, injection of IL-6 instead of Poly(I:C) to E12.5 dams was sufficient to produce IL-17a, and IL-17Ra mRNA expression was increased in fetal E14.5 brains after maternal Poly(I:C) injection at

E12.5[21]. Indeed, IL-17a as an outcome of maternal Poly(I:C) injection at E12.5 caused cortical lamination abnormalities (such as inversions and protrusions) in fetal E14.5 cortex, which was rescued by co-administration with anti-IL-17a antibodies[21]. Furthermore, ultrasonic vocalizations of day 9 postnatal pups was promoted by IL-17a (suggesting defective communication), and abolished with pre-treatment with anti-IL-17a antibodies prior to MIA with Poly(I:C)[21]. Since IL-6 promotes T_H17 cell differentiation, and T_H17 cells produce IL-17a[19,20], *Choi et al.* investigated whether or not maternal T_H17 cells were producing IL-17. To do so, *Choi et al.* used RORγt deficient mice specifically in the $CD4^+$ T cell compartment; RORγt is a critical regulator of the IL-17a pathway. RORγt $CD4^+$ T cell deficient mothers failed to produce IL-17a even after Poly(I:C) injection[21]. Furthermore, the MIA-induced behavioral defects and cortical abnormalities were abolished in offspring from RORγt $CD4^+$ T cell deficient mothers[21]. Lastly, direct intraventricular injection of IL-17a was sufficient to promote the MIA-induced cortical anomalies and behavioral phenotypes; blocking IL-17a signaling in pregnant dams two days after Poly(I:C) injection had therapeutic effects in attenuating MIA-induced behavior changes in the offspring[21]. Altogether, *Choi et al.* convincingly demonstrate that IL-17a is produced by maternal T_H17 cells following Poly(I:C)-induced MIA, and that IL-17a crosses the placenta to cause cortical lamination abnormalities that promote ASD-like behavior changes in the offspring[21].

It is known that mice produce an abundance of T_H17 cells when segmented filamentous bacteria (SFB) colonize the intestinal microbiota compared to mice that are SFB-free[22]. Therefore, *Kim et al.* sought to explore the connection between the maternal microbiota and effects of MIA on offspring[23]. Intriguingly, using the broad-spectrum antibiotic vancomycin on WT C57BL/6 mice before Poly(I:C)-induced MIA abolished the increase of ultrasonic volcalizations and cortical patches seen in the offspring of non-antibiotic treated dams[23], suggesting that maternal bacteria can promote MIA-induced behavioral anomalies. Only IL-17a was detected in the plasma of dams that did not receive vancomycin, further suggesting a cellular source of IL-17 dependent on the microbiota[23]. Notably, T_H17 cells from the small intestine of vancomycin-treated dams were also diminished[23]. Since SFB disproportionally contributes to the differentiation of T_H17 cells in the small intestine[22], *Kim et al.* used mice with and without SFB during MIA. C57BL/6 wildtype mice from Jackson Laboratories (Jax) are SFB-free, while C57BL/6 wildtype mice from Taconic Biosciences (Tac) are colonized by SFB[23]. Predictably, Taconic mice had abundant T_H17 cells from the small intestine while Jax mice had very few T_H17 cells[23]. Unlike offspring from Taconic mothers, Poly(I:C)-induced MIA of Jax mothers did not show any MIA-associated behavioral phenotypes nor cortical patches[23]. Only after co-housing with Taconic mice, or oral-gavage of SFB, could MIA phenotypes in the offspring of Jax mothers be captured[23]. Collectively, these data powerfully demonstrate that the maternal microbiota can influence *in utero* brain development[23].

In another milestone paper, *Yim et al.* demonstrated that these behavioral abnormalities in MIA offspring can be reversed[24]. The cortical abnormalities previously identified by *Choi et al.* in E14.5 and E18.5 brains after Poly(I:C)-induced MIA persist into adulthood, mostly localizing as “cortical patches” within the primary somatosensory cortex[24]. Remarkably, driving neural activity in these regions using optogenetics induces MIA behavioral phenotypes within WT mice; similarly, reducing activity in these regions

via optogenetics corrects the MIA behavioral abnormalities[24]. Thus, a nexus among the putative circuitries mediating MIA-induced ASD-like behavior changes has been convincingly identified.

Taken altogether, maternal IL-17a (downstream of IL-6) derived by T_H17 cells (responsive to specific bacteria found within the microbiota) negatively impacts brain development by affecting the cortical lamination of offspring within the primary somatosensory cortex[21,23,24]. These cortical patches persist into adulthood, constituting a node of circuitry mediating ASD-like behavior changes[24]. Thus, the maternal IL-17a axis remains the best defined mechanism yet to explain the ASD-like behavior changes in offspring from Poly(I:C)-induced MIA mothers.

While these studies beautifully highlight the maternal immune contribution to ASD-like behaviors in offspring within the MIA model, the fetal contribution itself to ASD-like behaviors has received more limited attention in comparison. A prominent study by *Hsiao et al.* demonstrates that the microbiota within MIA offspring in adulthood can modulate their behavioral anomalies[25]. MIA treatment results in gut dysbiosis in offspring[25]. Oral treatment of MIA offspring with the bacterium *Bacteroides fragilis* corrected gut permeability issues, and also remarkably attenuated anxiety-like behaviors, restricted/repetitive burying of marbles, restored communication (as measured by USVs), and improved sensorimotor gating[25]. However, MIA offspring treated with *B. fragilis* retained defects in sociability and social preference[25]. Since *B. fragilis*' palliative effects were not due to changes in systemic immunity, Hsiao *et al.* found metabolites produced by *B. fragilis* that travel in the serum to help correct loose tight junctions mediating the increase in gut permeability, and/or modulate the microbial composition in the GI tract[25]. Thus, the microbiota in MIA offspring also modulate ASD-like behavior changes. However, because not all core behavior abnormalities were corrected with *B. fragilis* treatment, this likely reflects that core sociability changes have occurred during development, which are intractable to intervention after birth. Furthermore, it could be that MIA causes permanent immune dysregulation *in utero* that causes the compositional microbiota changes in adulthood, in addition to core ASD-like sociability changes. Thus, exploring the fetal immune response itself during development is worthy of investigation.

3.3 Investigating fetal immunity during MIA: design and rationale for our study.

Myeloid cells exist throughout the embryonic body, including the brain, as early as E10.5[26]. Myeloid cells, though undergoing their own migration, proliferation, and general developmental programming[26-28], may be immunologically competent enough to respond to MIA. Indeed, it is an attractive hypothesis, because direct or indirect sensing of MIA (and the subsequent cytokine and chemokine production thereof), could influence the development of fetal bystander cells nearby and represent an underappreciated arm of ASD development.

As discussed in more detail within the introductory chapter (section 1.2), the first wave of myeloid cells descends from erythromyeloid progenitor (EMP) cells of the yolk sac islands. EMPs infiltrate the primordial organ buds by E9.5[26,29,30]. By E10.5, organogenesis has begun[31]. Upon entry to the primordial organ buds, EMPs define their molecular programs attuned to their destination, and become long-lasting tissue-

resident macrophages with limited contribution from hematopoietic derived monocytes in certain contexts dependent on the organ[26-30,32]. It isn't until after E14.5 that the overlapping waves of hematopoiesis begin to produce lymphoid cells[26]. Thus, there is no expected adaptive immune component of an appreciable amount during the height of organogenesis between E10.5 and E13.5.

Neurogenesis begins at E12.5[13]. Therefore, the tissue resident macrophages of the brain, microglia, are already present in the developing brain prior to immature neurons[33,34]. Furthermore, border-associated macrophages (BAMs) and monocytes are also present[35,36]. Since MIA is typically induced at E12.5[1,2], the cell populations to consider within the fetal brain include microglia, BAMs, monocytes, radial glial precursors, immature neurons, as well as maturing and migrating neurons[13,14,33-36]. Notably, glial cells do not begin to arise from asymmetric division of radial glia until after E16.5[13,14,33-36]; therefore, oligodendrocytes and astrocytes are not considered relevant to the early phase of MIA-induced responses. The myeloid fraction of the brain is thought to be is immunologically competent due to the restricted expression of immune adapters (such as TLRs and adapter molecules like TRIF and MYD88). Thus, this fraction would likely contain fetal immune responders, if any, to MIA.

In order to identify if there is a fetal innate immune response component to the MIA-induced ASD-like behavior changes, we incorporate mouse genetics, live viral infections, behavior assays, and single cell RNA sequencing (scRNAseq) approaches. When using the MIA model, we injected TLR agonists to E12.5 dams and conducted behavioral assays on offspring at 10-16 weeks of age (see Methods). We looked for transcriptional signatures of an innate immune response in the brain myeloid fraction ($CD45^{+}Cd11b^{+}$ cells) 24 hours after MIA induction via scRNA-seq.

We hypothesized that viral sensing by TLR3 (activated by Poly(I:C) and mediated by TRIF signaling) will more strongly induce MIA phenotypes rather than other TLR agonists, such as LPS, that mimic bacterial infections. Since microglia are in the brain parenchyma at E12.5[33,34,37], including active zones of neurogenesis[37] (see Introduction section 1.2 for more information), we hypothesized that fetal microglia respond to Poly(I:C)-induced MIA. If indeed direct sensing of MIA by the fetal innate immune system is important, we hypothesized that only viruses that can pass the placenta will induce ASD-like behavior changes in the offspring.

Results

3.4 Only Poly(I:C)-induced MIA causes ASD-like behavior changes.

In order to infer which TLR agonists are relevant for inducing ASD-like behavior changes in MIA offspring, we considered agonists for TLR3, TLR4, and TLR9—Poly(I:C), LPS, and CpG oligodeoxynucleotides (ODN), respectively. Poly(I:C) mimics double-stranded RNA typical of many RNA viruses, LPS is derived from the outer membrane of Gram-negative bacteria, and ODN mimics unmethylated DNA typical of bacteria[38]. TLR3 signals through the TRIF adapter molecule, TLR9 through the MYD88 adapter, and LPS signals through both TRIF and MYD88 adapter molecules[9].

We injected TLR agonists or a vehicle saline control (PBS) to dams at E12.5 to activate maternal immunity (**Figure 3.1A**). 10-16 weeks after birth, offspring were used in behavior assays to assess all core and associated ASD-like behavior changes. The ASD-like core behavioral traits we assayed included sociability, restricted/repetitive behavior, and learning and memory. For sociability, three assays were utilized: the reciprocal social interaction, three-chamber, and food preference social transmission assays. For restricted/repetitive-like behaviors, the marble burying and open field (for grooming) assays were used. For learning and memory, the T-maze and fear conditioning (contextual and cued) assays were used. The associated ASD-like behavioral traits we assayed included hyperactivity and anxiety. For hyperactivity-like behaviors, we utilized the open field assay for general movement. For anxiety-like behaviors, we used the elevated plus maze and the open field assay (center vs. peripheral ratio). These assays are considered standard in the field[4].

Remarkably, only the TLR3 agonist Poly(I:C) was able to recapture the core ASD-like behavioral phenotype (**Figure 3.1B,C**). Male offspring from Poly(I:C)-injected dams had a significant reduction in the time spent approaching the stranger mouse within the social interaction assay (**Figure 3.1B**), suggesting impaired sociability consistent with a previous report[21]. Male offspring from Poly(I:C)-injected dams also buried a significantly higher amount of marbles in the marble burying assay, suggesting they exhibited highly restricted/repetitive behaviors (**Figure 3.1C**); this is also consistent with previous reports[1,21]. Meanwhile, male offspring from LPS- and ODN- injected mothers did have significant behavior changes, though they do not indicate classic ASD-like behavior changes. For example, male offspring from LPS-injected dams had a significant reduction in time spent approaching the stranger mouse in the social interaction assay (**Figure 3.1B**), yet did not bury a significantly greater amount of marbles (**Fig. 3.1C**). These data suggest that, while sociability was impaired in offspring of LPS-injected dams, they appeared like WT in that they did not have restricted/repetitive digging behaviors. Male offspring from ODN-injected mothers had no significant changes in the time spent approaching the stranger mouse in the social interaction assay (**Fig. 3.1B**), suggesting sociability is intact. However, male offspring from ODN-injected mothers buried a significantly reduced amount of marbles relative to WT mice (**Fig. 3.1C**), and therefore did not exhibit any restricted/repetitive behaviors; in fact, general burying was suppressed. Thus, male offspring from ODN-injected mothers did not exhibit any of the classic core ASD-like behavior changes. All male offspring exposed to maternal Poly(I:C), LPS, and ODN demonstrated learning and memory

deficits (data not shown). Poly(I:C)-exposed male offspring displayed hyperactivity/hypoanxiety, while LPS- and ODN-exposed offspring showed aggressive behaviors and high levels of anxiety (data not shown). Therefore, of the TLR three agonists, Poly(I:C)-induced MIA recaptures the most ASD-like behavioral phenotype.

Strikingly, female mice were largely protected from all three TLR agonist-induced MIA behavioral phenotypes (data not shown). An exception to this is that female offspring exposed to ODN-induced MIA had decreased restricted/repetitive behaviors in the marble burying assay (though, this is due to sleeping behaviors; data not shown). Thus, we also recaptured the male bias seen in ASD cases.

Altogether, these data suggest that TLR agonists clearly matter in the MIA model of ASD, replete with a male bias. Surprisingly, however, a clear segregation between TRIF-dependent and MYD88-dependent immune responses during MIA was observed for the core ASD-like behavior changes. Since TLR4 uses both TRIF and MYD88 to transmit its signal, it might make sense that sociability was impaired in offspring after LPS-induced MIA because of partial dependence on TRIF. Since TLR9 primarily uses MYD88 to transmit its signal, it may also make sense that sociability was intact in ODN-induced MIA offspring due to the lack of TRIF activation. Since offspring from LPS-induced and ODN-induced MIA did not exhibit restricted/repetitive behaviors within the marble burying assay, it could be that a MYD88-mediated signaling pathway is responsible for suppressing formation of the restricted/repetitive behaviors typical of Poly(I:C)-induced MIA offspring.

These data suggest that classic innate immune sensing is at play. While understanding how other agonists in MIA can lead to differential behavioral outcomes is worthy of further investigation in of itself, we decided to first investigate the contribution of TRIF signaling to MIA phenotypes because TRIF signaling appears to be the main driver of the core ASD-like behavior changes. Furthermore, we wondered if TRIF sensing of the mother or the fetus was more important to the ASD-like phenotypes of Poly(I:C) induced MIA.

3.5 Fetal immunity, mediated by TRIF signaling, is required for ASD-like defects in sociability.

In order to understand the maternal vs. fetal TRIF contribution to the Poly(I:C)-induced MIA phenotype in offspring, we used a mouse genetics approached combined with our mouse behavioral assays. We used a *Trif*$^{-/-}$ mouse line. To infer the fetal contribution of TRIF signaling, we first bred *Trif*$^{-/-}$ female mice with *Trif*$^{+/+}$ male mice such that each littermate had one functional copy of TRIF; these are heterozygous mice (*Trif*$^{+/-}$) (**Figure 3.2A).** When Poly(I:C) was injected to *Trif*$^{-/-}$ dams at E12.5 to induce MIA, *Trif*$^{+/-}$ male offspring exhibited defective sociability by having a significantly decreased interaction time with the stranger mouse in the social interaction assay (**Figure 3.2B**). However, male offspring did not exhibit restricted/repetitive tendencies as assayed by the marble burying test—they did not bury any significant amount of marbles above or below PBS vehicle control offspring (**Figure 3.2C**). These data suggest that maternal TRIF sensing is required for promoting restricted/repetitive behaviors. In another experiment, we bred heterozygous *Trif*$^{+/-}$ female and *Trif*$^{+/-}$ male mice such that the mother was competent for TRIF sensing, while there was a mix of

littermates who were and were not TRIF competent (**Figure 3.3A**). This experiment is ideal because *Trif*$^{+/-}$ and *Trif*$^{-/-}$ littermate behaviors can be compared side-by-side. Remarkably, only male offspring with the *Trif*$^{+/-}$ genotype captured the core ASD-like behavior changes: these offspring had a significant reduction in interaction time in the social interaction assay compared to PBS controls, as well as a significant increase in the number of marbles buried during the marble burying assay (**Figure 3.3B**). Male offspring with the *Trif*$^{-/-}$ genotype did not have a significant decrease in social interaction time, nor a significant increase in the number of marbles buried relative to PBS control offspring (**Figure 3.3C**). Because marble burying was not significantly increased in the Poly(I:C) MIA *Trif*$^{-/-}$ offspring from *Trif*$^{+/-}$ mothers, these data suggest that maternal TRIF sensing is not sufficient for producing restricted/repetitive behaviors in male MIA offspring (**Figure 3.3B,C**).

These data collectively demonstrate that fetal TRIF sensing is required for the core ASD-like sociability changes seen in Poly(I:C)-induced MIA male offspring, and that both maternal and fetal TRIF sensing is required to promote restricted/repetitive behaviors. These data also suggest that there is direct sensing of Poly(I:C) by fetal immune cells independent of TRIF sensing by the mother.

3.6 Trans-placental viral infections cause ASD-like behavior changes.

In order to test the idea that direct pathogen sensing by fetal immune cells could promote the MIA behavioral phenotypes, we use two murine viruses in live infections: murine gammaherpesvirus 68 (MHV-68), and murine cytomegalovirus (MCMV). MHV-68 models the human pathogen Kaposi's sarcoma-associated herpesvirus (KSHV)[39], and MCMV models human cytomegalovirus (HCMV) infection[40]. Both are DNA viruses[39,40]. Gammaherpesviruses like MHV-68 generally establish persistent latent infections in lymphocytes, and are of little concern in immunocompetent hosts who are largely asymptomatic[39]. Similarly, cytomegaloviruses like MCMV also can establish latent infections with the potential of re-activation and immunocompetent hosts are largely asymptomatic[40]. HCMV has the reputation of being the most common cause of congenital and perinatal viral infections around the world[41], though whether or not they increase the risk of ASD in the offspring is unclear[42-44]. Generally, the placenta is regarded as a physical and immunological barricade against viral infections[45]; indeed, MHV-68 and MCMV are thought to be unable to pass the placenta[46,47]. But, in immunodeficient backgrounds, MCMV can cross the placenta[48], and vertical transmission of MHV-68 was confirmed in one study[49]. Therefore, it may be possible that MHV-68 can cross the placenta to infect our mice. While it is not expected that TLR3 (mediated by TRIF signaling) is the primary sensor of intracellular infection from these viral pathogens with DNA genomes, TLR3 signaling was shown to be necessary to control MHV-68 infection and involved in the response to KSHV[46,50,51]. TLR3 response was also shown to be important during the course of MCMV infection in other studies[52,53]. Therefore, these two viruses may be ideal to test the requirement of fetal immune sensing.

We infected dams at E12.5 with live virus and conducted behavior assays on offspring 10-16 weeks later (**Figure 3.4A**). Only MHV-68, and not MCMV, could promote defects in sociability and increases in restricted/repetitive behaviors in male

mice, as assayed by the social interaction assay and marble burying assay, respectively (**Figure 3.4B-E**). In contrast, female offspring exposed to MHV-68 did not have significant behavior changes compared to uninfected controls (data not shown). Curiously, female offspring from mothers infected with MCMV did show variable restricted/repetitive behaviors and hypoanxiety (data not shown). In the male offspring of MHV-68 infected dams, we detected viral DNA by nested PCR and electrophoresis within fetal organs (**Figure 3.5**). This data suggests that trans-placental infection of the fetus from the mother disproportionately affects males, and that virus that can cross the placenta promote ASD-like behavior changes. Altogether, the data supports the idea that there is direct TRIF sensing in the fetus as a consequence of MIA. However, the TRIF-responsive fetal cell identity is unknown.

3.7 We recovered robust microglial and border-associated macrophage (BAM) populations in the E13.5 brain by scRNA-seq.

To identify the fetal TRIF-responsive cells, we used a single-cell RNA-sequencing (scRNA-seq) approach on the myeloid cell fraction ($Cd45^+Cd11b^+$ cells) of WT and *Trif*$^{-/-}$ fetal brains 24 hours after Poly(I:C) injection to dams (**Figure 3.6A,B**). We included two treatment replicates (with 1-2 litters per replicate; **Figure 3.6C**). We achieved a median capture of at least 10,000 UMIs per batch with less than 15% mitochondrial gene content per cell per batch, constituting a high-quality dataset of unprecedented breadth and depth for E13.5 brain myeloid cells (**Figure 3.7A-C**). Captured mRNA corresponded to meaningful feature content (**Figure 3.7D**). Features include genes and long non-coding RNA species. We recovered a total of 49,865 cells from 88 E13.5 brains traversing eighteen transcriptionally distinct cell clusters (**Figure 3.8A**). 37,339 cells were positive for *Fcrls* gene expression. *Fcrls* gene expression is found in both border-associated macrophage (BAM) and microglial cells of the brain, but is thought to be higher in the microglial fraction[35,36,54]. BAMs have been found to highly express *Mrc1*, *Lyve1*, and *Ms4a7*, while microglia have been found to highly express *P2ry12*, *Sparc*, and *Olfml3*. Consistent with the previous literature, we also detected these BAM and microglial gene signatures in the *Fcrls*$^+$ cell fractions (**Figure 3.8B**)[35,36,55,56]. Based on expression of *Fcrls* and these canonical marker genes, we define clusters 1, 2, and 4 as BAMs, and clusters 0, 6, and 7 as microglial (**Figure 3.8C**). We also found 12,526 *Fcrls*$^-$ cells likely to be monocytes and neural cells (**Figure 3.8C**). Some of the top differentially expressed marker genes are plotted as a heatmap in **Figure 3.9A**. Genes are displayed on the left, cell identity is annotated on the right, and cluster ID is color coded at the top of the heatmap. The top 20 differentially expressed marker genes per cluster is summarized in **Supplementary Table 1**.

3.8 We identified a putative WT fetal responder cell population to Poly(I:C)-induced MIA.

We found one cluster significantly enriched by cells from the Poly(I:C) condition in the *Fcrls*$^+$ (but not *Fcrls*$^-$) cell fraction. Cluster 13 is a unique cluster found in the Poly(I:C) condition (**Figure 3.10A,B**). Cluster 13 has 1118 cells, and these are almost exclusively WT, and not *Trif*$^{-/-}$, cells (**Figure 3.10A,C**). These data suggest that cells in Cluster 13 are the candidate *Trif*-competent responders to Poly(I:C)-induced MIA. Aside

from enrichment in monocytic clusters in WT, *Trif*$^{-/-}$ cells do not substantially differ in clustering from WT suggesting major fetal brain myeloid cell development is intact (**Figure 3.10A**).

Intriguingly, gene ontology analysis of the top twenty marker genes in Cluster 13 are enriched with terms that suggest an inflammatory immune response (**Figure 3.11A**). Furthermore, Cluster 13 exhibited both BAM and microglial-like signatures, so its identity is unknown from marker gene identification alone (**Figure 3.11B,C**). In order to extensively validate the putative fetal brain myeloid responder cells in Poly(I:C)-induced MIA, and to see if responder cells are in the fetal brain borders or parenchyma, we identified markers that define Cluster 13. We chose *S100a8* and *S100a9* as viable markers for tissue staining (**Figure 3.11D**). *S100a8* and *S100a9* were among the highest differentially expressed genes defining Cluster 13 in most cells (**Figure 3.9A** and **Figure 3.11D**). *S100a8* and *S100a9* have been identified previously as top highly expressed genes in an choroid plexus macrophage population after a mouse model of autoimmune encephalitis[57]. S100A8/A9 is also produced by macrophages in response double-stranded RNA[58]. IFN-γ and TNF regulate *S100a8* expression[59], and the S100A8/A9 heterodimer amplifies proinflammatory cytokine production by macrophages[60]. At the time of filing this dissertation, the biological validation of S100A8/A9 heterodimers has not yet been completed.

Validation is particularly important because only one replicate is largely represented in Cluster 13 (**Figure 3.12A**). In order to rule out if Cluster 13's separation is due to technical factors, such as differential UMI and cell counts, we down-sampled every cell to 1000 random UMIs and every batch to 4800 random cells (**Figure 3.12B**). Cluster 13 persisted despite downsampling in either case (UMI data shown in **Figure 3.12B**; downsampled cell data not shown), suggesting it is biologically relevant. Indeed, this is consistent with the fact that the top genes defining Cluster 13 are significantly enriched with gene ontology terms consistent with an inflammatory response (**Figure 3.11A**). Cluster 13 contains 1118 cells and is about 9% of cells in its replicate. If the 10 fetal brains within this replicate are equally represented (see batch summary in **Figure 3.6C**), we estimate that $Cd45^{+}Cd11b^{+}$ cells from multiple embryonic brains must populate Cluster 13. Therefore, we are likely observing variability litter-to-litter.

3.9 Putative fetal responder cells to Poly(I:C)-induced MIA resolve back towards a BAM-like state.

Cluster 13 has no clear origin from BAMs or microglia (**Figure 3.11**), so it is difficult to predict whether or not fetal responders to maternal Poly(I:C) will resolve back toward a BAM- or microglial-like cell state. In order to infer the cell state of clusters within our dataset, we used an RNA velocity approach called Velocyto[61] (**Figure 3.13**). RNA velocity is the time derivative of the gene expression state, meaning that time can be resolved from a snapshot of collected RNA[61]. This is inferred from the balance of spliced and unspliced RNA variants in the dataset[61]. Therefore, dynamic elements are uncovered within a dataset, such as differentiation processes[61]. The direction of the arrows indicate cells' trend toward another cell state. From **Figure 3.13**, we see that the BAM and microglial sub-clusters are trending toward a terminal cell state represented by clusters 1 and 3 (respectively). Clusters 1 and 3 are G1 cells, while sub-clusters 0, 7

and 2, 4 are in the G2M and S stages (**Figure 3.14**). These data suggest that sub-clusters 0, 7 and 2, 4 are actively proliferative cells filling the BAM and microglial niches, respectively (**Figure 3.14**). Importantly, Cluster 13 is trending towards a BAM-like cell state rather than microglial cell state (**Figure 3.13**), signifying that, irrespective of origin, responder cells become BAMs. These data also indicate that we captured a "resolution" state rather than an "emergent" responder state; in the future, repeating this work at an earlier time point (6-12 hours after MIA rather than 24 hours) may capture an earlier and more consistent immune response among replicates. To note, the data presented in **Figure 3.13** is of the WT (and not *Trif*$^{-/-}$) portion of the dataset. At time of filing, our analysis pipeline is still undergoing refinement.

Taken altogether, we propose a working model depicted in **Figure 3.15**. Maternal immune activation, induced by Poly(I:C) at E12.5 (**Figure 3.15**), is sensed by a subset of BAMs within the fetal brain. Because BAMs are situated along the borders of the brain, including ventricles and developing vasculature (choroid plexus included), perhaps Poly(I:C) is transmitted through vessels and picked up by BAMs rather than parenchymal microglia. BAMs sensing maternal Poly(I:C) challenge become "activated", producing pro-inflammatory cytokines (**Figure 3.15B**). Because BAMS are positioned at the borders of the brain, secretion of neurotoxic inflammation can potentially be systemic throughout the developing brain; cytokines may diffuse through the ventricle lumen, which is adjacent to neurogenic zones. It is possible that pro-inflammatory mediators negatively impact neural development by altering the neural precursor cell (NPC) pool, and/or altering differentiation and migration of immature neurons to their putative circuits. The aberrant circuits then produce ASD-like behavior changes. While this hypothesis is attractive to consider, much work will be required in the future to test this working model.

Discussion

3.10 Fetal brain myeloid cells are responsive to MIA.

The behavioral and transcriptomics data presented herein cumulatively suggest that fetal innate immune cells are responsive to MIA. Thus, a new layer of complexity is added in our attempt to understand how maternal infection translates to an increased risk of abnormal brain development.

Our conclusion may partially fit in with previous findings. *Hsiao et al.* discovered that core ASD-like behaviors could be attenuated by the microbial composition of the gut, except for sociability[25]. These data suggest that serum derivatives from the microbiota modulate plasticity of existing circuits in ways that help compensate for the theorized excitatory/inhibitory imbalances in ASD brains[62-64]. Yet, circuits encoding social behaviors are intractable to such modulation by microbiota metabolites; in other words, the changes to circuits mediating sociability are beyond rescue by modulating synaptic plasticity. It is likely that changes to circuits mediating sociability are engrained before circuits are established, at the cellular level. This would make sense given the larger picture: MIA is induced as neurogenesis begins at E12.5[13]. It isn't until about E15.5-E16.5 that synapses are formed within a newly established circuit[13,14]. From our own data, aberrant social behaviors required fetal TRIF signaling. Fetal TRIF was necessary and sufficient to drive core ASD-like sociability changes and was necessary, but not sufficient, to promote restricted/repetitive behaviors (**Figure 3.2** and **Figure 3.3**). ASD-like restricted/repetitive behaviors in Poly(I:C)-induced MIA offspring also required maternal TRIF sensing; but, maternal TRIF sensing was not sufficient alone to promote restricted/repetitive behaviors (**Figure 3.2** and **Figure 3.3**). Thus, fetal and maternal sensing was required for this core ASD-like behavioral symptom. This piece of data can fit in with the current concept of the field that maternal immune sensing is required, perhaps mediated by the IL-17 axis defined by *Choi et al.*, *Yim et. al.*, and *Kim et al.*[21,23,24].

However, in one critical way that our conclusion does not fit with the IL-17 and T_H17 axis delineated by *Choi et al.*, *Yim et. al.*, and *Kim et al.* is that we did not observe that maternal innate immune sensing (mediated by TRIF) was sufficient to drive all core and associated ASD-like behavior changes, particularly for sociability[21,23,24]. This is unexpected because IL-17 (downstream of Poly(I:C) sensing by IL-6 producing cells) from maternal T_H17 cells was shown to be necessary and sufficient to promote ASD-like behavior changes in Poly(I:C)-induced MIA offspring[21,23,24]. Presumably, this adaptive immune component would be downstream of innate immune sensing. While we did not look for a T_H17 cell population in our mice, we did detect minimal amounts of SFB in our WT mice derived from Jackson Laboratories (data not shown). Therefore, it is still possible that IL-17 is relevant to our system. Another possibility is that our mice have differing microbial communities beyond SFB that promote a different cytokine milieu, which potentiates a different behavioral outcome in Poly(I:C)-induced MIA offspring.

3.11 Study limitations and future experimental modifications.

Our study has several limitations that should be considered while interpreting our results. I will first consider limitations to our behavioral studies, to our live viral infections, and then to our scRNA-seq study.

The microbial composition in the maternal and fetal gut is important for modulating ASD-like behavior changes[25]. In our study, we did not profile the microbiota of our mice, but did detect minimal levels of SFB by qRT-PCR (data not shown). Similarly, we did not do any immunophenotyping of mothers, prior to and during pregnancy, to identify maternal cytokines (and the possible cellular sources thereof). Thus, it is tough to evaluate how well our results fit in with the current concept of the field. Future work is needed to gain more mechanistic insight into how the maternal and fetal immune responses synergize *in utero* to produce altered behavior.

Our live viral infections also have important considerations that may complicate our interpretation. The route of injection used in our infection model differs from natural modes of transmission—we used intraperitoneal injections. Infections started from intraperitoneal delivery may engage a different form of immunity. Indeed, mucosal immunity functions independently from systemic immunity that may lend itself to generating different immune responses and/or different timing of immune responses[65]. For future work, mimicking the natural route of infection as much as possible may better recapitulate the human maternal infection risk factors. For example, intranasal injections can be considered as an alternative to intraperitoneal injections.

It is also intriguing that our behavioral phenotype of MHV-68 exposed offspring, the only virus that we detected crossing the placenta, is not phenocopying ODN-induced MIA. We'd expect that MHV-68 would engage TLR9 and MYD88-dependent signaling pathway similar to activation by ODN. Perhaps, since TLR3 mechanisms may also be involved[46,50,51], they are driving the majority of this behavioral phenotype. If TRIF signaling were indeed important during our live infection of MHV-68, we would need to repeat our study with *Trif* $^{-/-}$ breeder mice. Due to the pandemic and sheltering-in-place starting mid-March 2020, we did not have time to finish these experiments in *Trif* $^{-/-}$ mice; it is my hope that the reader can view a more complete version of this work in a future peer-reviewed publication. We are also not sure if our behavioral phenotype in the offspring of MHV-68 mothers is due to re-activation of MHV-68 in adulthood. To test this possibility, we need to use a strain of MHV-68 that is not capable of re-activation after primary infection. These experiments have been planned at the time of this dissertation's submission; I hope that the reader can also view the conclusion of this experiment in a future peer-reviewed work. Lastly, MCMV infection did promote some behavioral changes in female offspring despite being established as a virus that can't cross the placenta[46,47] (data not shown). This data may suggest maternal factors crossing the placenta to affect female brain development; future studies are required to understand this more.

Our scRNA-seq study also has limitations; some of these were already mentioned earlier. At the outset of this study in 2018, border-associated macrophages were not well defined[35,36]. The transcriptional heterogeneity of fetal microglia, particularly during brain development, was also not known[55,56]. This influenced the design of my study. From our previous work implicating fetal microglial lytic cell death in the brain (as discussed in Chapter 2), we knew that even low numbers of cells (an estimated 400-500 cells) potentially affect discrete neural circuit development. Because

my hypothesis was that fetal microglia are responsive to Poly(I:C)-induced MIA, and because we wanted to maximally resolve the possible transcriptional heterogeneity of microglia in the fetal brain (and find low numbers of responder cells), we sought to load as many myeloid brain cells as possible from a litter of E13.5 mice on the 10X Chromium chip. The recommended maximum is about 10,000 cells—the doublet rate increases considerably 10,000 or more cells loaded. We loaded cells such that we aimed for 9-10k cells per library. We also wanted to gain a decent depth of sequencing by pooling four libraries on one S4 lane of the NovaSeq 6000; users may get up to 3 billion reads back from a full lane. We ended up getting back nearly 50k cells with a median of 10-15k UMIs and median of 2-4k features per cell. My dataset, therefore, has an excellent breadth and depth for E13.5 brain myeloid cells. While this is impressive, our dataset does exclude non-myeloid cells; E13.5 brain myeloid cells are only 1-2% of the total live brain cell fraction. Including a fraction of non-myeloid cells in my scRNAseq-pipeline would have been informative for seeing if we could detect any abnormalities in the neural compartment as a consequence of Poly(I:C)-induced MIA. For example, one enriched GO term I found in my data of fetal myeloid responder cells is “regulation of extrinsic apoptosis” (not shown)—perhaps, we would have seen an enrichment of neural cells in some clusters, which fits with the hypothesis that fetal microglia regulate the neural precursor cell pool[33,34,37,66-68]. Since we saw litter-to-litter variability, we recommend including at least three biologically distinct replicates for future studies. Using a limited breeding window overnight can also reduce litter-to-litter variability. Furthermore, taking maternal serum the day of the experiment to look for IL-6 and IL-17 cytokines can help inform which libraries to pool, because perhaps our additional Poly(I:C) replicate may not have had an adequate immune activation. Though laborious, these additional measures would ensure precise developmental staging of the embryos and reduce potential litter-to-litter variability. As mentioned, we captured a resolution state in fetal myeloid responder cells. In the future, conducting this experiment 6- to 12-hours after maternal injection may capture a more informative emergent immune response. To facilitate this, the ability to sort cells and use the 10X Genomics kit independently of core resources will be required. Because these experiments are time-intensive and rigorous, a team of three people is also recommended.

The advent of “cell hashing” technology will also improve future scRNA-seq experiments. Cell hashing describes the addition of barcodes to the surface of cells, enabling users to pool cells from different treatments, animals, etc. within the same library[69]. For our purpose, individually barcoding cells from each embryo will allow embryos of Vehicle and Poly(I:C) treatments to be in the same library, reducing technical variability from slight alterations during cell isolation and library prep. Furthermore, the identity of cells can be decoded such that the embryo it came from is known. This is powerful, because while we suspect multiple embryos contributed to the responder cell population we identified, cell hashing would have provided a definitive answer. One very last consideration is that we did not yet biologically validate the fetal myeloid responder cells. This is important because our responder population is from one litter. Additionally, dry lab analysis is still ongoing. I hope that the readers can refer to a future peer-reviewed work that has the crucial validation experiments included, in addition to any updated figures from the scRNA-seq dataset.

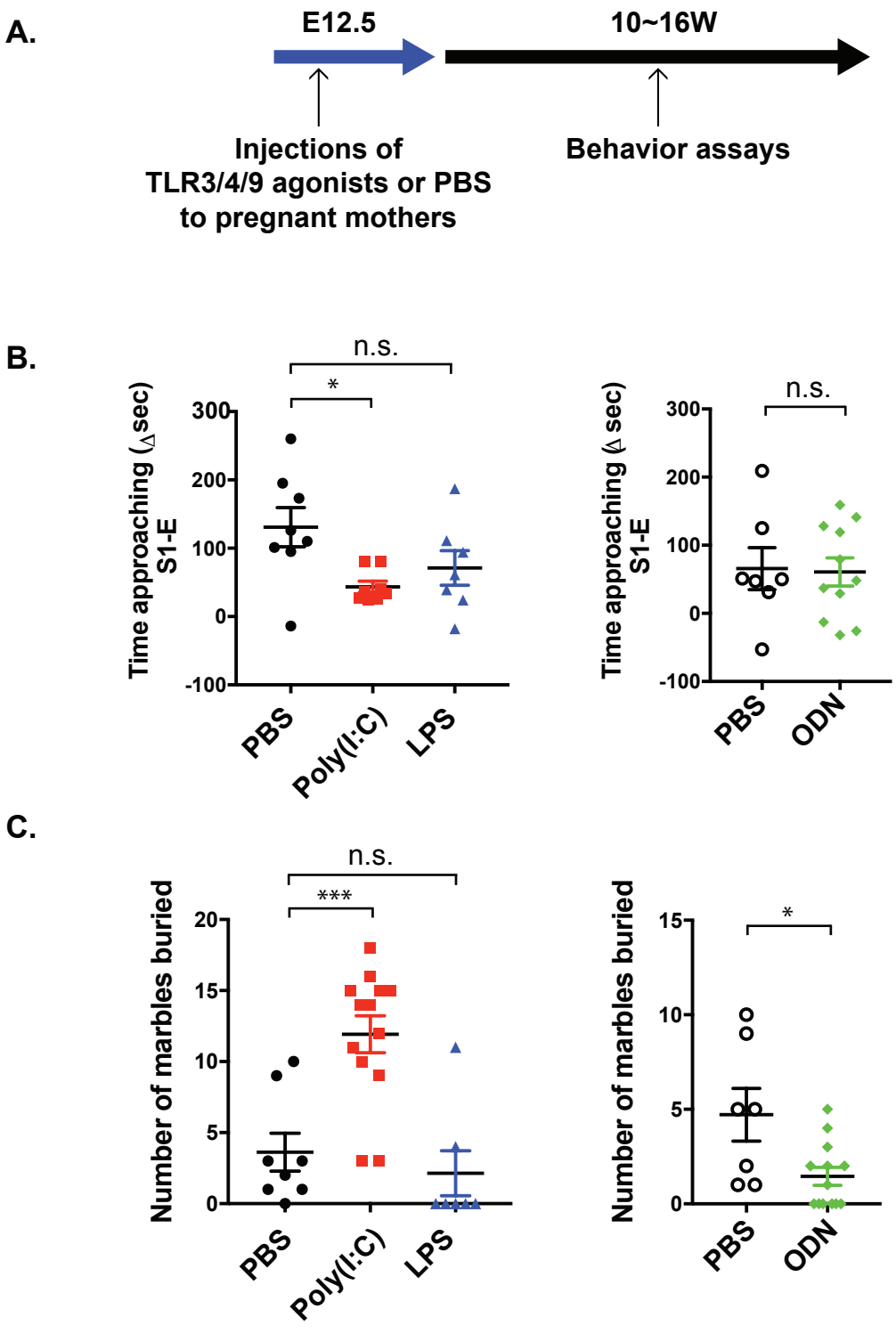

A.
E12.5
10~16W
Injections of
TLR3/4/9 agonists or PBS
to pregnant mothers
Behavior assays
B.
n.s.
*
Time approaching (Δsec)
S1-E
300
200
100
0
-100
PBS
Poly(I:C)
LPS
n.s.
Time approaching (Δ sec)
S1-E
300
200
100
0
-100
PBS
ODN
C.
n.s.
***
Number of marbles buried
20
15
10
5
0
PBS
Poly(I:C)
LPS
*
Number of marbles buried
15
10
5
0
PBS
ODN

Figure 3.1: *Only the TLR3 agonist, Poly(I:C), was sufficient to promote core ASD-like behavior changes in the MIA model.*
A. Experimental scheme. Dams at E12.5 were injected with TLR3, TLR4, or TLR9 agonists as well as a PBS vehicle control. 10-16 weeks after birth, offspring underwent behavior assays.
B. Sociability was determined with the reciprocal social interaction assay. The time spent approaching the stranger mouse (seconds) is shown for male mice. PBS-exposed control offspring (filled black circles, N=8), Poly(I:C)-exposed offspring (red squares, N=8), LPS-exposed offspring (blue triangles, N=7) are shown. ODN-exposed offspring (green diamonds, N=12) behaviors are shown separately because PBS-exposed control offspring (open black circles, N=7) were ran separately from previous TLR-agonist cohorts.
C. Restricted/repetitive behaviors are measured as the number of marbles buried during the marble-burying assay. PBS-exposed control male offspring (filled black circles, N=8), Poly(I:C)-exposed male offspring (red squares, N=13), LPS-exposed male offspring (blue triangles, N=7) data is shown. ODN-exposed male offspring (green diamonds, N=12) behaviors are shown separately because PBS-exposed control offspring (open black circles, N=7) were ran separately from previous TLR-agonist cohorts.
(*) shows $p < 0.05$, (**) shows $p < 0.01$, (***) shows $p < 0.001$; n.s. = not significant.

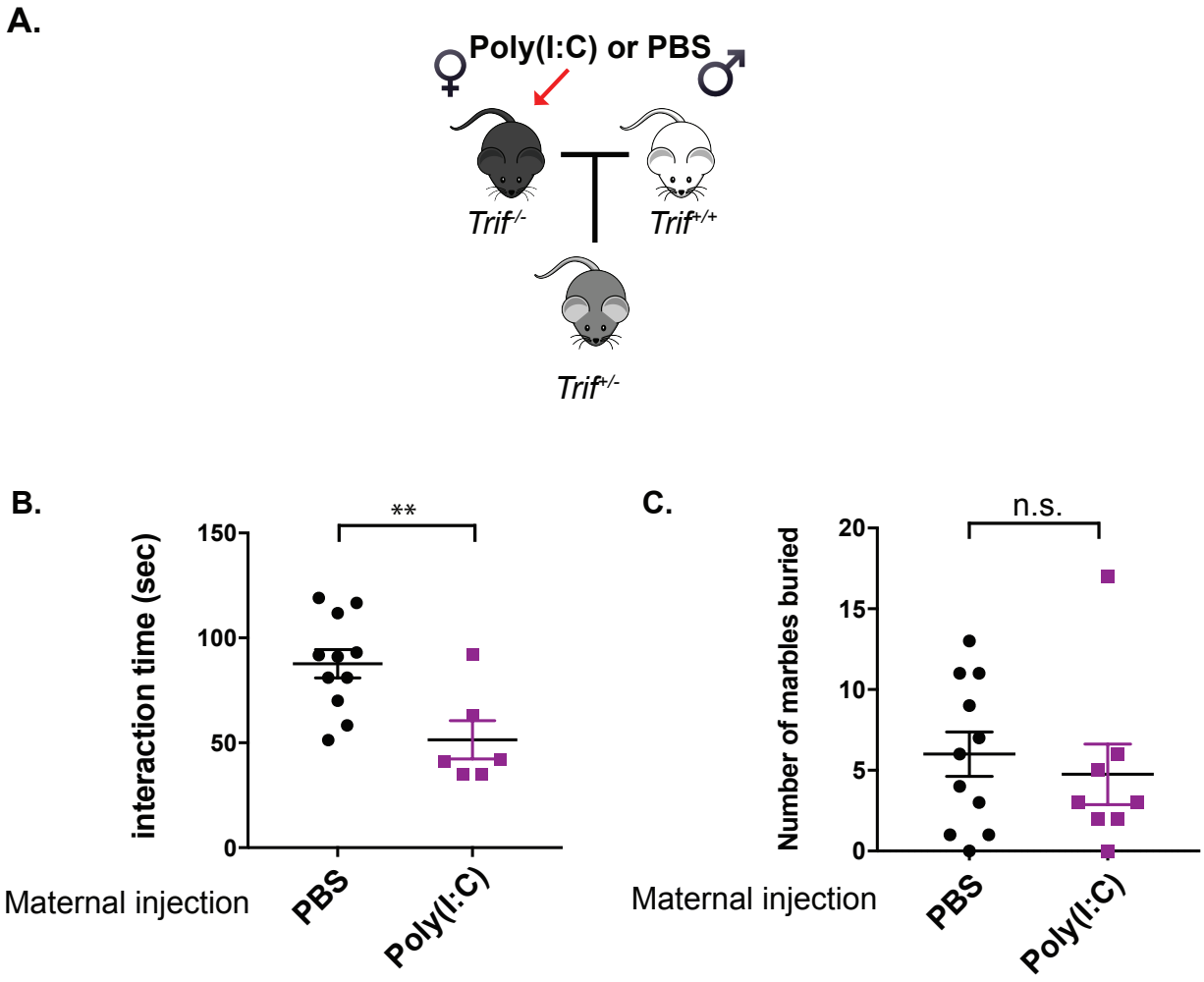
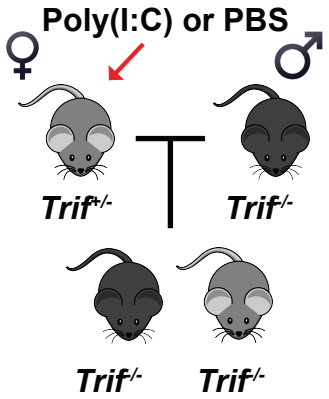
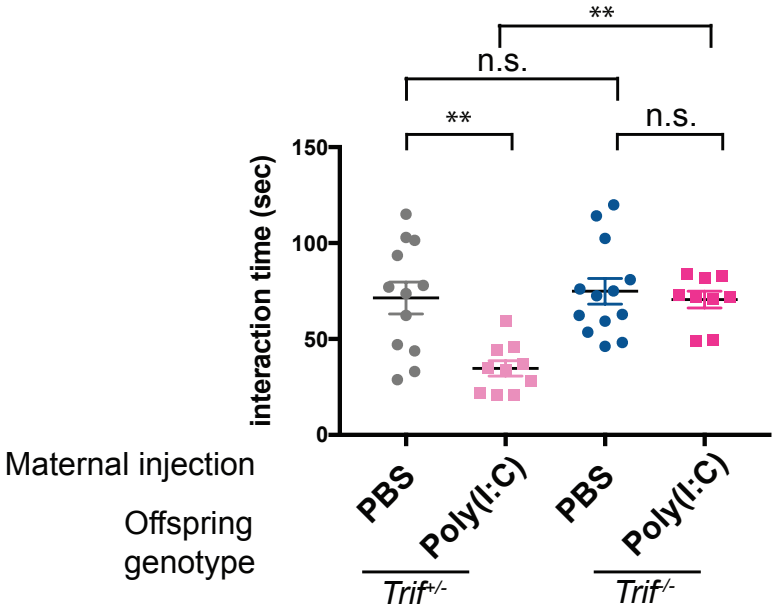

A.
Poly(I:C) or PBS
♀
♂
Trif-/-
Trif+/+
Trif+/-
B.
interaction time (sec)
150
100
50
0
**
PBS
Poly(I:C)
Maternal injection
C.
Number of marbles buried
20
15
10
5
0
n.s.
PBS
Poly(I:C)
Maternal injection

Figure 3.2: *Maternal TRIF sensing is necessary for producing restricted/repetitive behaviors in male offspring of Poly(I:C)-induced MIA mice.*
A. Breeding scheme shown. *Trif*$^{-/-}$ mothers were bred with *Trif*$^{+/+}$ father mice. *Trif*$^{-/-}$ mothers received an intraperitoneal injection of Poly(I:C) or PBS at day E12.5. *Trif*$^{+/-}$ offspring were ran in behavior assays 10-16 weeks after birth.
B. Total interaction time (seconds) is recorded during the reciprocal social interaction assay of male PBS-exposed control offspring (black circles, N=11) or male Poly(I:C)-exposed offspring (purple squares, N=5).
C. Restricted/repetitive behaviors are measured as the number of marbles buried during the marble-burying assay. PBS-exposed control male offspring (black circles, N=11) and male Poly(I:C)-exposed offspring (purple squares, N=8) data is shown.
(**) shows $p < 0.01$; n.s. = not significant.

A.


Poly(I:C) or PBS
♀
♂
Trif+/-
Trif-/-
Trif-/-
Trif-/-

B.


**
n.s.
**
n.s.
interaction time (sec)
150
100
50
0
Maternal injection
PBS
Poly(I:C)
PBS
Poly(I:C)
Offspring genotype
Trif+/-
Trif-/-

C.

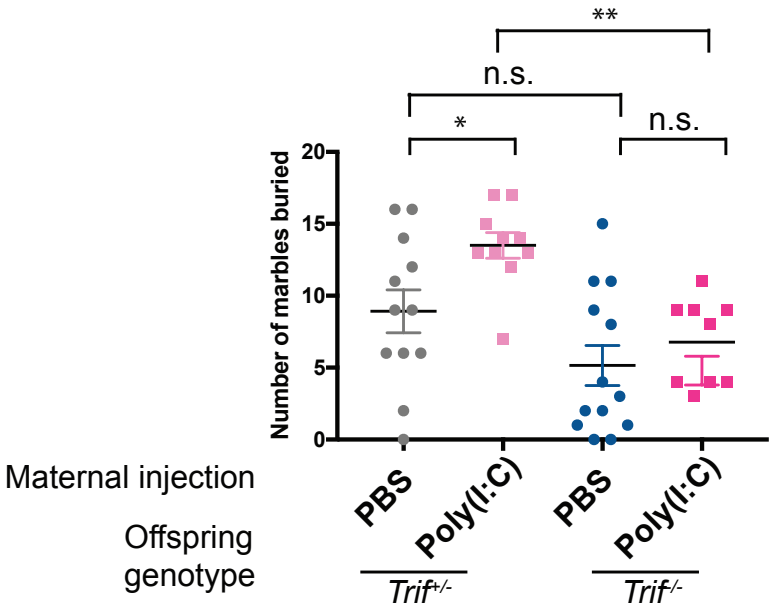

**
n.s.
*
n.s.
Number of marbles buried
20
15
10
5
0
Maternal injection
PBS
Poly(I:C)
PBS
Poly(I:C)
Offspring genotype
Trif+/-
Trif-/-

Figure 3.3: *Fetal TRIF sensing is necessary and sufficient for producing a core sociability deficit in male offspring of Poly(I:C)-induced MIA mice.*
A. Breeding scheme shown. *Trif*$^{+/-}$ mothers were bred with *Trif*$^{-/-}$ father mice to produce litters of *Trif*$^{-/-}$ and *Trif*$^{+/-}$ offspring. Mothers received an intraperitoneal injection of Poly(I:C) or PBS at day E12.5. *Trif*$^{-/-}$ and *Trif*$^{+/-}$ offspring were ran in behavior assays 10-16 weeks after birth. Since WT mice are not possible to produce in this breeding scheme, age-matched WT mice are used for comparisons in the subsequent behavior assays.
B. Total interaction time (seconds) is recorded during the reciprocal social interaction assay. Data from male *Trif*$^{+/-}$ offspring (PBS-exposed: gray circles, N=12; Poly(I:C)-exposed: pink squares, N=10) and *Trif*$^{-/-}$ offspring (PBS-exposed: teal circles, N=13; Poly(I:C)-exposed: magenta squares, N=9) is shown.
C. Restricted/repetitive behaviors are measured as the number of marbles buried during the marble-burying assay. Data from male *Trif*$^{+/-}$ offspring (PBS-exposed: gray circles, N=12; Poly(I:C)-exposed: pink squares, N=10) and *Trif*$^{-/-}$ offspring (PBS-exposed: teal circles, N=13; Poly(I:C)-exposed: magenta squares, N=9) is shown.
(*) shows $p < 0.05$, (**) shows $p < 0.01$; n.s. = not significant.

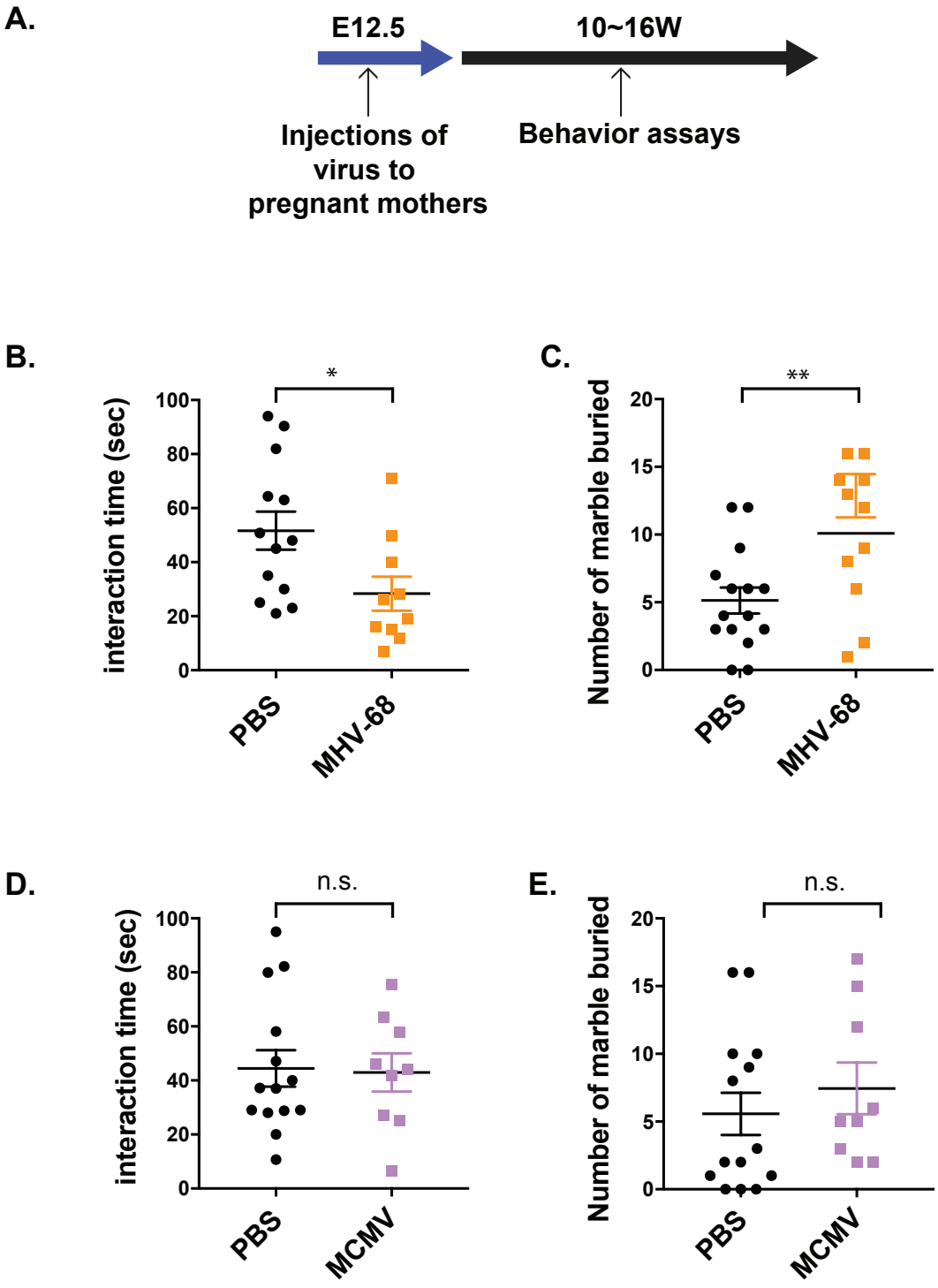

A.
E12.5
10~16W
Injections of virus to pregnant mothers
Behavior assays
B.
interaction time (sec)
*
PBS
MHV-68
C.
Number of marble buried
**
PBS
MHV-68
D.
interaction time (sec)
n.s.
PBS
MCMV
E.
Number of marble buried
n.s.
PBS
MCMV

Figure 3.4: *Infection of MHV-68, and not MCMV, at E12.5 promoted ASD-like behavior changes in male offspring.*
A. Experimental scheme is shown. Dams at E12.5 were injected with live MHV-68 virus, MCMV virus, or PBS vehicle control. 10-16 weeks after birth, offspring were ran in behavior assays.
B. Total interaction time (seconds) is recorded during the reciprocal social interaction assay. Data from male PBS-exposed control offspring (black circles, N=13) or male MHV-68-exposed offspring (orange squares, N=10) is shown.
C. Restricted/repetitive behaviors are measured as the number of marbles buried during the marble-burying assay. Data from PBS-exposed control male offspring (black circles, N=15) or male MHV-68-exposed offspring (orange squares, N=11) is shown.
D. Total interaction time (seconds) is recorded during the reciprocal social interaction assay. Data from PBS-exposed control male offspring (black circles, N=14) or male MCMV-exposed offspring (purple squares, N=9) is shown.
E. Restricted/repetitive behaviors are measured as the number of marbles buried during the marble-burying assay. Data from male PBS-exposed control offspring (black circles, N=14) or male MCMV-exposed offspring (orange squares, N=9) is shown.
(*) shows $p < 0.05$, (**) shows $p < 0.01$; n.s. = not significant.

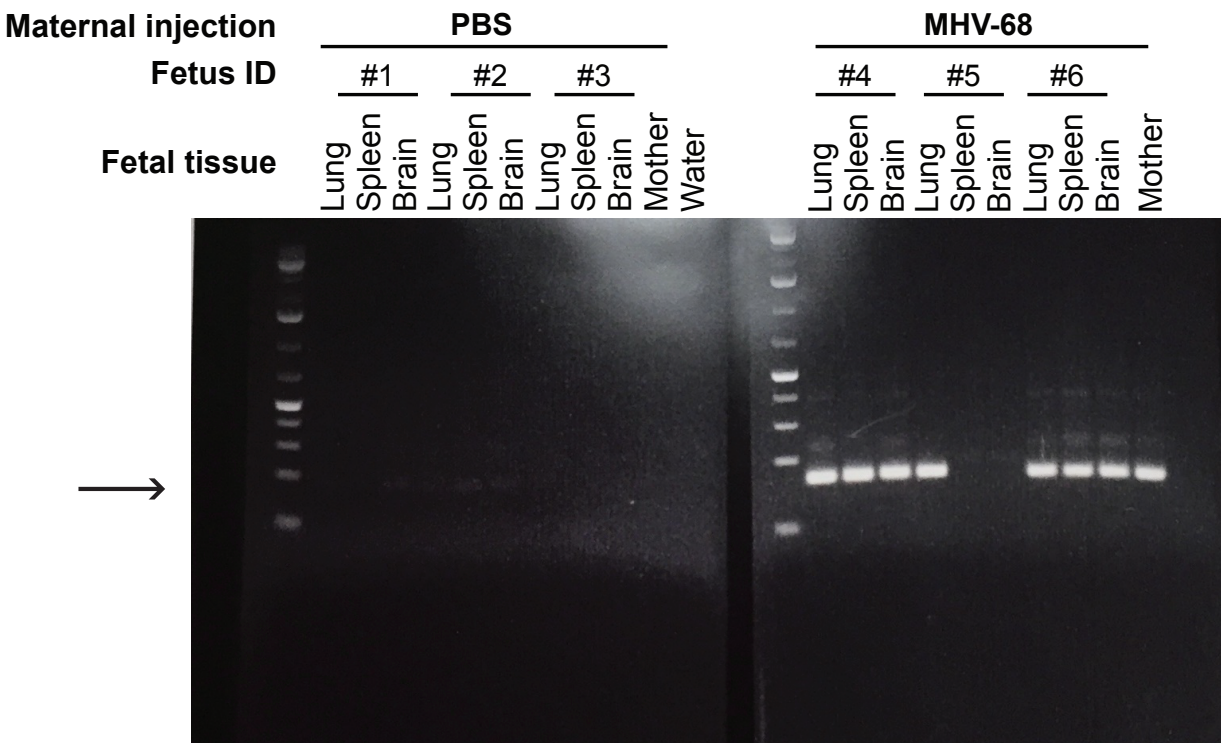
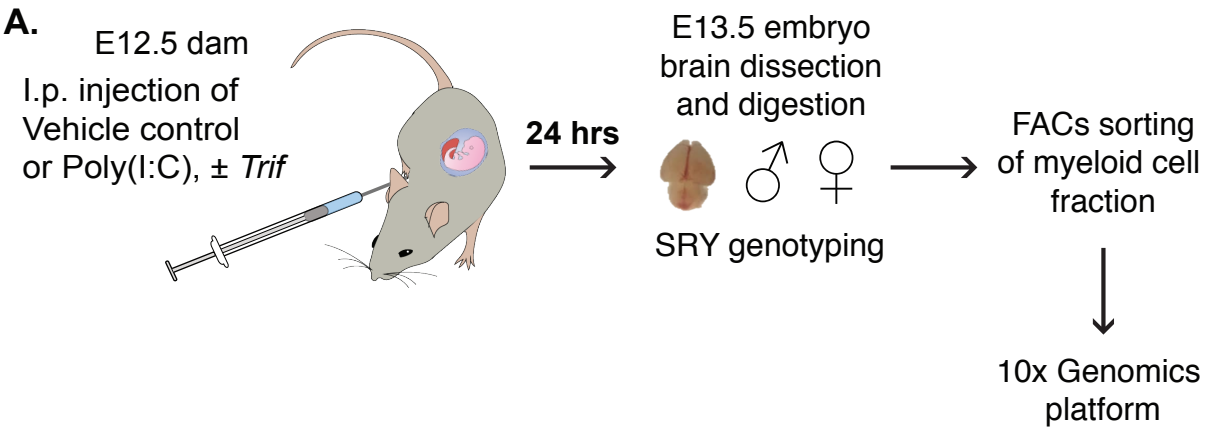
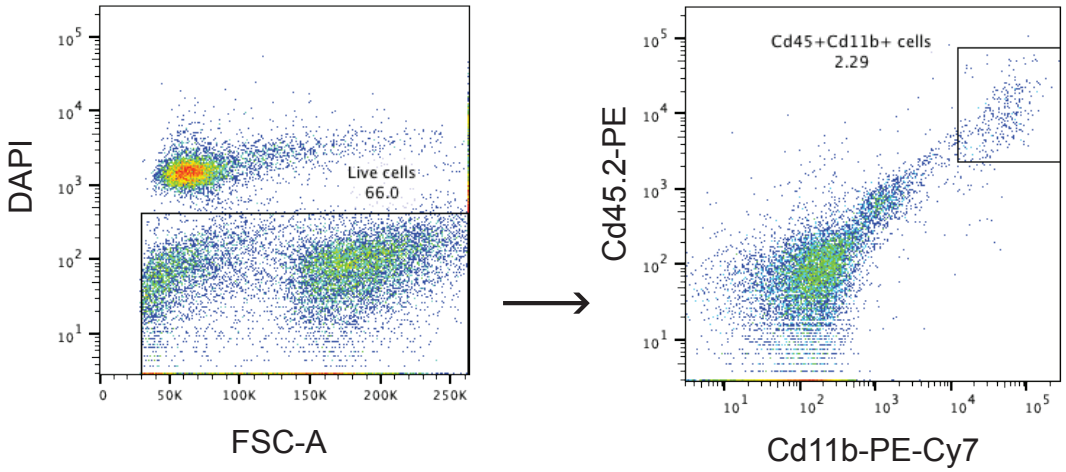

Maternal injection
PBS
MHV-68
Fetus ID
#1
#2
#3
#4
#5
#6
Fetal tissue
Lung
Spleen
Brain
Lung
Spleen
Brain
Lung
Spleen
Brain
Mother
Water
Lung
Spleen
Brain
Lung
Spleen
Brain
Lung
Spleen
Brain
Mother

Figure 3.5: MHV-68 can cross the placenta.
Nested PCR results five days post-infection (E17.5) from DNA of harvested organs. The PCR targeted the gp150 gene of MHV-68.

A.



B.

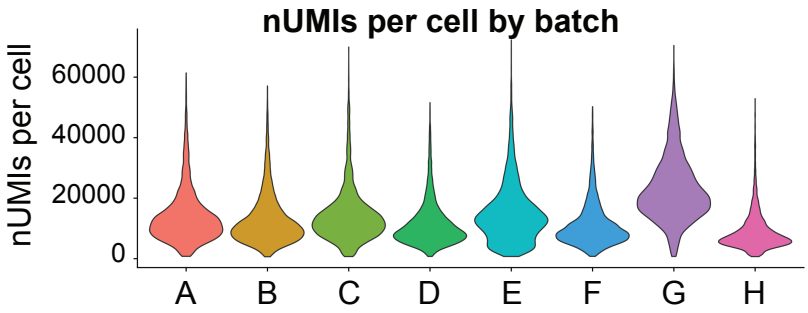


C.

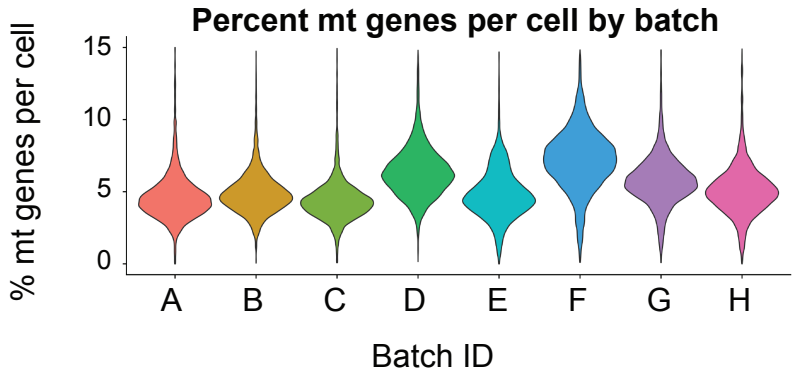
	Batch ID							
	A	**B**	**C**	**D**	**E**	**F**	**G**	**H**
Genotype	TrifKO	TrifKO	TrifKO	TrifKO	WT	WT	WT	WT
Treatment_replicate	Poly(I:C)_1	Poly(I:C)_2	Vehicle_1	Vehicle_2	Poly(I:C)_1	Poly(I:C)_2	Vehicle_1	Vehicle_2
Number of litters	2	2	1	1	1	1	1	1
Total embryos	19	18	9	7	10	9	8	8
Total male embryos	5	3	3	1	6	3	4	4
Total female embryos	14	15	6	6	4	6	4	4
Total cells (post quality control)	5745	6670	5715	7446	12069	5389	6585	6849

Figure 3.6: *Using a single-cell RNA sequencing approach to identify potential fetal myeloid cells following MIA.*
A. Experimental scheme. E12.5 WT or *Trif*$^{-/-}$ dams received an intraperitoneal injection of Poly(I:C) or PBS vehicle control. 24 hours later, E13.5 fetal brains were isolated and underwent a single cell isolation protocol. gDNA was isolated from embryonic tails and genotyped for presence of SRY, distinguishing males from female mice. Whenever possible, an equal amount of male and female brain cells were pooled prior to staining and sorting. The myeloid cell fraction, Cd45^{+}Cd11b^{+} cells, were sorted and concentrated before the 10X Genomics single-cell capture and library prep platform.
B. Representative flow plots of cell size- and singlet-gated cells from E13.5 fetal brain. Live cells (DAPI^{-}) were gated for Cd45^{+}Cd11b^{+} double-positive cells. Cd45^{+}Cd11b^{+} double-positive cells were 1-2% of the total live cell population.
C. Table of dataset composition. Eight total batches went into the dataset: four *Trif*$^{-/-}$ and four WT litters; two of these per genotype are PBS- and Poly(I:C)-exposed litters.

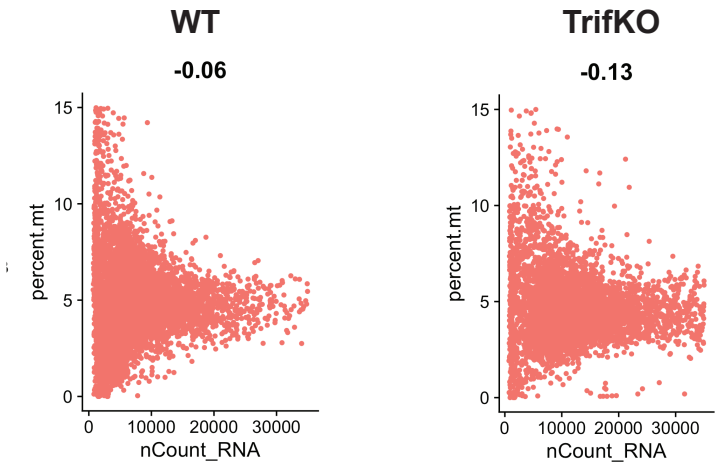
A.


nUMIs per cell by batch
nUMIs per cell
60000
40000
20000
0
A
B
C
D
E
F
G
H

B.


Percent mt genes per cell by batch
% mt genes per cell
15
10
5
0
A
B
C
D
E
F
G
H
Batch ID

C.


WT
-0.06
TrifKO
-0.13
percent.mt
15
10
5
0
0
10000
20000
30000
nCount_RNA

D.

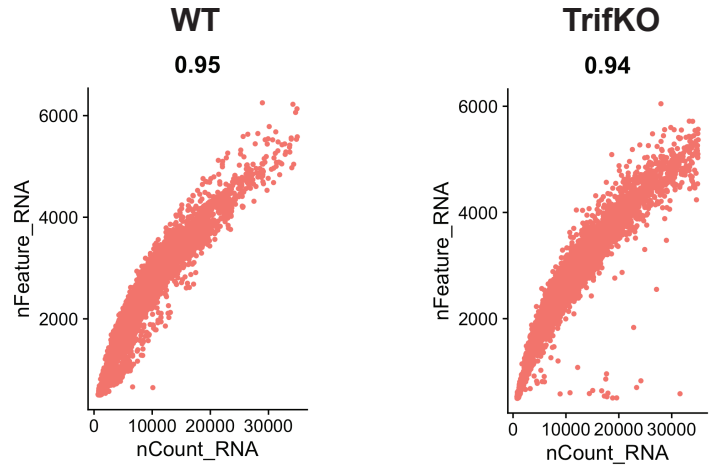

WT
0.95
TrifKO
0.94
nFeature_RNA
6000
4000
2000
0
10000
20000
30000
nCount_RNA

Figure 3.7: *Quality control metrics of our scRNAseq dataset show high-quality cells.*
A. Violin plots of number of unique molecular identifiers (UMI's) (nUMIs) per cell in each batch post quality control. UMIs correspond to barcoded mRNA captured per cell. Median nUMIs for the batches are around 10000-15000 per cell.
B. Violin plots of percent (%) mitochondrial genes found per cell for each batch post quality control. Percent mitochondrial genes are thought to reflect the health of the captured cells, because release of mitochondrial gene content is associated with dying cells.
C. Scatterplots of percent mitochondrial gene content (percent.mt) versus mRNA counts (nCount_RNA) from a representatitve WT (here, batch G) and *Trif*$^{-/-}$ (here, batch B) batches post quality-control. Every dot is a cell. The negative correlation coefficient is reflective of the fact that the vast majority of RNA content in cells is not largely composed of mitochondrial genes.
D. Representative scatterplots of the number of unique features mapped (mostly genes; nFeature_RNA) versus the number of mRNA counts (nCount_RNA) from a representatitve WT (here, batch G) and *Trif*$^{-/-}$ (here, batch B) batches post-quality control. Every dot is a cell. The high correlation coefficient is reflective of the fact that cells that have more nCount_RNAs generally have more detected features (mostly genes) and vice versa; cells greatly deviating from this are low-quality cells and/or possible doublet/multiplet cells.

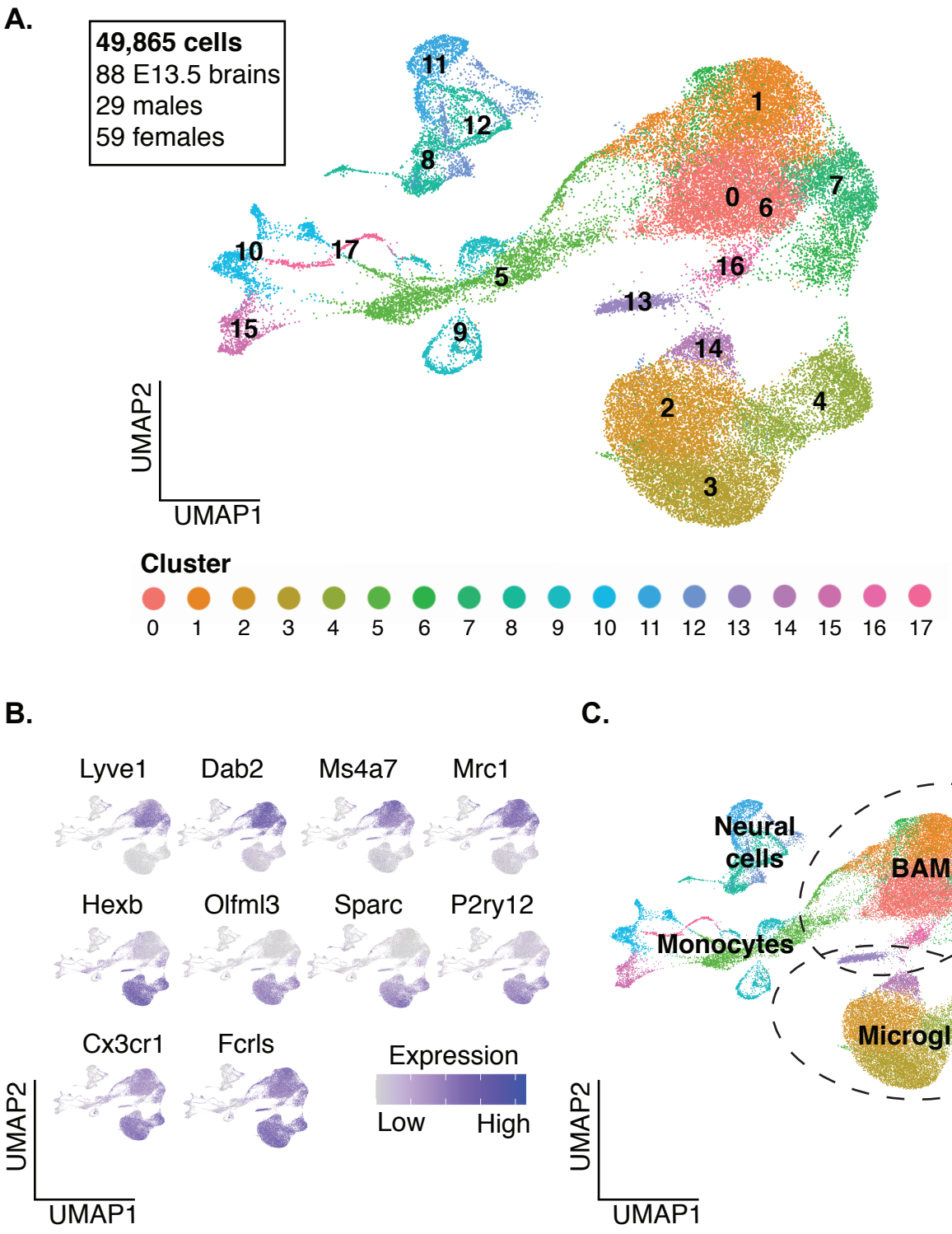

A.
49,865 cells
88 E13.5 brains
29 males
59 females
11
12
8
1
0
6
7
10
17
5
16
13
15
9
14
2
4
3
UMAP2
UMAP1
Cluster
0 1 2 3 4 5 6 7 8 9 10 11 12 13 14 15 16 17
B.
Lyve1
Dab2
Ms4a7
Mrc1
Hexb
Olfml3
Sparc
P2ry12
Cx3cr1
Fcrls
Expression
Low
High
UMAP2
UMAP1
C.
Neural cells
BAMs
Monocytes
Microglia
UMAP2
UMAP1

Figure 3.8: *We recovered 49,865 cells that are primarily E13.5 microglia and border-associated macrophage cells.*
A. UMAP projection (a dimensionality reduction method) of all 49,865 cells in the dataset. Every dot is a cell, and from the Euclidean distance between cells and among clusters allows inference of the transcriptional identity relatedness[70,71]. We identify eighteen transcriptionally distinct clusters from unsupervised clustering. Our dataset contains WT and *Trif*$^{-/-}$ cells from 88 E13.5 brains, 29 of which are male and 59 of which are female.
B. UMAP projection in (**A.**) colored by canonical BAM and microglia marker gene expression identified from previous works in the field. *Cx3cr1* marks cells of the mononuclear phagocyte system (including monocytes, microglia, and BAMs). *Fcrls* is considered to be restricted to brain myeloid cells (including microglia and BAMs).
C. UMAP projection in (**A.**) with cell population identifiers overlaid on top. Expression patterns of marker genes identified previously in the neural and myeloid cell fields informed their identification (approach as in **B.**).

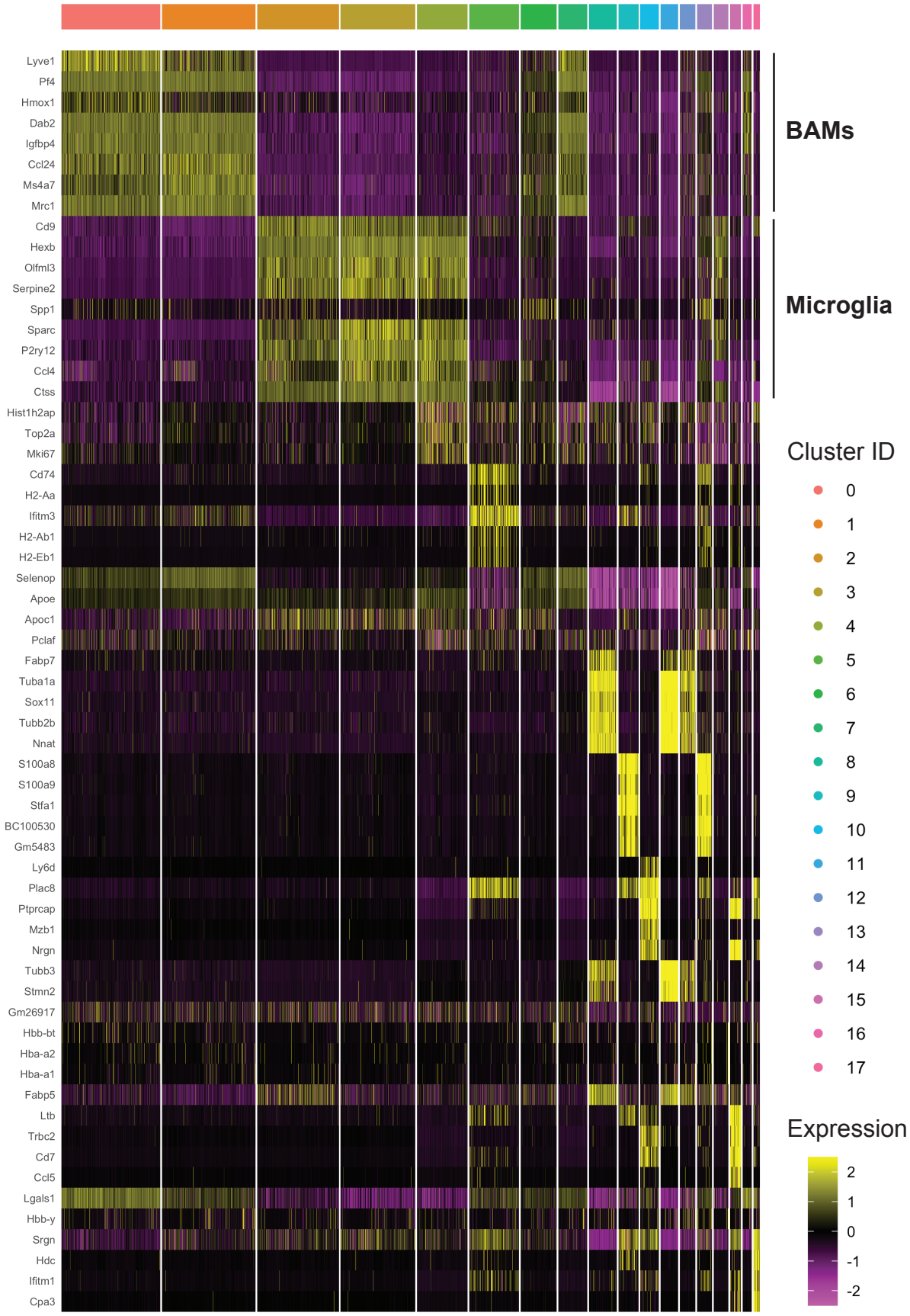

Lyve1
Pf4
Hmox1
Dab2
Igfbp4
Ccl24
Ms4a7
Mrc1
Cd9
Hexb
Olfml3
Serpine2
Spp1
Sparc
P2ry12
Ccl4
Ctss
Hist1h2ap
Top2a
Mki67
Cd74
H2-Aa
Ifitm3
H2-Ab1
H2-Eb1
Selenop
Apoe
Apoc1
Pclaf
Fabp7
Tuba1a
Sox11
Tubb2b
Nnat
S100a8
S100a9
Stfa1
BC100530
Gm5483
Ly6d
Plac8
Ptprcap
Mzb1
Nrgn
Tubb3
Stmn2
Gm26917
Hbb-bt
Hba-a2
Hba-a1
Fabp5
Ltb
Trbc2
Cd7
Ccl5
Lgals1
Hbb-y
Srgn
Hdc
Ifitm1
Cpa3
BAMs
Microglia
Cluster ID
0
1
2
3
4
5
6
7
8
9
10
11
12
13
14
15
16
17
Expression
2
1
0
-1
-2

Figure 3.9: Heatmap of some of the top differentially expressed genes that distinguish the cell clusters.
We identified eighteen transcriptionally distinct clusters. Using the FindAllMarkers function in the Seurat program[72], up to ten of the top differentially expressed genes defining the clusters (the marker genes) are plotted; the top twenty markers are listed in **Supplementary Table 1**. Each row is a gene, and individual bars in each row belong to a cell within a cluster. The relative expression level of that gene is depicted; high expression is in yellow and low expression is in magenta. Gene names are on the left. On the right, the cell population identifier is written. Cluster ID is color coded at the top of the heatmap.

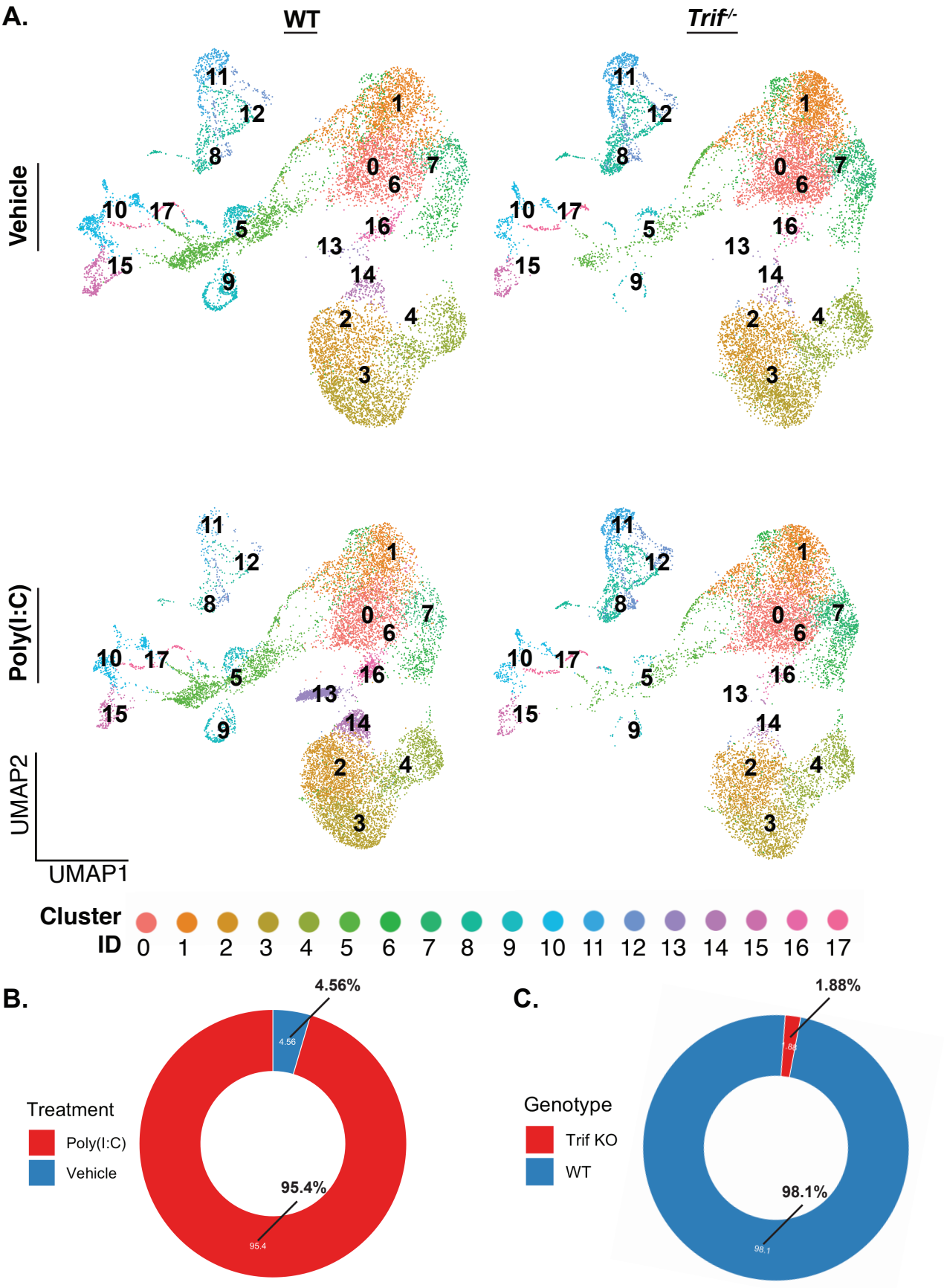
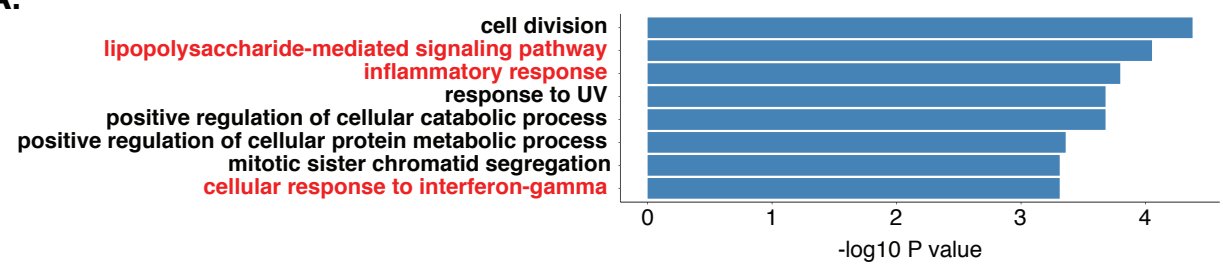
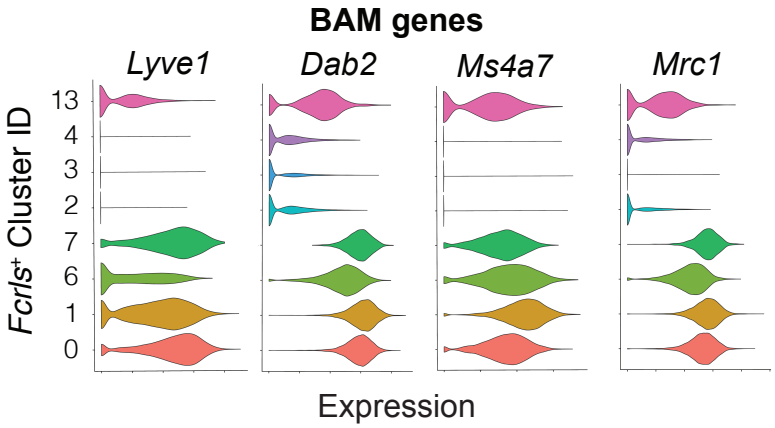

A.
WT
Trif-/-
Vehicle
Poly(I:C)
UMAP2
UMAP1
Cluster ID
0 1 2 3 4 5 6 7 8 9 10 11 12 13 14 15 16 17
B.
4.56%
95.4%
Treatment
Poly(I:C)
Vehicle
C.
1.88%
98.1%
Genotype
Trif KO
WT

Figure 3.10: *We identify a putative WT fetal responder cell population to Poly(I:C)-induced MIA.*
A. UMAP projection (a dimensionality reduction method[70,71]) of all 49,865 cells in the dataset, split by treatment and genotype. Every dot is a cell, and from the Euclidean distance between cells and among clusters allows inference of the transcriptional identity relatedness. Cluster 13 is a unique cluster found in the Poly(I:C) condition and are primarily WT.
B. Pie chart depicting the percent contribution of Vehicle and Poly(I:C) cells to Cluster 13.
C. Pie chart depicting the percent contribution of *Trif*$^{-/-}$ and WT cells to Cluster 13.

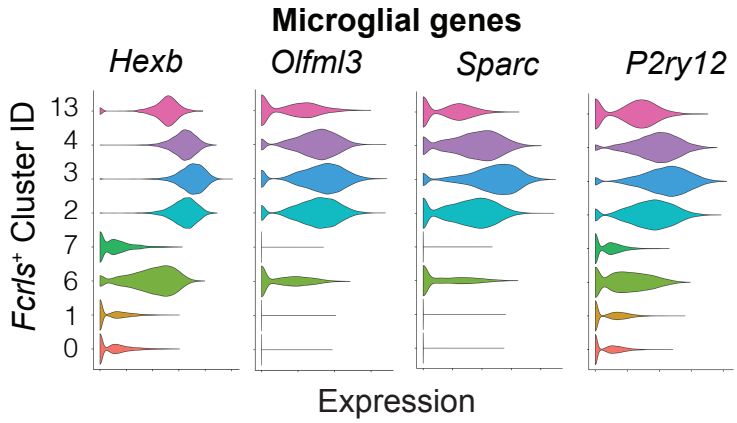
A.


cell division
lipopolysaccharide-mediated signaling pathway
inflammatory response
response to UV
positive regulation of cellular catabolic process
positive regulation of cellular protein metabolic process
mitotic sister chromatid segregation
cellular response to interferon-gamma
0
1
2
3
4
-log10 P value

B.


BAM genes
Lyve1
Dab2
Ms4a7
Mrc1
Fcrls+ Cluster ID
13
4
3
2
7
6
1
0
Expression

C.


Microglial genes
Hexb
Olfml3
Sparc
P2ry12
Fcrls+ Cluster ID
13
4
3
2
7
6
1
0
Expression

D.

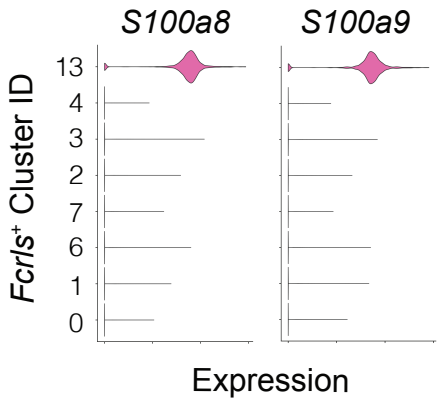
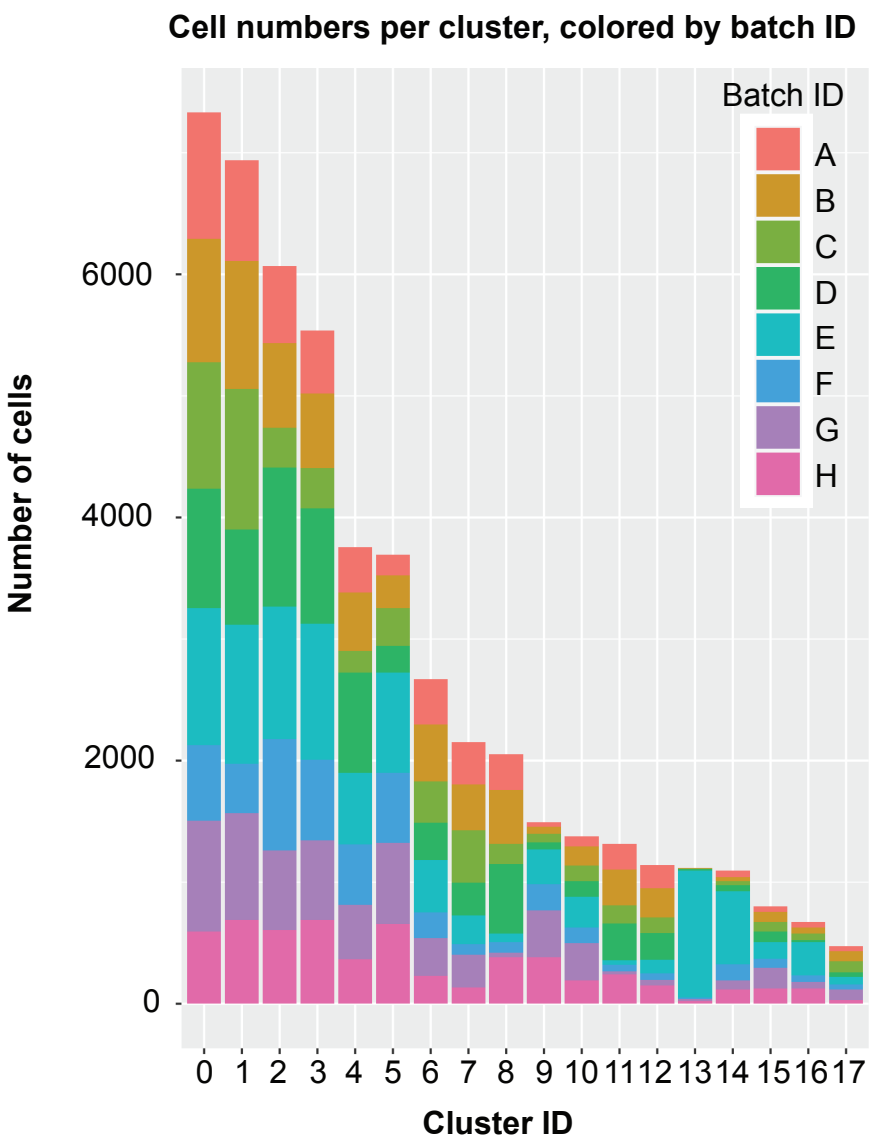

S100a8
S100a9
Fcrls+ Cluster ID
13
4
3
2
7
6
1
0
Expression

Figure 3.11: *The putative WT fetal responder cells are inflammatory, and express both microglial and BAM-associated genes.*
A. The top twenty differentially expressed genes belonging to Cluster 13 were used as input for gene ontology (GO) analysis. Enriched GO terms explicitly related to immune responses are highlighted in red.
B. Violin plots of the gene expression levels of canonical BAM genes in cells belonging to each *Fcrls*$^{+}$ cluster.
C. Violin plots of the gene expression levels of canonical microglial genes in cells belonging to each *Fcrls*$^{+}$ cluster.
D. Cluster 13 is defined by high expression of *S100a8* and *S100a9* within the *Fcrls*$^{+}$ clusters. We propose to use these marker genes for biological validation.

A.


Cell numbers per cluster, colored by batch ID
Batch ID
A
B
C
D
E
F
G
H
Number of cells
6000
4000
2000
0
0 1 2 3 4 5 6 7 8 9 10 11 12 13 14 15 16 17
Cluster ID

B.

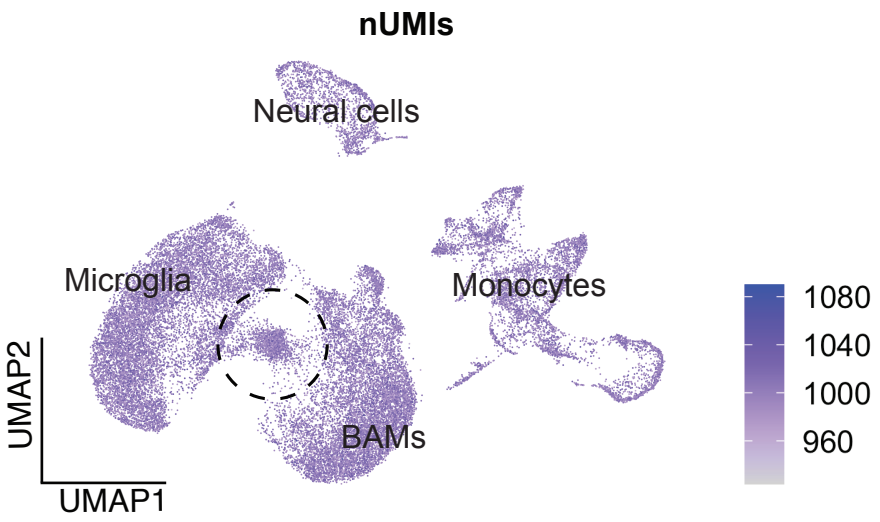

nUMIs
Neural cells
Microglia
Monocytes
BAMs
UMAP2
UMAP1
1080
1040
1000
960

Figure 3.12: *Batch composition and downsampling: testing for robustness.*
A. Barplot depicting the number of cells per cluster colored by batch. Cluster 13, the putative fetal myeloid responder population to Poly(I:C)-induced MIA, largely belongs to one treated replicate (Batch E).
B. The dataset was downsampled such that every cell contains 1000 random UMIs. Cluster 13 (here, numbered Cluster 6—not all clusters in the original dataset remained) persisted despite downsampling.

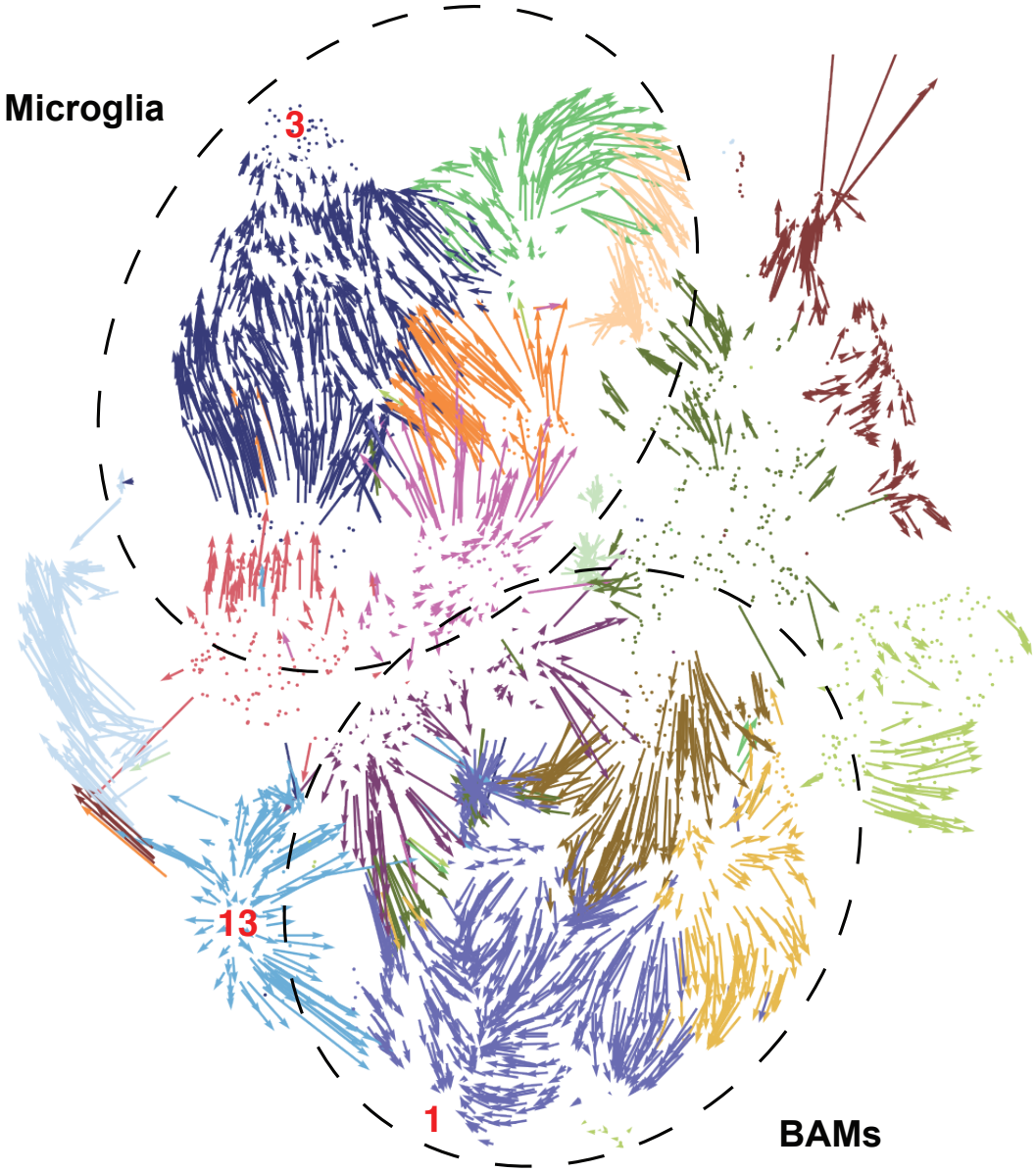

Microglia
3
13
1
BAMs

Figure 3.13: *RNA velocity analysis shows that the putative WT fetal responder cells resolve back toward a BAM cell state.*
The dataset was dimensionally reduced and presented as a tSNE[73] plot with cluster IDs overlaid on top. Dashed circles indicate the microglial and BAM cell neighborhoods as defined previously. The dataset was analyzed using the Velocyto program[61]; the direction of the arrows indicate progression toward a terminal cell state. Cluster 3 represents a terminally differentiated cell state within the microglial cell neighborhood, while Cluster 1 represents a terminally differentiated cell state within the BAM neighborhood. Only the WT portion of the dataset is presented here. For clarity, only three of the clusters are labeled. Since the dataset is still undergoing refinement, the exact cluster coordinates are not the same as previously shown; they are re-labeled to maintain the same notation.

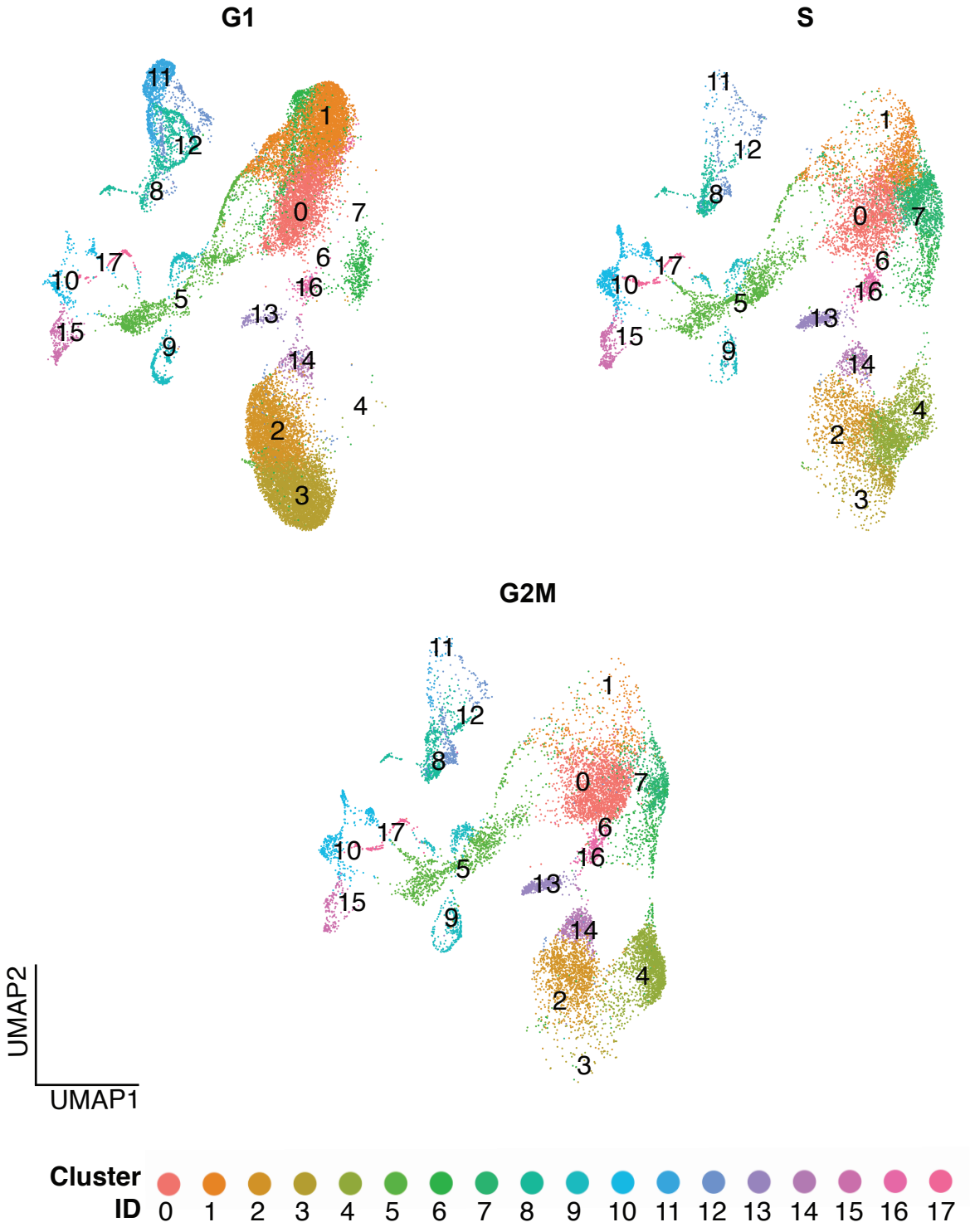
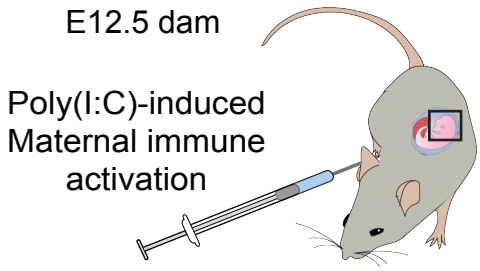

G1
S
G2M
UMAP2
UMAP1
Cluster ID
0 1 2 3 4 5 6 7 8 9 10 11 12 13 14 15 16 17

Figure 3.14: Cell cycle phasing of the dataset.
The entire dataset is presented as UMAPs split by cell cycle phase. Each cell was assigned a G1, S, and G2M score (see Methods).

A.

Working Model



B.

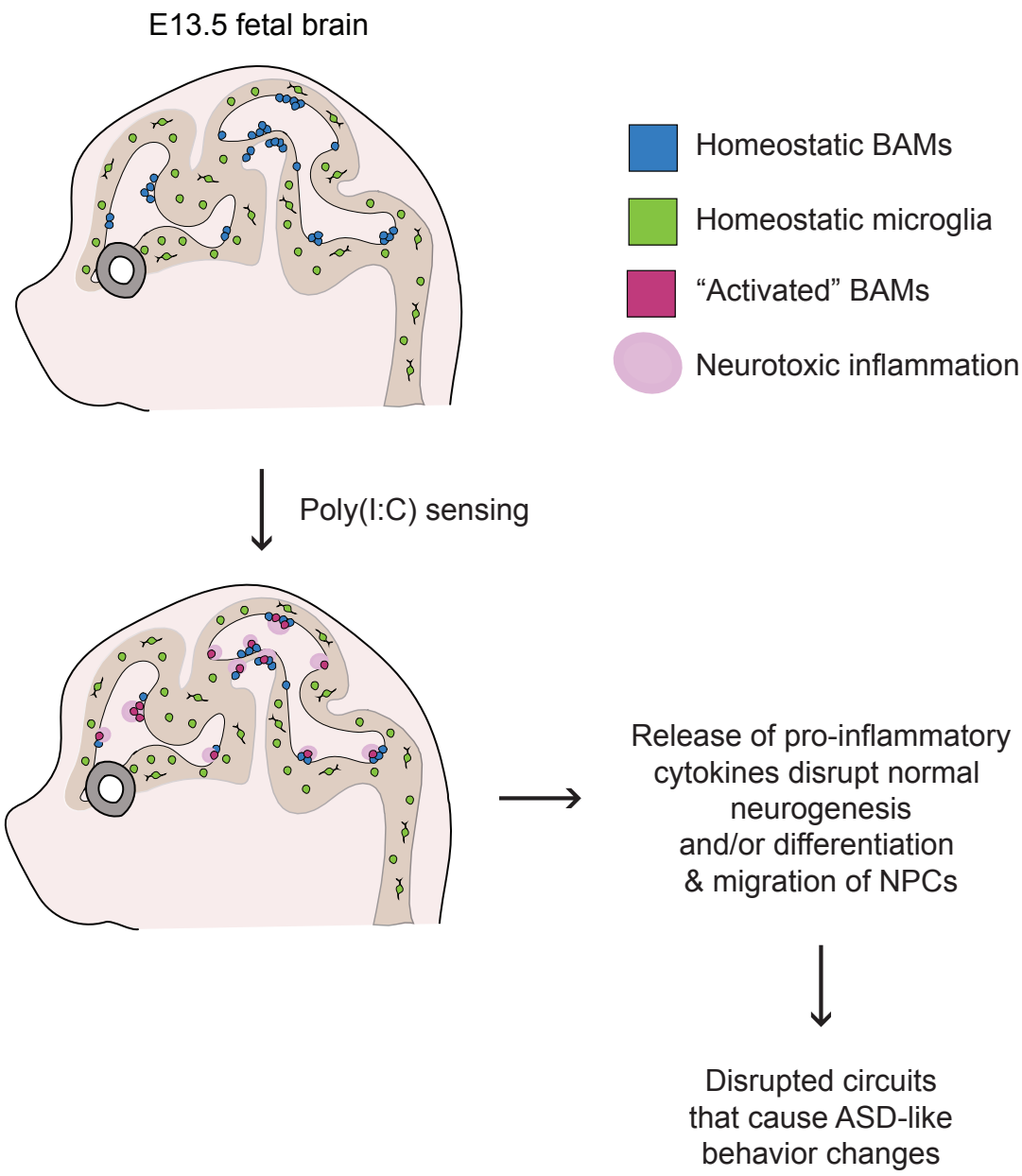


Figure 3.15: *Working model—WT fetal myeloid cells, likely BAMs, respond to Poly(I:C)-induced MIA and promote the formation of ASD-like behavior changes.*
A. Experimental scheme as shown previously.
B. Inset in (**A.**) expanded to depict E13.5 fetal brains 24 hours after Poly(I:C)-induced MIA or vehicle injection. We propose that a subset of BAMs are responsive to Poly(I:C)-induced MIA. Upon sensing Poly(I:C), a subset of BAMs secrete pro-inflammatory factors that disrupt normal brain development. Because BAMs are associated with the borders of the developing brain, secretion of cytokines within the ventricles can potentially be systemic because of diffusion across neurogenic zones. Perhaps, pro-inflammatory cytokines modulate the neural precursor cell pool such that normal neurogenesis and/or differentiation and migration of immature neurons create aberrant circuitry. As a result, this disrupted circuitry underlies the ASD-like behavior changes in adulthood.

Supplementary Table 1. Top 20 marker genes defining the eighteen clusters of the scRNA-seq dataset in descending order of significance, exported from Seurat's FindAllMarkers function[72]. As the Seurat's documentation says, the p_val is the unadjusted p-value[72]. Avg_logFC is the log fold-change of the average expression between two groups; positive values indicate that the feature is more highly expressed in the first group[72]. Pct.1 and pct.2 is the percentage of cells where the feature is detected in the first and second group, respectively[72]. P_val_adj is the adjusted p-value based on the Bonferroni correction on all features within the dataset[72].

Gene	Cluster	p_val	avg_logFC	pct.1	pct.2	p_val_adj
Lyve1	0	0	1.354557364	0.975	0.67	0
Pf4	0	0	1.145967279	1	0.797	0
Hmox1	0	0	1.05523366	0.994	0.911	0
Dab2	0	0	1.023484559	1	0.841	0
Igfbp4	0	0	0.952792825	0.999	0.9	0
Ednrb	0	0	0.942234542	0.991	0.76	0
F13a1	0	0	0.939928405	0.995	0.761	0
Snx2	0	0	0.927085596	1	0.965	0
Mrc1	0	0	0.907727346	0.999	0.801	0
Lgals1	0	0	0.887381629	0.999	0.93	0
Ccl24	0	0	0.801396089	0.986	0.777	0
Stab1	0	0	0.764789501	0.999	0.875	0
Serpinb6a	0	0	0.762535897	0.996	0.845	0
Folr2	0	0	0.753938259	0.984	0.768	0
Ccl7	0	0	0.746547588	0.986	0.874	0
Blvrb	0	0	0.743931659	0.998	0.912	0
Fcgrt	0	0	0.698968004	0.999	0.933	0
Snx6	0	0	0.68271523	0.998	0.961	0
Gas6	0	0	0.677762467	0.998	0.908	0
Fcna	0	0	0.638943622	0.958	0.744	0
Pf4	1	0	1.331467797	1	0.799	0
Ccl24	1	0	1.203023041	0.988	0.779	0
Dab2	1	0	1.188034963	1	0.842	0
Ms4a7	1	0	1.181318171	0.995	0.819	0
Mrc1	1	0	1.175543866	1	0.803	0
Ccl7	1	0	1.175205032	0.986	0.875	0
Selenop	1	0	1.151859673	1	0.986	0
Fcgrt	1	0	1.148848241	0.999	0.933	0
F13a1	1	0	1.111812314	0.997	0.763	0
Igfbp4	1	0	1.068224146	0.999	0.901	0
Stab1	1	0	1.065961176	0.999	0.876	0
Gas6	1	0	0.962534295	0.999	0.908	0
Ednrb	1	0	0.955724493	0.991	0.762	0

Gene	Cluster	p_val	avg_logFC	pct.1	pct.2	p_val_adj
Adrb2	1	0	0.953558055	0.997	0.93	0
Folr2	1	0	0.919343151	0.977	0.772	0
Serpinb6a	1	0	0.905192086	0.993	0.847	0
Blvrb	1	0	0.9016222	0.996	0.914	0
Igf1	1	0	0.849941156	0.983	0.793	0
Clec4a1	1	0	0.839796813	0.98	0.755	0
Maf	1	0	0.834818439	1	0.925	0
Cd9	2	0	1.054700993	0.994	0.865	0
Hexb	2	0	1.028036354	1	0.937	0
Olfml3	2	0	0.821084689	0.986	0.777	0
Serpine2	2	0	0.787129717	0.969	0.794	0
Ctsd	2	0	0.770408922	1	0.989	0
Ctss	2	0	0.755853871	0.999	0.982	0
P2ry12	2	0	0.731565888	0.997	0.91	0
Gpr34	2	0	0.718339113	0.985	0.882	0
Mt1	2	0	0.686404531	0.985	0.929	0
F11r	2	0	0.642230448	0.981	0.8	0
Mpeg1	2	0	0.641725904	0.979	0.805	0
Syngr1	2	0	0.62479312	0.91	0.701	0
Ly86	2	0	0.580638294	0.998	0.965	0
Lair1	2	0	0.574734363	0.969	0.781	0
Cryba4	2	0	0.563899435	0.971	0.885	0
Crybb1	2	0	0.54917997	0.94	0.843	0
Ctsl	2	0	0.541805081	0.998	0.976	0
Sparc	2	0	0.536857771	0.967	0.813	0
Lpcat2	2	0	0.517995867	0.99	0.881	0
Tmem119	2	0	0.511192482	0.958	0.8	0
Sparc	3	0	1.608273941	0.989	0.812	0
Hexb	3	0	1.399530163	1	0.938	0
P2ry12	3	0	1.372242784	0.998	0.911	0
Ccl4	3	0	1.255438314	0.979	0.911	0
Ctss	3	0	1.224920742	1	0.982	0
Rhob	3	0	1.159326338	0.998	0.947	0
Junb	3	0	1.10118507	0.991	0.927	0
Serpine2	3	0	1.058038675	0.983	0.794	0
Lpcat2	3	0	1.049755235	0.993	0.882	0
Tgfbr1	3	0	1.039788456	0.984	0.798	0
F11r	3	0	1.0386503	0.988	0.802	0
Olfml3	3	0	1.029817632	0.982	0.78	0
Il1a	3	0	1.028551759	0.919	0.762	0
Klf2	3	0	1.002524051	0.985	0.944	0
Sgk1	3	0	0.940480787	0.934	0.787	0

Gene	Cluster	p_val	avg_logFC	pct.1	pct.2	p_val_adj
Lair1	3	0	0.931244659	0.975	0.783	0
Tmem119	3	0	0.923409737	0.971	0.801	0
Atf3	3	0	0.914047041	0.975	0.898	0
Btg2	3	0	0.90826576	0.979	0.891	0
Mpeg1	3	0	0.891389586	0.979	0.807	0
Hist1h2ap	4	0	1.323017542	0.903	0.705	0
Ccl4	4	0	0.979936031	0.989	0.913	0
Top2a	4	0	0.917820482	0.925	0.682	0
Hexb	4	0	0.897328045	1	0.941	0
Mki67	4	0	0.859434265	0.917	0.703	0
Pclaf	4	0	0.840699774	0.961	0.763	0
P2ry12	4	0	0.796261934	0.999	0.914	0
Cdk1	4	0	0.783641437	0.974	0.847	0
Olfml3	4	0	0.748041535	0.993	0.787	0
Ccl3	4	0	0.720624291	0.998	0.954	0
Ube2c	4	0	0.718029905	0.914	0.803	0
Smc2	4	0	0.716679103	0.962	0.775	0
Serpine2	4	0	0.687273349	0.979	0.802	0
Tmem119	4	0	0.681290855	0.986	0.806	0
Tgfbr1	4	0	0.679996773	0.99	0.805	0
F11r	4	0	0.675591273	0.994	0.808	0
Ctss	4	0	0.649889901	1	0.983	0
Hmgb2	4	0	0.63884342	0.995	0.955	0
Sparc	4	0	0.633855168	0.983	0.819	0
Pmepa1	4	0	0.614070916	0.949	0.714	0
Cd74	5	0	2.857666099	0.948	0.742	0
H2-Aa	5	0	1.892491717	0.72	0.593	0
Ifitm3	5	0	1.887742317	0.964	0.756	0
Napsa	5	0	1.54374903	0.97	0.647	0
Plac8	5	0	1.497123815	0.957	0.625	0
Crip1	5	0	1.409841026	0.952	0.743	0
Lsp1	5	0	1.377018213	0.989	0.851	0
S100a10	5	0	1.353809833	0.977	0.74	0
Ccr2	5	0	1.312162857	0.956	0.674	0
Ifi203	5	0	1.243100736	0.942	0.58	0
Vim	5	0	1.216162314	0.992	0.911	0
Lgals3	5	0	1.125838126	0.936	0.69	0
Cd52	5	0	1.100877366	0.996	0.911	0
Mndal	5	0	1.097096571	0.969	0.735	0
Plbd1	5	0	0.991154282	0.912	0.638	0
Fxyd5	5	0	0.957061286	0.982	0.783	0
Tspo	5	0	0.940936802	0.997	0.945	0

Gene	Cluster	p_val	avg_logFC	pct.1	pct.2	p_val_adj
S100a11	5	0	0.929554922	0.948	0.65	0
Emb	5	0	0.910167154	0.971	0.779	0
Alox5ap	5	0	0.874548011	0.998	0.932	0
Selenop	6	0	0.628179737	1	0.987	0
Ms4a7	6	0	0.527621611	0.979	0.836	0
Igf1	6	0	0.445903743	0.964	0.812	0
Apoe	6	7.13E-303	0.547393981	1	0.987	1.43E-299
Abca1	6	8.49E-302	0.386183665	0.977	0.863	1.70E-298
Fth1	6	2.09E-283	0.332680606	1	0.999	4.18E-280
Zfp36l1	6	2.40E-245	0.347779011	0.98	0.884	4.81E-242
Serpinb6a	6	8.12E-238	0.340247844	0.978	0.861	1.62E-234
Maf	6	1.01E-233	0.333366742	0.997	0.932	2.03E-230
Ehd4	6	4.29E-228	0.28983275	0.99	0.92	8.59E-225
Cxcl2	6	1.01E-222	0.353908259	0.855	0.766	2.03E-219
Ms4a6c	6	2.88E-220	0.351474503	0.992	0.89	5.75E-217
Cltc	6	2.71E-219	0.269977531	0.991	0.914	5.43E-216
Cd83	6	4.19E-218	0.327932583	0.964	0.848	8.38E-215
Stab1	6	1.70E-213	0.287359766	0.994	0.888	3.39E-210
Klf6	6	4.25E-209	0.316651712	0.995	0.941	8.49E-206
Atf3	6	7.80E-207	0.295753256	0.979	0.902	1.56E-203
Clec4n	6	2.58E-200	0.286496879	0.869	0.754	5.16E-197
Ier3	6	3.54E-199	0.340354796	0.994	0.938	7.07E-196
Ms4a6b	6	9.87E-192	0.307001247	0.994	0.931	1.97E-188
Hist1h2ap	7	0	0.935351964	0.91	0.712	0
Lyve1	7	0	0.886094535	0.976	0.703	0
Pclaf	7	0	0.813507707	0.974	0.769	0
Pf4	7	0	0.804173747	1	0.819	0
Mrc1	7	0	0.794153124	1	0.822	0
Dab2	7	0	0.733966609	1	0.858	0
Igfbp4	7	0	0.695792942	1	0.911	0
F13a1	7	0	0.661866887	0.997	0.787	0
Snx2	7	0	0.654937598	1	0.969	0
Cdk1	7	0	0.647726951	0.989	0.85	0
Mcm6	7	0	0.646357517	0.982	0.819	0
Tyms	7	0	0.638819766	0.974	0.794	0
Gmnn	7	0	0.618169889	0.987	0.816	0
Cxcl2	7	0	0.617327004	0.927	0.764	0
Mcm5	7	0	0.616386394	0.978	0.819	0
Stab1	7	0	0.602176447	0.998	0.889	0
Top2a	7	0	0.577019979	0.932	0.689	0
Rrm2	7	0	0.575302047	0.948	0.734	0
Hat1	7	0	0.568338382	0.981	0.864	0

Gene	Cluster	p_val	avg_logFC	pct.1	pct.2	p_val_adj
Hmgb2	7	0	0.564371467	0.999	0.957	0
Fabp7	8	0	2.459730746	0.929	0.57	0
Tuba1a	8	0	2.193010558	0.996	0.817	0
Sox11	8	0	2.097929063	0.941	0.519	0
Tubb2b	8	0	2.083622061	0.988	0.827	0
Nnat	8	0	2.022653632	0.99	0.637	0
Tubb3	8	0	1.813365548	0.813	0.575	0
Mdk	8	0	1.731647106	0.929	0.53	0
Cdkn1c	8	0	1.68776467	0.876	0.56	0
Ptn	8	0	1.631953562	0.899	0.531	0
Stmn1	8	0	1.528784347	0.988	0.967	0
Prdx2	8	0	1.496480618	0.993	0.972	0
Hmgb3	8	0	1.471021236	0.966	0.766	0
Pantr1	8	0	1.442130476	0.865	0.458	0
Nfib	8	0	1.433036407	0.877	0.484	0
H1fx	8	0	1.413653384	0.938	0.528	0
Tagln3	8	0	1.383278506	0.788	0.497	0
Cd24a	8	0	1.371088163	0.924	0.575	0
Igfbp2	8	0	1.347921741	0.839	0.532	0
Ddah2	8	0	1.326992149	0.977	0.764	0
Sox4	8	0	1.307788103	0.944	0.727	0
S100a8	9	0	5.656088105	0.969	0.613	0
S100a9	9	0	5.570323072	0.898	0.601	0
Stfa1	9	0	5.027780484	0.992	0.616	0
BC100530	9	0	4.886369609	0.881	0.602	0
Gm5483	9	0	4.26462082	0.897	0.538	0
Lcn2	9	0	3.902645851	0.78	0.558	0
Stfa3	9	0	3.246562997	0.929	0.452	0
Olfm4	9	0	3.062607965	0.847	0.539	0
Lyz2	9	0	2.77531892	0.997	0.966	0
Pglyrp1	9	0	2.73632393	0.937	0.462	0
Anxa1	9	0	2.688302404	0.994	0.724	0
S100a6	9	0	2.670206834	0.9	0.655	0
Wfdc21	9	0	2.651772706	0.817	0.476	0
Hp	9	0	2.600231635	0.995	0.561	0
S100a11	9	0	2.435579186	0.997	0.663	0
Thbs1	9	0	2.167144935	0.94	0.506	0
Ifitm6	9	0	2.124376269	0.946	0.559	0
Lgals3	9	0	2.041202504	0.957	0.701	0
2010005H15Rik	9	0	2.026083456	0.784	0.521	0
Slpi	9	0	1.962363353	0.913	0.494	0
Ly6d	10	0	2.21925933	0.811	0.486	0

Gene	Cluster	p_val	avg_logFC	pct.1	pct.2	p_val_adj
Plac8	10	0	2.130563706	1	0.64	0
Ptprcap	10	0	1.802917137	0.995	0.576	0
Mzb1	10	0	1.704190009	0.912	0.445	0
Nrgn	10	0	1.608943693	0.93	0.52	0
Cox6a2	10	0	1.540501189	0.856	0.471	0
H2afy	10	0	1.530052201	1	0.969	0
Trbc2	10	0	1.488606136	0.92	0.475	0
Lsp1	10	0	1.375628097	1	0.858	0
Cd7	10	0	1.336537711	0.945	0.525	0
Bcl11a	10	0	1.180273293	0.974	0.545	0
Tsc22d1	10	0	1.133803393	0.983	0.749	0
Igkc	10	0	1.111722865	0.759	0.42	0
Gpr171	10	0	1.098059831	0.978	0.493	0
Ccr9	10	0	1.088584866	0.941	0.513	0
Atp1b1	10	0	1.060122023	0.855	0.459	0
Tmsb10	10	0	1.011004946	0.999	0.977	0
Ramp1	10	0	0.991684563	0.983	0.809	0
Crip1	10	0	0.954356231	0.971	0.752	0
S100a10	10	0	0.910978234	0.987	0.751	0
Tuba1a	11	0	3.446561807	1	0.82	0
Nnat	11	0	3.18455826	1	0.642	0
Tubb2b	11	0	3.14708737	1	0.829	0
Tubb3	11	0	3.026917651	0.998	0.573	0
Stmn2	11	0	2.734178071	0.989	0.518	0
Rtn1	11	0	2.546863068	0.995	0.633	0
Stmn3	11	0	2.399108401	0.991	0.537	0
Cd24a	11	0	2.311400945	0.998	0.579	0
Sox11	11	0	2.29154304	1	0.523	0
Hist3h2ba	11	0	2.252049256	0.989	0.629	0
Uchl1	11	0	2.19646257	0.995	0.517	0
Stmn1	11	0	2.164984076	1	0.967	0
Tmsb10	11	0	2.136171543	1	0.977	0
Mllt11	11	0	2.133394319	0.995	0.69	0
Pfn2	11	0	2.051254253	0.989	0.544	0
Cnih2	11	0	2.000761295	0.98	0.544	0
Bex2	11	0	1.987724552	0.992	0.536	0
Tagln3	11	0	1.973434064	0.991	0.495	0
Ndn	11	0	1.87200455	0.952	0.559	0
Gng3	11	0	1.854082605	0.968	0.513	0
Tubb2b	12	0	1.222361818	0.949	0.831	0
Tuba1a	12	0	1.159499862	0.976	0.821	0
Nnat	12	0	1.138211443	0.907	0.646	0

Gene	Cluster	p_val	avg_logFC	pct.1	pct.2	p_val_adj
Sox11	12	0	1.100897445	0.863	0.528	0
Stmn1	12	0	1.010894649	0.989	0.967	0
Prdx2	12	0	0.873385279	0.968	0.973	0
Tmsb10	12	4.22E-236	0.674630792	0.993	0.977	8.43E-233
Tubb5	12	1.70E-219	0.733562479	0.993	0.99	3.40E-216
Junb	12	2.92E-207	-0.884731692	0.87	0.936	5.84E-204
Tubb3	12	7.42E-206	0.945287108	0.801	0.579	1.48E-202
Ccl3	12	3.08E-203	-1.10014442	0.867	0.96	6.15E-200
Atf3	12	3.87E-184	-0.771263205	0.745	0.91	7.74E-181
Bex2	12	1.53E-181	0.839116828	0.777	0.543	3.05E-178
Ptma	12	7.04E-178	0.499674856	0.998	0.996	1.41E-174
Ccl4	12	5.33E-177	-1.204371421	0.847	0.92	1.07E-173
Ctss	12	3.16E-174	-0.959248806	0.936	0.985	6.31E-171
Basp1	12	1.55E-173	0.671214949	0.954	0.932	3.09E-170
Srgn	12	1.16E-172	-0.695468749	0.909	0.946	2.32E-169
Rgs2	12	2.02E-171	-0.644121643	0.898	0.949	4.04E-168
Fabp5	12	4.65E-167	0.660998396	0.906	0.843	9.31E-164
S100a9	13	0	0.703643871	0.968	0.601	0
S100a8	13	0	0.666368564	0.973	0.615	0
Stfa1	13	0	0.657640121	0.954	0.62	0
BC100530	13	0	0.621633074	0.941	0.603	0
Gm5483	13	0	0.440034161	0.816	0.542	0
Lyz2	13	0	0.38630768	0.987	0.967	0
Lcn2	13	6.96E-258	0.457944756	0.728	0.56	1.39E-254
Cd74	13	4.60E-216	0.320155524	0.788	0.756	9.20E-213
Tcf4	13	2.19E-201	-0.485857136	0.247	0.86	4.37E-198
Kcnq1ot1	13	1.96E-184	-0.302283238	0.226	0.844	3.92E-181
Stfa3	13	5.77E-181	0.435286744	0.601	0.463	1.15E-177
Zfhx3	13	4.42E-162	-0.375304035	0.163	0.786	8.85E-159
Gas7	13	1.80E-158	-0.301115372	0.234	0.826	3.60E-155
Gm26522	13	7.81E-157	-0.343252704	0.185	0.787	1.56E-153
Smc2	13	3.41E-154	-0.255550936	0.204	0.802	6.81E-151
Nrp1	13	1.20E-152	-0.276855586	0.182	0.788	2.40E-149
Maf	13	5.94E-142	-0.660713976	0.685	0.941	1.19E-138
Wwp1	13	1.80E-133	-0.271749165	0.203	0.78	3.61E-130
Sox4	13	2.44E-130	-0.39249043	0.174	0.749	4.89E-127
Dek	13	1.03E-128	-0.350314195	0.425	0.91	2.07E-125
Gm6377	14	0	-0.423321243	0.41	0.856	0
Klf4	14	0	-0.42665906	0.361	0.83	0
Nfkbia	14	0	-0.535575944	0.396	0.892	0
Egr2	14	0	-0.584655465	0.439	0.886	0
Kcnq1ot1	14	0	-0.586526379	0.268	0.843	0

Gene	Cluster	p_val	avg_logFC	pct.1	pct.2	p_val_adj
Fosb	14	0	-0.662161419	0.335	0.832	0
Tcf4	14	0	-0.69783681	0.317	0.859	0
Gm26532	14	0	-0.788567263	0.416	0.899	0
Btg2	14	0	-0.791089843	0.431	0.911	0
Zfp36l1	14	0	-0.952062519	0.357	0.901	0
Egr1	14	0	-0.970902152	0.378	0.856	0
Neat1	14	0	-0.977996474	0.41	0.917	0
Cited2	14	0	-1.048607802	0.451	0.924	0
Marcksl1	14	0	-1.169411768	0.596	0.976	0
Junb	14	0	-1.214424524	0.5	0.944	0
Klf2	14	0	-1.282074236	0.51	0.958	0
Klf6	14	0	-1.374683949	0.491	0.954	0
Ier3	14	0	-1.540827487	0.456	0.952	0
Ccl7	14	0	-1.575433041	0.42	0.901	0
Ccl3	14	0	-1.587215349	0.598	0.966	0
Ltb	15	0	2.419659785	0.99	0.635	0
Trbc2	15	0	2.295081209	0.964	0.479	0
Nrgn	15	0	2.294634978	0.991	0.524	0
Cd7	15	0	2.027681609	0.986	0.529	0
Tcf7	15	0	1.872039981	0.983	0.455	0
Il7r	15	0	1.784186675	0.975	0.617	0
Ptprcap	15	0	1.720692457	0.985	0.581	0
Id2	15	0	1.637257771	0.99	0.712	0
Hmgn3	15	0	1.605770308	0.911	0.52	0
Nkg7	15	0	1.421143965	0.908	0.338	0
S100a10	15	0	1.40399813	0.995	0.753	0
Emb	15	0	1.387333543	0.998	0.79	0
S100a4	15	0	1.383605397	0.928	0.519	0
Runx3	15	0	1.276524139	0.959	0.549	0
Il17f	15	0	1.244698009	0.879	0.504	0
Tmsb10	15	0	1.235614436	1	0.977	0
Rorc	15	0	1.234662406	0.958	0.545	0
Cd82	15	0	1.180470249	0.979	0.75	0
Lsp1	15	0	1.156013964	0.999	0.859	0
Tagln2	15	0	1.150032689	1	0.915	0
Btg2	16	1.33E-210	-0.752784573	0.515	0.906	2.66E-207
Neat1	16	1.83E-200	-0.676811934	0.476	0.912	3.65E-197
Junb	16	2.48E-191	-0.969235496	0.562	0.94	4.97E-188
Rgs2	16	1.70E-184	-0.841872695	0.592	0.953	3.41E-181
Egr1	16	1.81E-179	-0.826729004	0.397	0.852	3.63E-176
Rgs1	16	1.11E-173	-0.649058477	0.391	0.834	2.22E-170
Lgals1	16	7.94E-172	0.946007666	0.97	0.939	1.59E-168

Gene	Cluster	p_val	avg_logFC	pct.1	pct.2	p_val_adj
Ccl3	16	4.34E-170	-1.428209503	0.696	0.961	8.68E-167
Ccl4	16	2.14E-166	-1.637043598	0.571	0.923	4.29E-163
Fosb	16	1.70E-161	-0.446025248	0.323	0.828	3.39E-158
Jun	16	6.93E-161	-0.923360798	0.689	0.967	1.39E-157
Ier3	16	1.02E-160	-1.001931265	0.64	0.945	2.04E-157
Egr3	16	9.63E-159	-0.450015283	0.433	0.821	1.93E-155
Nr4a1	16	6.84E-158	-0.333237413	0.426	0.801	1.37E-154
Klf6	16	6.83E-157	-0.690439771	0.644	0.948	1.37E-153
Skil	16	9.87E-157	-0.571868858	0.25	0.759	1.97E-153
Egr2	16	2.95E-156	-0.375845107	0.531	0.881	5.90E-153
Kcnq1ot1	16	4.74E-156	-0.484312186	0.509	0.834	9.47E-153
Tspan13	16	6.60E-151	-0.576785509	0.452	0.835	1.32E-147
Srgn	16	1.28E-149	-0.708628914	0.676	0.949	2.57E-146
Scin	17	0	0.326249138	0.797	0.056	0
Srgn	17	4.90E-261	1.967898903	1	0.944	9.80E-258
Hdc	17	4.10E-249	1.974822375	0.939	0.536	8.21E-246
Nedd4	17	6.35E-233	0.915048913	0.989	0.595	1.27E-229
Rab44	17	7.38E-228	0.674163275	0.911	0.372	1.48E-224
Perp	17	1.11E-226	0.833912017	0.919	0.576	2.23E-223
Ptprcap	17	1.25E-225	1.160523282	0.96	0.584	2.50E-222
Tespa1	17	3.19E-223	0.746276109	0.928	0.492	6.39E-220
Il13	17	4.63E-223	0.796546131	0.761	0.148	9.27E-220
Ifitm1	17	7.22E-223	4.257500495	0.928	0.492	1.44E-219
Tagln2	17	3.80E-222	1.146473895	0.994	0.915	7.59E-219
Gata2	17	1.15E-220	1.212837928	0.9	0.421	2.30E-217
Cpa3	17	1.61E-216	2.123658167	0.896	0.454	3.22E-213
Plac8	17	1.15E-214	1.725310138	0.975	0.647	2.31E-211
Mpo	17	2.60E-210	1.617847513	0.896	0.462	5.21E-207
Itgb7	17	5.26E-208	0.987765709	0.943	0.509	1.05E-204
P2ry14	17	1.97E-207	0.700531361	0.922	0.533	3.93E-204
Pglyrp1	17	1.48E-205	0.5815801	0.928	0.472	2.96E-202
Sept1	17	1.52E-205	0.567677878	0.951	0.578	3.04E-202
Fut8	17	2.80E-202	0.850915634	0.943	0.648	5.61E-199

Methods

Animals

All mice were maintained in specific pathogen free conditions at the Association of Laboratory Care-approved animal facility at the Li Ka Shing, University of California, Berkeley, CA. A 12-h light/dark cycle (lights off at 19:00) was maintained in the housing and test rooms. Food and water were accessed *ad libitum*. Wild-type C57BL/6J (WT) mice were originally obtained from the The Jackson Laboratory or Charles River Laboratories and bred in our facilities, *Trif*$^{-/-}$ mice were originally provided by Gregory Barton. *Trif*$^{+/-}$ female mice were generated by *Trif*$^{-/-}$ founders and then further crossed to *Trif*$^{-/-}$ male to produce *Trif*$^{+/-}$ or *Trif*$^{-/-}$ offspring. All of the animals were cohoused in mix-genotype or mix-treatment groups of 3-5 mice per cages upon weaning or, if not possible, their bedding was mixed. Animals at 2-4 months of age were used for behavioral assays. The order of behavioral tests was elevated plus maze, marble burying assay, followed by social behavioral test including reciprocal social interaction and three-chamber. Then, the mice were subjected to T-maze to test their spatial learning and memory. After, the mice were maintained in housing room for more than 2 weeks after the test of T-maze and followed by the open field assay. The above assays were carried out between 10:00 and 18:00 h to prevent fluctuations due to the circadian rhythm.

Detection of MHV-68 DNA by nested PCR

C57BL/6J female mice were bred and infected intraperitoneally at embryonic day E12.5 with either 200 mL 5×10^5 PFU or PBS (control group). Five days post-infection (dpi), pregnant mice were sacrificed, and organs of containing lungs, spleen, and brain in mother and pup mice were harvested. The DNA of organs was prepared by directly using the quick-DNA miniprep kit (Zymo Research) and analyzed for the presence of MHV-68 DNA by nested PCR targeting the gp150 gene of MHV-68. The sequences of primers were as follows: the outer primers were 5'- ACAACTTAGTATGGGTGCCCG-3' (forward) and 5'- CTCAGTCTCCCCAACATGCC-3' (reverse); the inner primers were 5'-ACAAAGGCACCATCTAGCGG-3' (forward) and 5'- GTTCTGAGGTGGTGGGATCG-3' (reverse).

Maternal immune activation by Poly(I:C), LPS, and ODN

On embryonic day E12.5, pregnant mice were given a single dose of either of Poly(I:C) (2 mg/kg; Sigma-Aldrich, cat. no. P9582), LPS (100 mg/kg; Sigma-Aldrich, cat. no. L3024), ODN (100 mg/kg; InvivoGen, cat. no. ODN1826), or saline (control group) given intraperitoneally. Their offspring at 10-16 weeks of age were used for the behavioral assays.

Maternal immune activation by MHV-68 and MCMV

Pregnant wildtype and *Trif*$^{-/-}$ mice were infected intraperitoneally at E12.5 with MHV-68 (5×10^5 plaque forming units (PFU)), MCMV (2×10^6 PFU), or PBS alone (control group). Their offspring at 2-4 months of age were used for the behavioral assays.

Behavioral assays

Open field test

Mice were individually placed in the center of a transparant plastic box (22 x 42.5 x 21 cm) for 1 hour and allowed to freely explore the arena in the dark. Animal movement including the total travelled distance was monitored by computerized photobeam using the MotorMonitor SmartFrame System (Kinder Scientific).

Elevated plus maze

For the elevated plus maze test, each arm of the maze was 30 × 5 cm, and they extended out from a central platform (area 5 × 5 cm). Animals were individually placed onto the central platform and allowed to freely explore the maze for 10 min. A Smart Video Tracking System (Panlab) was used to determine the time spent in the open arms, the closed arms, and the central area during the test.

Reciprocal social interaction

A test mouse was first housed individually for at least 7 days. During the test session, an unfamiliar mouse was put into the home cage of the isolated test mouse, where it was allowed to freely interact with the test mouse. The social interactions of the test mice were recorded using a digital camera for 3 min. The time that the test mouse spent interacting with the non-familiar mouse including sniffing, mounting, and grooming were subsequently measured. The number of test mice observed for the aggressive behaviors included chasing, tail rattling, and biting was also recorded.

Three-chamber social behavior test

A three-chambered rectangular box with two dividing walls that marked the left, center, and right chambers (20 × 40 × 22 cm) was used. This box had openings that allowed a test mouse to freely move into each chamber. During the habituation phase, the mice were placed in the center chamber and allowed to freely explore for 10 min. In the sociability test, a cylindrical grid cage (7 cm in diameter and 15 cm in height) housing an unfamiliar adult mouse (S1), and an identical empty cage (E) were placed on opposite side chambers. The test mouse was allowed to freely explore the chambers with the S1 and E cages for 10 min. In the last preference for social novelty test, the test mouse was allowed to freely explore and selectively interact with either the already-investigated familiar (S1) mouse or the new unfamiliar (S2) mouse placed into the empty cage in a 10-min session. The movements of the test mice were recorded with a digital camera and the time spent interacting or sniffing each cylindrical cage was measured using the

Smart Video Tracking System (Panlab). The time spent on the top of the cylindrical cage designated as the climbing behavior was also recorded.

Marble burying assay

The fresh unscented bedding material was evenly distributed into a flat surface across the clean cage (27 × 16.5 × 12.5 cm) with a depth of approximately 5 cm. During the habituation phase, the mouse was individually placed to each cage without any marbles. After freely exploring the cage for 20 min, the mouse was temporarily removed. Then, twenty glass marbles (1.5 mm in diameter) were gently spaced in a 4 × 5 arrangement on the surface of the bedding. During the testing phase each mouse was placed in the cage with marbles and allowed to explore it for 20 min. At the end of the test, mice were removed from cage and the number of marbles buried (>50% marble covered by bedding material) was counted.

Statistical analysis

Statistical analysis was performed using the Prism 6 (GraphPad) software. We used the Student's t-test to compare two groups and one-way ANOVA to compare more than three groups with the Tukey post-test, except when showing the differences between the littermate controls and experimental groups. P values <0.05 were considered to be statistically significant.

scRNAseq

Tissue dissection and cell isolation

One or two E13.5 dams were sacrificed per replicate (24 hours after MIA), and individual embryos collected in ice-cold 1xPBS or DMEM F12 media (with 10% FBS, 5% HS, and 1% PS antibiotics). Embryonic tails were taken for SRY genotyping, and entire fetal brains were dissected, minced by feather blade, and triturated with a flame-polished Pasteur pipette until pieces were <1mm in size. Whenever possible, samples were kept on ice and at 4^{o}C during centrifugation and sorting. At least seven embryos were used per replicate; whenever possible, an equal number of male and female brain samples were pooled together. After pooling, samples were spun at 1000*xg* for 5 minutes and re-suspended in pre-warmed digestion buffer (10mL 1xHBSS with Ca^{2+} and Mg^{2+} containing Liberase-TM and 400 U of DNAse-I). Samples were rotated end-over-end at 37^{o}C for 10-15 minutes, with further trituration by flame-polished Pasteur pipette every five minutes. 200-400 U of DNAse-I was added if DNA precipitate was visible in solution. Next, the sample was strained on ice through a 100um cell strainer and washed with 4mL of ice-cold Wash Buffer 1 (1xHBSS without Ca^{2+} and Mg^{2+} containing 200 U of DNAseI and 10% FBS) into a 50mL conical tube. This process was repeated once more with a 70um cell strainer and a fresh 50mL conical tube. 22mL of ice-cold Wash Buffer 2 (1xHBSS without Ca^{2+} and Mg^{2+} containing 10% FBS) was spun down at 1200*xg* for 10 minutes; cell staining followed after.

Myeloid cell staining and flow cytometry sorting

After centrifugation, the cell pellet was re-suspended in blocking solution (Wash Buffer 2 Fc Block at a 1:16 dilution factor) and incubated on ice for at least 10 minutes in a 2mL lo-bind Eppendorf tube. After, Cd11b-PE-Cy7 (eBioscience, cat. no. 25-0112-81) and CD45.2-PE (Invitrogen, cat. no. 12-0454-83) antibodies were added at a 1:100 dilution factor, and the sample was incubated for an additional 15 minutes on ice. 500uL of Wash Buffer 2 was added directly to the tub for a half-rinse; this was spun down at 800*xg* for 5 minutes and re-suspended in about 750uL of media (DMEM F12 without phenol red, 10% FBS, and 5% HS) per fetal brain pooled. The sample was filtered through a 40um cell strainer prior to sorting. For dead cell exclusion, 0.001% v/v of DAPI was added for every 100uL of solution. An estimated 3-10x10^6< cells per litter were stained, and on average 56,000 live- and singlet-gated $Cd45^+Cd11b^+$ was sorted into media using a BD FACSAria™ Fusion flow cytometer available at the Cancer Research Laboratory Flow Cytometry Facility at UC Berkeley. $Cd45^+Cd11b^+$ cells were about 1-2% of the total live cell fraction, and were not partitioned into $Cd11b^{hi}$ or $Cd11b^{lo}$ groups (see **Figure 3.6B**).

SRY genotyping

Genomic DNA from embryonic tails was isolated by digestion in 100 uL of 50 mM NaOH until no longer visible; 25 uL of 1 mM Tris-HCl was then added. 1 uL of this gDNA prep was used in a fast SRY genotyping protocol using the KAPA2G Fast HotStart genotyping kit and SRY forward and reverse primers (SRY F 5'-TTGTCTAGAGAGCATGGAGGGC-3' and SRY R 5'-CCACTCCTCTGTGACACTTTAGC-3').

Library prep, sequencing, and raw data processing

Immediately after sorting, cells were spun down 800*xg* for 5-10 minutes, and concentrated in media to an estimated 500-1100 cells/uL. The 10X Chromium Single Cell 3' Reagent Kit (v3 chemistry) platform was at the Functional Genomics Lab, UC Berkeley. To maximally resolve any cellular heterogeneity in our system, we aimed for a cell capture of 9-10,000 cells per batch. The 10X Chromium Single Cell 3' Reagent Kit (v3 chemistry) was used. All four libraries (per genotype) were pooled and sequenced on one S4 lane of the Illumina NovaSeq 6000 platform at the Vincent J. Coates Genomics Sequencing Laboratory at UC Berkeley and the UCSF Center for Advanced Technology. Sequencing reads were processed using the 10X Cell Ranger software in cluster mode.

Data import, filtering, and variable feature selection

The raw filtered gene expression matrices generated by the 10X Cell Ranger software was analyzed primarily using the Seurat R package[72] (version 2.1.4) within RStudio (version 1.1.463)[74]. The matrices were read into Seurat and made into Seurat objects. Only cells with a minimum of three cells and a minimum of 200 features were present

for downstream steps. The treatment, genotype, batch, percent mitochondrial genes (percent.mt), and percent ribosomal genes (percent.ribo) were added to the metadata for every cell. Next, each Seurat object was further filtered such that only cells containing equal to or more than 500 features (but less than 6500) and equal to or less than 15% mitochondrial genes per cell were included for downstream analysis. The data was then log normalized using the NormalizeData function, in which the feature counts in each cell are divided by the total counts for that cell, then multiplied by a scale factor of 10,000[72]. Then, these values are natural-log transformed using log1p[72]. Next, 2000 variable features are selected for every cell using the FindVariableFeatures function and the vst selection method[72]. These variable features were used as input for principle component analysis.

Cell sex separation

The sex of every cell was identified by first merging the batches via the merge function in Seurat[72]. The merged object for each genotype underwent sex gene expression characterization in order to infer the sex of every cell. Briefly, the lists of all genes from the Y and X mouse chromosomes were extracted from Ensembl's biomaRt using the "ENSEMBL_MART_MOUSE" mart and the "mmusculus_gene_ensembl" dataset[75]. The merged object data was then normalized and scaled only on features found only on the Y- and X-chromosomes. These sex gene lists was used to find all Y and X chromosome genes expressed in the dataset; only 8 total Y-chromosome features were found (*Eif2s3y*, *Kdm5d*, *Gm29650*, *Uty*, *Ddx3y*, *Gm29554*, *Gm47283*, and *Zfy1*). Meanwhile, 610 total X-chromosome genes were found; we chose *Xist* as the representative X-chromosome gene[76]. Density histograms of gene expression were constructed for all 8 Y-chromosome genes and *Xist*; cutoff values were determined at the first minimum. For any cell that has expression of any Y-chromosome gene above the cutoff, and below the cutoff for *Xist*, were counted as male. Conversely, any cells with *Xist* expression above its cutoff, and below that of all Y-chromosome genes, were counted as female. Any cells that did not fall in this category were deemed indeterminate and removed from the study; all remaining cells had its sex assigned to the metadata.

Additional cell quality control, scaling, and regression

Any low-quality cells, such as doublets remaining after filtering, were identified using the DoubletFinder tool (version 2.0.3)[77]. We then used Seurat's CellCycleScoring function to infer the cell cycle phase of every cell; each cell received a G2M and S score (S.Score and G2M.Score, respectively) based on phase markers. We used the Scater package (version 1.14.6)[78] to further assess dataset quality. Next, the batches were batch-corrected using Seurat's FindIntegrationAnchors and IntegrateData functions using 40 dimensions and normalized using the log normalization method. The integrated dataset was then scaled using Seurat's ScaleData function; here, the percent.mt, nCounts_RNA, S.Score, and G2M.Score variables were regressed out, and all variable features in the dataset were scaled.

Principle components selection, dataset integration, and clustering

In order to infer how many useful principal components (PCs) to include, we used Seurat's ElbowPlot function and decided to use 15 PCs in the downstream analysis[72]. These PCs were used to reduce the dimensionality of the dataset via Seurat's RunPCA function, which was used on the integrated assay[72]. RunUMAP, FindNeighbors, and FindClusters functions were used next to visualize results[72]. We used a resolution parameter of 0.4, as inferred by Clustree analysis[79]. A total of eighteen clusters were identified. The top marker genes (positive and negative) defining the clusters were found using Seurat's FindAllMarkers function (with parameters min.pct and thresh.use at 0.25)[72]. These are considered to be differentially expressed genes. The top five markers per cluster were visualized in a heat map generated by Seurat's DoHeatmap function[72]. Seurat's DimPlot, FeaturePlot, and DotPlot functions were used to generate figures[72]. KableExtra[80], ggplot2[81], and cowplot[82] were also used to generate figures.

Gene ontology analysis

To perform a gene ontology analysis on the genes defining Cluster 13, Cluster 13 was first subsetted using Seurat's SubsetData function[72]. Then, the topGO package was used[83]. First, genes were selected that are expressed in at least 75% of cells. Second, a topGOdata object was made using the biological process ontology. Then, genes were tested for enrichment using Fisher's Exact Test. ggplot[81] was used to plot the –log10 of the adjusted P values.

RNA velocity analysis

RNA velocity analysis was done using the Velocyto package[61] performed by Rick Z. Li from the Chris Glass Lab. Fastq files were trimmed and mapped using STAR to the mouse reference genome (*mm10*). From the annotation files, intronic and exonic information was extracted. From this information, ratios of the spliced and unspliced variants of each gene in every cell is known; changes in these ratios for a gene in a cell allow for inferences in cell state changes among the population[61]. Arrows point to the position of the future state. The data presented here comes from the WT (and not *Trif*$^{-/-}$) portion of the dataset. The arrow embeddings were plotted and visualized by tSNE[73].

References

1. Malkova, N. V., Yu, C. Z., Hsiao, E. Y., Moore, M. J. & Patterson, P. H. Maternal immune activation yields offspring displaying mouse versions of the three core symptoms of autism. *Brain Behavior and Immunity* **26,** 607–616 (2012).
2. Patterson, P. H. Modeling autistic features in animals. *Pediatric Research* **69,** 34R–40R (2011).
3. Ey, E., Leblond, C. S. & Bourgeron, T. Behavioral profiles of mouse models for autism spectrum disorders. *Autism Res* **4,** 5–16 (2011).
4. Bey, A. L. & Jiang, Y.-H. Overview of mouse models of autism spectrum disorders. *Curr Protoc Pharmacol* **66,** 5.66.1–26 (2014).
5. Provenzano, G., Zunino, G., Genovesi, S., Sgadó, P. & Bozzi, Y. Mutant mouse models of autism spectrum disorders. *Dis. Markers* **33,** 225–239 (2012).
6. Atladóttir, H. Ó. *et al.* Maternal Infection Requiring Hospitalization During Pregnancy and Autism Spectrum Disorders. *J Autism Dev Disord* **40,** 1423–1430 (2010).
7. Takeda, K. & Akira, S. TLR signaling pathways. *Seminars in Immunology* **16,** 3–9 (2004).
8. Sen, G. C. & Sarkar, S. N. Transcriptional signaling by double-stranded RNA: role of TLR3. *Cytokine and Growth Factor Reviews* **16,** 1–14 (2005).
9. Takeda, K. & Akira, S. TLR signaling pathways. *Seminars in Immunology* **16,** 3–9 (2004).
10. Lu, Y.-C., Yeh, W.-C. & Ohashi, P. S. LPS/TLR4 signal transduction pathway. *Cytokine* **42,** 145–151 (2008).
11. Patterson, P. H. Immune involvement in schizophrenia and autism: Etiology, pathology and animal models. *Behavioural Brain Research* **204,** 313–321 (2009).
12. Estes, M. L., Farrelly, K., Cameron, S., bioRxiv, J. A.2019. Enhancing rigor and reproducibility in maternal immune activation models: practical considerations and predicting resilience and susceptibility using baseline immune …. *biorxiv.org* doi:10.1101/699983
13. Martinez, S., Puelles, E., Puelles, L. & Echevarria, D. in *The Mouse Nervous System* 2–18 (Elsevier, 2012). doi:10.1016/B978-0-12-369497-3.10001-9
14. Semple, B. D., Blomgren, K., Gimlin, K., Ferriero, D. M. & Noble-Haeusslein, L. J. Brain development in rodents and humans: Identifying benchmarks of maturation and vulnerability to injury across species. *Progress in Neurobiology* **106-107,** 1–16 (2013).
15. Brown, A. S. & Derkits, E. J. Prenatal infection and schizophrenia: a review of epidemiologic and translational studies. *Am J Psychiatry* **167,** 261–280 (2010).
16. Smith, S. E. P., Li, J., Garbett, K., Mirnics, K. & Patterson, P. H. Maternal immune activation alters fetal brain development through interleukin-6. *J. Neurosci.* **27,** 10695–10702 (2007).
17. Kishimoto, T. Interleukin-6: discovery of a pleiotropic cytokine. *Arthritis Res.*

Ther. **8 Suppl 2,** S2–6 (2006).
18. Tanaka, T., Narazaki, M. & Kishimoto, T. IL-6 in inflammation, immunity, and disease. *Cold Spring Harbor Perspectives in Biology* **6,** a016295 (2014).
19. Jin, W. & Dong, C. IL-17 cytokines in immunity and inflammation. *Emerg Microbes Infect* **2,** e60–5 (2013).
20. Iwakura, Y., Nakae, S., Saijo, S. & Ishigame, H. The roles of IL-17A in inflammatory immune responses and host defense against pathogens. *Immunol. Rev.* **226,** 57–79 (2008).
21. Choi, G. B. *et al.* The maternal interleukin-17a pathway in mice promotes autism-like phenotypes in offspring. *Science* **351,** 933–939 (2016).
22. Ivanov, I. I. *et al.* Induction of intestinal Th17 cells by segmented filamentous bacteria. *Cell* **139,** 485–498 (2009).
23. Kim, S. *et al.* Maternal gut bacteria promote neurodevelopmental abnormalities in mouse offspring. *Nature* **549,** 528–532 (2017).
24. Yim, Y. S. *et al.* Reversing behavioural abnormalities in mice exposed to maternal inflammation. *Nature* **549,** 482–487 (2017).
25. Hsiao, E. Y. *et al.* Microbiota Modulate Behavioral and Physiological Abnormalities Associated with Neurodevelopmental Disorders. *Cell* **155,** 1451–1463 (2013).
26. Perdiguero, E. G. & Geissmann, F. The development and maintenance of resident macrophages. *Nat Immunol* **17,** 2–8 (2016).
27. Mass, E. *et al.* Specification of tissue-resident macrophages during organogenesis. *Science* **353,** (2016).
28. Amit, I., Winter, D. R. & Jung, S. The role of the local environment and epigenetics in shaping macrophage identity and their effect on tissue homeostasis. *Nat Immunol* **17,** 18–25 (2016).
29. Ginhoux, F. *et al.* Fate mapping analysis reveals that adult microglia derive from primitive macrophages. *Science* **330,** 841–845 (2010).
30. Ginhoux, F. & Jung, S. Monocytes and macrophages: developmental pathways and tissue homeostasis. *Nat. Rev. Immunol.* **14,** 392–404 (2014).
31. Kojima, Y., Tam, O. H. & Tam, P. P. L. Timing of developmental events in the early mouse embryo. *Semin. Cell Dev. Biol.* **34,** 65–75 (2014).
32. Matcovitch-Natan, O. *et al.* Microglia development follows a stepwise program to regulate brain homeostasis. *Science* **353,** aad8670 (2016).
33. Thion, M. S. & Garel, S. On place and time: microglia in embryonic and perinatal brain development. *Current Opinion in Neurobiology* **47,** 121–130 (2017).
34. Reemst, K., Noctor, S. C., Lucassen, P. J. & Hol, E. M. The Indispensable Roles of Microglia and Astrocytes during Brain Development. *Front Hum Neurosci* **10,** 566 (2016).
35. Utz, S. G. *et al.* Early Fate Defines Microglia and Non-parenchymal Brain Macrophage Development. *Cell* (2020). doi:10.1016/j.cell.2020.03.021
36. Van Hove, H. *et al.* A single-cell atlas of mouse brain macrophages reveals unique transcriptional identities shaped by ontogeny and tissue environment. *Nat Neurosci* **22,** 1021–1035 (2019).
37. Swinnen, N. *et al.* Complex invasion pattern of the cerebral cortex

bymicroglial cells during development of the mouse embryo. *Glia* **61,** 150–163 (2013).
38. Krieg, A. M. CpG motifs in bacterial DNA and their immune effects. *Annu. Rev. Immunol.* **20,** 709–760 (2002).
39. Simas, J. P. & Efstathiou, S. Murine gammaherpesvirus 68: a model for the study of gammaherpesvirus pathogenesis. *Trends Microbiol.* **6,** 276–282 (1998).
40. Krmpotic, A., Bubic, I., Polic, B., Lucin, P. & Jonjic, S. Pathogenesis of murine cytomegalovirus infection. *Microbes Infect.* **5,** 1263–1277 (2003).
41. Alford, C. A., Stagno, S., Pass, R. F. & Britt, W. J. Congenital and perinatal cytomegalovirus infections. *Rev. Infect. Dis.* **12 Suppl 7,** S745–53 (1990).
42. Engman, M.-L. *et al.* Prenatal acquired cytomegalovirus infection should be considered in children with autism. *Acta Paediatr.* **104,** 792–795 (2015).
43. Sakamoto, A., Moriuchi, H., Matsuzaki, J., Motoyama, K. & Moriuchi, M. Retrospective diagnosis of congenital cytomegalovirus infection in children with autism spectrum disorder but no other major neurologic deficit. *Brain Dev.* **37,** 200–205 (2015).
44. Maeyama, K. *et al.* Congenital Cytomegalovirus Infection in Children with Autism Spectrum Disorder: Systematic Review and Meta-Analysis. *J Autism Dev Disord* **48,** 1483–1491 (2018).
45. Delorme-Axford, E., Sadovsky, Y. & Coyne, C. B. The Placenta as a Barrier to Viral Infections. *Annu Rev Virol* **1,** 133–146 (2014).
46. Cardenas, I. *et al.* Viral infection of the placenta leads to fetal inflammation and sensitization to bacterial products predisposing to preterm labor. *J. Immunol.* **185,** 1248–1257 (2010).
47. Johnson, K. P. Mouse cytomegalovirus: placental infection. *J. Infect. Dis.* **120,** 445–450 (1969).
48. Woolf, N. K., Jaquish, D. V. & Koehrn, F. J. Transplacental murine cytomegalovirus infection in the brain of SCID mice. *Virol. J.* **4,** 26 (2007).
49. ŠTIGLINCOVÁ, V. *et al.* Vertical transmission of murine gammaherpesvirus 68 in mice. *Acta Virol.* **55,** 55–59 (2011).
50. Shen, Y. *et al.* Inhibition of murine herpesvirus-68 replication by IFN-gamma in macrophages is counteracted by the induction of SOCS1 expression. *PLoS Pathog* **14,** e1007202 (2018).
51. Bussey, K. A. *et al.* The gammaherpesviruses Kaposi's sarcoma-associated herpesvirus and murine gammaherpesvirus 68 modulate the Toll-like receptor-induced proinflammatory cytokine response. *J. Virol.* **88,** 9245–9259 (2014).
52. Tabeta, K. *et al.* Toll-like receptors 9 and 3 as essential components of innate immune defense against mouse cytomegalovirus infection. *Proceedings of the National Academy of Sciences* **101,** 3516–3521 (2004).
53. Becker, M. *et al.* Mast cells as rapid innate sensors of cytomegalovirus by TLR3/TRIF signaling-dependent and -independent mechanisms. *Cell Mol Immunol* **12,** 192–201 (2015).
54. Prinz, M., Erny, D. & Hagemeyer, N. Ontogeny and homeostasis of CNS myeloid cells. *Nat Immunol* **18,** 385–392 (2017).

55. Hammond, T. R. *et al.* Single-Cell RNA Sequencing of Microglia throughout the Mouse Lifespan and in the Injured Brain Reveals Complex Cell-State Changes. *Immunity* **50,** 253–271.e6 (2019).
56. Li, Q. *et al.* Developmental Heterogeneity of Microglia and Brain Myeloid Cells Revealed by Deep Single-Cell RNA Sequencing. *Neuron* **101,** 207–223.e10 (2019).
57. Jordão, M. J. C. *et al.* Single-cell profiling identifies myeloid cell subsets with distinct fates during neuroinflammation. *Science* **363,** (2019).
58. Endoh, Y., Chung, Y. M., Clark, I. A., Geczy, C. L. & Hsu, K. IL-10-dependent S100A8 gene induction in monocytes/macrophages by double-stranded RNA. *J. Immunol.* **182,** 2258–2268 (2009).
59. Xu, K. & Geczy, C. L. IFN-gamma and TNF regulate macrophage expression of the chemotactic S100 protein S100A8. *J. Immunol.* **164,** 4916–4923 (2000).
60. Sunahori, K. *et al.* The S100A8/A9 heterodimer amplifies proinflammatory cytokine production by macrophages via activation of nuclear factor kappa B and p38 mitogen-activated protein kinase in rheumatoid arthritis. *Arthritis Res. Ther.* **8,** R69 (2006).
61. La Manno, G. *et al.* RNA velocity of single cells. *Nature* **560,** 494–498 (2018).
62. Nelson, S. B. & Valakh, V. Excitatory/Inhibitory Balance and Circuit Homeostasis in Autism Spectrum Disorders. *Neuron* **87,** 684–698 (2015).
63. Rubenstein, J. L. R. & Merzenich, M. M. Model of autism: increased ratio of excitation/inhibition in key neural systems. *Genes Brain Behav.* **2,** 255–267 (2003).
64. Polleux, F. & Lauder, J. M. Toward a developmental neurobiology of autism. *Ment Retard Dev Disabil Res Rev* **10,** 303–317 (2004).
65. Holmgren, J. & Czerkinsky, C. Mucosal immunity and vaccines. *Nature Medicine* **11,** S45–53 (2005).
66. Cunningham, C. L. & Martinez-Cerdeno, V. Microglia regulate the number of neural precursor cells in the developing cerebral cortex. *Journal of …* (2013). doi:10.1523/JNEUROSCI.3441-12.2013
67. Ashwell, K. The distribution of microglia and cell death in the fetal rat forebrain. *Brain Res. Dev. Brain Res.* **58,** 1–12 (1991).
68. Dalmau, I. *et al.* Development of microglia in the prenatal rat hippocampus. *J. Comp. Neurol.* **377,** 70–84 (1997).
69. Stoeckius, M. *et al.* Cell Hashing with barcoded antibodies enables multiplexing and doublet detection for single cell genomics. *Genome Biol.* **19,** 224–12 (2018).
70. McInnes, L., Healy, J. & Melville, J. UMAP: Uniform Manifold Approximation and Projection for Dimension Reduction. (2018).
71. Becht, E. *et al.* Dimensionality reduction for visualizing single-cell data using UMAP. *Nature Biotechnology* (2018). doi:10.1038/nbt.4314
72. Satija, R., Farrell, J. A., Gennert, D., Schier, A. F. & Regev, A. Spatial reconstruction of single-cell gene expression data. *Nature Biotechnology* **33,** 495–502 (2015).

73. Maaten, L. V. D. & Hinton, G. Visualizing Data using t-SNE. *Journal of Machine Learning Research* **9,** 2579–2605 (2008).
74. Young, M. E. *et al.* Facilitating admissions of diverse students: A six-point, evidence-informed framework for pipeline and program development. *Perspect Med Educ* **6,** 82–90 (2017).
75. Yates, A. D. *et al.* Ensembl 2020. *Nucleic Acids Research* **48,** D682–D688 (2020).
76. Staedtler, F. *et al.* Robust and tissue-independent gender-specific transcript biomarkers. *Biomarkers* **18,** 436–445 (2013).
77. McGinnis, C. S., Murrow, L. M. & Gartner, Z. J. DoubletFinder: Doublet Detection in Single-Cell RNA Sequencing Data Using Artificial Nearest Neighbors. *Cell Syst* **8,** 329–337.e4 (2019).
78. McCarthy, D. J., Campbell, K. R., Lun, A. T. L. & Wills, Q. F. Scater: pre-processing, quality control, normalization and visualization of single-cell RNA-seq data in R. *Bioinformatics* **33,** 1179–1186 (2017).
79. Zappia, L. & Oshlack, A. Clustering trees: a visualization for evaluating clusterings at multiple resolutions. *Gigascience* **7,** (2018).
80. Hao Zhu (2019). kableExtra: Construct Complex Table with 'kable' and Pipe Syntax. R package version 1.1.0. https://CRAN.R-project.org/package=kableExtra
81. Wickham H (2016). *ggplot2: Elegant Graphics for Data Analysis*. Springer-Verlag New York. ISBN 978-3-319-24277-4, https://ggplot2.tidyverse.org.
82. Claus O. Wilke (2019). cowplot: Streamlined Plot Theme and Plot Annotations for 'ggplot2'. R package version 1.0.0. https://CRAN.R-project.org/package=cowplot
83. Adrian Alexa and Jorg Rahnenfuhrer (2019). topGO: Enrichment Analysis for Gene Ontology. R package version 2.38.1.

Chapter 4

Discussion and future directions

4.1 Fetal immunity and development: considerations for public health.

Broadly, our work suggests that there is likely exquisite coordination of fetal brain myeloid cells and neural cell development throughout brain formation. Disruption of fetal brain myeloid cell functions, either by interrupting microglial lytic cell death or activating border-associated macrophage immunity, can negatively impact brain circuit development—even in the absence of overt structural brain abnormalities. These observations may have important implications for human maternal and fetal health. In this section, I will discuss how we may contextualize our findings within the larger framework of public health. However, I caution the reader that our work (and my interpretation thereof) should be cautiously regarded; at time of filing this dissertation, our work has not yet appeared in a peer-reviewed journal (and, some data analysis is still ongoing). More studies are required to gain additional mechanistic insight. As always, by using a mouse model, our interpretations to human health are already quite limited.

Much of our studies concerned mouse brain development between E12.5 and E14.5. Embryology studies in mice and humans have created the Carnegie Staging method, a means of comparative analysis of developmental events among species[1]. Days E12.5 through E14.5 of mouse gestation correlate to days 40 through 52 during human pregnancy; the Carnegie stages are 16-20[2]. In humans, organogenesis begins at Carnegie stage 9 (E20) and ends at Carnegie stage 23 (E56)[2]. Thus, our experimental window of E12.5-E14.5 in mouse correlates to a 12-day window in human pregnancy when organogenesis is well underway and reaching a flourish[3].

Because of the organogenesis process, this time is appreciated as a highly sensitive window of development. Any alterations in this time window to the developing fetal brain can confer permanent changes in cellular composition and character that is causative for neurodevelopmental disorders. A well-known example is fetal alcohol syndrome, in which maternal alcohol consumption can cause severe intellectual disability (among other behavioral symptoms) in the child[4]. Thus, by utilizing the E12.5-E14.5 window of mouse gestation, we model a critical vulnerability window of human gestation and fetal brain development.

Infection during pregnancy as a maternal risk factor for ASD is gaining appreciation[5,6]. Our work shows that, unexpectedly, fetal immunity in addition to maternal immunity may also be a factor into the overall risk of maternal infection. Perhaps, one public health outcome would be to ensure people are up-to-date on vaccinations (such as the seasonal flu vaccine) prior to pregnancy. Additionally, during flu season, additional measures can include wearing facemasks, limiting touch to the face, and frequent hand washing (these are precautions that everyone should be taking normally).

We also learned that maternal use of drugs that affect the pyroptosis pathway might cause permanent changes in behavior that appear like ADHD. Caspase-1 ICE inhibitors is under active investigation for use in autoimmune conditions, like myasthenia gravis in which using an ICE inhibitor demonstrated improvements in symptoms[7]. ICE inhibitors are also being explored for other clinical applications[8-11]. Further investigation should be done to see if ingesting ICE inhibitors confers any additional risk to the already known link between maternal autoimmunity and neurodevelopmental

disorders[12,13]. If there is, limiting drug use that may impact pyroptosis during the first trimester may reduce that risk. Additionally, we show that acetaminophen exposure during the window of active neurogenesis and differentiation in mice produce ADHD-like behaviors, perhaps in part by downregulating aspects of the pyroptosis pathway. Acetaminophen use during pregnancy is already acknowledged as a risk factor for hyperactivity[14,15]. Since acetaminophen is frequently marketed as the only "safe" painkiller for pregnant women, and is the most commonly used drug during pregnancy[14,16], limiting its use during the first trimester can mitigate concerns for this risk factor.

Ultimately, there should be no fear mongering—the timing, duration, and intensity of the maternal risk factors clearly matter. For example, maternal hospitalizations due to infection remain low[5,6,17]. I am personally heartened to see that, despite the marvelous complexity of molecular and cellular mechanisms guiding organogenesis, it more often proceeds normally than not. Using our model systems, we now have tools to begin understanding how these basic biological mechanisms—particularly between fetal myeloid cells and neural cells—synergize to form a complex organ like the brain. I will discuss some of these outstanding questions and future directions in the next section.

4.2 Outstanding questions and future directions of study.

I think the most exciting part of using the *Casp1*$^{-/-}$ and MIA mouse models in future works is to explore how fetal brain myeloid cells and neural cells coordinate cell functions to establish neurotypical circuitry. In the process, we can learn more about the neural circuits underlying fundamental behaviors, especially for behaviors like sociability, that are less well understood. To study the basic biology of fetal myeloid cells during brain development, more refined mouse genetics tools are needed—namely, generation of fluorescence reporter strains and conditional deletion strains in a microglial-, BAM-, and neural-subtype specific manner. Advances in scRNA-seq will aid in the identification of cellular subsets and the marker genes defining them. Advances in genetic engineering, particularly mediated by Cas9[18-20], should aid in the swift creation of these mice. I provide a few examples of outstanding questions that can make use of these future tools.

In the data presented in this thesis, only male mouse data was shown. Unless otherwise indicated, female mice did not show as striking behavior changes compared to male mice. Why did we observe a male bias in our *Casp1*$^{-/-}$ and MIA mouse models? This is perhaps our greatest outstanding question. Many neurodevelopmental disorders have a male bias, including ASD and ADHD[21-24]. It is unknown why male mice are more susceptible (or, female mice more resilient) to *Casp1* deficiency and maternal immune challenge. When considering our models of neurodevelopmental disorders, two major hypotheses are immediately thought of: 1. Genetic elements on the sex chromosomes confer susceptibility or resiliency. Male mice have the Y-chromosome that may harbor factors that confer increased susceptibility. Female mice have two X-chromosomes; additional elements escaping X-inactivation may confer protection for female mice. 2., Gonadal (or sex hormones) confer susceptibility or resiliency. To test these hypotheses, combining our models with the four-core genotypes model (FCG) may help us dissect genetic or hormonal contributions to our mouse behavioral phenotypes[25]. In the FCG

mice, the testis-determining gene *Sry* is deleted from the Y-chromosome and inserted elsewhere onto an autosome as a transgene[25-27]. XY^- mice are gonadal female. When the *Sry* transgene is present, the mice are gonadal male (XY^-*Sry*)[25]. So, XX & XY mice with testes, and XX & XY mice with ovaries, are made[25]. Thus, XX females (XXF), XY^- females (XYF), XX*Sry* males (XXM), and XY^-*Sry* males (XYM) are produced when XYM mice are mated with XXF mice[25].

Two important parameters can be evaluated with the FCG model. First, the sex factor (*Sry* present or absent), and the ovarian and testicular secretions thereof, is the first key comparison[25]. If testicular hormones are a principle driver in the susceptibility of male mice to *Casp1*- and MIA-induced behavioral phenotypes, we would anticipate that XXM mice will phenocopy XYM mice. We would also anticipate that XXF and XYF would phenocopy each other. If ovarian sex hormones are a principle driver that promotes resiliency in female mice to *Casp1*- and MIA-induced behavioral phenotypes, we would predict that XYF mice will phenocopy XXF mice more closely. Secondly, sex chromosome complementation is the second key parameter to consider in the FCG model[25]. If Y-chromosome genes contribute to the susceptibility of *Casp1* deficiency- and MIA-induced behavioral phenotypes, we would expect to see XYF behavior phenocopy XYM behaviors. If there is no effect, we would expect to see XYF behavior phenocopy XXF behavior more closely. If X-chromosome genes confer resiliency to *Casp1* deficiency- and MIA-induced behavioral phenotypes, we may expect to see XXM mouse behavior phenocopy XXF female mouse behaviors. If there is no X-chromosome gene protection, we expect that XXM mouse behavior will mirror that of XYM male mouse behavior. The caveats of the FCG mouse model is that the gonads of XX and XY mice of the same gonadal sex have differences in both morphology and function[25], which may complicate the interpretation of this behavioral study. This is because there could be different levels of hormones produced. To circumvent this, gonadectomizing mice and treating with equivalent levels of respective hormones may help[25]. Still, different sex hormone levels may be present before production by gonads themselves *in utero* during critical periods[28-31]. And, microglia express the estrogen receptor β (ERβ); 5-androsten-3β,17β-diol (ADIOL) was demonstrated to function as a selective modulator of ERβ by negatively suppressing inflammatory responses of microglia and astrocytes[32]. Thus, the fetal brain may be competent to sense sex hormones even before gonadal development. Therefore, the biology of sex and the brain is a very complicated one. Perhaps the FCG model, and more targeted genetic approaches along sex hormone pathways, can help answer this question.

Another major question is, what is the maternal and fetal cytokine milieu promoting neurotypical brain development *in utero*? And, what cytokines, in addition to IL-6 and IL-17, promote abnormal brain development? What are the effects on neural cells? From our work using *Casp1*$^{-/-}$ mice, it's likely that there is not be a one-size-fits-all answer. IL-1β exerts differential effects in the brain[33]; in development from our own studies, IL-1β may promote the death of specific neural subsets in the thalamus. Yet, other subsets in the thalamic nuclei may have been depleted with cells in *Casp1*$^{-/-}$ mice (data not shown), suggesting that IL-1β may be a candidate factor promoting the survival of other neural cells in the vicinity of lytic cell death. An alternative explanation is that cytokines may skew the differentiation of neural cell types akin to immune cells in the periphery. So, perhaps the neural precursor cells are less likely to produce

oligodendrocytes later in brain development during asymmetric division. Indeed, IL-6 and is implicated in both normal and abnormal brain development[34,35]. Therefore, context is key. Differential cytokine action in the fetal brain, in our models and others, can be clarified with conditional cytokine and cytokine receptor knockout mice in a microglia-, BAM-, and neural subtype-dependent manner. A boon to this process is that the genetic neuroanatomy is fairly well defined[36] (see also the Allen Institute for Brain Science online resources), and is increasingly being refined, by scRNA-seq and spatial transcriptomics methods[37-44]. However, in contrast, fetal brain myeloid cell mapping is behind.

Thus, another major question is, what is the spatiotemporal localization of fetal brain myeloid cells over the developmental brain landscape? *Swinnen et al.* has an excellent baseline characterization of fetal microglia in brain development[45], but to my knowledge, extensive mapping of markers identified by scRNA-seq has not yet been done. In order to fully understand how fetal brain myeloid cells and neural precursor cell development is coordinated, high-definition atlases involving both of these major cell lineages should be constructed. These data are important because, while largely qualitative, they help contextualize and refine our hypotheses. For example, fetal microglia directly impacting neurogenesis may make less sense if there are few fetal microglia within the neurogenic zones. By making inferences among the literature, *Swinnen et al.* noted a key switch in microglial morphology at E15.5, which lines up with the key developmental switch noted by *Matcovitch-Natan et al*. Other parallels yet-to-be-discovered may exist. Furthermore, since the developmental sites of fetal myeloid cell migration into the brain is not known, fate mapping and lineage tracing tools can be used to trace the migratory routes of microglia and BAMs throughout brain development. These studies are laborious because of the technical skills (and time) required to serial section and stain tissue. However, with the advent of modern tissue processing methods, tissue sectioning and staining may soon be antiquated. It is now possible to process intact tissue samples for whole volumetric imaging[46-58], with improvements in computational analysis tools[52,59]. I anticipate that these modern tissue processing, microscopy, and computational analysis methods will vastly accelerate future studies.

4.3 Conclusion.

Fetal immunity, mediated by both microglia and border associated macrophages, matters for typical brain development in mice. Future works will be aimed toward mechanistically defining how fetal immunity in the brain shapes proper circuit formation. This is only the beginning of an exciting frontier at the intersection of developmental neuroscience and immunology.

References

1. O'Rahilly, R. & Müller, F. Developmental stages in human embryos: revised and new measurements. *Cells Tissues Organs (Print)* **192,** 73–84 (2010).
2. Hill, M.A. (2020, May 17) **Embryology** *Animal Development*. Retrieved from https://embryology.med.unsw.edu.au/embryology/index.php/Animal_Development.
3. B.M. Carlson. Human Embryology and Developmental Biology. Mosby, St. Louis (2004).
4. Riley, E. P., Infante, M. A. & Warren, K. R. Fetal alcohol spectrum disorders: an overview. *Neuropsychol Rev* **21,** 73–80 (2011).
5. Osokine, I. & Erlebacher, A. Inflammation and Autism: From Maternal Gut to Fetal Brain. *Trends in Molecular Medicine* **23,** 1070–1071 (2017).
6. Lee, B. K. *et al.* Maternal hospitalization with infection during pregnancy and risk of autism spectrum disorders. *Brain Behavior and Immunity* **44,** 100–105 (2015).
7. Wang, C.-C. *et al.* Caspase-1 inhibitor ameliorates experimental autoimmune myasthenia gravis by innate dendric cell IL-1-IL-17 pathway. *J Neuroinflammation* **12,** 118 (2015).
8. Wannamaker, W. *et al.* (S)-1-((S)-2-{[1-(4-amino-3-chloro-phenyl)-methanoyl]-amino}-3,3-dimethyl-butanoyl)-pyrrolidine-2-carboxylic acid ((2R,3S)-2-ethoxy-5-oxo-tetrahydro-furan-3-yl)-amide (VX-765), an orally available selective interleukin (IL)-converting enzyme/caspase-1 inhibitor, exhibits potent anti-inflammatory activities by inhibiting the release of IL-1beta and IL-18. *J Pharmacol Exp Ther* **321,** 509–516 (2007).
9. Flores, J. *et al.* Caspase-1 inhibition alleviates cognitive impairment and neuropathology in an Alzheimer's disease mouse model. *Nature Communications* **9,** 3916–14 (2018).
10. Yang, X.-M. *et al.* The Highly Selective Caspase-1 Inhibitor VX-765 Provides Additive Protection Against Myocardial Infarction in Rat Hearts When Combined With a Platelet Inhibitor. *J. Cardiovasc. Pharmacol. Ther.* **22,** 574–578 (2017).
11. Cornelis, S., Kersse, K., Festjens, N., Lamkanfi, M. & Vandenabeele, P. Inflammatory caspases: targets for novel therapies. *Curr. Pharm. Des.* **13,** 367–385 (2007).
12. Nielsen, P. R., Benros, M. E. & Dalsgaard, S. Associations Between Autoimmune Diseases and Attention-Deficit/Hyperactivity Disorder: A Nationwide Study. *J Am Acad Child Adolesc Psychiatry* **56,** 234–240.e1 (2017).
13. Edmiston, E., Ashwood, P. & van de Water, J. Autoimmunity, Autoantibodies, and Autism Spectrum Disorder. *Biological Psychiatry* **81,** 383–390 (2017).
14. Bauer, A. Z., Kriebel, D., Herbert, M. R., Bornehag, C.-G. & Swan, S. H. Prenatal paracetamol exposure and child neurodevelopment: A review. *Horm Behav* **101,** 125–147 (2018).
15. Liew, Z., Ritz, B., Rebordosa, C., Lee, P.-C. & Olsen, J. Acetaminophen use during pregnancy, behavioral problems, and hyperkinetic disorders. *JAMA Pediatr* **168,** 313–320 (2014).
16. Werler, M. M., Mitchell, A. A., Hernandez-Diaz, S. & Honein, M. A. Use of over-the-counter medications during pregnancy. *Am. J. Obstet. Gynecol.* **193,** 771–

777 (2005).
17. Atladóttir, H. Ó. *et al.* Maternal Infection Requiring Hospitalization During Pregnancy and Autism Spectrum Disorders. *J Autism Dev Disord* **40,** 1423–1430 (2010).
18. Ran, F. A. *et al.* Genome engineering using the CRISPR-Cas9 system. *Nature Protocols* **8,** 2281–2308 (2013).
19. Andersson-Rolf, A. *et al.* One-step generation of conditional and reversible gene knockouts. *Nat Meth* (2017). doi:10.1038/nmeth.4156
20. Modzelewski, A. J. *et al.* Efficient mouse genome engineering by CRISPR-EZ technology. *Nature Protocols* **13,** 1253–1274 (2018).
21. May, T., Adesina, I., McGillivray, J. & Rinehart, N. J. Sex differences in neurodevelopmental disorders. *Current Opinion in Neurology* **32,** 622–626 (2019).
22. Arnold, L. E. Sex differences in ADHD: conference summary. *J Abnorm Child Psychol* **24,** 555–569 (1996).
23. Davies, W. Sex differences in attention Deficit Hyperactivity Disorder: candidate genetic and endocrine mechanisms. *FRONTIERS IN NEUROENDOCRINOLOGY* **35,** 331–346 (2014).
24. Trent, S. & Davies, W. The influence of sex-linked genetic mechanisms on attention and impulsivity. *Biol Psychol* **89,** 1–13 (2012).
25. Arnold, A. P. & Chen, X. What does the 'four core genotypes' mouse model tell us about sex differences in the brain and other tissues? *FRONTIERS IN NEUROENDOCRINOLOGY* **30,** 1–9 (2009).
26. Lovell-Badge, R. & Robertson, E. XY female mice resulting from a heritable mutation in the primary testis-determining gene, Tdy. *Development* **109,** 635–646 (1990).
27. Mahadevaiah, S. K. *et al.* Mouse homologues of the human AZF candidate gene RBM are expressed in spermatogonia and spermatids, and map to a Y chromosome deletion interval associated with a high incidence of sperm abnormalities. *Hum. Mol. Genet.* **7,** 715–727 (1998).
28. Money, J. & Ehrhardt, A. A. Fetal hormones and the brain: Effect on sexual dimorphism of behavior-A review. *Arch Sex Behav* **1,** 241–262 (1971).
29. Reinisch, J. M. Fetal hormones, the Brain, and human sex differences: A heuristic, integrative review of the recent literature. *Arch Sex Behav* **3,** 51–90 (1974).
30. Ehrhardt, A. A. & Meyer-Bahlburg, H. F. Effects of prenatal sex hormones on gender-related behavior. *Science* **211,** 1312–1318 (1981).
31. Berenbaum, S. A. & Beltz, A. M. How Early Hormones Shape Gender Development. *Curr Opin Behav Sci* **7,** 53–60 (2016).
32. Saijo, K., Collier, J. G., Li, A. C., Katzenellenbogen, J. A. & Glass, C. K. An ADIOL-ERβ-CtBP transrepression pathway negatively regulates microglia-mediated inflammation. *Cell* **145,** 584–595 (2011).
33. Depino, A., Ferrari, C., Pott Godoy, M. C., Tarelli, R. & Pitossi, F. J. Differential effects of interleukin-1beta on neurotoxicity, cytokine induction and glial reaction in specific brain regions. *J. Neuroimmunol.* **168,** 96–110 (2005).
34. Smith, S. E. P., Li, J., Garbett, K., Mirnics, K. & Patterson, P. H. Maternal immune

activation alters fetal brain development through interleukin-6. *J. Neurosci.* **27,** 10695–10702 (2007).
35. Hattori, Y. *et al.* Transient microglial absence assists postmigratory cortical neurons in proper differentiation. *Nature Communications* **11,** 1631 (2020).
36. Joyner, A. L. & Sudarov, A. *Chapter 3 - Genetic Neuroanatomy*. *The Mouse Nervous System* 36–50 (Elsevier Inc., 2011). doi:10.1016/B978-0-12-369497-3.10003-2
37. Ofengeim, D., Giagtzoglou, N., Huh, D., Zou, C. & Yuan, J. Single-Cell RNA Sequencing: Unraveling the Brain One Cell at a Time. *Trends in Molecular Medicine* **23,** 563–576 (2017).
38. Kolodziejczyk, A. A., Kim, J. K., Svensson, V., Marioni, J. C. & Teichmann, S. A. The technology and biology of single-cell RNA sequencing. *Molecular Cell* **58,** 610–620 (2015).
39. Cuevas-Diaz Duran, R., Wei, H. & Wu, J. Q. Single-cell RNA-sequencing of the brain. *Clin Transl Med* **6,** 20–14 (2017).
40. Moor, A. E. & Itzkovitz, S. Spatial transcriptomics: paving the way for tissue-level systems biology. *Current Opinion in Biotechnology* **46,** 126–133 (2017).
41. Rodriques, S. G. *et al.* Slide-seq: A scalable technology for measuring genome-wide expression at high spatial resolution. *Science* **363,** 1463–1467 (2019).
42. Codeluppi, S. *et al.* Spatial organization of the somatosensory cortex revealed by osmFISH. *Nat Meth* **15,** 932–935 (2018).
43. Ståhl, P. L. *et al.* Visualization and analysis of gene expression in tissue sections by spatial transcriptomics. *Science* **353,** 78–82 (2016).
44. Wang, X. *et al.* Three-dimensional intact-tissue sequencing of single-cell transcriptional states. *Science* **361,** (2018).
45. Swinnen, N. *et al.* Complex invasion pattern of the cerebral cortex bymicroglial cells during development of the mouse embryo. *Glia* **61,** 150–163 (2013).
46. Ueda, H. R. *et al.* Tissue clearing and its applications in neuroscience. *Nat Rev Neurosci* **21,** 61–79 (2020).
47. Susaki, E. A. *et al.* Advanced CUBIC protocols for whole-brain and whole-body clearing and imaging. *Nature Protocols* **10,** 1709–1727 (2015).
48. Tainaka, K. *et al.* Whole-Body Imaging with Single-Cell Resolution by Tissue Decolorization. *Cell* **159,** 911–924 (2014).
49. Susaki, E. A. *et al.* Whole-brain imaging with single-cell resolution using chemical cocktails and computational analysis. *Cell* **157,** 726–739 (2014).
50. Chung, K. & Deisseroth, K. CLARITY for mapping the nervous system. *Nat Meth* **10,** 508–513 (2013).
51. Park, Y.-G. *et al.* Protection of tissue physicochemical properties using polyfunctional crosslinkers. *Nature Biotechnology* (2018). doi:10.1038/nbt.4281
52. Murray, E. *et al.* Simple, Scalable Proteomic Imaging for High-Dimensional Profiling of Intact Systems. *Cell* **163,** 1500–1514 (2015).
53. Kim, S.-Y. *et al.* Stochastic electrotransport selectively enhances the transport of highly electromobile molecules. *Proc. Natl. Acad. Sci. U.S.A.* **112,** E6274–83 (2015).
54. Epp, J. R. *et al.* Optimization of CLARITY for Clearing Whole-Brain and Other Intact Organs. *eNeuro* **2,** 1–15 (2015).

55. Tomer, R., Ye, L., Hsueh, B. & Deisseroth, K. Advanced CLARITY for rapid and high-resolution imaging of intact tissues. *Nature Protocols* **9,** 1682–1697 (2014).
56. Keller, P. J. & Dodt, H.-U. Light sheet microscopy of living or cleared specimens. *Current Opinion in Neurobiology* **22,** 138–143 (2012).
57. Santi, P. A. Light sheet fluorescence microscopy: a review. *J. Histochem. Cytochem.* **59,** 129–138 (2011).
58. Power, R. M. & Huisken, J. A guide to light-sheet fluorescence microscopy for multiscale imaging. *Nat Meth* **14,** 360–373 (2017).
59. Swaney, J. *et al.* Scalable image processing techniques for quantitative analysis of volumetric biological images from light-sheet microscopy. *biorxiv.org* doi:10.1101/576595